The Structure and Properties of Surfactant and Polymer Mixtures in Glycerol/Water Solutions

The University Of Sheffield.

James Cosby

Department of Chemistry

Faculty of Science

University of Sheffield

Submitted to the University of Sheffield in partial fulfilment of the requirements for the degree of Doctor of Philosophy.

Declaration

The work conducted in this thesis was carried out at the University of Sheffield under the supervision of Prof. Anthony J. Ryan and Dr. Oleksandr O. Mykhaylyk between October 2016 and May 2021. It has not been submitted, either wholly or in part, for this or any other degree. All work is the original work of the author except when acknowledged by means of references.

James Cosby

30/04/2021

Acknowledgements

My greatest thanks to Prof. Tony Ryan and Dr. Oleksandr Mykhaylyk for over four years of knowledge, guidance, and patience. Whether it was help with an instrument, a theory or just general advice you have always been there whenever I needed it. I have truly relished this PhD and I thank you both for giving me this opportunity. Your supervision has been incredible, and I leave this PhD a better chemist thanks to both of you.

Pierre, thank you for being a great industrial supervisor. Your excitement and encouragement have meant a lot. You have been understanding and helped me anyway you can. I would also like to thank everyone at Unilever I have interacted with, either on placement or otherwise. A big thank you especially to Andre, Dave, Dawn, Rob, and everyone in the oral care team. You are all kind and knowledgeable, and learning from you has been so rewarding.

Thank you to Keith Owen for providing Karl Fisher measurements and Craig Robertson for the XRD measurements. Thank you to Emma Brown for all your help in the MIF.

I would like to thank Unilever and EPSRC for providing funding for this project. Thanks are extended to the Centre for Doctoral training in Polymers, Soft Matter and Colloids, for providing exemplary training throughout this PhD.

A big thank you to everyone in that has helped me through my journey. Adam, Chris, James and Lloyd, thanks for always being there even if we couldn't meet up. Thanks to James Jennings for being a great friend always on hand to help. To my friends in Sheffield, including Debs, Harry, and Tom thanks for making it enjoyable, I'll miss our times together. Thanks to the Ryan-Mykhaylyk group, who have always been so helpful and are a genuinely great group of people to be around.

To my mum, dad, and brother, it's been quite a while since you first dropped me off at the halls of residence during my undergraduate degree, I don't think any of us expected me to be a student for this long! Thank you for all your unwavering love and encouragement and being there no matter what, those weekends home after a long week helped more than you knew. Soon we will be able to spend more time together again. Thank you as well to Artur and Ewa, it has been amazing staying with you, hopefully, we will get to go on forest adventures shortly.

Finally, Alex, you are truly wonderful, without you I could not have gotten this far. From last minute train journeys after a day in the lab, to the unwavering love and support during writing, you have shared this journey with me and been with me every step of the way. Thank you.

Publication

J. Cosby, P. Starck, D. Littlewood, O. O. Mykhaylyk and A. J. Ryan, Co-assembly and Structure of Sodium Dodecylsulfate and other n-Alkyl Sulfates in Glycerol: n-Alkyl Sulfate-Glycerol Crystal Phase, *Journal of Colloid and Interface Science*, 2021, 596, 442–454. https://doi.org/10.1016/j.jcis.2021.03.063

Abstract

The use of non-aqueous and mixed-aqueous solvents can add therapeutic and performance benefits to personal care and pharmaceutical formulations. The understanding of these colloidal systems, however, is limited compared to the wealth of information available for aqueous systems. This thesis describes the impact of solvent composition and additives on the phase behaviour and physical properties of model surfactant systems. Polymer solution behaviour is studied alongside, with the aim of understanding the interactions between solutes in complex formulations. Sodium dodecyl sulfate (SDS) in glycerol and glycerol-aqueous mixtures was used as a model system and was studied in detail due to the commonality and characteristic behaviour of each component. Analogous polyol solvent-anionic surfactant systems were used to study systematic behaviour, while iota-carrageenan was used as a model structuring polymer, as it is commonly utilized and is compatible with SDS.

SDS was found to crystallize into ribbon-like morphologies at room temperature forming a freestanding gel at 2 Wt.% and above. Under continuous shear, the brittle gels break up and align to the shear field, causing strong shear-thinning behaviour. The structure of the crystal phase was investigated using small and wide angle x-ray scattering, with electron density information along the lamellar axis obtained from Bragg peak diffraction data. It was found that SDS and glycerol formed highly crystalline co-assembled structures, with glycerol incorporated between surfactant headgroups. The formation of the phase was independent of tail group, and similar phases were systematically formed in homologous n-alkyl sulfates (C12-C18) in glycerol. Co-assembly was not limited to glycerol: the same phenomenon was observed in ethylene glycol, suggesting potential for tuneable surfactant-solvent crystalline gels.

Addition of small amounts of water were shown to disrupt the formation of the SDS-glycerol phase, with the dominance of anhydrous SDS crystals at 6 Wt.% water of solution and above. This caused a loss of structure in mixtures. Moreover, anhydrous SDS crystals formed in solvent mixtures containing less than 20 Wt.% water exhibited an unexpected feather-like morphology, in contrast to the expected platelets and needles. Analysis of micellar structures using SAXS showed that whilst SDS in glycerol formed small oblate micelles, SDS in glycerol-rich mixed solvent had hydrated head groups, affecting the micelle shell thickness. This is in contrast to the larger prolate ellipsoids that formed in water-rich and aqueous mixtures. The complex crystallization and micelle behaviour was attributed to a dynamic equilibrium for water, existing in the bulk solvent and micelle surface. 1-Dodecanol, a synthetic precursor to SDS, co-crystallized with SDS in glycerol mixtures, replacing the SDS-glycerol phase. The change in phase was linear with respect to 1-dodecanol concentration when cooled quiescently. At elevated temperatures, 1-dodecanol acted as a co-surfactant, swelling the micelle cores. The effect of NaCl addition on crystal structure was also probed, which led to the formation of a new, previously unreported crystal phase at 3 Wt.% NaCl.

1 Wt.% solutions of iota-carrageenan formed weak gel-like structures in mixed solvents, with a viscosity maximum at ~20 Wt.% water, irrespective of processing conditions. This behaviour was rationalised through preferential exclusion of co-solvents, leading to conformational changes from coil to helix, previously demonstrated using inverse Kirkwood-Buff theory in the literature. Despite its interaction with water, this biopolymer did not alter the preference for anhydrous crystal formation in the presence of water.

These results show that both surfactant and polymer phase behaviour is changeable over a narrow formulation region. The work in this thesis can be used to characterise and predict material behaviour in more complex industrial mixtures, thus aiding formulation design.

Abbreviations

ATR	Attenuated total reflection
c*	Critical overlap concentration
Ce	Critical entanglement concentration
CMC	Critical micelle concentration
CMT	Critical micelle temperature
CPP	Critical packing parameter
DSC	Differential scanning calorimetry
EDP	Electron density profile
FCN	Fat crystal network
G'	Storage modulus
G''	Loss modulus
IR	Infrared
KB theory	Kirkwood Buff theory
LMWG	Low molecular weight gels
LVER	Linear viscoelastic range
M_w	Weight averaged molecular weight
NMR	Nuclear magnetic resonance
OM	Optical microscopy
POM	Polarised optical microscopy
q	Scattering vector
RED	Relative energy difference
SaFiN	Self-assembled fibrillar networks
SANS	Small angle neutron scattering
SAXS	Small angle x-ray scattering
SCMC	Sodium carboxymethyl cellulose
SDS	Sodium dodecyl sulfate
SIPLI	Shear induced polarisation of light imaging
SLD	Scattering length density
SWAXS	Simultaneous small and wide angle scattering
T_{init}	Lag/initiation time
T_K	Krafft temperature
WAXS	Wide angle scattering
Wt.%	Weight percent
η	Viscosity
η_0	Zero shear viscosity
η_{inf}	Infinite shear viscosity
ξ	Correlation length

Table of Contents

1. Introduction

1.1. Project Context: The Use of Toothpaste and the Emergence of Non-aqueous Formulations

Cleaning materials for oral hygiene have been used for over 3000 years, but the use of a particulate slurry to abrade and clean the teeth is more recent, dating from the 1800's.[1] Advances in the field of oral care has led to a greater understanding of what is required to combat the effects of a modern diet on oral health.[2,3] while providing additional functionality in the form of whitening,[4] sensitivity and odour.[5] Modern toothpaste comes in two main forms, gel or paste.[1] Paste comprise a high solids particulate as an abrasive and rheology modifier at concentrations of around 50 Wt.%,[6] whereas gels contains far less undissolved matter.[6] For gels, silica abrasives are commonly used instead of carbonates as they are more abrasive (to counteract their lower concentration),[7] and refractive index matching of the solution ensures transparancy.[8] Their lower solid content results in a higher reliance on structuring agents, typically organic polymers (such as polyacrylic acid), to achieve the rheology required for application and brushing.

Most toothpastes act through two mechanisms: abrasive cleaning in combination with a toothbrush, and fluoridisation. The first, often credited due to inorganic particle abrasives, removes food debris as well as a harmful biofilm called plaque, although the impact of abrasives is questionable.[1,5,9,10] The second, is the formation of acid-resistant fluorapatite in place of hydroxyapatite.[11] This creates a stronger enamel which protects against damage even at relatively low concentrations.[12] Modern toothpaste requires a range of controlled material behaviour to achieve the correct experiential properties. The rheology of toothpaste is crucial for successful application on the dental surface. Multiple shear events over different length scales must be considered when designing the product's rheology[13–15]. For the consumer this encompasses two main events. Firstly the toothpaste is squeezed under low shear onto a brush, whereby the toothpaste experiences primarily planar squeeze flow (or plug flow).[16] After this the cylindrical 'ribbon' of toothpaste must recover and maintain its shape on the brush. The next event is high shear brushing where the material must lose its initial viscosity and disperse uniformly in the mouth and on the teeth.[17]

By removing water, active ingredients which are either reactive to, or insoluble in water can be included in a toothpaste formulation. This is encapsulated within one of the earliest commercial examples in 1933, where the use of a carrier oil allowed for the presence of acid and alkaline materials, which were reported to result in deposition of inorganic chalk particles in aqueous mixtures.[18] Further examples of

non-aqueous toothpaste can be found throughout the 20th century, reportedly with an oil or polyol carrier liquid.[1,19] In the early 21st century, formulations targeting the remineralisation of enamel at the tooth surface, with non-aqueous mixtures used to confine the reaction in vivo, as water is introduced on application in the mouth.[3,20] Most commercial formulations of toothpaste exist as a mixed aqueous system, where the humectants (typically glycerol and sucrose) act as minor cosolvents. However as water content is reduced and materials such as glycerol become the predominant or sole solvent; the nature of solvation changes due to the polarity and hydrogen bonding ability of the new solvent mixture.[21] Because aqueous formulations are the most common within the personal care industry, most ingredients are not intended for a non-aqueous environment. Solubility, and hence stability, in alternative solvents may result in unexpected changes to the physical properties of the resulting formulation, e.g. rheological profile. Thus, fundamental work is required to characterise mixtures related to non-aqueous toothpaste formulation.

This body of work has been undertaken to better characterise the effect of non-aqueous and mixed-aqueous solvents, predominantly containing glycerol and water, on commonly used surfactants and polymers. Thus their phase behaviour can be determined, along with any key processing parameters that may result from variations in micro- and macroscale behaviour. The enhanced understanding should inform toothpaste formulation and processing, taking advantage of specific effects only possible within narrow formulation ranges. This fundamental understanding can be applied to more complex application scenarios in the future.

1.2. Solvation and Solubility

1.2.1. Solubility

When a compound is in solution, it forms into single molecules or clusters[22,23] surrounded by solvent molecules. What determines whether an homogeneous solution forms, as opposed to two liquids or a solid in a liquid, is whether the process of mixing is thermodynamically favourable i.e. there is negative Gibbs free energy on mixing, ΔG_{mix} (in the context of the Gibbs equation, $\Delta G = \Delta H - T\Delta S$).[24] This is dependent on physical properties such as pressure and temperature along with chemical properties such as concentration and solvent, all affecting the chemical potential (partial molar Gibbs quantity) of the constituents in the mixture.[25] While toothpastes can contain a high degree of particulate material for abrasion, the active ingredients, rheology modifiers, and surfactants and fragrance oils all typically exist in a molecularly dissolved state,[26] and are therefore affected by solvent and cosolvent.

There are numerous methods that have been constructed to rationalise and predict solubility behaviour for different solvents and solutes.[27] One established way is to use solubility parameters. These are often empirically derived and relate to bonding and polarity. The Hildebrand solubility parameter (δ) is one of the earliest attempts which utilise cohesive energy density (CED).[28] This is the amount of energy to move all molecules to infinite separation,[29,30] and equates to the total (molar) interaction energy between the molecules. It can be obtained through measurement of heat of vaporisation (H_{vap}, Equation 1.1).

$$\delta = CED^{\frac{1}{2}} = \sqrt{\frac{\Delta H_{vap} - RT}{n}} \qquad \text{eq. 1.1}$$

Where R is the gas constant, T is the absolute temperature and n is the number of moles. This method is simple, but it does not account for non-ideal solutions, nor the contribution of hydrogen bonding, limiting its efficacy in aqueous or alcoholic environments. The Hansen solubility parameter was developed to consider hydrogen bonding.[31] Empirically based; it attempts to describe solubility using three parameters. These are dispersion (D) forces, dipole forces (P), and hydrogen bonding (H). The values correspond to their contribution to total cohesion energy divided by the molecules molar volume and give a 3-point coordinate space. The distance can be compared against with another molecule to predict solubility. To calculate distance (R_a), the terms combine (Equation 1.2), where the '4' coefficient was determined from empirical findings to account for the relative contribution to solubility.[21]

$$(R_a)^2 = 4(\delta_{D2} - \delta_{D1})^2 + (\delta_{P2} - \delta_{P1})^2 + (\delta_{H2} - \delta_{H1})^2 \qquad \text{eq. 1.2}$$

Where δ_x corresponds to the partial solubility parameter of a certain type (x) of interaction, and the species being mixed (i). The distance (R_a) can also be divided by an interaction radius: the 'sphere of solubility' s a value which describes the potential or solubility, called the relative energy difference (RED).

Hansen solubility parameters have been utilised in a range of applications beyond traditional solubility, from predicting polymer swelling,[32] to supramolecular gelation and cocrystal formation,[33,34] and have been further developed to incorporate other variables (e.g. temperature).[31] Using Hansen solubility parameters, a molecule can be predicted to be soluble (RED<1), partially soluble (RED=1), or insoluble (RED>1), for a wide range of components. However, it cannot account for specific donor-acceptor interactions such as H-bonding or 3D structures. Most importantly, mixed solvents are treated as volume averages.[25] This is problematic for biological matter and other systems, where conformational change of molecules or preferential localisation of solvent can occur.[35–37] Venkatram found that for a

set of 75 polymers, both Hildebrand and Hansen parameters correctly predicted solvents (or non-solvents) in 60-76% of the cases, with Hansen parameters having slightly greater accuracy.[38] Whilst solubility parameters have limited predictive power, other methods, including the quantum based COSMO-RS[39] can achieve high accuracy through more extensive computing, although this is also limited in some systems.[40]

Kirkwood Buff (KB) statistical mechanical theory[41] describes solubility as whether a solute molecule prefers to be localised about like molecules (i.e. insoluble), solvent molecules (i.e. soluble) or a particular solvent in binary solvent mixtures. It does this by defining (Kirkwood-Buff) integrals (G_{12} for a two-component system containing species 1 and 2) which describe an excess or a deficiency of the number of molecules of one type surrounding another.

$$G_{12} = \int_0^\infty [g_{12}(R) - 1] 4\pi R^2 dR \qquad \text{eq. 1.3}$$

Where R is the distance from the centre of mass. $g_{12}(R)$ is the pair-average correlation function at a distance R (also known as the radial distribution function). Although originally it was designed to predict thermodynamic quantities, and measurement $g_{12}(R)$ is experimentally possible, prediction of KB integrals is difficult. Molecular simulations to solve this problem are limited as it is not possible to model an infinite system which the theory requires, although improvements in modified finite solutions have been made.[42] In 1978 Ben-Naim showed that 'inverse KB' is a valuable tool[40] because measurement of thermodynamic parameters could be used to calculate interaction parameters and hence probe molecular packing. This is useful as it can be used to study the microstructure of solutions from experimental data. Notably, it has also been used to explain the enhanced structuring of carrageenan, a polymer often used in toothpaste,[43–45] when in mixed alcoholic-aqueous solvent. Shimizu was able to determine[45] that, through a change in the secondary structure of the polymer, preferential exclusion of solvent is determined, which leads to aggregation and changes in viscosity and gelation. There is no perfect solution for predicting solubility, but considering different approaches enables better prediction.

1.2.2. Non-aqueous Solvents and Glycerol

Water is highly polar and has a high degree of ionizability and hydrogen bonding, in contrast to non-aqueous solvents that are often less polar and typically have a lower hydrogen bonding ability. [31,46] This introduces a challenge in formulating in non-aqueous mixtures, as the change in solvent can affect the

solubility and behaviour of materials. For biocompatible solvents and carrier liquids used on a frequent basis, choice is generally restricted to oils, which may benefit delivery of apolar compounds,[47] or biocompatible polar solvents.[1,48] The benefit of using polar solvents is the lack of oily residue, and the ability to use similar (hydrophilic ingredients). Polar solvents can be categorised into two types: protic and aprotic. A common category of solvents used in personal care are polyalcohols, which are protic, whereas polar aprotic solvents are rarer. Many polar aprotic solvents, lacking the hydrogen bonding (donating) ability seen in water are toxic, meaning they are generally less relevant in the applications discussed in this work. Dimethyl sulfoxide, a cryopreservation agent and known therapeutic,[49,50] with a similar polarity to the polyol glycerol,[51] has come under scrutiny for its toxicity.[52,53] One of the few aprotic polar solvents used in personal care is low molecular weight poly(ethylene glycol).[54] Glycerol, propylene glycol, and sorbitol are common protic solvents or cosolvents that are used regularly in formulations.

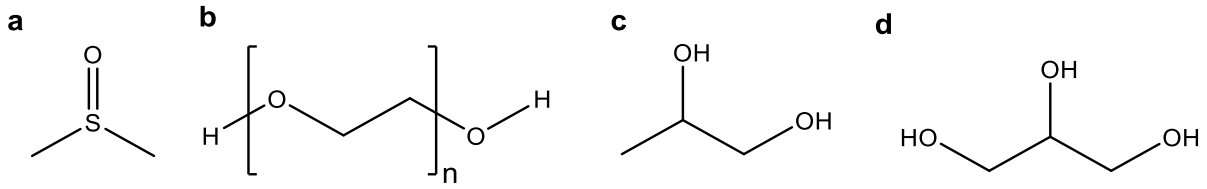

Figure 1.1: Common non-aqueous polar solvents that have been used in medicine or personal care. a) Dimethyl sulfoxide (aprotic) b) poly(ethylene glycol)l (aprotic) c) propylene glycol (protic) d) glycerol.

Glycerol is of particular interest as a widely used polar protic solvent which also acts as a humectant.[55] It is miscible with water at all temperatures and compositions, has three hydrogen bond donating sites (Figure 1.1) and has a dielectric constant ~60% of that of water,[56] illustrating its lower polarity. While water is ultimately the most cost effective and safe solvent, glycerol has many advantages over other organic solvents, including biocompatibility, humectancy, viscosity, and cost effectiveness all while being a 'green solvent' that can be sustainably derived as a biproduct.[48,55,57,58] Many toothpastes already contain glycerol or sorbitol as minor cosolvents to act as humectants.[59] This does not mean solubility is assured and moving from a binary glycerol-aqueous system to glycerol can incur changes in formulation solubility and stability. An important example is the considerable reduction in micellar solubility for sodium dodecyl sulfate surfactant.[60]

1.3. Crystallization

1.3.1. Nucleation and Growth

A phase change from liquid to 3D ordered solid assemblies for a liquid or gas is the process of crystallization, which occurs in two stages.[61] Firstly, nucleation occurs, which is the initial formation of organised assemblies, followed by a growth stage which consists of addition to the nuclei to form larger assemblies.[62] The maximum amount of solute that a solvent can dissolve is called the saturation limit and solutions above this are supersaturated. A transition from a higher to lower temperature without agitation or disturbance causes the solubility to drop and a mixture can become supersaturated, which can lead to an unstable, or metastable state.[63–65] If it is the former, crystals can nucleate without external interference, and if the latter, the solution can remain stable indefinitely without crystals forming, but will crystallize if nucleation occurs. There often exists a metastable zone that is accessible beyond a certain temperature/concentration range.[66,67] Nucleation can be primary, where formation occurs without a prior crystal, or secondary where nucleation is directly attributed to crystals that are already present. Primary nucleation can also be heterogeneous, occurring on a foreign surface due to lower energy of organisation at the interface, or homogeneous i.e. occurs within the same phase (Figure 1.2).[68] A popular method for crystal growth is to use seed crystals to promote secondary nucleation and growth.[69]

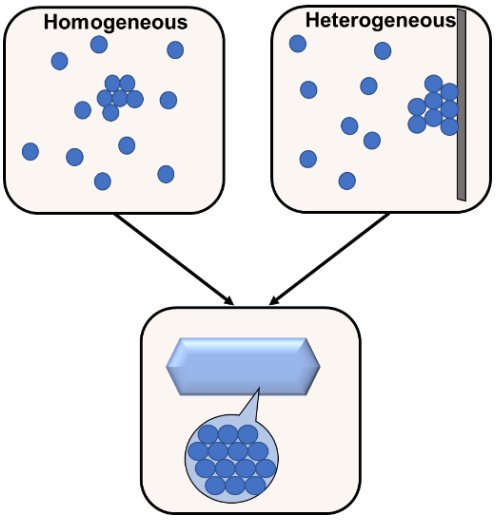

Figure 1.2: Modes of primary nucleation leading to crystallization. Heterogeneous nucleation occurs within one phase where clusters form within the liquid. Homogeneous nucleation forms with an additional interface e.g. at the surface of a solid.

Variation in crystal arrangement is called polymorphism, which can change the structure and properties of a crystal. This is evident in 'fat bloom' that occurs when chocolate is improperly stored.[70,71] The pathways to different crystal polymorphs are commonly described by Ostwald's rule of stages, which

states the fastest growing (kinetic product) forms in preference to the most stable form.[72] This means that polymorphic transformation can occur due to the negative Gibbs energy when transitioning to a more thermodynamically stable polymorph. However, this the rule is not infallible and has exceptions.[73–75] Crystals can also be 'hydrates' or solvates' when they contain either water or solvent molecules crystallized within the structure.[71] Interconversion may also occur as well during crystallization, further complicating matters. Solvate crystals contain a molecule and a solvent molecule both in the ordered structure. They exhibit more order when compared to an anhydrous crystal with all solvent in the bulk, as two or more species must present in an ordered structure,[76] and therefore their formation is driven by enthalpy. This arises from solvent-molecule interactions, and hydrates are common due to the ability of water to form noncovalent bonds such as hydrogen bonding, with ionic or polar species.[77,78] The complexity of crystallization processes means that prediction or isolation of one type of crystal may be difficult, but not impossible. Other methods can be used to purify specific crystal types, such as antisolvent addition, or solvent evaporation, as in the case of 1/8th hydrate SDS formation.[79,80] Nevertheless, the degree of undercooling and concentration of solute can have a large impact on phase formation. When competing solid-liquid equilibrium profile of different crystal types are overlayed, regions of accessible crystal type can be visualised.[74] An example is shown in Figure 1.3, where two different solutions at different concentrations are cooled to different temperatures. In scenario B, a higher degree of undercooling leads to hydrate formation which is not the thermodynamic product at this point. In contrast, scenario A produces the anhydrate, which is the thermodynamic product.

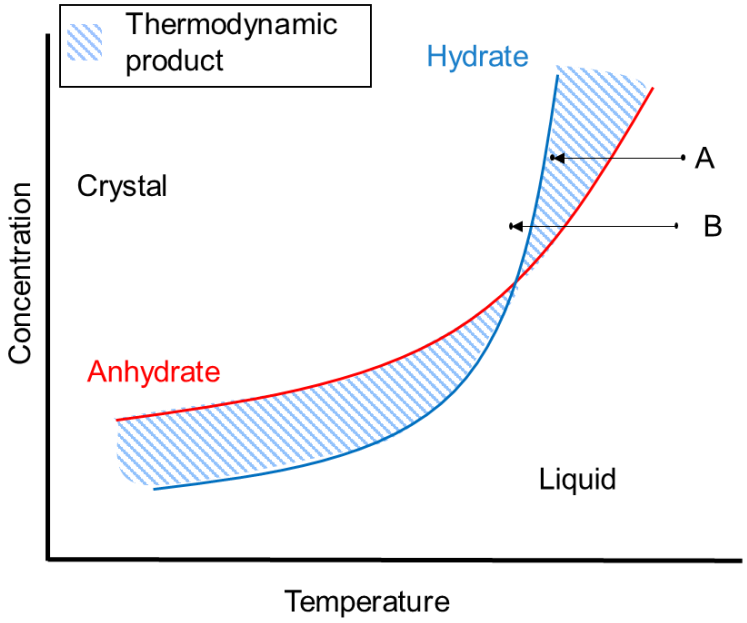

Figure 1.3: Phase diagram showing theoretically accessible hydrate or anhydrous (anhydrate) states of a crystal when it is isothermally cooled. Depending on the degree of undercooling, either a kinetic or thermodynamic (shaded) crystal is accessible, which can vary depending on solvent concentration. Two scenarios are presented at different concentrations and undercooling rates where A) a lower degree of undercooling leads to a thermodynamic product of an anhydrate crystal or B) a higher degree of undercooling leads to competition between kinetic and thermodynamic product of a hydrate crystal. Figure adapted from Tian et al.[74]

When forming crystals, the cooling regime can either be isothermal or non-isothermal. Isothermal cooling allows for a uniform degree of supersaturation and chemical potential but is limited by heat transfer as the cooling rate must be fast and hence may can be problematic in large scale batch production. The isothermal kinetics of crystallization have been modelled using the semi-empirical Johnson-Mehl-Avrami-Kolmogorov (Avrami) equation for many years (Equation 1.4).[81] and although other methods are available, but they are less popular. It is possible to model crystal evolution over time, thus gain information regarding dimensionality and spontaneity of nucleation. This method is used regularly in fat crystallization,[81–83] where it is sometimes modified to include a lag time parameter.

$$X(t) = 1 - e^{-kt^n} \qquad \text{eq. 1.4}$$

Where $X(t)$ is the volume fraction of crystallized species, t is time, t_{init} is the lag time, n is the Avrami exponent, and k is the overall crystallization rate constant. The Avrami exponent informs whether growth is in 1 (rod shape), 2 (plate shape) or 3 (spherical shape) dimensions and whether nucleation is spontaneous or sporadic.[84] The Avrami equation (or Ozawa equation for non-isothermal growth[85]) is subject to assumptions and limitations,[83,86,87]and is an oversimplification of the process. Moreover,

results can yield non-integer exponents e.g. from intermediate sporadicity or secondary processes.[88] Nevertheless, its simplicity and comparative ability can still yield useful information.[89,90]

1.3.2. Crystal Morphology

While the unit cell of a crystal is determined by its symmetry and arrangement of atoms in the lattice, the crystal habit is determined by the growth rate of each crystal face relative to each other. Factors that can affect habit include impurities/additives,[91] solvent,[92] and temperature. An additive can affect habit formation in different ways and can be either a small molecule or polymer.[62] A solvent can also form noncovalent interactions with a growing crystal face, affecting its growth.[93] SDS primarily forms platelets or needles depending on degree of hydration and cooling parameters.[94] Many other shapes exist: dendritic and feather like structures are also common,[95,96] and are facilitated through thermal and chemical gradients. High aspect ratio fibres/rod crystals can be twisted either as a result of molecular chirality,[97] or microstructural stress on the structure during crystallization.[97]

1.4. Surfactants

1.4.1. Structure and Micelle Formation

Amphiphilicity is the phenomenon of distinct regions of polarity and apolarity in a single molecule and is what defines a surfactant. Surfactant are used heavily in cleaning, where they can solubilise unwanted material through adsorption and micelle formation, as well as being a key stabilising agent for foams.[79] Most products within the beauty and personal care market are aqueous (but can be oil based), therefore the majority of surfactants are designed to work in water, and any change in solvent can drastically alter their performance and properties. This is true for toothpaste, where surfactants act as foaming agents, promote wetting, and aid oil solubility.[1] For toothpastes, ionic surfactants predominate, but non-ionic surfactants such as lauryl glucoside are used as well.[98] The most common small molecule ionic surfactants used in toothpaste consist of a charged head group with accompanying counterion, and a nonpolar tail (Figure 1.4) made of an alkyl or amido-alkyl chain.[98] The headgroup charge may be negative (anionic), positive (cationic) or mixed (zwitterionic). Non-ionic surfactants can be small molecule (e.g. lauryl glucoside) or polymeric, e.g. block copolymers with distinct regions of monomer repeat units of differing polarity found along a chain. An example of this is Poloxamer 407/Pluronic F127,[99] a triblock copolymer consisting of a poly(propylene oxide) block sandwiched

between two polyethylene oxide blocks, which can be formulated into toothpaste.[100] Due to their small size, and charge, small molecule surfactants can be more mobile and in some cases foam better.[101]

Due to the relevance to personal care and toothpaste, this work will focus on small molecule ionic surfactants, namely sodium dodecyl sulfate (Figure 1.4), which has a sulfate head group, and a 12-carbon alkyl chain tail. Surfactants are known to form various different micelle structures depending on their concentration, including liquid crystal structures at higher concentrations.[102] In toothpaste, surfactants are formulated above the CMC, and exist as micelles; they present below 5 Wt.% in typical formulations.[6] The number of molecules within each micelle is described by aggregation number (n_{agg}), and can vary from less than 10, to more than 100, which can be greatly impacted by solvent choice.[103,104] Surfactants in a micellar solution are in dynamic equilibrium with the bulk solvent and the air-water interface, as micelles are not ordered structures like crystals. The minimum concentration for micelle formation is the critical micelle concentration (CMC),which varies depending on temperature, solvent, and mixture composition.[105–107]

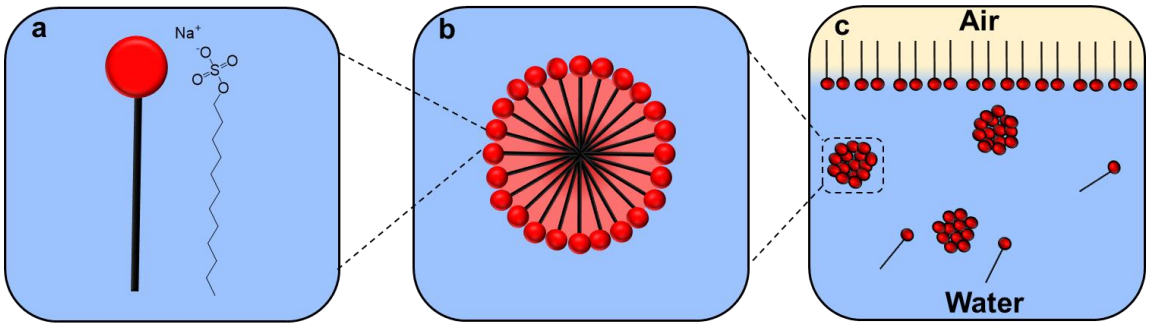

Figure 1.4: a) Generalised structure of a small molecule ionic surfactant with polar head and nonpolar tail, in comparison to sodium dodecyl sulfate. b) Generalised arrangement of surfactants within a micelle. C) Micellar solution where surfactant molecules either align at the interface, form micelles, or are numerically dissolved.

1.4.2. Thermodynamic Rationalisation of Surfactant Behaviour

For non-polar compounds, miscibility is thermodynamically unfavourable in highly polar solvents such as water. This is because of the increase in entropy that occurs when polar compounds form ordered structures at the interface to accommodate the non-polar component. The ordered structuring of polar compounds, typically water, is known as the hydrophobic effect.[108,109] As a result of the hydrophobic effect, ΔG_{mix} is positive, meaning that it cannot occur without input of energy, and will not occur spontaneously. This results in compounds with different polarities undergoing phase separation. However, but because of their composition, the monomeric dissolution of surfactants is

thermodynamically mostly unfavourable due to the hydrophobic effect. To satisfy both polar and non-polar groups, surfactants often organise into micelles which maximise positive interactions with the solvent, while minimising exposure of non-polar tails to the solvent which leads to the hydrophobic effect.[110] This leads to an assembly into a shape with a core comprised of non-polar groups and a shell comprised of polar groups. Hence, micelles represent a higher degree of order compared to randomly dispersed molecules, but the hydrophobic effect means micelles have a lower entropy than monomeric surfactants (Figure 1.5). Micellization is therefore an entropy driven process which causes a drop in ΔG_{mic} resulting in spontaneous formation in the right conditions. This is not true for all scenarios and is both concentration and temperature dependent.

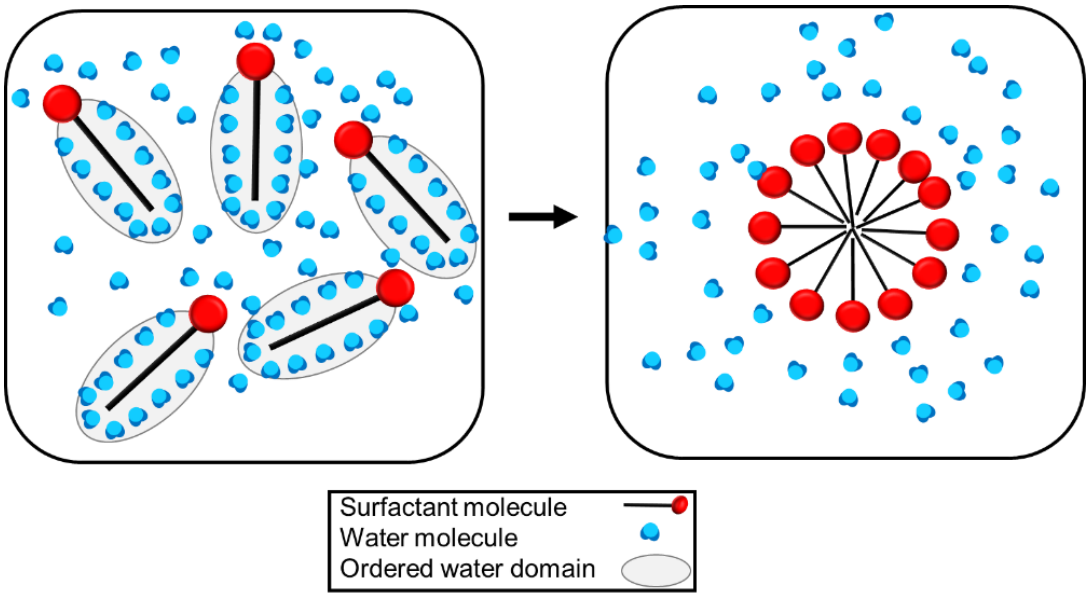

Figure 1.5: Visualisation of the change in water structure upon micellization. For unimeric solutions, the hydrophobic effect causes ordered water domains around the nonpolar tail. The hydrophobic effect is minimised for micelles. This has the result of increasing the overall entropy under certain conditions making Gibbs energy negative and the transition spontaneous.

The critical micelle concentration (CMC) is the minimum concentration at which micelles form, while below this, monomeric solubility dominates. Due to the polarity gradient at the air-water interface, surfactant molecules readily align (Figure 1.4C) in equilibrium with the bulk. It is only when the interface becomes saturated, that micellization occurs. Measurement of surface tension can therefore be used for CMC determination, as the surfactant population is proportional to the surface tension.[111] Measurement of solution conductivity or dye fluorescence are two other techniques that can be used to probe the CMC.[112,113] The CMC is strongly dependent on temperature, although behaviour differs for ionic, zwitterionic and non-ionic surfactants.[79] CMC and temperature does not scale linearly and

parabolic type trends are seen for ionic surfactants like SDS,[114,115] although not always.[116] The trend is likely due to competing interactions, where the solubility of surfactant chain increases (disfavouring micellization), while the degree of head group hydration reduces.[79] There is general reduction in radii and aggregate at higher temperature.[117,118]

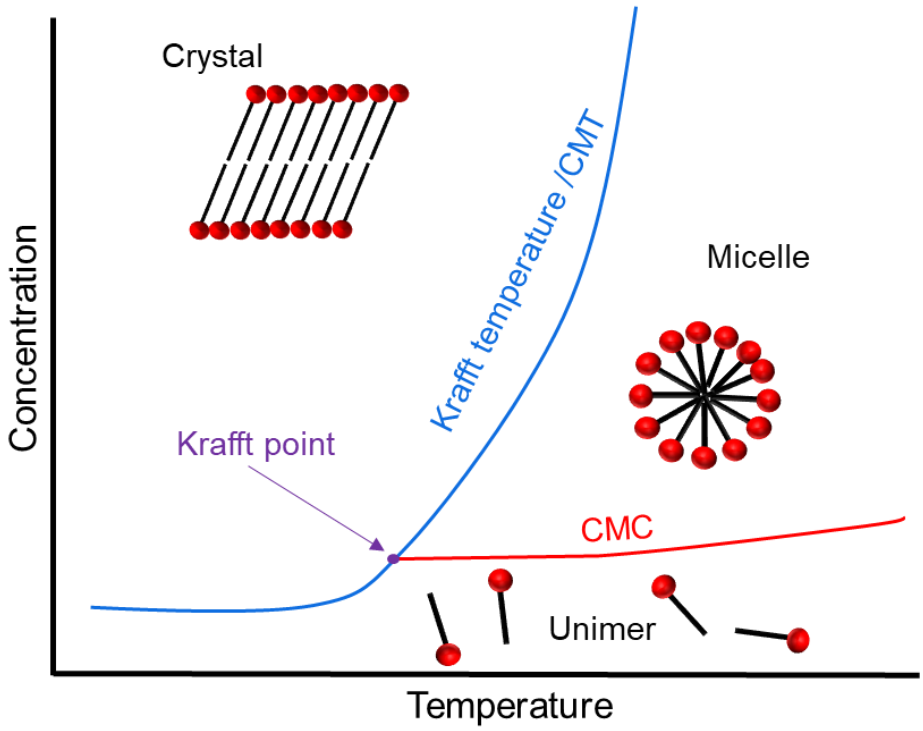

Figure 1.6: Generalised phase diagram of an ionic surfactant. At low concentration non-aggregated unimers are present in solution. As concentration increases, the surfactant will either form a crystalline or micellar phase, depending on whether the temperature is below or above the Krafft temperature.

The lowest temperature and concentration at which a micelle can form is called the Krafft Point.[119] The lowest temperature (concentration above the Krafft Point) at which a micelle can form is called the Krafft temperature, or critical micelle temperature (CMT). Below this boundary, only unimer solubility occurs (Figure 1.6). Moving from a higher temperature to below this value can cause liquid-liquid separation or crystallization.[120] Krafft temperature can be determined by DSC,[121] conductivity,[120] or other methods.

1.4.3. Micelle Shape

Micelles are often visualised as spherical objects, but this is just one possible shape. Worm/cylinder geometries,[122–124] vesicle bilayers,[125,126] reverse micelles,[127–129] (Figure 1.7), can all form from surfactants depending on the molecular structure. The critical packing parameter (CPP) is most commonly used to draw the relationship between structure and accessible shape (Figure 1.7).[130] The CPP is defined as the volume of the surfactant divided by the product of the tail length and cross sectional area. For small molecule ionic surfactants like SDS, a low CPP is observed due to the relatively large size of the ionic head group compared to the tail, yielding spherical micelles.[131–133] However, this can be altered to worm-like micelles when NaCl is added,[134,135] which has the effect of reducing the ionic radii through charge screening, thus increasing the CPP. For polymeric surfactants, stimuli responsiveness can be achieved through careful selection of monomer and block length, adding functionality.[136] CPP is one of the most common methods for rationalising surfactant self-assembly, but is not fully representative for all systems.[137,138]

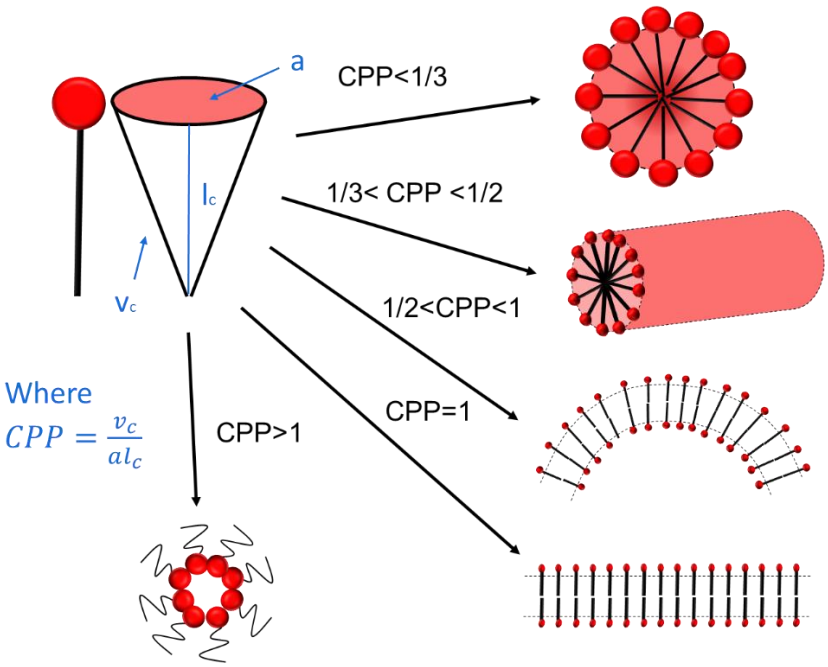

Figure 1.7: Critical packing parameter (CCP) equation and relationship to different surfactant structures. CPP is calculated from the volume of a surfactant 'cone' (v_c) divided by the product of the head group surface area (a) and surfactant length (l_c) . When CPP < 1/3 spherical micelles form. From ⅓ to ½ cylindrical, rod or wormlike micelles are formed. From ½ to 1 curved bilayers or vesicles are obtained. At 1, the 'cone' exists as a cylinder and planar bilayers are formed. Above this, reverse micelles form.

Moreover, in contrast to CPP prediction, some scattering (x-ray and neutron) experiments indicate that micelles are ellipsoids rather than spheres e.g. for SDS.[118,139–141] There have been attempts to rationalise such observations and also identify what type of ellipsoid (prolate vs oblate) is formed, suggesting that

while ambiguity for some mixtures remain, addition of solutes such as salt can have a real effect on ellipsoid formation.[142] Oliver et al. showed the effect of the surfactant structure on ellipsoid aspect ratio, with different length tail groups affecting the size but not aspect ratio.[143] While some disagree with idea of ellipsoid micelle shapes entirely,[144] It has been reported that ellipsoid formation is thermodynamically feasible, adding support for their existence.[145]

1.4.4. Impact of Solvent Composition on Surfactant Behaviour

The addition of less polar alcohols with lower CED and H-bonding ability than solely aqueous mixtures, will reduce the hydrophilicity of the solvent mixture. An example of this is the reduction of the dielectric constant for glycerol-water mixtures as the glycerol content is increased.[56,146,147]. For solutions of ionic micelles, this can cause a reduction in micellar solubility, increasing the Krafft temperature and CMC.[113,148,149] There are two reasons for this: the increase in electrostatic repulsion between surfactant headgroups lowers enthalpy of micellization, and increase in solubility of tail groups upon non-aqueous solvent addition, leading to a reduction in the entropy drop.[150–152] This can also be a non-linear trend, and different solvents can change the CMC values by varying amounts.[153] Rodriguez et al., showed a general negative trend between Gordon parameter of solvent (CED) and the Gibbs free energy of micellization, indicating the reduced favourability of formation in less polar media.[154]

The behaviour of SDS in glycerol/water mixtures has been explored by numerous authors,[60,113,155,156] notably with work by Khan et al.[60] exploring the phase boundary of SDS/glycerol/water mixtures with and without NaCl. The addition of glycerol dramatically reduces the micellar solubility, increasing the Krafft point temperature from 14 °C to 31 °C, and the CMC from 0.17 Wt.% to 1.0 Wt.%. Thus the room temperature solubility is limited, and most SDS would be expected to be in solid (crystalline form) in pure glycerol. Similar large increases in the CMC of SDS have also been achieved with a range of other protic and aprotic solvents.[103,153-159] Initial reductions in CMC can be observed at low cosolvent concentrations, especially if the molecule is surface active, causing competition with the surfactant at the interface.[160] Non-ionic surfactants do not experience a change in ionic repulsion on addition of polar solvent addition. Despite this, using mixed aqueous solvents lead to a similar, sometimes even more dramatic increase in CMC.[146] This can be at least in part attributed to an increase in monomer solubility.[161]

The effect of stronger electrostatic interactions caused by (co)solvent addition can affect the micelle structure.[162] This can be advantageous: micelle shape can be tuned for the most appropriate physical properties, for example wormlike micelles[163] effect the rheological behaviour of a formulation. This choice can produce drastically different effects, depending on the solvency with respect to both head groups and tails. Generally, addition of an alcoholic cosolvent (or solvent) to ionic surfactants, lead to smaller, more spherical micelles[164] due to the greater headgroup repulsion. Comparatively, for non-ionic ethylene oxide-propylene oxide copolymer surfactants, a decrease, small change or increase in micelle size cab be observed depending on solvent.[165] Without a change in ionic repulsion, micelle size is dictated by solvation and partition of solvent molecules into the micelle core or corona.

1.4.5. Effect of Electrolyte on Surfactant Behaviour

Inorganic salts have large effects on both micelle formation and structure by ionic surfactants owing to charge screening at the head group, which reduces the ionic radii and hence altering the packing parameter.[166] A well-known method for increasing viscosity in personal care formulations is the addition of NaCl to surfactants such as sodium lauryl ether sulfates to form wormlike micelles.[166] The CMC is also lowered due to the lower repulsive interactions between the headgroups, making micellization more favourable. Corrin and Harkins reported a double-log dependence for the relationship between salt concentration and CMC.[167] They interpreted this in terms of the number of ions adsorbed in the Stern layer, or the first layer found at a charged surface (micelle surface). However, prediction using the Corrin-Harkins equation is reportedly limited for mixed solvents.[168] Addition of small quantities of NaCl has a moderate effect on the Krafft temperature in the case of SDS/glycerol/water ternary mixtures[60] but the effect of NaCl in a sodium salt surfactant system is not necessarily representative of other salt mixtures. The Hofmeister series describes a series of ions that are chaotropic, which disrupt solvent networks, and kosmotropic, that enhance solvent structure.[169] It was originally found that proteins could be more soluble (salting in), or less soluble (salting out) depending on the solvent.[169] This effect is not limited to proteins: it also applies to non-ionic and ionic surfactants.[170] For cationic cetylpyridinium chloride aqueous mixtures, chaotropic ions raise the Krafft temperature Whereas the inverse is observed for kosmotropic ions. This is due to the formation of ion pairs with surfactant and chaotropic ions, causing salting out.[171] While less chaotropic ions increase micellar solubility through the previously mentioned mechanisms, although this does not strictly follow the Hofmeister series.[171] Similar trends were also seen in aqueous mixtures of SDS,[172] and such behaviour is applicable in non-aqueous solvents as well.[170]

1.4.6. Effect of Additives on Surfactant Behaviour

Impurities or other additives can change the shape and formation of micelles. Polar additives or compounds will predominantly reside in the bulk for aqueous (or polar solvent) mixtures, whereas if a hydrophobic compound is present, it will tend to reside in the core of the micelle. Many small molecule polar additives act as co-solvents, affecting micelle formation in a similar manner.[168] One exception is any acidic/basic additives, which can change the pH of a system. For SDS, the CMC is stable above pH 5, with a lower CMC observed below pH 5 attributed to protons reducing the surface charge density of the anionic micelle.[173] Furthermore, if additives are pH sensitive, their hydrophilicity and interaction with a micelle, as well as locality about the core/shell can change when the pH is adjusted. This can manifest in micelle shape changes, as evidenced by Patel et al. for cetyltrimethylammonium bromide with pH-sensitive aromatic compounds, where different transitions from worms to ellipsoids or vesicles can occur when the pH is switched.[174] Finally, surfactants can be designed to be stimuli responsive, (particularly block copolymers), with shape change occurring on pH adjustment.[175]

The polarity of an additive will affect its distribution within a micellar system. Primary alcohols are interesting compounds to probe this, as polarity varies depending on the alkyl chain length.[174] Many authors consider short to medium chain alcohols (C4-C10) to be co-surfactants, due to their ability to align at interfaces.[176–180] The inclusion of such alcohols can affect curvature and packing, demonstrated by emulsion stability.[181] Longer chained alcohols such as 1-dodecanol can align as well,[182,183] giving rise for potential to affect micellar shape and formation as it is a synthetic precursor of SDS, and therefore a common impurity.[184]

For aqueous SDS mixtures, Førland et al. found that medium chain C5-C6 (propanol, hexanol) alcohols primarily lie in the micelle as a cosurfactant, causing elongation of the micelle from spheres to rods as determined using SANS.[185] In comparison, C4 (butanol) acted like a water soluble smaller chain alcohol (e.g. methanol): it reduced micelle size initially, before causing an increase in size. Putra and Patriati evaluated C2-C10 (ethanol to 1-decanol) in aqueous SDS solutions.[133] Upon addition of C2-C5 alcohols both micelle size and aspect ratio decreased, producing smaller, more spherical micelles, acting as an alcoholic cosolvent. This effect is reduced as the chain length is increased and hexanol appeared to be the minimum chain length to induce cosurfactant-like behaviour, with elongation of the micelle and increase in size. Simulations of similar mixtures from C6-C12 suggest transitions to cylinder and bilayer structures at high alcohol contents, facilitated by the migration of alcohol into the core from the palisade,[186] with NMR data by Totland and Blokus support the previous findings.[187] Depending on whether a molecule acts as a cosolvent or cosurfactant, an increase or decrease in the CMC is observed which is evidenced in SDS solutions.[188] The effect of added alcohols is also applicable for other ionic

surfactants, e.g. CTAB forms ellipsoidal micelles with addition of C6 alcohol.[189] Moreover this effect is also seen for non-ionic surfactants.[190]

1.4.7. Surfactant Crystallization

Surfactant solubility is different than other small molecules owing to micelle formation. The CMC, Krafft temperature, and Krafft point define additional phase boundaries. Below the Krafft temperature, the surfactant is only soluble as unimers, meaning that the majority of surfactant is not soluble. Ionic surfactants, containing crystallizable alkyl tails, and two regions with distinct polarities, tend to crystallize into lamellar structures (Figure 1.8), with regions of polarity and apolarity. Ionic surfactants share similarities to fats due to the alkyl tail, although fats typically experience more polymorphism.[82,83,191] Ionic surfactants readily form hydrates,[192–195] as they can intercalate between surfactant head groups.[196] The stoichiometry of hydrates can alter molecular packing constraints substantially, with the tilt of the molecules ranging from 5 to 45 ° against the layer normal (Figure 1.8) for SDS hydrates.[196–198] Solutions of hydrated crystals can form gelled mixtures called coagels.[199]

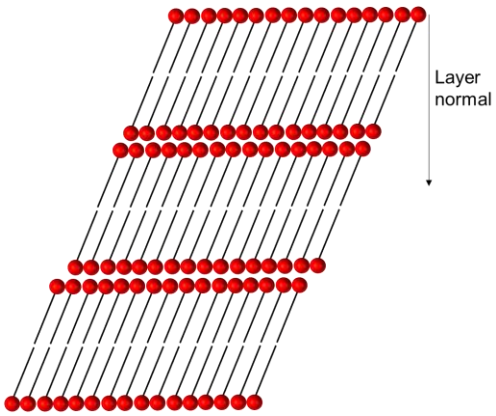

Figure 1.8: Lamellar structure of a surfactant crystal, consisting of an 'infinite' number of bilayers arranged to maximise like-like interactions between polar and apolar regions of the molecule. Surfactant is shown with tilt in the primary axis against the layer normal. This tilt can extend to another dimension aside from the primary axis (Layer normal) when in 3D space.

In recent years, the crystallization of SDS has gained renewed interest. General unit cell data of certain hydrates of SDS and its alkyl chain homologues were reported in the 1950's.[200] Coiro et al. subsequently determined various dodecyl crystals and hydrates.[196,197] A precise structure of anhydrous SDS was published by Smith in 2000,[198] with subsequent work identifying crystal morphology along with crystallization with different counterions.[201,202] Miller et al.[203] showed different hydrate crystals were

accessible via different linear and isothermal cooling regimes in aqueous solution.[204] Furthermore, Summerton et al., showed that cocrystallization was possible with 1-dodecanol, significantly raising the melting point of the SDS crystals for aqueous systems.[184] In contrast, addition of n,n-dimethyldodecylamine *n*-oxide was shown to reduce crystallization temperatures, without cocrystallization.[205]

1.5. Polymers

1.5.1. Polymer Solutions

Polymers are long chained molecules comprised of repeating units called monomers. They are widely used for their viscosifying properties owing to chain entanglement and potential for cross-linking to form a gel. Monomers can be one type, forming a homopolymer, or two or more types, forming a copolymer. The former is used primarily for viscosity modification, while the latter can add functionality and surface activity, although copolymers are also used for structuring toothpaste.[26] The choice of monomer can affect solubility and rigidity, while the degree of polymerisation/molecular weight can affect solubility. For toothpastes, polymers are generally formulated in the semi-dilute regime, and generally exist as either bioderived sugar based biopolymers e.g. xanthan gum, or synthetic polymers such as poly(vinyl alcohol), poly(ethylene glycol) or copolymers.[1,26,98] The high functionality in the form of acid, alcohol, or charged groups both ensures solubility in aqueous mixtures and potential for crosslinking. Adsorption to particulate solids including silicas used in toothpaste, is also possible, potentially stabilising dispersions.[26]

Small molecules can be soluble, insoluble, or lie in a metastable region, but polymer solution behaviour is more complicated. ΔG_{mix} must be negative to ensure spontaneous mixing or dissolution. While a small molecule may be 'soluble' or 'not soluble', polymers conformation in space will change, to maximise or minimise interactions depending on the solvent. This is referred to as 'quality', where solvents are classed as non-solvent, poor solvent, theta solvent or good solvent. If a polymer is dissolved, increasing 'goodness' of a solvent generally causes a transition from a globule to an expanded coil. If the solvent quality is higher, the solvent is a theta solvent,[26,206] the excess chemical potential is zero, meaning that the polymer does not seek to avoid or increase its interactions with other polymer chains. It also conforms to random-walk type behaviour, which is referred to as a Gaussian chain.[207] If the solvent quality is higher, it is a good solvent where the polymer expands to maximise solvent interactions. Quantifying the size of polymers is commonly done using the radius of gyration (R_g) which is the root-mean-square averaged distance of monomer repeat units from the centre of mass.

Polymer solutions exist in three broad concentration regimes relative to the critical overlap concentration (C*) of the chains. At low concentrations, a polymer rarely interacts with other polymer chains in solution. When the concentration reaches c*, the polymer is in the semi-dilute regime. Above this, overlap occurs between neighbouring chains, which become indistinguishable in the concentrated regime.[207] In the case of polyelectrolytes, electrostatic interactions complicate matters, and semi-dilute entangled and semi-dilute unentangled regimes become more apparent than for uncharged polymers.[208,209] The semidilute unentangled regime (C=C*) describes when the hydrodynamic interaction is screened by the neighbouring chains, without the chain physically overlapping (Figure 1.9).[210] Higher concentrations correspond to the critical entanglement concentration (C_e), which is where chains overlap. This is the semidilute entangled regime. The specific viscosity of a polymer solution scales as a power law, with a change of gradient at each boundary, with the viscosity behaviour described by a different model for each region.[210]

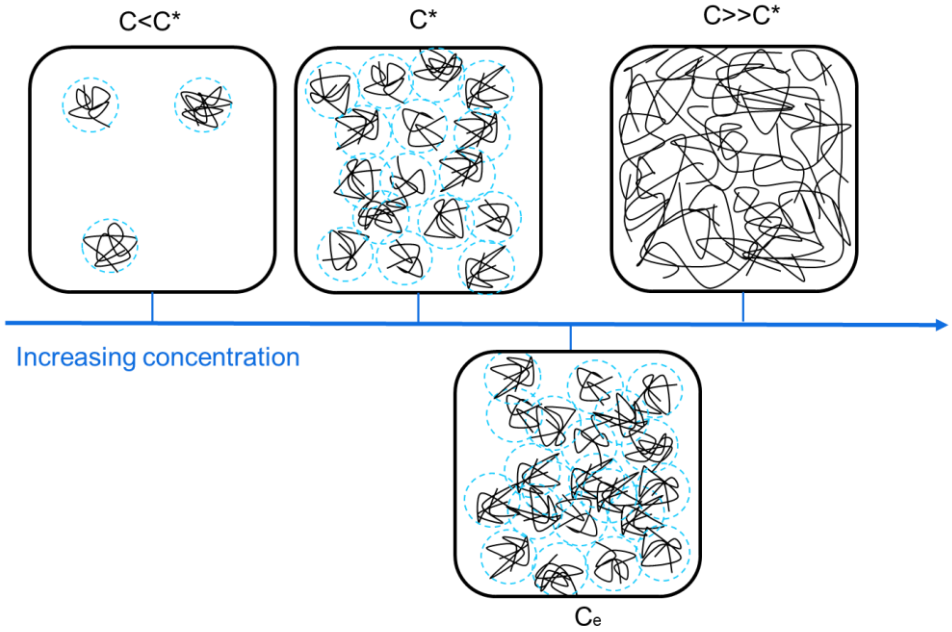

Figure 1.9: Visualisation of concentration regimes for polymer solutions, relative to the critical entanglement concentration. Dilute solutions show polymer coils in solution with little influence from neighbouring polymers (C<C). Semi-dilute solutions occur at the critical entanglement concentration (C*), marking the start of chain overlap and the boundary of a defined excluded volume (C=C*). Concentrated regimes show entanglement between chains. (C>C*). For polyelectrolytes in particular, semidilute unentangled regimes (C=C*) occur when hydrodynamic interactions are screened by the neighbours, whereas the semidilute entangled regime occurs at the boundary of chain entanglement (C=C_e) at the critical entanglement concentration (C_e).*

Solubility parameters are used regularly for polymer solutions, and the original Hansen solubility parameter thesis focused heavily on polymer solubility.[31] Similar restrictions to small molecule solubility apply as well. As solvent quality effects chain conformation, scaling and concentration regimes differ.[207]

Moreover, the response to changing solvent is not uniform, as mixed solvents can have unique structuring effects for biopolymer systems.[44] Solvent type therefore has an impact on structuring and entanglement, which must be considered when selecting a solvent system for a given formulation.

1.5.2. Biopolymers and Hydrocolloids

Polysaccharide biopolymers used in toothpaste occupy a category called 'hydrocolloids': they are water-soluble but can thicken and gel aqueous solutions. This can be achieved through either thermal transitions or addition of chemical crosslinkers. They can be obtained from plants, such as carrageenan from seaweed and cellulose from plant-based pulp, or from bacteria in some cases.[210–212] Although all such biopolymers all contain a sugar backbone, their ability to modify rheology and form gels depending on their structure (Figure 1.10).[213,214] A wide range of polysaccharides form interacting helices, which can be thermally or chemically induced, to either form gels or thicken solutions.[215] Because of their ability to self-assemble, the effect of solvent can vary. Antoniou et al. showed that, for non-ionic Dextran T500, an increase in intrinsic viscosity occurred on switching from water to both protic and aprotic polar solvents.[215,216] This was associated with an increase in coil volume indicating that all non-aqueous solvents were better than water. However, explanations differed depending on the composition. Comparatively, xanthan gum, an ionic polysaccharide, precipitates in the presence of ethanol (>30%).[217] However, the addition of non-aqueous solvents does not entirely depend on ionic functionality: carrageenan can form a gel in mixed aqueous alcoholic/polyalcohol solvents,[44,218] but minimally interact in pure non-aqueous solvent. This is due to helix formation which leads to a network structure. Therefore, self-assembly, hydrophilicity and composition must all be considered when exploring cosolvent behaviour on aqueous solutions of biopolymers.

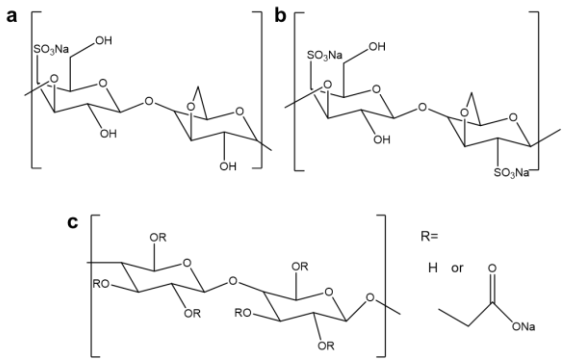

Figure 1.10: Molecular structure of some common thickening and gelling polysaccharides. a) Kappa-carrageenan, with a single sulfate group per disaccharide and a galactan (glactanopyranose) based backbone. b) Iota-carrageenan, with two sulfate groups per dimer. c) Sodium carboxymethyl cellulose, consisting of glucopyranose monomers with varying degree of substitution of carboxylic salt in place of alcohol.

1.6. Gels

1.6.1. Polymer Gels

Despite toothpaste comprising either a high solid content paste or a low solid content gel, polymers are used in a similar way for both types of formulations. Furthermore, the majority of gels used for toothpaste are hydrogels, (i.e. water is the solvent). The ability to arrest suspensions and mixtures is key for the comprehensive application and dispersion of material, particularly within the personal care and medical sector. Gels have an elastic component, or storage modulus (G'), greater than the liquid/viscous component, or loss modulus (G'') within the linear viscoelastic range. As a result, they do not flow until a force causes the structure to break (e.g. shear on application). Both synthetic and bioderived polymers can gel solutions, although modes of gelation vary according to their composition. However, all polymers must form a crosslinked matrix to form a gel (Figure 1.11). Crosslinking can be chemical i.e. comprising covalent bonds between different chains, or physical, i.e. dynamic non-covalent linkages originating from weaker forces such as ionic interactions or H-bonds.[219] Physical gels can even form following thermal transitions in an appropriate solvent, mediated by supramolecular assembly: e.g. helix formation in polysaccharides.[220] Microgels are a different class of gel[221] comprising crosslinked polymer particles that can swell and structure solutions.

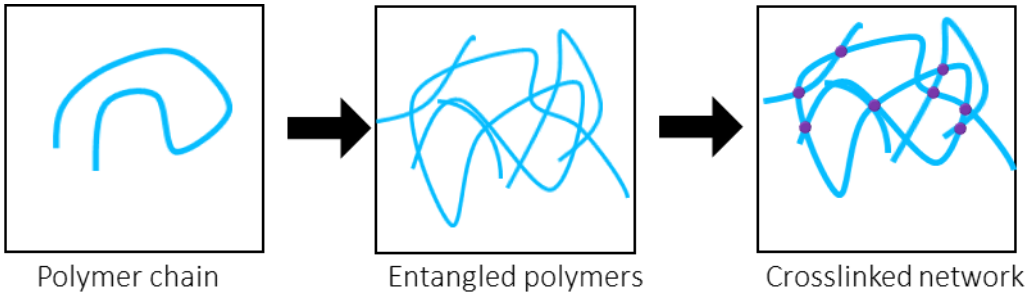

Figure 1.11: Schematic of polymer gelation through crosslinking of an entangled solution to form a network/matrix.

Polysaccharide based gels can provide different textures and rheology depending on their structure, but the gelation mechanisms are similar in principle. There are two mechanisms of gelation for gelling polysaccharides: addition of electrolytes to form ionic crosslinked gels, and thermally induced gelation which occurs due to a conformational change in the polymer to produce helixes. Alginate forms a gel through the eggbox model,[222,223] where polymers arrange to form antiparallel chains surrounding the ion (the 'egg') responsible for crosslinking, subsequently forming eggbox-like dimers which further aggregate. In contrast, ionic gelation of carrageenan occurs through aggregation and ionic crosslinking

of helices.[224] Different ions induce gelation in different polysaccharides. For example, kappa-carrageenan primarily gels in the presence of potassium ions,[225] although can form gels with calcium ions,[226] or be tuned by using mixtures of ions.[227] Iota-carrageenan, is used to form ionic gels and gellan gum, which is (carboxylic) acid functionalised, also forms gels with calcium ions.[228] Thermally induced gelation for polymers such as carrageenan, involves the formation of secondary helical structures and aggregation but does not require an ionic crosslinker.[229] Firstly, gels are heated to form dissolved coils, before cooling to generate an aggregate network. The structure of these helices can differ,[230] and there is some debate over regarding their precise conformations.[231]

1.6.2. Low Molecular Weight Gels and Supramolecular Assemblies

The benefits of low molecular weight gels (LMWGs) are numerous and exciting. A polymeric gel exists as a matrix of crosslinked chains, where the chains are formed of covalently linked monomers. In contrast LMWGs exist as single or multiple small molecules which form a gel through supramolecular self-assembly utilising non-covalent interactions.[232] This is often facilitated through directional interactions (e.g. H-bonding). Unlike a traditional polymeric gel, LMWGs can be optimised for targeted formation and degelation with a stimulus such as temperature and pH, which has great potential for drug delivery.[233–235] However, because of the weaker nature of the forces holding the assemblies together, the mechanical strength is often inferior to traditional polymer based gels.[236,237] LMWGs typically form micro or nanosized fibres which are formed through one dimensional hierarchical assembly, in contrast to long range 3D order in crystalline structures (Figure 1.12). Although high aspect ratio structures is beneficial for gelation, the precise organisation of molecules to form the larger assemblies varies. Tubular, helical, lamellar, and worm-like organisations of molecules can all form LMWGs. Moreover, LMWGs can either be single component or multicomponent, with the latter adding potential for additional functionality e.g. triggered gelation when a cogelator is introduced.[238] Self assembled fibrillar networks (SaFiNs) are an important subset of LMWGs that rely on gelator-solvent interactions to form gels using inexpensive gelator molecules.[239] The formation of molecule-solvent assemblies in SaFiNs is similar to a solvate crystal, except the latter always exhibit high degrees of order in three dimensions.

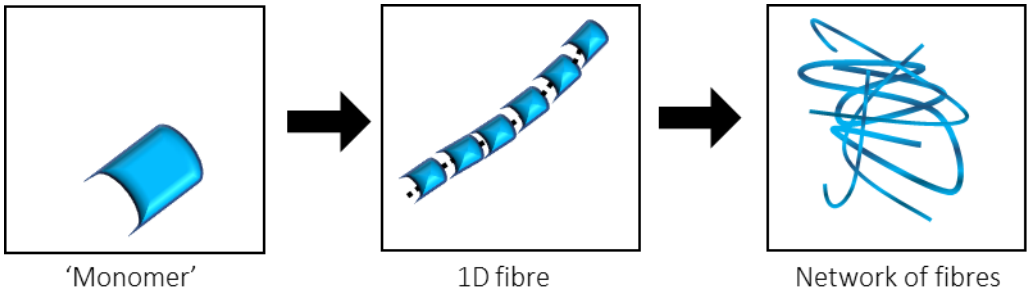

Figure 1.12: Schematic of 1D assembly of low molecular weight gels. Monomers do not covalently bond and therefore gelation is mediated through noncovalent bonding such as hydrogen bonding. The 1D assemblies then form gel networks.

The role of crystallinity within LMWGs is debated,[232] with some definitions such as SaFiNs sometimes used for both crystalline and non-crystalline gels.[240,241] Draper and Adams regard the majority of LMWGs as amorphous, with any implication of crystallinity being a minor or insignificant proportion of the gel phase.[242] For a large proportion of LMWGs, their lack of crystallinity is evident with Draper and Adams reporting amorphous ordered structures.[243] However it is not so simple; an alternative perspective by Weiss is that many LMWGs (particularly SaFiNs) are polymorphous, with thermodynamically unstable structures.[244] Although crystal structures do exist, growth of large single crystals (for XRD), or removal of solvent is often not possible without altering the structure. Very recently, crystal structures of multi-component (supramolecular) LMWGs have been evidenced[245] through single crystal XRD, further exemplifying the rich and diverse nature of LMWGs. A distinction between 'traditional LMWGs' was made for clarity, as crystalline suspensions also have the ability to gel solutions, while forming 3D ordered assemblies instead of more one-dimensional structures.

Solvents can have a large impact on the feasibility of gelation. Solvation properties such as cohesive energy, hydrogen bond density and their polarity determine if the gelator is compatible within the network. Attempts have been made to predict and rationalise gelation using Hansen solubility parameters, particularly important for SaFiNs.[246–249] Organogels (non-aqueous gels) are also used on a smaller scale, and are often oil based, and hence rely on interactions such as π-π stacking in apolar solvents.[250] By using alternative solvents, certain benefits can be achieved, for example, greater solubilisation and delivery of less polar therapeutic ingredients.[251]

1.6.3. Gels from Crystals

Fat crystal networks (FCN) consist of relatively low aspect ratio crystals that form networks of clusters or agglomerates, held together through weak forces (Figure 1.13) such as Van der Waals.[252] They are commonly used in foods,[252] and their hardness can be altered by increasing crystal content.[253] However, unlike non-aggregating polymer gels, both cooling rate and processing can affect rheological properties.[254]

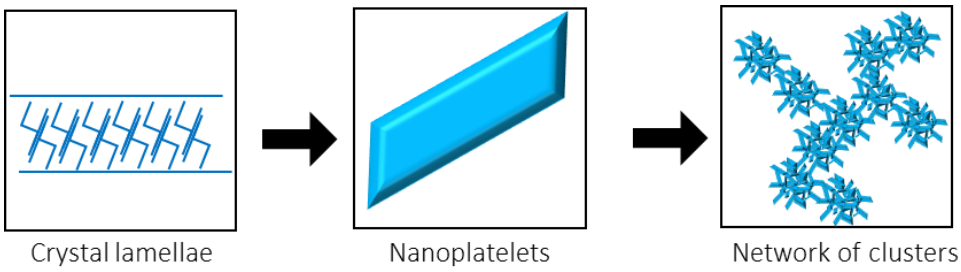

Figure 1.13: Schematic of fat crystal network gels, where organisation into crystals, and subsequently clusters and flocs cause gelation.

Coagels are similar as they are crystalline, or semicrystalline aggregate networks, with similar heterogeneity to FCNs, but are based on amphiphiles (Figure 1.14). They are hydrated surfactant crystals, and sometimes escribed as a β-phase crystals.[255] While coagels can be ionic or nonionic,[256,257] they are not comprised of polymeric surfactants, which self-assemble differently. While coagels can form different morphologies, the most effective shapes are ribbons and fibres.[258] This is because their high aspect ratio lead to entanglements and network formation. They share many similarities to SaFiNs, although exhibit have 3D ordering, instead of 1D. Gels from crystal/coagels behave differently to polymer gels. Instead of breaking of the weak interparticle/floc bonds or breaking of the crystals which gives rise to yielding and spreading,[230] polymer gels can deform more elastically,[259] although this varies on polymer composition and degree of crosslinking.

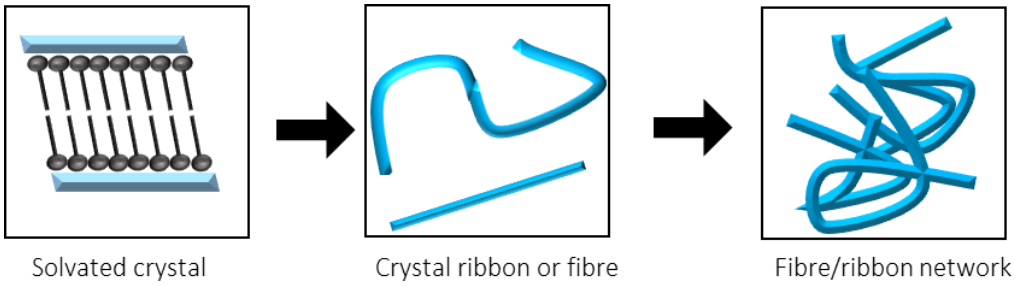

Figure 1.14: Schematic representation of coagel and crystalline surfactant gel formation where ribbons and fibres form a network which can gel.

While polymer structurants can gel at low concentrations, crystal gel strength depends on the growth and formation of crystal morphologies and aggregates This introduces an additional processing consideration, evidenced by the effect of fractality and size on rheology of fat crystal networks.[260] Finally, crystal gels are highly temperature dependent, which may aid, or limit applicability depending on formulation.

1.7. Research Objectives and Organisation

The general aim for this work is to explore the properties and structure of surfactants and polymers in mixed and non-aqueous solvents. SDS was chosen as a model surfactant to study in detail for two reasons: its ubiquity within personal care formulations and its typicality as an ionic surfactant: it has a similar structure to many other surfactants used in industry. An additional benefit is that SDS is synthetically derived and can be prepared in high purity compared to naturally derived alternatives.[261] Other surfactants can then be used to probe systematic behaviour. The main polymer used in this work is iota-carrageenan, which is a common additive within both food and personal care.[262] This biopolymer provides adequate model behaviour representing the widely used helical forming polysaccharides.

It was reported at the start of this project that SDS formed hydrated crystal in glycerol rich media.[155] However, little work has been conducted on the nature and dynamics of SDS in glycerol, especially in an industrial context. Therefore the aims of the first results chapter is to establish an understanding of the microstructure for crystals that form in glycerol and if hydrated crystals form, as well as examining processing effects on phase behaviour. This is primarily achieved using x-ray scattering in combination

with polarised optical microscopy. The physical properties of the crystalline suspension are then probed using rheology and DSC. Following this, the study of analogous surfactants and polyol solvents is undertaken to determine whether the behaviour of SDS in glycerol is systematic or anomalous.

The next chapter covers ternary systems. The initial focuses on water as a minor cosolvent, as phase behaviour is less known in this formulation space. This is then extended across the solvent composition range. The effects of adding a co-surfactant additive, 1-dodecanol, which is likely to be present as additives or impurities within industrial formulations, was then studied to see whether crystal structure and micelle behaviour are significantly altered. Finally, as inorganic electrolytes are often present in toothpastes and personal care formulations, the effect of addition of a model salt (NaCl) on crystallization was then studied. In the final results chapter microstructure and rheology of carrageenan as a model polymer is studied in various glycerol/water mixtures. Following characterisation of the polymer, its influence on the behaviour of SDS at room temperature is studied in glycerol/water mixtures. These interconnecting themes can then be used as a roadmap for more complex formulations, as summarised in Figure 1.15.

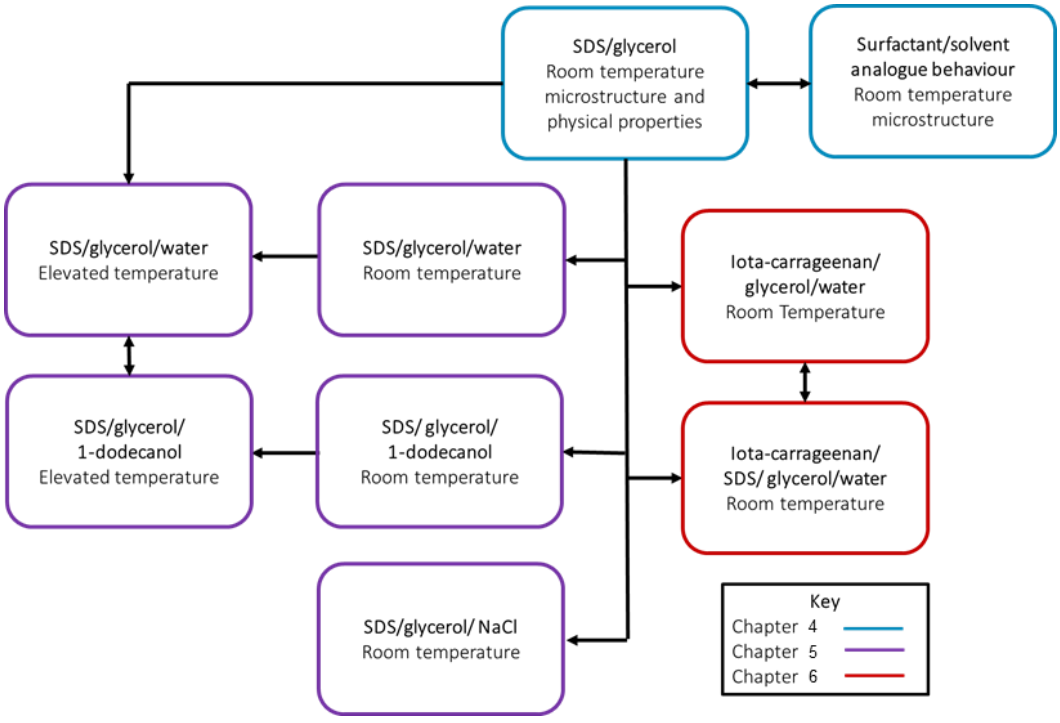

Figure 1.15: Flow chart for the content and organisation of work produced in this thesis, where Chapter 4 aims to provide fundamental understanding of binary surfactant mixtures in polyols, Chapter 5 increasing complexity to ternary mixtures, and Chapter 6 covering the behaviour of polymers (iota-carrageenan) in glycerol/water mixtures, as well as quaternary systems including SDS.

1.8. References

1 F. Lippert, *Monographs in Oral Science*, 2013, **23**, 1–14.
2 S. Twetman, S. Axelsson, H. Dahlgren, A. K. Holm, C. Källestål, F. Lagerlöf, P. Lingström, I. Mejàre, G. Nordenram, A. Norlund, L. G. Petersson and B. Söder, *Acta Odontologica Scandinavica*, 2003, 61, 347–355.
3 X. Li, J. Wang, A. Joiner and J. Chang, *Journal of Dentistry*, 2014, **42**, S12–S20.
4 A. Joiner, *Journal of Dentistry*, 2010, **38**, e17-24.
5 C. Valkenburg, D. E. Slot, E. W. P. Bakker and F. A. Van der Weijden, *Journal of Clinical Periodontology*, 2016, **43**, 1050–1058.
6 *Chemistry and Technology of the Cosmetics and Toiletries Industry*, Chapman & Hall, London, 1992.
7 I. M. C. Camargo, M. Saiki, M. B. A. Vasconcellos and D. M. Ávila, *Journal of Cosmetic Science*, 2001, **52**, 163–167.
8 *Formulating Toothpaste Using Carbopol Polymer*, The Lubrizol Corporation, 2010.
9 C. Ganss, M. Möllers and N. Schlueter, *Caries Research*, 2017, **51**, 52–57.
10 E. Macdonald, A. North, B. Maggio, F. Sufi, S. Mason, C. Moore, M. Addy and N. X. West, *Journal of Dentistry*, 2010, **38**, 509–516.
11 G. Rølla, B. Øsard and R. de Almeida Cruz, *Journal of Clinical Periodontology*, 1993, **20**, 105–108.
12 N. R. Mohammed, R. J. M. Lynch and P. Anderson, *Journal of Dentistry*, 2014, **42**, 613–618.
13 A. Ahuja and A. Potanin, *Rheologica Acta*, 2018, **57**, 459–471.
14 H. Cai, Y. Li and J. Chen, *Biotribology*, 2017, **10**, 17–25.
15 A. Ahuja, G. Luisi and A. Potanin, *Journal of Non-Newtonian Fluid Mechanics*, 2018, **258**, 1–9.
16 L. Fusi, A. Farina and F. Rosso, *Journal of Non-Newtonian Fluid Mechanics*, 2015, **225**, 1–9.
17 A. Ahuja, I. Pappas and A. Potanin, *Rheologica Acta*, 2020, **59**, 133–145.
18 U.S. *pat.*, 2,089,529, 1937.
19 O. Raubenheimer, *The Journal of the American Pharmaceutical Association (1912)*, 1916, **5**, 1397–1400.
20 B. J. Tai, Z. Bian, H. Jiang, D. C. Greenspan, J. Zhong, A. E. Clark and M. Q. Du, *Journal of Clinical Periodontology*, 2006, **33**, 86–91.
21 C. M. Hansen, *Hansen Solubility Parameters A User's Handbook*, Second ed., CRC press, Boca Raton, 2013.
22 O. Gereben and L. Pusztai, *Chemical Physics*, 2017, **496**, 1–8.
23 S. Pothoczki, I. Pethes, L. Pusztai, L. Temleitner, D. Csókás, S. Kohara, K. Ohara and I. Bakó, *Journal of Molecular Liquids*, 2021, **329**, 115592.
24 T. F. Tadros, *Applied Surfactants: Principles and Applications*, Wiley, Weinheim, 2005.
25 S. Abbott, *Solubility Science : Principles and Practice*, TCNF Ltd., 2017.
26 E. Vranić, A. Lacević, A. Mehmedagić and A. Uzunović, *Bosnian Journal of Basic Medical Sciences*, 2004, **4**, 51–58.
27 S. Chackalamannil, D. Rotella, S. Ward, A. Martinez and C. Gil, Eds., *Comprehensive Medicinal Chemistry III: Volume 1 General perspective -The future of drug discovery*, Elsevier Ltd., Amsterdam, 2017.
28 J. H. Hildebrand, *The solubility of non-electrolytes*, Reinhold Publishing corporation, New York, First Edit., 1936.
29 G. Scatchard, *Chemical Reviews*, 1931, **8**, 321–333.
30 G. Scatchard, S. E. Wood and J. M. Mochel, *Journal of the American Chemical Society*, 1939, **61**, 3206–3210.
31 C. M. Hansen, *The Three Dimensional Solubility Parameter and Solvent Diffusion Coefficient*, Danish Technical Press, Copenhagen, 1967
32 T. B. Nielsen and C. M. Hansen, *Polymer Testing*, 2005, **24**, 1054–1061.

33 M. A. Mohammad, A. Alhalaweh and S. P. Velaga, *International Journal of Pharmaceutics*, 2011, **407**, 63–71.
34 M. Raynal and L. Bouteiller, *Chemical Communications*, 2011, **47**, 8271–8273.
35 K. Gekkot and S. N. Timasheff, *Biochemistry Ruwart & Suelter Bradburg & Jakoby*, 1981, **20**, 4667–4676.
36 X. Li, Y. Liu, Y. Cao, Y. Cong, A. Farajtabar and H. Zhao, *Journal of Chemical and Engineering Data*, 2018, **63**, 2219–2227.
37 N. Chéron, M. Naepels, E. Pluhařová and D. Laage, *Journal of Physical Chemistry B*, 2020, **124**, 1424–1437.
38 S. Venkatram, C. Kim, A. Chandrasekaran and R. Ramprasad, *Journal of Chemical Information and Modeling*, 2019, **59**, 4188–4194.
39 A. Klamt, *Journal of Physical Chemistry*, 1995, **99**, 2224–2235.
40 A. Klamt, *WIREs Computational Molecular Science*, 2018, **8**, 1–11.
41 J. G. Kirkwood and F. P. Buff, *The Journal of Chemical Physics*, 1951, **19**, 774–777.
42 N. Dawass, P. Krüger, S. K. Schnell, J. M. Simon and T. J. H. Vlugt, *Fluid Phase Equilibria*, 2019, **486**, 21–36.
43 D. Yang, S. Gao and H. Yang, *Food Hydrocolloids*, 2020, **99**, 105317.
44 D. Yang and H. Yang, *LWT - Food Science and Technology*, 2020, **126**, 109281.
45 R. Stenner, N. Matubayasi and S. Shimizu, *Food Hydrocolloids*, 2016, **54**, 284–292.
46 I. M. Smallwood, *Handbook of Organic Solvent Properties*, Halsted Press, New York, 1996.
47 *US. Pat.,* 3,574,824, 1971.
48 A. Skaare, V. Kjærheim, P. Barkvoll and G. Rølla, *Acta Odontologica Scandinavica*, 1997, **55**, 133–136.
49 J. M. Trice and R. S. Pinals, *Seminars in Arthritis and Rheumatism*, 1985, **15**, 45–60.
50 S. W. Jacob and D. C. Wood, *The American Journal of Surgery*, 1967, **114**, 414–426.
51 A Structural Approach to Reveal the Cryoprotective Action of Glycerol, J. J. Towey, PhD thesis,University of Leeds, 2013.
52 M. Verheijen, M. Lienhard, Y. Schrooders, O. Clayton, R. Nudischer, S. Boerno, B. Timmermann, N. Selevsek, R. Schlapbach, H. Gmuender, S. Gotta, J. Geraedts, R. Herwig, J. Kleinjans and F. Caiment, *Scientific Reports*, 2019, **9**, 1–12.
53 X. Yi, M. Liu, Q. Luo, H. Zhuo, H. Cao, J. Wang and Y. Han, *FEBS Open Bio*, 2017, **7**, 485–494.
54 D. S. Jones, B. C. O. Muldoon, A. D. Woolfson, G. P. Andrews and F. D. Sanderson, *Biomacromolecules*, 2008, **9**, 624–633.
55 M. R. Rosen, Ed., *Delivery System Handbook for Personal Care and Cosmetic Products Technology, Applications, and Formulations*, William Andrew, Inc., New Jersey, 2005.
56 *Physical properties of glycerol and its solutions*, Glycerine Producers' Association, New York, 1963.
57 H. W. Tan, A. R. Abdul Aziz and M. K. Aroua, *Renewable and Sustainable Energy Reviews*, 2013, **27**, 118–127.
58 N. S. Cheng, *Industrial and Engineering Chemistry Research*, 2008, **47**, 3285–3288.
59 Y. Lu, *International Journal of Cosmetic Science*, 2001, **23**, 175–181.
60 H. Khan, J. M. Seddon, R. V Law, N. J. Brooks, E. Robles and J. T. Cabral, *Journal of Colloid And Interface Science*, 2018, **538**, 75–82.
61 J. J. De Yoreo and P. G. Vekilov, *Reviews in Mineralogy and Geochemistry*, 2003, **54**, 57–93.
62 A. S. Myerson, D. Erdemir and A. Y. Lee, *Handbook of industrial crystallization*, Cambridge University Press, 2019.
63 J. Dalmolen, PhD thesis, University of Groningen, 2005.
64 M. Steiger and W. Voigt, *Journal of Solution Chemistry*, 2019, **48**, 1009–1024.
65 H. Dai, X. Lu, Y. Peng, Z. Yang and H. Zhu, *Desalination and Water Treatment*, 2017, **62**, 192–199.
66 P. Barrett and B. Glennon, *Trans IChemE*, 2002, **80**, 799–805.

67 A. Chianese, A. Contaldi and B. Mazzarotta, *Journal of Crystal Growth*, 1986, **78**, 279–290.
68 G. C. Sosso, J. Chen, S. J. Cox, M. Fitzner, P. Pedevilla, A. Zen and A. Michaelides, *Chemical Reviews*, 2016, **116**, 7078–7116.
69 S. Xu, Y. Wang, Z. Hou and X. Chuai, *Industrial and Engineering Chemistry Research*, 2020, **59**, 18335–18356.
70 T. Koyano, I. Hachiya And K. Sato, *Food structure (USA)*, 1990, **9**, 231–240.
71 D. Braga, F. Grepioni, L. Maini and M. Polito, *Structure and Bonding*, 2009, **132**, 25–50.
72 J. W. P. Schmelzer and A. S. Abyzov, in *Thermal Physics and Thermal Analysis*, Springer, Cham, 2017, pp. 195–211.
73 R. A. Chiarella, A. L. Gillon, R. C. Burton, R. J. Davey, G. Sadiq, A. Auffret, M. Cioffi and C. A. Hunter, *Faraday Discussions*, 2007, **136**, 179–193.
74 F. Tian, H. Qu, A. Zimmermann, T. Munk, A. C. Jørgensen and J. Rantanen, *Journal of Pharmacy and Pharmacology*, 2010, **62**, 1534–1546.
75 L. O. Hedges and S. Whitelam, *The Journal of Chemical Physics*, 2011, **135**, 164902.
76 A. J. Cruz-Cabeza, S. E. Wright and A. Bacchi, *Chemical Communications*, 2020, **56**, 5127–5130.
77 R. Thakuria, B. Sarma and A. Nangia, in *Comprehensive Supramolecular Chemistry II*, Elsevier, Oxford, 2017, vol. 7, pp. 25–48.
78 R. Chidambaram, *The Journal of Chemical Physics*, 1962, **36**, 2361–2365.
79 D. Myers, *Surfactant Science and Technology*, John Wiley & Sons, Hoboken, 2020.
80 T. Lee, K. L. Yeh, J. X. You, Y. C. Fan, Y. S. Cheng and D. E. Pratama, *ACS Omega*, 2020, **5**, 1068–1079.
81 I. Foubert, K. Dewettinck and P. A. Vanrolleghem, *Trends in Food Science and Technology*, 2003, **14**, 79–92.
82 C. Himawan, V. M. Starov and A. G. F. Stapley, *Advances in Colloid and Interface Science*, 2006, **122**, 3–33.
83 S. Padar, S. A. K. Jeelani and E. J. Windhab, *Journal of the American Oil Chemists' Society*, 2008, **85**, 1115–1126.
84 A. G. Marangoni, in *Kinetic Analysis of Food Systems*, Springer International Publishing, Cham, 2017, pp. 113–134.
85 T. Ozawa, *Polymer*, 1971, **12**, 150–158.
86 E. Piorkowska, A. Galeski and J.-M. Haudin, *Progress in Polymer Science*, 2006, **31**, 549–575.
87 The Crystallization of Poly(ethylene terephthalate) Studied by Thermal Analysis and FTIR Spectroscopy, Z. Chen, *PhD Thesis*, 2012.
88 A. T. Lorenzo, M. L. Arnal, J. Albuerne and A. J. Müller, *Polymer Testing*, 2007, **26**, 222–231.
89 Y. Liu, R. Y. Wang, J. L. Li, B. Yuan, M. Han, P. Wang and X. Y. Liu, *CrystEngComm*, 2014, **16**, 5402–5408.
90 J. F. Toro-Vazquez, E. Dibildox-Alvarado, M. Charó-Alonso, V. Herrera-Coronado and C. A. Gómez-Aldapa, *JAOCS, Journal of the American Oil Chemists' Society*, 2002, **79**, 855–866.
91 S. J. Urwin and J. H. t. Horst, in *50th Annual Conference of the British Association of Crystal Growth,* 2019.
92 C. J. Tilbury, D. A. Green, W. J. Marshall and M. F. Doherty, *Crystal Growth and Design*, 2016, **16**, 2590–2604.
93 C. Stoica, P. Verwer, H. Meekes, P. J. C. M. Van Hoof, F. M. Kaspersen and E. Vlieg, *Crystal Growth and Design*, 2004, **4**, 765–768.
94 R. M. Miller, A. S. Poulos, E. S. J. Robles, N. J. Brooks, O. Ces and J. T. Cabral, *Crystal Growth and Design*, 2016, **16**, 3379–3388.
95 H. J. Wood, J. D. Hunt and P. V. Evans, *Acta Materialia*, 1997, **45**, 569–574.
96 M. E. Glicksman and A. O. Lupulescu, *Journal of Crystal Growth*, 2004, **264**, 541–549.
97 B. Lotz and S. Z. D. Cheng, *Polymer*, 2005, **46**, 577–610.

98 S. R. Aspinall, J. K. Parker and V. V. Khutoryanskiy, *Colloids and Surfaces B: Biointerfaces*, 2021, **200**, 111567.
99 Pluronic® F-127 (Poloxamer 407) NF | VWR, https://uk.vwr.com/store/product/18046895/pluronic-f-127-poloxamer-407-nf, (accessed 8 April 2021).
100 Y. Seok Jung, W. Park, H. Park, D. K. Lee and K. Na, *Carbohydrate Polymers*, 2017, **156**, 403–408.
101 E. Carey and C. Stubenrauch, *Journal of Colloid and Interface Science*, 2010, **346**, 414–423.
102 P. Kékicheff, *Journal of Colloid and Interface Science*, 1989, **131**, 133–152.
103 R. Nagarajan and C. C. Wang, *Langmuir*, 2000, **16**, 5242–5251.
104 K. Esumi and M. Ueno, Eds., *Structure-Performance Relationships in Surfactants*, CRC Press, Boca Raton, Second Edition, 2003.
105 H. U. Kim and K. H. Lim, *Colloids and Surfaces A: Physicochemical and Engineering Aspects*, 2004, **235**, 121–128.
106 M. J. Schick, *Journal of Physical Chemistry*, 1964, **68**, 3585–3592.
107 J. H. Clint and J. H. Clint, *Surfactant Aggregation*, 1992, 82–129.
108 L. R. Pratt and D. Chandler, *The Journal of Chemical Physics*, 1977, **67**, 3683–3704.
109 D. Chandler, *Nature*, 2005, **437**, 640–647.
110 L. Maibaum, A. R. Dinner and D. Chandler, *Journal of Physical Chemistry B*, 2004, **108**, 6778–6781.
111 J. Dey, D. Ray, S. Kumar, N. Sultana, V. K. Aswal, J. Kohlbrecher and K. Ismail, *Journal of Molecular Liquids*, 2016, **216**, 450–454.
112 A. K. Sood, R. Kaur and T. S. Banipal, *Indian Journal of Chemistry - Section A Inorganic, Physical, Theoretical and Analytical Chemistry*, 2016, **55A**, 34–43.
113 C. C. Ruiz, L. Díaz-lópez, J. Aguiar, L. Díaz-López and J. Aguiar, *Journal of Dispersion Science and Technology*, 2008, **29**, 266–273.
114 S. S. Sakhawat and Ejaz-ur-Rehman, in *Interactions of Water in Ionic and Nonionic Hydrates*, Springer Berlin Heidelberg, Berlin, Heidelberg, 1987, 251–255.
115 E. Junquera, L. Peña and E. Aicart, *Journal of Solution Chemistry*, 1994, **23**, 421–430.
116 S. K. Mehta, K. K. Bhasin, R. Chauhan and S. Dham, *Colloids and Surfaces A: Physicochemical and Engineering Aspects*, 2005, **255**, 153–157.
117 A. Malliaris, J. Le Moigne, J. Sturm and R. Zana, *Journal of Physical Chemistry*, 1985, **89**, 2709–2713.
118 B. Hammouda, *Journal of Research of the National Institute of Standards and Technology*, 2013, **118**, 151.
119 A. D. McNaught and A. Wilkinson, *The IUPAC Compendium of Chemical Terminology*, International Union of Pure and Applied Chemistry (IUPAC), Research Triangle Park, NC, 2019.
120 J. Ž. Manojlovi, Thermal Science, 2012, **16**, 631–640.
121 H. Matsuki, R. Ichikawa, S. Kaneshina, H. Kamaya and I. Ueda, *Journal of Colloid and Interface Science*, 1996, **181**, 362–369.
122 J. Karayil, S. Kumar, P. A. Hassan, Y. Talmon and L. Sreejith, *RSC Advances*, 2015, **5**, 12434–12441.
123 Z. Lin, *Langmuir*, 1996, **12**, 1729–1737.
124 L. M. Walker, *Current Opinion in Colloid & Interface Science*, 2001, **6**, 451–456.
125 R. Oda, L. Bourdieu and M. Schmutz, *Journal of Physical Chemistry B*, 1997, **101**, 5913–5916.
126 A. S. Poulos, M. Nania, P. Lapham, R. M. Miller, A. J. Smith, H. Tantawy, J. Caragay, J. Gummel, O. Ces, E. S. J. Robles and J. T. Cabral, *Langmuir*, 2016, **32**, 5852–5861.
127 L. K. Shrestha, O. Glatter and K. Aramaki, *Journal of Physical Chemistry B*, 2009, **113**, 6290–6298.
128 R. E. Riter, J. R. Kimmel, E. P. Undiks and N. E. Levinger, *Journal of Physical Chemistry B*, 1997, **101**, 8292–8297.

129 L. K. Shrestha, R. G. Shrestha, D. Varade and K. Aramaki, *Langmuir*, 2009, **25**, 4435–4442.
130 R. A. Khalil and A. H. A. Zarari, *Applied Surface Science*, 2014, **318**, 85–89.
131 K. Schäfer, H. B. Kolli, M. Killingmoe Christensen, S. L. Bore, G. Diezemann, J. Gauss, G. Milano, R. Lund and M. Cascella, *Angewandte Chemie*, 2020, **132**, 18750–18757.
132 T. H. Ito, R. K. Rodrigues, W. Loh and E. Sabadini, *Langmuir*, 2015, **31**, 6020–6026.
133 E. G. R. Putra and A. Patriati, in *AIP Conference Proceedings*, 2015, vol. 1656, p. 020001.
134 S. Hayashi and S. Ikeda, *Journal of Physical Chemistry*, 1980, **84**, 744–751.
135 G. V. Jensen, R. Lund, J. Gummel, T. Narayanan and J. S. Pedersen, *Angewandte Chemie*, 2014, **126**, 11708 –11712.
136 Y. Cai, C. Burguiere and S. P. Armes, *Chemical Communications*, 2004, **4**, 802–803.
137 R. Nagarajan, *Langmuir*, 2002, **18**, 31–38.
138 V. Lutz-Bueno, S. Isabettini, F. Walker, S. Kuster, M. Liebi and P. Fischer, *Physical Chemistry Chemical Physics*, 2017, **19**, 21869–21877.
139 E. Summerton, M. J. Hollamby, C. S. Le Duff, E. S. Thompson, T. Snow, A. J. Smith, C. Jones, J. Bettiol, S. Bakalis and M. M. Britton, *Journal of Colloid and Interface Science*, 2019, **535**, 1–7.
140 M. Bergström and J. S. Pedersen, *Physical Chemistry Chemical Physics*, 1999, **1**, 4437–4446.
141 M. Kakitani, T. Imae and M. Furusaka, *Journal of Physical Chemistry*, 1995, **99**, 16018–16023.
142 S. Vass, J. S. Pedersen, J. Pleštil, P. Laggner, E. Rétfalvi, I. Varga and T. Gilányi, *Langmuir*, 2008, **24**, 408–417.
143 R. C. Oliver, J. Lipfert, D. A. Fox, R. H. Lo, S. Doniach and L. Columbus, *PLoS ONE*, 2013, **8**, e62488.
144 Israelachvili, J. N.; Mitchell, D. J.; Ninham, B. W. , Journal of the Chemical Society, Faraday Transactions 2: Molecular and Chemical Physics 2, 1976, **72**, 1525−1568.
145 J. Iyer and D. Blankschtein, *Journal of Physical Chemistry B*, 2012, **116**, 6443–6454.
146 G. D'Errico, D. Ciccarelli and O. Ortona, *Journal of Colloid and Interface Science*, 2005, **286**, 747–754.
147 G. E. McDuffie, R. G. Quinn and T. A. Litovitz, *Journal of Chemical Physics*, 1962, **37**, 239–242.
148 S. K. Shah, S. K. Chatterjee and A. Bhattarai, *Journal of Molecular Liquids*, 2016, **222**, 906–914.
149 S. Das, B. Naskar and S. Ghosh, *Soft Matter*, 2014, **10**, 2863–2875.
150 H. Gharibi, B. M. Razavizadeh and A. A. Rafati, *Colloids and Surfaces A: Physicochemical and Engineering Aspects*, 1998, **136**, 123–132.
151 J. B. Huang, M. Mao and B. Y. Zhu, *Colloids and Surfaces A: Physicochemical and Engineering Aspects*, 1999, **155**, 339–348.
152 F. Golmohammadi, M. Amiri, H. Gharibi, A. Yousefi and M. Safari, *Journal of Solution Chemistry*, 2020, **49**, 16–33.
153 G. Colafemmina, D. Florentino, A. Ceglie, E. Carretti, E. Fratini, L. Dei, P. Baglioni and G. Palazzo, *Journal of Physical Chemistry B*, 2007, **111**, 7184–7193.
154 A. Rodríguez, M. Del Mar Graciani, M. L. Moya, A. Rodriguez, M. Graciani Mdel and M. L. Moya, *Langmuir*, 2008, **24**, 12785–12792.
155 R. A. Abdel-Rahem, *Journal of Dispersion Science and Technology*, 2013, **34**, 932–940.
156 M. Almgren, S. Swarup and J. E. Loefroth, *Journal of Physical Chemistry*, 1985, **89**, 4621–4626.
157 R. Zana, *Advances in Colloid and Interface Science*, 1995, **57**, 1–64.
158 G. M. Førland, J. Samseth, M. I. Gjerde, H. Høiland, A. O. Jensen and K. Mortensen, *Journal of Colloid and Interface Science*, 1998, **203**, 328–334.
159 H. N. Singh, S. M. Saleem, R. P. Singh and K. S. Birdi, Journal of Physical Chemistry, 1980, **84**, 2191–2194.
160 A. Pan, B. Naskar, G. K. S. Prameela, B. V. N. P. Kumar, A. B. Mandal, S. C. Bhattacharya and S. P. Moulik, *Langmuir*, 2012, **28**, 13830–13843.
161 B. Sarkar, S. Lam and P. Alexandridis, *Langmuir*, 2010, **26**, 10532–10540.
162 S. K. Shah, S. K. Chatterjee and A. Bhattarai, *Journal of Surfactants and Detergents*, 2016, **19**, 201–207.

163 H. Jiang, G. Beaucage, K. Vogtt and M. Weaver, *Journal of Colloid and Interface Science*, 2018, **509**, 25–31.
164 M. A. Dyakonova, Y. Li, I. N. Besiri, Z. Di, I. Grillo, C. Tsitsilianis and C. M. Papadakis, *Colloid and Polymer Science*, 2021, **299**, 419–428.
165 P. Alexandridis and L. Yang, *Macromolecules*, 2000, **33**, 5574–5587.
166 D. Gaudino, R. Pasquino and N. Grizzuti, *Journal of Rheology*, 2015, **59**, 1363–1375.
167 M. L. Corrin and W. D. Harkins, *Journal of the American Chemical Society*, 1947, **69**, 683–688.
168 J. Dey, N. Sultana and K. Ismail, *Journal of Molecular Liquids*, 2015, **207**, 107–111.
169 Y. Zhang and P. S. Cremer, *Current Opinion in Chemical Biology*, 2006, **10**, 658–663.
170 V. Mazzini and V. S. J. Craig, *Current Opinion in Colloid and Interface Science*, 2016, **23**, 82–93.
171 M. Nazrul Islam, K. C. Sarker and G. Aktaruzzaman, *Journal of Surfactants and Detergents*, 2014, **17**, 525–530.
172 K. K. Sharker, M. Nazrul Islam and S. Das, *Journal of Surfactants and Detergents*, 2019, **22**, 249–258.
173 A. Rahman and C. W. Brown, *Journal of Applied Polymer Science*, 1983, **28**, 1331–1334.
174 V. Patel, N. Dharaiya, D. Ray, V. K. Aswal and P. Bahadur, *Colloids and Surfaces A: Physicochemical and Engineering Aspects*, 2014, **455**, 67–75.
175 A. S. Lee, A. P. Gast, V. Bütün and S. P. Armes, *Macromolecules*, 1999, **32**, 4302–4310.
176 H. Durmaz and M. İşcan, *Nanosystems: Physics, Chemistry, Mathematics*, 2019, **10**, 176–183.
177 Y. Nan, W. Li and Z. Jin, *Langmuir*, 2020, **36**, 5198–5207.
178 S. Y. Choi, S. G. Oh, S. Y. Bae and S. K. Moon, *Korean Journal of Chemical Engineering*, 1999, **16**, 377–381.
179 M. Sun, Y. Wang and A. Firoozabadi, *Energy and Fuels*, 2012, **26**, 5626–5632.
180 C. Leal, A. Bilalov and B. Lindman, *Journal of Physical Chemistry B*, 2006, **110**, 17221–17229.
181 M. Kahlweit, R. Strey and G. Busse, *Journal of Physical Chemistry*, 1991, **95**, 5344–5352.
182 Y. Einaga, Y. Totake and H. Matsuyama, *Polymer Journal*, 2004, **36**, 971–978.
183 V. K. Paruchuri, J. Nalaskowski, D. O. Shah and J. D. Miller, *Colloids and Surfaces A: Physicochemical and Engineering Aspects*, 2006, **272**, 157–163.
184 E. Summerton, G. Zimbitas, M. Britton and S. Bakalis, *Journal of Crystal Growth*, 2016, **455**, 111–116.
185 G. M. Førland, J. Samseth, H. Høiland and K. Mortensen, *Journal of Colloid and Interface Science*, 1994, **164**, 163–167.
186 J. G. Méndez-Bermúdez and H. Dominguez, *Journal of Molecular Modeling*, 2016, **22**, 1–9.
187 C. Totland and A. M. Blokhus, *Physical Chemistry Chemical Physics*, 2017, **19**, 7708–7713.
188 S. Shirzad and R. Sadeghi, *Journal of the Iranian Chemical Society*, 2018, **15**, 1365–1375.
189 T. Schmutzler, T. Schindler, M. Schmiele, M. S. Appavou, S. Lages, A. Kriele, R. Gilles and T. Unruh, *Colloids and Surfaces A: Physicochemical and Engineering Aspects*, 2018, **543**, 56–63.
190 S. Vierros and M. Sammalkorpi, *Physical Chemistry Chemical Physics*, 2018, **20**, 6287–6298.
191 C. V. Kulkarni, *Nanoscale*, 2012, **4**, 5779–5791.
192 M. Ricaurte, J. Torré, J. Diaz, C. Dicharry, M. Ricaurte, J. Torré, J. Diaz and C. Dicharry, .
193 R. P. Sperline, *Langmuir*, 1997, **13**, 3715–3726.
194 K. Takeda, Y. Andoh, W. Shinoda and S. Okazaki, *Langmuir*, 2019, **35**, 9011–9019.
195 P. Lo Nostro, M. Ambrosi, B. W. Ninham and P. Baglioni, *Journal of Physical Chemistry B*, 2009, **113**, 8324–8331.
196 V. M. Coiro, M. Manigrasso, F. Mazza and G. Pochetti, *Acta Crystallogr.*, 1987, **C43**, 850–854.
197 V. M. Coiro, F. Mazza and G. Pochetti, *Acta Crystallogr.*, 1986, **C42**, 991–995.
198 L. A. Smith, R. B. Hammond, K. J. Roberts, D. Machin and G. McLeod, *Journal of Molecular Structure*, 2000, **554**, 173–182.
199 P. Kékicheff, C. Grabielle-Madelmont and M. Ollivon, *Journal of Colloid And Interface Science*, 1989, **131**, 112–132.
200 J. A. Prins and W. Prins, *Nature*, 1956, **177**, 535–536.

201 L. A. Smith, A. Duncan, G. B. Thomson, K. J. Roberts, D. Machin and G. Mcleod, *Journal of Crystal Growth,* 2004, **263**, 480–490.
202 L. A. Smith, G. B. Thomson, K. J. Roberts, D. Machin and G. McLeod, *Crystal Growth & Design*, 2005, **5**, 2164–2172.
203 R. M. Miller, J. T. Cabral, E. S. J. Robles, N. J. Brooks and O. Ces, *CrystEngComm*, 2018, **20**, 6834–6843.
204 R. M. Miller, O. Ces, N. J. Brooks, E. S. J. Robles and J. T. Cabral, *Crystal Growth & Design*, 2017, **17**, 2428–2437.
205 E. Summerton, M. J. Hollamby, G. Zimbitas, T. Snow, A. J. Smith, J. Sommertune, J. Bettiol, C. Jones, M. M. Britton and S. Bakalis, *Journal of Colloid and Interface Science*, 2018, **527**, 260–266.
206 F. Brochard and P. G. de Gennes, *Macromolecules*, 1977, **10**, 1157–1161.
207 U.W. Gedde, *Polymer Physics*, Springer Netherlands, Dordrecht, 1999.
208 E. A. Litmanovich, S. O. Zakharchenko and G. V. Stoichev, *Journal of Physical Chemistry B*, 2007, **111**, 8567–8571.
209 E. Zhang, X. Dai, Z. Dong, X. Qiu and X. Ji, *Polymer*, 2016, **84**, 275–285.
210 H. Chen, E. Zhang, X. Dai, W. Yang, X. Liu, X. Qiu, W. Liu and X. Ji, *Journal of Polymer Research*, 2019, **26**, 39.
211 H. Toğrul and N. Arslan, *Carbohydrate Polymers*, 2003, **54**, 73–82.
212 H. J. Bixler and H. Porse, *Journal of Applied Phycology*, 2011, **23**, 321–335.
213 M. Glicksman, *Food hydrocolloids, Volume 1*, CRC Press, Boca Raton, 1982.
214 G. O. Phillips and P. A. Williams, *Handbook of Hydrocolloids: Second Edition*, Woodhead Publishing Limited,Cambridge, 2009.
215 G. Fittolani, P. H. Seeberger and M. Delbianco, *Peptide Science*, **112**, 2020, e24124.
216 E. Antoniou and P. Alexandridis, *European Polymer Journal*, 2010, **46**, 324–335.
217 R. Gonzales, M. R. Johns, P. F. Greenfield and G. W. Pace, *Carbohydrate Polymers*, 1990, **13**, 317–333.
218 S. Ramakrishnan and R. Prud'homme, *Carbohydrate Polymers*, 2000, **43**, 327–332.
219 N. Stavrouli, Z. Iatridi, T. Aubry and C. Tsitsilianis, *Polymer Chemistry*, 2013, **4**, 2097–2105.
220 Z. Yang, H. H. Yang and H. H. Yang, *Food Research International*, 2018, **107**, 738–746.
221 M. T. Islam, N. Rodríguez-Hornedo, S. Ciotti and C. Ackermann, *Pharmaceutical Research*, 2004, **21**, 1192–1199.
222 L. Cao, W. Lu, A. Mata, K. Nishinari and Y. Fang, *Carbohydrate Polymers*, 2020, **242**, 116389.
223 D. Renard, F. Van De Velde and R. W. Visschers, *Food Hydrocolloids*, 2006, **20**, 423–431.
224 S. Liu and L. Li, *Food Hydrocolloids*, 2016, **61**, 793–800.
225 P. M. Visakh, O. Bayraktar and G. Menon, *Bio Monomers for Green Polymeric Composite Materials*, Wiley, Chichester, 2019.
226 S. Liu and L. Li, *Food hydrocolloids*, 2016, **61**, 793–800.
227 A. M. Hermansson, E. Eriksson and E. Jordansson, *Carbohydrate Polymers*, 1991, **16**, 297–320.
228 D. Kang, H.-B. Zhang, Y. Nitta, Y.-P. Fang and K. Nishinari, in *Polysaccharides*, Springer, Cham, 2015, pp. 1–48.
229 F. Tanaka and Y. Tamura, *AIP Conference Proceedings*, 2004, **708**, 221–224.
230 M. Rayner, K. Östbring and J. Purhagen, in *Natural Polymers*, ed. O. Olatunji, Springer International Publishing, Cham, 2016, pp. 115–161.
231 M. Diener, J. Adamcik, A. Sánchez-Ferrer, F. Jaedig, L. Schefer and R. Mezzenga, *Biomacromolecules*, 2019, **20**, 1731–1739.
232 E. R. Draper and D. J. Adams, *Chem*, 2017, **3**, 390–410.
233 S. M. M. Reddy, G. Shanmugam, N. Duraipandy, M. S. Kiran and A. B. Mandal, *Soft Matter*, 2015, **11**, 8126–8140.
234 M. Marlow, M. Al-Ameedee, T. Smith, S. Wheeler and M. J. Stocks, *Chemical Communications*, 2015, **51**, 6384–6387.

235 D. Ghosh, M. T. Mulvee and K. K. Damodaran, *Molecules*, 2019, **24**, 24–32.
236 D. J. Cornwell and D. K. Smith, *Materials Horizons*, 2015, **2**, 279–293.
237 P. R. A. Chivers and D. K. Smith, *Chemical Science*, 2017, **8**, 7218–7227.
238 J. Buendia, E. Matesanz, D. K. Smith and L. Sanchez, *Cryst. Eng. Comm.*, 2015, **17**, 8146–8152.
239 Y. Lan and M. A. Rogers, *CrystEngComm*, **17**, 8031–8038.
240 P. Dastidar, *Gels*, 2019, **5**, 15.
241 M. A. Rogers and A. G. Marangoni, *Langmuir*, 2016, **32**, 12833–12841.
242 J. Raeburn and D. J. Adams, *Chemical Communications*, 2015, **51**, 5170–5180.
243 E. R. Draper, B. Dietrich, K. McAulay, C. Brasnett, H. Abdizadeh, I. Patmanidis, S. J. Marrink, H. Su, H. Cui, R. Schweins, A. Seddon and D. J. Adams, *Matter*, 2020, **2**, 764–778.
244 R. G. Weiss, *Journal of the American Chemical Society*, 2014, **136**, 7519–7530.
245 D. Ghosh, A. D. Farahani, A. D. Martin, P. Thordarson and K. K. Damodaran, *Chemistry of Materials*, 2020, **32**, 3517–3527.
246 P. Lin, N. X. Zhang, J. J. Li, J. Zhang, J. H. Liu, B. Zhang and J. Song, *Chinese Chemical Letters*, 2017, **28**, 771–776.
247 J. Bonnet, G. Suissa, M. Raynal and L. Bouteiller, *Soft Matter*, 2014, **10**, 3154–3160.
248 M. G. Corradini and M. A. Rogers, *Current Opinion in Food Science*, 2016, **9**, 84–92.
249 J. Bonnet, G. Suissa, M. Raynal and L. Bouteiller, *Soft Matter*, 2015, **11**, 2308–2312.
250 S. Murdan, *Expert Opinion on Drug Delivery*, 2005, **2**, 489–505.
251 R. M. Martinez, C. Rosado, M. V. R. Velasco, S. C. S. Lannes and A. R. Baby, *International Journal of Cosmetic Science*, 2019, **41**, 109–117.
252 J. M. Deman and A. M. Beers, *Journal of Texture Studies*, 1987, **18**, 303–318.
253 A. G. Marangoni, N. Acevedo, F. Maleky, E. Co, F. Peyronel, G. Mazzanti, B. Quinn and D. Pink, *Soft Matter*, 2012, **8**, 1275–1300.
254 S. Sandra, C. Cooper, M. Alexander and M. Corredig, *Food Research International*, 2011, **44**, 951–956.
255 B. M. McKenna, Ed., *Texture in food. Volume 1: Semi-solid foods*, Woodhead Publishing Limited, Cambridge, 2003.
256 P. S. Dubey, H. Srinivasan, V. K. Sharma, S. Mitra, V. G. Sakai and R. Mukhopadhyay, *Scientific Reports*, 2018, **8**, 1–16.
257 E. Carretti, V. Mazzini, E. Fratini, M. Ambrosi, L. Dei, P. Baglioni and P. Lo Nostro, *Physical Chemistry Chemical Physics*, 2016, **18**, 8865–8873.
258 S. Ogawa, M. Koga, K. Asakura, I. Takahashi and S. Osanai, *Journal of Surfactants and Detergents*, 2017, **20**, 255–261.
259 G. M. Kavanagh and S. B. Ross-Murphy, *Progress in Polymer Science* , 1998, **23**, 533-562 .
260 S. S. Narine and A. G. Marangoni, *Physical Review E - Statistical Physics, Plasmas, Fluids, and Related Interdisciplinary Topics*, 1999, **59**, 1908–1920.
261 M. Bährle-Rapp, in *Springer Lexikon Kosmetik und Körperpflege*, Springer Berlin Heidelberg, Berlin, Heidelberg, 2007, pp. 514–514.
262 V. T. N. T. Bui, B. T. Nguyen, F. Renou and T. Nicolai, *Journal of Applied Phycology*, 2019, **31**, 1947–1953.

2. Analytical Techniques

2.1. Scattering of Electromagnetic Waves by Matter

2.1.1. Scattering Principles

Scattering techniques are ubiquitous in the characterisation of molecules and macromolecular assemblies, where structural determination is achieved through interaction of electromagnetic radiation, or elemental particles, with matter. For characterisation of colloidal objects and crystals using x-rays, radiation interacts elastically (coherently) with no energy transfer between the incoming photon and matter. This involves Rayleigh and Thompson scattering, where the incident wave interacts with the electrons surrounding the nucleus of the atoms being studied. Thompson scattering is the dominant process in x-ray scattering.[1] The Bragg condition (Equation 2.1) states that the wavelength of radiation is related to the resolution. For small distances, on the atomic or nano-scale, the small wavelengths of x-rays are perfect for structural characterisation. Alternatively, elemental particles with a small associated de Broglie wavelength can be used including neutrons.[2]

$$\frac{n\lambda}{2d} = \sin\theta \qquad \text{eq. 2.1}$$

Where λ is the radiation wavelength, d is lattice spacing, n is an integer of order, and θ is half of the scattering (or diffraction) angle.[3] In general, the majority of x-rays pass unperturbed through a sample. But when an x-ray interacts elastically (coherently) with a point scatterer, radiation of the same wavelength is scattered as a spherical wave. If multiple scatterers are arranged in a lattice, then constructive and destructive interaction of the coherent waves causes differences in the scattered intensity depending on the scattering angle. The differences in intensity can then be measured and compared against the scattering angle, which can be transformed into real space information. For labile systems such as liquids and gases, inhomogeneities in the distribution of electrons within the sample (e.g. a micelle and solvent) causes scattering of incoming radiation, which is measured in a scattering experiment. For ordered systems, the regular array of scatterers (e.g. atoms), produces an interference pattern from the long-range repeating spacings, which is called diffraction.

Scattering angle is inversely proportional to the sizes and distances measured. Thus, recording at wider scattering angles (up to about 160 °) yields information at sub-Angstrom distances, which can be used to probe atomic positions, particularly in crystals. If larger structures (up to a few microns)[4] are to be measured, small angles must be used instead. Differing experimental setups are required to measure intensity of the radiation scattered by materials into these two angle regions. Because of this, x-ray

scattering is differentiated into small-angle and wide-angle X-ray scattering (SAXS/WAXS). Small angle scattering is used to measure large assemblies and structures including polymers, micelles, and liquid crystals. Detailed atomic positions cannot be resolved using small angle scattering results, but motifs of electron density distribution can be measured.[5]

2.1.2. Small and Wide-angle X-ray Scattering

In SAXS, the scattering angles that are resolved by the instruments are below 10 °. Most experiments are conducted in transmission mode, meaning that the x-rays pass through the sample as they are scattered. Therefore, a beam-stop must be used to absorb the non-scattered x-rays and prevent damage to the detecting sensors. A reflection/grazing incidence setup can also be used to probe surface structures. The momentum transfer of an x-ray photon scattered by a material is called the scattering vector, $\vec{q}$, and its modulus is expressed as:

$$q = \frac{4\pi sin\theta}{\lambda} \qquad \text{eq. 2.2}$$

Where q is usually measured in $Å^{-1}$ or nm^{-1}. The closer a detector is to the sample, the wider the scattering angles that can be recorded, and vice versa. Therefore, in order to gain structural information using SAXS, the detector must be placed some distance away from the sample. Flight tubes under vacuum are used to provide a means for the scattered x-rays to travel without interference from collisions with air molecules (Figure 2.1).The sample to detector distance can vary in length as the flux of x-rays, their collimation and the sensitivity of the detector also dictate what angles can be resolved.

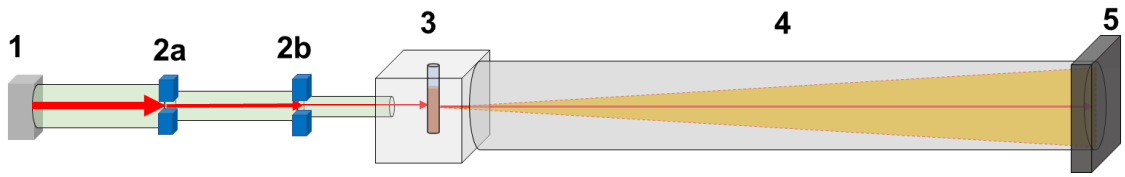

Figure 2.1: Example of the small angle x-ray scattering equipment setup for liquid (solution) samples. X-rays generated by x-ray source are focused and deflected using a 3D mirror (1) passing through collimation slits (2a and 2b) to create a narrow focused beam. The x-rays continue into the sample stage (3), where it passes through a solution in a capillary. The resulting x-rays pass through the flight chamber (4) with the scattered x-rays spreading out at different angles. The x-rays are collected at the detector camera, with the non-scattered radiation absorbed by the beam stop (not pictured). In nearly all cases, components (2) and (4) are under vacuum to prevent scattering of x-rays by air molecules. Depending on experiment the sample chamber (3) can be either in an atmosphere or under vacuum.

Scattering information is then recorded as 2D patterns using a detector, acting as a camera. If samples are isotropically averaged, i.e. randomly orientated and distributed in space, the patterns will be isotropic around the centre. Conversely, if the materials are orientated and aligned, this will be represented by an anisotropic pattern. This anisotropy can be quantified in one dimension by integrating the intensity pattern as a function of the scattering angle. In order to improve the statistics for isotropic samples, 2D data are integrated azimuthally to determine the intensity as a function of the distance from the centre of the pattern, which equates to the scattering vector length. This is then averaged over all (angles around) the detector (Figure 2.2).

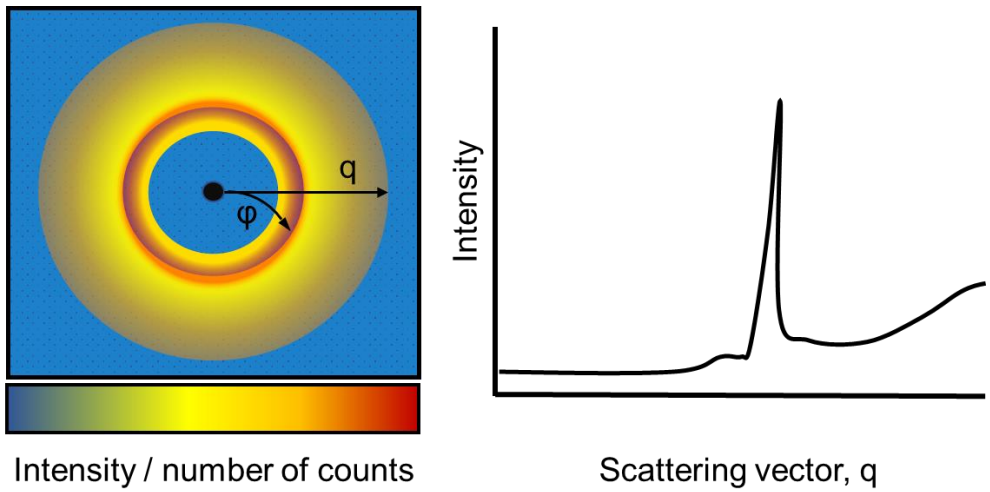

Figure 2.2: Example of an isotropic 2D scattering pattern (left), with the arrows indicating the direction of the scattering vector length (q) and the azimuthal angle (φ). 1D integrated scattering pattern calculated from the 2D image. The peak corresponds to the intense (red) scattering region with the highest x-ray intensity.

The intensity $I(q)$, at a given scattering vector (q), is the product of the scatterers concentration, their shape and distribution in space, and the scattering length density (SLD) contrast (Equation 2.3). SLD is the relative scattering power and is defined by the number of electrons per unit length of a particular compound, which is dependent on the chemical composition and mass density.

$$I(q) = S(q)P(q)DV^2\Delta\rho^2 \qquad \text{eq. 2.3}$$

Where S(q) is the structure factor which describes how the scatterers are distributed in space with respect to each other, P(q) is the form factor that describes shape of the scatterers, D is the number of scatterers per unit volume, V is the volume of the scatterer, and $\Delta\rho$ is the difference in SLD or contrast. For successful measurements to occur, there must be adequate contrast between the SLD (Equation 2.4) of the medium and the scatterer. This is problematic in some cases where the composition and

density of the solvent and scatterer are similar, in which case alternative techniques such as neutron scattering can be used.

$$\rho = \frac{D_m N_a b_e}{M_w} \sum n_i b_i \qquad \text{eq. 2.4}$$

Where D_m is the mass density, N_a is Avogadro's constant, b_e is the scattering length of an electron, M_w is the weight average molecular weight (weight averaged), n_i is number of *i*th atoms in the molecule, and b_i is the number of electrons in the *i*th atom.

There are two types of function that describe inhomogeneities in electron density for solutions that give rise to scattering. Firstly, the form factor P(q) describes the scattering arising from objects in space, in particular their size and shape (Figure 2.3). Secondly the structure factor S(q) describes the distribution of particles in space. Particle interactions are weak at low concentrations and hence have minimal effect on scattered intensity. Thus, the structure factor term can be neglected for such colloidal systems. Comparatively, if scatterers are more concentrated, or are charged, effect of particle interactions is more pronounced and has to be accounted by the structure factor term. An example of this is the organisation of ionic surfactant micelles in solution to minimise inter-micelle repulsion, often modelled using the Hayter-Penfold mean spherical approximation (Figure 2.3).[6,7]

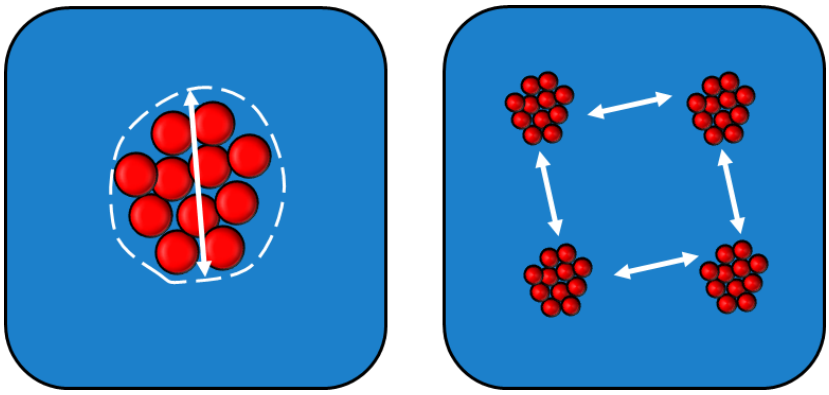

Figure 2.3: Visualization of (left) particle shape, which is accounted for by the form factor P(q) and (right) interaction of charged micelles in semidilute solution experiencing intermicellar ionic repulsion, which is accounted for by the structure factor S(q).

Wide-angle scattering is often captured using a separate instrument, using adjustable positions in space to collect signal at different angles. However recent iterations of SAXS instruments can implement a secondary stationary detector to collect WAXS simultaneously (SWAXS).[8] This is most beneficial for crystalline materials with nanoscale order.

2.1.3. Processing and Data Reduction

Following transformation of 2D data into 1D patterns, further processing must occur before the resulting scattering pattern can be analysed. The number of data points are reduced to minimise computational load. The background scattering of the sample and the instrument must then be subtracted.

In scattering experiments, the background scattering has multiple origins: Firstly, from incoherent scattering and from instrumental noise. This equates to a constant value that can be accounted for. Secondly, coherent background scattering originates from the material the scattered x-ray has to pass through, that are not the focus of the measurement. In solution scattering, this originates from thermal density fluctuations in the solvent and the sample holder or capillary that houses the mixture, as well as any barriers (windows) the x-ray must pass through. This is achieved by completing a background scan under the same conditions, which for solutions will contain only the solvent in a capillary tube. The background scattering pattern can then be subtracted from the sample, once the intensity is scaled appropriately. The resulting background-corrected scattering pattern can then either be used or scaled to absolute intensity to account for the flux of x-rays and the volume of irradiated material. An efficient method is to scale collected data to use a readily available scatterer with minimal structural features and a solvent with a known differential scattering cross-section value such as water. Scaling to absolute intensity is useful as some analytical models require this to calculate volume fractions of components.

2.1.4. Generalised Scattering Approximations

Generalised approximations and mathematical models are used to determine size and shape parameters of soft matter objects. While there are many different types, a brief overview of relevant systems is included. The Guinier approximation states that regardless of particle shape, the radius of gyration (R_g) can be measured at small values of scattering vector (q) (Equation 2.5).

$$P(q) \approx I_o e^{-\frac{q^2 Rg^2}{3}} \qquad \text{eq. 2.5}$$

Where I_0 is the intensity of the incident beam. The approximation is considered accurate only at very small angles ($qR_g << 1$). At high q ($qR_g >> 1$), the Porod approximation becomes valid. While the Guinier approximation relates to particle size, the Porod approximation relates to particle surface area (S). At the highest values of q, intensity I(q), decays uniformly (Equation 2.6).

$$I(q) \propto Sq^{-4} \qquad \text{eq. 2.6}$$

In the intermediate region between Guinier and Porod, the shape can also be elucidated. This is called the intermediate, fractal, or Fourier regime and mainly represents shape and internal structure of the scatterers.[1] The slope of the region informs the shape: a power law slope is observed, with integer values n = 1 (Equation 2.7) indicating rod-like particle shape, n = 2 corresponds to discs or Gaussian polymer chains, and n = 0 indicating spherical particles.

$$I(q) \propto q^{-n} \qquad \text{eq. 2.7}$$

Generalised slopes can also determine the type and degree of fractality in a system e.g. a gel matrix. From n = 2 to n = 3, mass fractals such as gels are seen, and above n = 3 and below 4 surface fractals are observed.[9]

2.1.5. Scattering by Soft Matter Materials

Modelling of globular polymers in solution that correspond to a Gaussian coil in theta solvent conditions can be achieved using the Debye function (Equation 2.8).[10] It comprises a low q component for the change in Rg, and a high q component that decays with a power law of 2. This does not correspond to extended or wormlike chains which are modelled differently.

$$P(q) = \frac{2\left(e^{-(q^2R_g^2)} + q^2R_g^2 - 1\right)}{(q^2R_g^2)^2} \qquad \text{eq. 2.8}$$

Where R_g is the polymer radius of gyration. While homopolymers in solvent have two SLD's (one for the scatterer, one for the solution), ionic surfactant micellar solutions have 3 regions of differing SLD (the core, shell, and the solvent). In aqueous solution, this generally results in the solvent having intermediate density compared to the less dense alkyl chain and the higher SLD shell, although the addition of organic cosolvents can change this scenario. To account for the component distribution in the particles (micelles), a core-shell structural model is used. The critical packing parameter (CPP) predicts spherical micelles, but ellipsoidal micelle models are often found to give better fits to the scattering curves. A robust method to assess micelle shape is therefore the core-shell ellipsoid model (Figure 2.4). While some models treat shell thickness (T_{shell}) as variable, for small molecule surfactants this is unphysical as the small ionic headgroup cannot change conformation unlike a polymer chain. Therefore, a constant value of T_{shell} around the micelle is assumed when fitting this model.

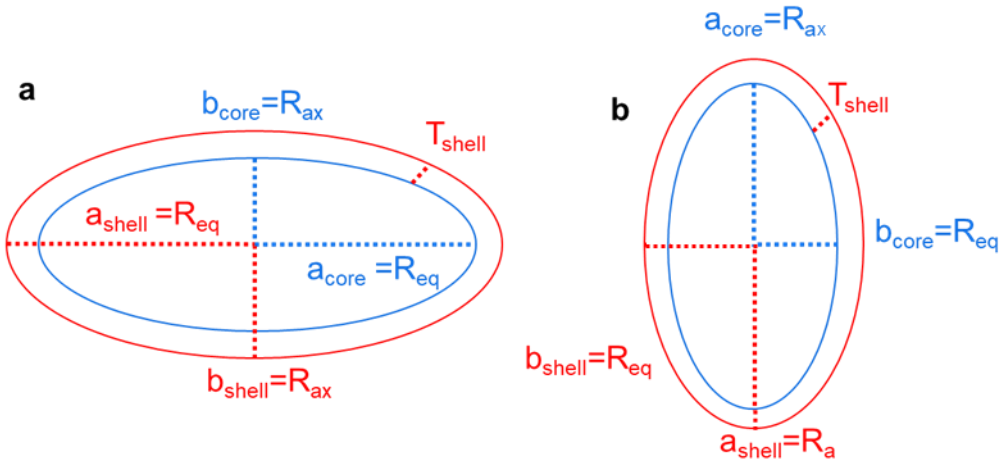

Figure 2.4: Visualisation of structural features of a core (blue) – shell (red) ellipsoid model, with fixed shell thickness. Ellipsoids can be a) oblate or b) prolate. The semi-major axis (a) and semi-minor axis (b) of the ellipsoid differs depending on which type is formed.

The generalised form factor of an (uniaxial) ellipsoid or core-shell ellipsoid is a function of the semi-major (a) and semi-minor axes (b), and an orientational variable (μ), which differ depending on the aspect ratio of the micelle.[11,12] To calculate the mean thickness, the shell is initially treated as a larger ellipsoid surrounding a smaller core ellipsoid, with the relationship as follows.

$$T_{shell} = a_{shell} - a_{core} = b_{shell} - b_{core} \quad \text{eq. 2.9}$$

To calculate the form factor ($\langle|P(q)|^2\rangle$) of a core-shell ellipsoid.[11,13,14]

$$\langle|P(q)|^2\rangle = scale \int_0^1 |P(a,b,\mu)|^2 d\mu \ + \text{background} \quad \text{eq. 2.10}$$

Where $P(a,b,\mu)$ is the single particle structure amplitude, which equates to

$$PP(q,a,b,\mu) = 3(\rho_{core} - \rho_{shell})V_{core}\left[\frac{j_1(u_{core})}{u_{core}}\right] + 3(\rho_{shell} - \rho_{solvent})V_{shell}\left[\frac{j_1(u_{shell})}{u_{shell}}\right] \quad \text{eq. 2.11}$$

When particle orientations are randomly oriented. Here V is the ellipsoid volume, ρ is the SLD and $j_i(u)$ is

$$j_1(x) = (sinx - xcosx)/x^2 \quad \text{eq. 2.12}$$

Values for V_{core} and V_{shell}, along with u_{core} and u_{shell} are calculated in the same way, with different coefficients representing the length of the axis etc. (Figure 2.4). However, the values for V and u depend on the aspect ratio of the micelle.[12] When the ellipsoid is prolate:

$$u = q[a^2(1-\mu^2) + b^2(1-u^2)]^{\frac{1}{2}} \quad \text{eq. 2.13}$$

and

$$\mathrm{V(a,b)} = \left(\frac{4\pi}{3}\right) ab^2 \quad \text{eq. 2.14}$$

Similarly, for an oblate ellipsoid

$$u = q[a^2(1-\mu^2) + b^2u^2]^{\frac{1}{2}} \quad \text{eq. 2.15}$$

and

$$\mathrm{V(a,b)} = \left(\frac{4\pi}{3}\right) a^2b \quad \text{eq. 2.16}$$

For particles with limited ionic functionality, the interaction between different particles will be primarily through steric or excluded volume interactions. For objects that possess significant charge density, including ionic micelles, repulsive interactions lead to maximising distance from other neighbouring objects to minimise the effects of the electrostatics. These interactions are captured by the structure factor. Structure factors generally describe spherical objects, and this should be considered when coupled with non-spherical form-factors. Organisation of repulsing ionic objects is described by Hayter and Penfold,[6,7] which is a function of the physical properties such as temperature, object size, and volume fraction, as well as electrical properties such as the charge density, the dielectric constant and salt concentration. This is required to account for the electrostatic repulsion.

2.1.6. Scattering by Ordered Periodic Structures

Diffraction from ordered structures is a type of structure factor, as it describes the periodic position, as opposed to their size and shape. While crystals exhibit long-range order in three dimensions, other molecular assemblies can also exhibit diffraction. For example, liquid crystals can exhibit diffraction,[15]

whereby a structure may exhibit positional order,[16] but not high levels of both long range orientational and positional order like a true crystal. When regular spacing occurs, a diffraction peak is observed in the scattering pattern (Figure 2.1). When the peak is sharp as opposed to broad and diffuse it is indicative of a high degree of long-range order, and such peaks are referred to as Bragg peaks. The relationship between the real spacing and the peak position expressed in units of scattering vector length is as follows:

$$d = \frac{2\pi}{q} \qquad \text{eq. 2.17}$$

Where d is the spacing. Due to the Bragg condition, peaks at low q correspond to the largest size. Large crystal unit cells, or large assemblies such as liquid crystals, will give rise to peaks in the SAXS region, as opposed to WAXS. The smallest representative structure that defines the repeating lattice of a crystal is called the unit cell. There are 14 Bravais lattices which describes types of all unit cells, which can be further categorised into point group and beyond depending on their symmetry.[17] Each can be characterised by different 'crystallographic planes' assigned by Miller indices (Figure 2.5).

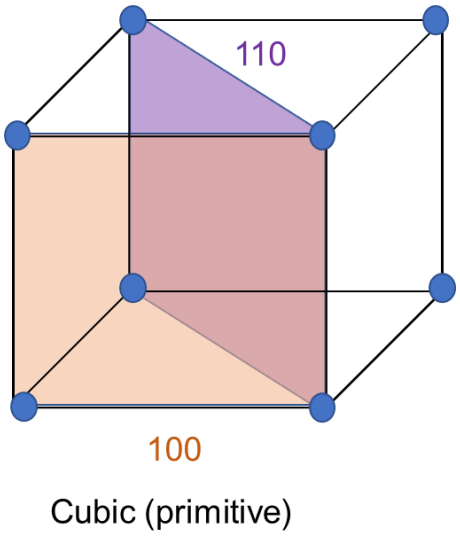

Figure 2.5: Example of a Bravais lattice: cubic primitive, with two examples of crystallographic planes with Miller indices 100, and 110 planes.

Miller indices can be determined through the Bragg peak position. Diffraction patterns are orientation-dependent and are best obtained from a single crystal. However, in an isotropic mixture such as a powder, this is averaged out to form Bragg peaks that are orientation independent. Bragg peaks can be used to determine unit cell structure. The more peaks that can be observed the more planes that are evident. However, while some peaks are easy to identify, others are difficult. Indexing can be used,

which can be conducted manually or through various algorithms, which uses peak spacing information to find a symmetry that satisfies all peaks.[18] Certain relative peak positions are indicative of specific structures. For example, lamellar structures have peak orders (e.g. in the 00x plane) that increases in a $q(n+1)$ manner (where q is first-order peak position and n is an integer), whereas hexagonal structures have peak ordering that increase by non-integer coefficients.[1]

While the peak position can reveal crystal symmetry, peak intensity can inform electron density distribution.[19] This extends to non-crystallizable ordered materials, where obtaining a single crystal is not possible. Instead, in certain cases, isotropic data such as powders can be studied to give electron density of a crystal across one dimension. This is evident for lamellar structures as they are packed along the lamellar normal in a repeatable fashion. The technique is most easily applied to molecules containing different atoms in distinct regions with identification of the different regions of electron density. This approach was developed for crystalline fats and lipids, where the positions of different regions (glycerol or head group, respectively) within a molecule can be identified (Figure 2.6).[19–21] The method can also be used for non-crystalline periodic structures provided a few diffraction peaks are generated.

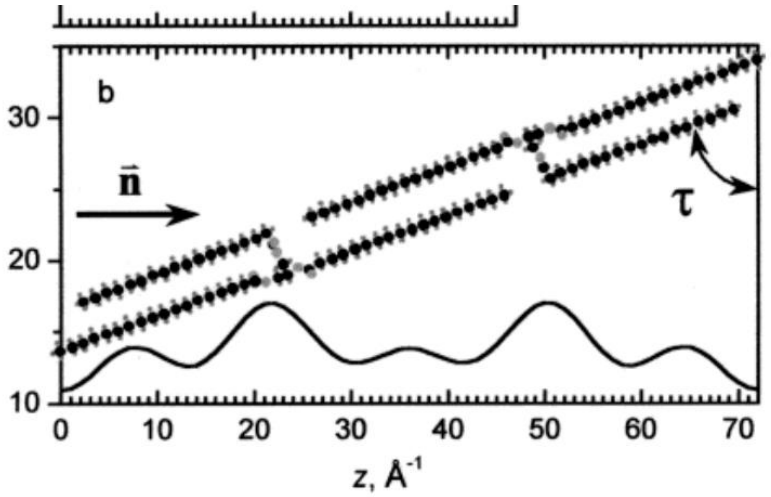

Figure 2.6: Reproduction from Mykhaylyk and Hamley.[21] Electron density profile along the layer normal of a triacylglyceride crystal, used as an aid for structural determination, and plotted as intensity versus distance along a bilayer. The presence of different glycerol groups can be shown to form the structure and molecular tilt evidenced by the structural diagram.

The construction of electron density profiles is achieved by an inverse Fourier transform to reconstruct the structure factor. The information used for this is the structure amplitudes originating from Bragg

peak position and intensity. Each peak contributes a single structure amplitude, leading to a wave term used to form the electron density profile.[22] The more diffraction peaks that are present, the more waves are used to reconstruct the electron density profile, theoretically giving better resolution of the profile. However, there is a complication, as the number of peaks is increased, the number of waves is subsequently increased. Due to the conditions of the transform, each experimental peak recorded will give rise to two possible outcomes, resulting in 2^n different combinations, where n is the number of peaks. While some combinations of waves are inverse or translated, only one combination of phases will correspond to the real electron density distribution in the unit cell. This is referred to as the phase problem.[23] In some cases phase determination can be solved by examining analogous structures. Alternatively, for non-crystalline systems, changing the spacings systematically can yield the correct phase. An example of this is in non-crystalline lamellar phases, where solvent content is increased to swell the molecule and increase the solvent region between the bilayers, which is reflected in the resulting electron density profile.[23] This technique is powerful, although not always applicable.

2.2. Optical microscopy

Optical microscopy (OM) is used to image and measure objects on the micron size scale in real space. It is complementary to scattering techniques, in particular SAXS, as larger aggregate structures can be compared to the microstructure previously determined. Polarised optical microscopy (POM) explores the birefringence of optically anisotropic micron-sized objects. Birefringence is a property of materials characterised by two or more refractive indexes depending on the material symmetry and orientation. Many crystals exhibit birefringence due to their structure which contains multiple indices of refraction. However, orientationally isotropic crystals such as the cubic crystal structure of NaCl do not exhibit this property as the refractive index is equivalent in all directions.[24] When light passes through optically anisotropic materials, it is split into two perpendicularly-polarised rays, called the ordinary and extraordinary, which travel via two different paths. This causes the exiting waves to be polarised in a different manner to the incident wave. The study of birefringence is not possible with unpolarised light, as the isotropic nature of the light source would negate the effect. While the colour of birefringence can be quantified,[25] the study of birefringent materials is used heavily in a qualitative manner to understand what types of phases present e.g. liquid crystals and crystals, as well as to determine the orientation and rotation of structures.

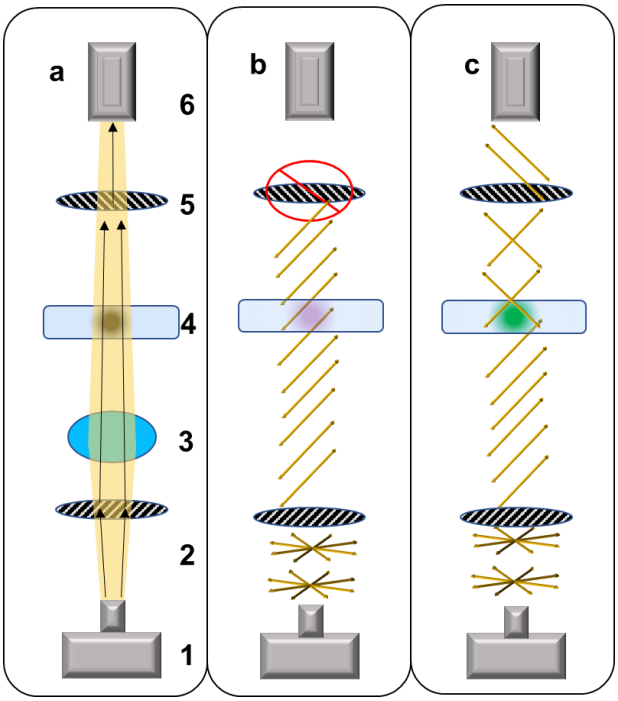

Figure 2.7: a) Generalised diagram of a polarised optical microscope. (1) Unpolarised light is generated and passes through a (2) polarised filter (polariser), before being focused using a condenser lens (3). The light then passes through the sample (4) before passing through another filter (analyser) (5) which is then recorded by a camera or detected by optics (6). b) Diagram showing the polarisation of light and the path through a non-birefringent (isotropic) sample. Non-polarised light passes through a filter to form linearly-polarised light in one direction. This does not change when interacting with the sample and is blocked at the analyser. c) Diagram showing the polarisation of light and the path through a birefringent sample, where the incoming linearly-polarised light changes the status of polarisation when passing through the sample. This allows light through the analyser with its plane of polarisation crossed at 90° to the polariser plane.

POM is achieved the same way as traditional optical microscopy, with the addition of polarised light filters (Figure 2.7). The first, called the polariser, is placed before the sample stage, and causes the light to become linearly-polarised along one direction. This polarised light then passes through the sample and then passes through a second polarisation filter (analyser) with its plane of polarisation crossed at 90° to the polariser plane. For isotropic systems, e.g. a liquid, the light passes through the material, experiences negligible change in orientation and is blocked by the second polarizing filter. For birefringent materials, the polarization direction is modified, and some light passes through the second filter.[26]

2.3. Rheology

2.3.1. Equipment

Rheology is the study of a material's deformation under an applied force. For example, a shear force can be applied to a soft matter material using two parallel discs separated by a fixed gap filled with the material, where one disc rotates around its central axis with respect to the other (Figure 2.8a). The rotation could be continuous (steady-state) or oscillatory when the disc rotation periodically changes its direction. The apparatus is called a rheometer and can use various geometries depending on the sample (Figure 2.8).

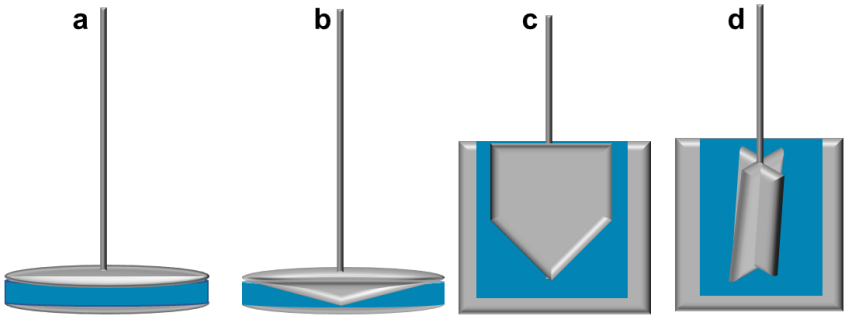

Figure 2.8: Common rheometer geometries (grey) containing sample (blue): a) parallel plate, b) cone and plate, c) Couette cell/ cup and bob cell/coaxial cylinder cell and d) vane/rotor geometry.

Each geometry confers practical benefits depending on the sample. Parallel plate geometries are the simplest (Figure 2.8a) and vary in size. The shear rate is not uniform across the diameter as the outer material must travel faster to conserve angular momentum. However, it is commonly exploited for oscillatory rheology where angular movement of the geometry fixtures, which are the same at all radial positions, are used for the measurements. Cone and plate geometry (Figure 2.8b) allows for more accurate measurement due to the uniform shear rate across the sample. This is because shear rate is a function of sample height, which varies with the distance from the centre. Thermal experiments are easily performed on plate-plate and cone-plate geometries due to the efficient heat transfer from the large sample surface area to its volume. Further improvement in measurement quality can be attained using a cup and bob, or Couette cell (Figure 2.8c), which can eliminate sample edge effects observed in plate-plate and cone-plate geometries. This includes material drying, or expulsion of material from the sample cell.[27,28] However larger sample volumes are required. For highly viscoelastic mixtures, vane geometries (Figure 2.8d) provide an alternative option that prevents a phenomenon called wall slip,

which can occur with lower surface area geometries. However, where only small sample volumes are available, plate-type geometries with rough or crosshatching surfaces can be used.

2.3.2. Steady-state Rheology

Steady-state rheology is the measurement of a material when a constant force (F) is applied in a certain direction. The applied force is normalised over area (A, Figure 2.9) to give a shear stress (τ).

$$\tau = F/A \qquad \text{eq. 2.18}$$

Shear rheology can be envisioned as plates moving in a response to shear force (Figure 2.9), where the bottom plate, representing the lower geometry is stationary and the top plate is the advancing front.[29] The magnitude of the moving geometry is defined by shear rate (Equation 2.19).

$$\dot{\gamma} = \frac{\left(\frac{x}{time}\right)}{h} = \frac{v}{h} \qquad \text{eq. 2.19}$$

Where *x* is the distance moved, *h* is the sample gap, and *v* is velocity. Shear strain is also used to define the amount of material deformed, which is the distance divided by the sample gap (Equation 2.20).

$$\gamma = \frac{x}{h} \qquad \text{eq. 2.20}$$

Viscosity is used to define how 'thick' a fluid is. It is defined as a measure of how much normalized force is required to move an object (equation 2.21).

$$\eta = \tau/\dot{\gamma} \qquad \text{eq. 2.21}$$

A fluid's response to shear can either be Newtonian or non-Newtonian. Newtonian materials respond uniformly to shear, regardless of the time of shearing and shear rate. Non-Newtonian liquids behave differently: their response to shear can be time-dependent and/or shear rate-dependent, which can be measured using steady-state rheology.

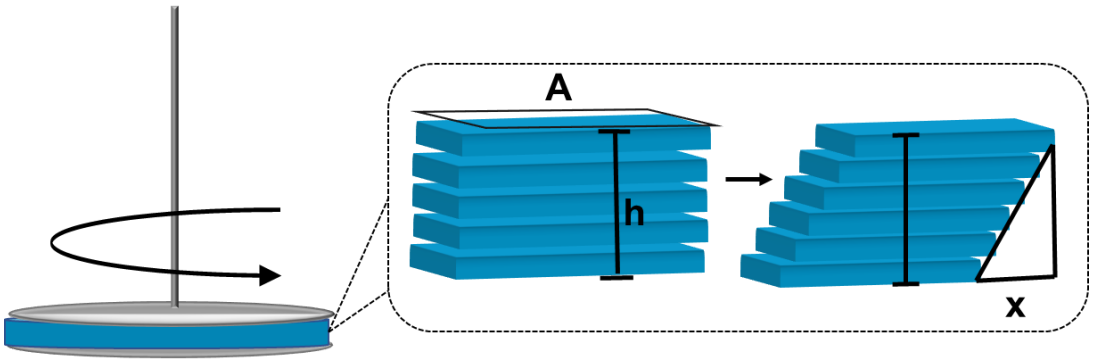

Figure 2.9: Visualisation of the plate model to describe shear rheology, where the deformation of a material caused from a force applied from a top moving geometry and stationary bottom plate. A is the plate area, h is the height or the sample gap, x is the displacement (distance moved).

Viscoelasticity is also a type of non-Newtonian behaviour often measured using oscillatory rheology. The most common time-dependent behaviour is thixotropy, which is when viscosity decreases over time. Shear rate-dependent viscosity is often described as shear-thickening or shear-thinning, although other types are possible, e.g. Bingham plastic. Shear rate-dependent behaviour is measured by flow curves where the shear rate is increased or decreased incrementally and the change in viscosity is measured. An example of a shear-thinning mixture is toothpaste, which is initially highly viscous but under shear of brushing, reduces its viscosity.

Various models exist to describe dependence of material viscosity on shear rate. The most common is the Cross model (Equation 2.22).[30] This is relevant for viscoelastic fluids that experience a high viscosity at low shear rates, and 'yield' at a specific point with a power law-dependent lowering of viscosity, until a limiting plateau value is reached (Figure 2.10).

$$\eta = \eta_{inf} + \frac{\eta_0 - \eta_{inf}}{1+(C\dot{\gamma})^n} \qquad \text{eq 2.22}$$

Where η_{inf} is the infinite shear viscosity plateau, η_0 is the zero shear viscosity plateau, C is the Cross constant, and n is the degree of shear-thinning (given as a positive value) representing the power law gradient of the shear-thinning region. An example of Cross behaviour is shown in Figure 2.10, with representation of the model's parameters. While this behaviour is not seen in all shear-thinning materials, it is highly applicable to polymer solutions, where a minimum shear rate is required to disentangle and align polymer chains parallel to the flow direction.[29] Other models can measure aspects of shear-thinning and thickening. The Sisko model[31] can be used if no zero shear viscosity plateau is present, which forgoes a zero shear plateau, but contains a power law dependency followed by a high shear plateau.

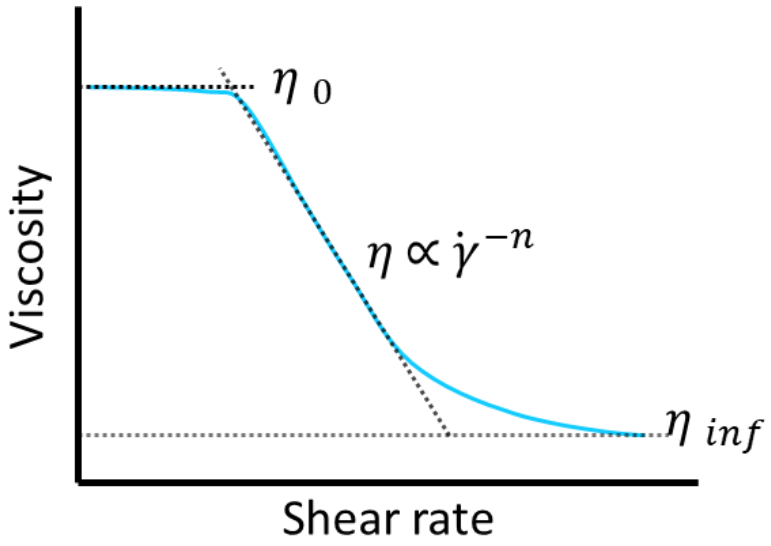

Figure 2.10: Shear-thinning behaviour, conforming to the Cross model, with visualisation of parameters for zero shear viscosity (η_0), infinite viscosity (η_{inf}), and degree of shear-thinning (n).

In addition, other tests can be used to probe behaviour undetectable by flow curves. Creep recovery tests are used to determine the deformation and recovery of materials, this is valuable for applicative properties in personal care, e.g. when squeezing a tube of toothpaste, the toothpaste is expected to recover and remain as a defined shape on a toothbrush. However, to measure the elasticity of a sample, oscillatory rheology must be used.

2.3.3. Oscillatory Rheology

Oscillatory rheology is performed to determine both the elastic (storage modulus, G') and viscous (loss modulus, G'') properties of a material. Instead of a steady shear, the rheometer geometry moves at a constant frequency through sinusoidal application of shear amplitude in two directions (Figures 2.11), with the material response being measured. In purely elastic solid, the material will respond in phase and follow the applied shear. For purely viscous materials, e.g. water or glycerol, the elastic component is negligible, so as one oscillation takes place (Figure 2.11), the material will respond out of phase as it is purely viscous, with a phase angle (δ) of 90 °. For a viscoelastic material, the response is an intermediate value, resulting in a phase difference lower than 90 ° which used to calculate viscoelastic properties (Figure 2.11).

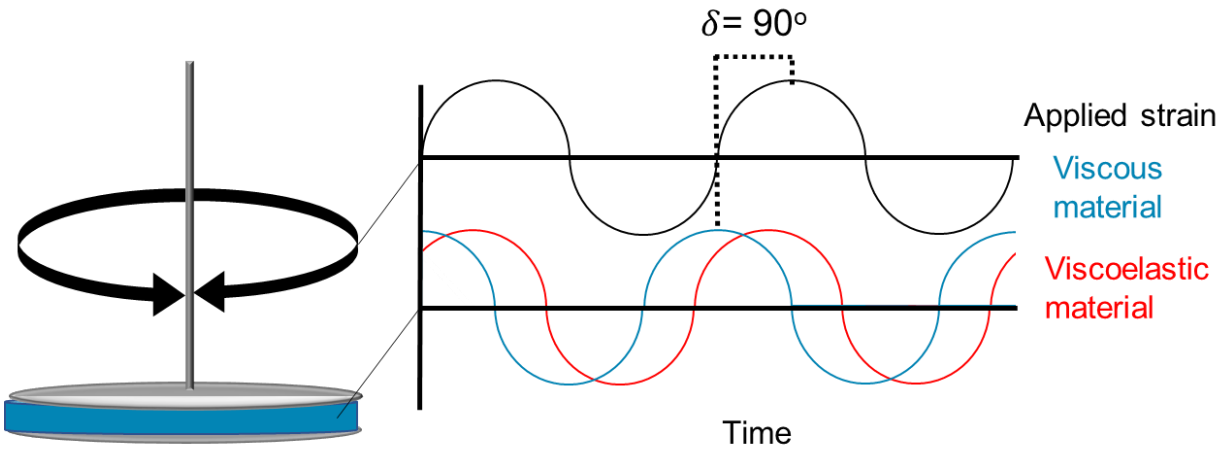

Figure 2.11: Example of oscillatory rheology measurement where a sinusoidal strain is applied (black) to a sample. A viscous material (blue) responds out of phase, with its response offset 90 ° compared to a wholly elastic material which responds in phase (not shown for clarity). A viscoelastic material (red) responds with an offset less than 90 ° due to contributions from both elastic and inelastic components.[32]

Materials do not respond similarly to all shear strains. There is a linear viscoelastic range (LVER), where stress and stain are linear, and beyond this range the material behaviour is less defined and more complex. Therefore, to measure the response of a material to different frequencies (frequency sweep), the linear viscoelastic range must be determined. This is achieved by performing an amplitude sweep at a fixed frequency, which consists of oscillatory strain increasing incrementally, with the response being measured (G', G''). The results show a plateau for the LVER, with a primarily negative dependence after this as the structure is 'broken'. A strain can then be chosen within the LVER to measure the response to frequency. Generally, the higher the strain within the LVER, the reduced amount of noise and more reliable measurements can be performed. Within the LVER, the storage modulus (G') can be defined from the ratio of the in-phase stress and strain.

$$G' = \frac{\tau}{\gamma}\cos(\delta) \qquad \text{eq. 2.22}$$

While the Loss modulus (G'') is derived from the out-of-phase stress and strain ratio.

$$G'' = \frac{\tau}{\gamma}\sin(\delta) \qquad \text{eq.2.23}$$

Complex viscosity can be defined as the frequency of the complex modulus, which is derived from the vector product of G' and G''. While it has a different meaning to viscosity under constant shear, empirical observations have shown in some cases there is a close relationship such as the Cox-Merz rule.[33,34]

2.3.4. Rheo-optical Techniques

Material birefringence and stress can be related via stress-optical coefficient. This property of materials is often exploited by rheo-optical techniques. In this respect, shear induced polarised light imaging (SIPLI) techniques, which is a combination of mechanical rheology with an optical polariscope (Figure 2.12), is developed to measure molecule birefringence/polarizability under shear.[35,36] The optical setup is similar to that used for polarised optical microscopy (Figure 2.7). However, for an isotropic mixture of birefringent particles, for example a crystalline suspension, the sample will be 'bright' only when the particles are aligned (for example, by a shear flow).

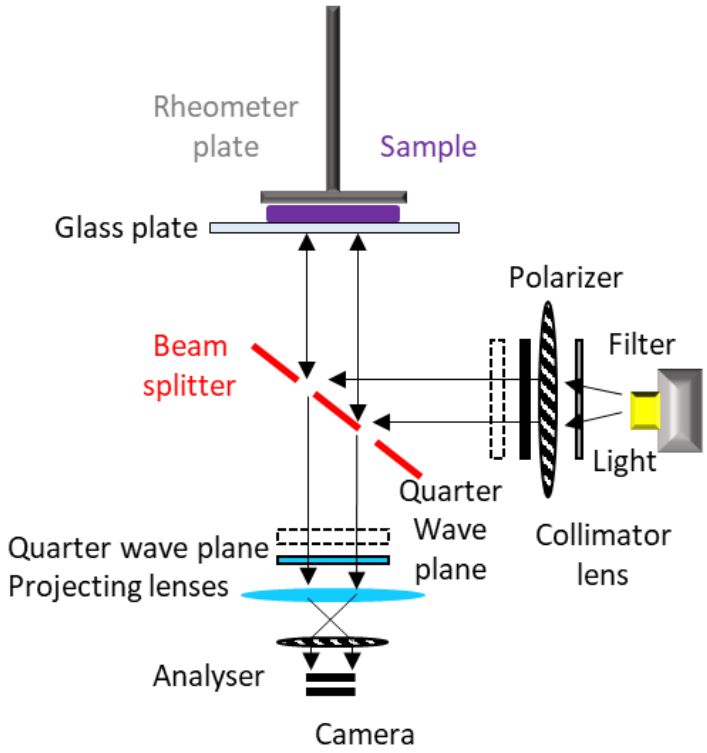

Figure 2.12: Schematic representation of SIPLI apparatus.[36] Polarised light is generated and reflected by the beam-splitter to pass through the sample which is in turn reflected by the rheometer mirror plate. Following this, the light is focused and passes through another polarised filter (analyser) with its plane of polarisation orientated at 90° with respect to the polariser plane, before being recorded by the camera.

When the particles align parallel to a shear direction the bulk material becomes birefringent and polarisation occurs, resulting in different polarised light images. For example, a Maltese cross will appear if the sample changes the polarisation of incoming light, and only then the light will pass through the analyser (Figure 2.13). This allows the determination of alignment under shear and hence interpretation of the sample's rheological behaviour, aiding characterisation of the microstructure. Furthermore, the contrast can indicate the degree of alignment of the structure. As a parallel plate

induces a gradient of shear, the observance of dark regions in the centre indicates the presence of a critical alignment shear rate, which must be exceeded to align the sample and form a Maltese cross.[36]

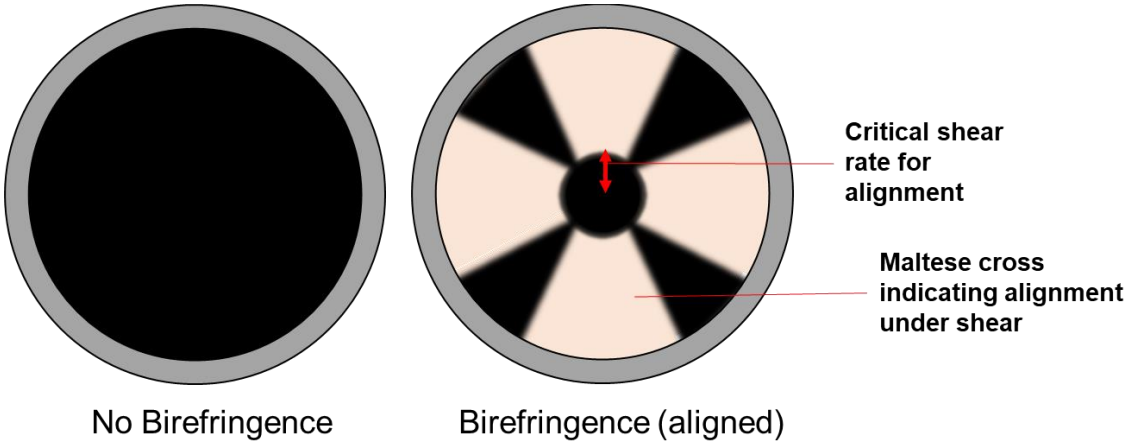

Figure 2.13: Schematic illustration of the orientation of birefringent material above a critical shear rate, resulting in Maltese cross formation, obtained using SIPLI apparatus while the sample is sheared. When no birefringence is observed, the sample is dark due to the plane polarised light being blocked by the analyser.

2.4. Differential Scanning Calorimetry

Differential scanning calorimetry (DSC) is the study of heat that is absorbed or released by a material when it undergoes a temperature-induced structural or phase change. It is used for primary phase transitions including melting and cooling, but it can also be used for the glass transition of polymers. Measurement of the transition is achieved by measuring a small amount of sample in a metal pan with a lid, compared to a reference empty pan. The difference in energy required to heat the sample to a given temperature is measured: any endothermic processes will require more energy to heat, and any exothermic processes will require less energy to heat when compared to the reference. A DSC experiment can be measured in two ways. In power-compensated DSC, the two pans are in separate insulated chambers and the difference in electrical energy required to heat the material equates to the energy of the transitions that occur. Alternatively, in heat flux DSC, the samples are contained in a single furnace and the difference in temperature equates to the change relative the reference material.[37] For some materials it is beneficial to take a baseline. In solutions this can be the solvent, so that only the thermal properties of the material in question are studied. This is applicable for melting and crystallization of solutes, e.g. a surfactant.

When measuring the melting transition of substances, a DSC trace should produce one distinct melting peak. However, non-equilibrated, impure, and non-uniform thermal transfer causes a melting range which consists of an onset, peak, and end-set. Choice of experimental conditions and cooling temperature can improve this situation, although it can be highly dependent on sample composition, it is common to observe melting ranges as opposed to specific melting points.[9]

2.5. Infrared Spectroscopy

Fourier transform Infrared (FT-IR) spectroscopy is the study of the vibrational energy of bonds within molecules. It can be performed in solution, or in the solid state. For solids/powders the spectrum is recorded via through attenuated total reflectance (ATR) of a crystal, on which the sample is placed. This technique can be used to identify different compounds or changes to structure. Moreover, non-covalent bonding can be probed, as it alters the vibrational frequency of adjacent covalent bonds. It is performed by irradiating the sample with infrared light (expressed as wavenumbers, which is inversely related to wavelength). The absorbance of radiation occurs when it is of the same energy as the vibrational frequency of a particular bond. This absorbance is then plotted against the wavenumber. Various types of bonds absorb have different associated energies, and therefore absorb in differing regions. One strongly absorbing group is the alcohols, with the O-H bond ranging from 2500-3500 cm^{-1}. Therefore for aqueous or alcoholic solutions the background must be subtracted.

2.6. References

1 H. Schnablegger and Y. Singh, *The SAXS Guide*, Austria, 3rd edn., 2013.
2 D. L. Price and K. Skold, *Methods in Experimental Physics*, 1986, **23**, 1–97.
3 L. A. Feigin and D. I. Svergun, *Structure Analysis by Small-Angle X-Ray and Neutron Scattering*, Springer US, Boston, 1987.
4 T. Narayanan, O. Diat and P. Bösecke, *Nuclear Instruments and Methods in Physics Research Section A: Accelerators, Spectrometers, Detectors and Associated Equipment*, 2001, **467–468**, 1005–1009.
5 R. den Adel, K. van Malssen, J. van Duynhoven, O. O. Mykhaylyk and A. Voda, *European Journal of Lipid Science and Technology*, 2018, **120**, 1–6.
6 J. B. Hayter and J. Penfold, *Molecular Physics*, 1981, **42**, 109–118.
7 J. Hansen and J. B. Hayter, *Molecular Physics*, 1982, **46**, 651–656.
8 In-situ SWAXS measurements in the lab are proving their worth - Xenocs, https://www.xenocs.com/in-situ-swaxs-measurements-in-the-lab-are-proving-their-worth/, (accessed 13 April 2021).
9 B. Hammouda, *Probing Nanosacle Structure - The SANS Toolbox*, 2008.
10 P. Debye, *The Journal of Physical and Colloid Chemistry*, 1947, **51**, 18–32.

11 S. S. Berr, *Journal of Physical Chemistry*, 1987, **91**, 4760–4765.
12 M. Kotlarchyk and S. H. Chen, *The Journal of Chemical Physics*, 1983, **79**, 2461–2469.
13 NIST, *SANS Model Function Documentation*, 2012.
14 S. L. Gawali, M. Zhang, S. Kumar, D. Ray, M. Basu, V. K. Aswal, D. Danino and P. A. Hassan, *Langmuir*, 2019, **35**, 9867–9877.
15 J. G. An, S. Hina, Y. Yang, M. Xue and Y. Liu, *Reviews on Advanced Materials Science*, 2016, **44**, 398–406.
16 C. Rodríguez-Abreu, Y. V. Kolen'ko, K. Kovnir, M. Sanchez-Dominguez, R. G. Shrestha, P. Bairi, K. Ariga and L. K. Shrestha, *Physical Chemistry Chemical Physics*, 2020, **22**, 23276–23285.
17 A. S. Myerson, D. Erdemir and A. Y. Lee, Eds., *Handbook of Industrial Crystallization*, Cambridge University Press, Cambridge, 2019.
18 L. Jiang, D. Georgieva and J. P. Abrahams, *Journal of Applied Crystallography*, 2011, **44**, 1132–1136.
19 O. O. Mykhaylyk, K. W. Smith, C. M. Martin and A. J. Ryan, *Journal of Applied Crystallography*, 2007, **40**, 297–302.
20 O. O. Mykhaylyk and C. M. Martin, *European Journal of Lipid Science and Technology*, 2009, **111**, 227–235.
21 O. O. Mykhaylyk and I. W. Hamley, *Journal of Physical Chemistry B*, 2004, **108**, 8069–8083.
22 N. Y. D. Li, Š. Perutková, A. Iglič and M. Rappolt, *Elektrotehniski Vestnik*, 2017, **84**, 69–75.
23 Z. W. Yu and P. J. Quinn, *Biochimica et Biophysica Acta - Biomembranes*, 2000, **1509**, 440–450.
24 A. K. Bain, *Crystal Optics*, Wiley-VCH Verlag GmbH, Weinheim, First Edit., 2019.
25 B. E. Sørensen, *European Journal of Mineralogy*, 2013, **25**, 5–10.
26 M. G. Corradini and D. Julian McClements, in *Encyclopedia of Analytical Science*, Elsevier, 2019, pp. 47–56.
27 J. Sato and V. Breedveld, *Applied Rheology*, 2005, **15**, 390–397.
28 R. L. Crawley and W. W. Graessley, *Trans Soc Rheol*, 1977, **21**, 19–49.
29 T. Mezger, *The Rheology Handbook*, Vincentz Network, Hanover, Fourth Edition., 2020.
30 M. M. Cross, *Journal of Colloid Science*, 1965, **20**, 417–437.
31 A. W. Sisko, *Industrial & Engineering Chemistry*, 1958, **50**, 1789–1792.
32 D. Weitz, H. Wyss and R. Larsen, *GIT Laboratory Journal Europe*, 2007, **11**, 68–70.
33 W. Gleissle and B. Hochstein, *Journal of Rheology*, 2003, **47**, 897–910.
34 S. Shafiei-Sabet, W. Y. Hamad and S. G. Hatzikiriakos, *Langmuir*, 2012, **28**, 17124–17133.
35 O. O. Mykhaylyk, *Soft Matter*, 2010, **6**, 4430-4440.
36 O. O. Mykhaylyk, N. J. Warren, A. J. Parnell, G. Pfeifer and J. Laeuger, *Journal of Polymer Science, Part B: Polymer Physics*, 2016, **54**, 2151–2170.
37 L. Pekař, *Advanced Analytic and Control Techniques for Thermal Systems with Heat Exchangers*, Academic Press, London, 2020.

3. Materials and Methods

3.1. Materials

Sodium dodecyl sulfate (> 99 %), sodium tetradecyl sulfate (> 95 %), sodium hexadecyl sulfate (~ 60 %), sodium octadecyl sulfate (> 93 %), sodium dodecanoate (99-100%) glycerol (> 99.5 %), sodium dodecyl benzenesulfonate (Technical grade), ethylene glycol (anhydrous 99.8%), 1,3-propanediol (98%), water (HPLC grade), and 1-dodecanol (> 98 %) were purchased from Sigma Aldrich. Sodium dodecyl sulfonate (HPLC grade), sodium decyl sulfate (99%) and NaCl (>99.5%) were purchased from Fisher Scientific. Genu Smart 236 (Iota carrageenan) was kindly donated by Unilever Port Sunlight.

Surfactant-glycerol crystal formation is strongly dependent on the presence of water, powdered materials were dried in a vacuum oven at 60 °C for 12 hours before use to minimise residual water. Water content in glycerol was measured using Karl Fisher titration, kindly performed by Keith Owen. Samples were stored in sealed containers under dry nitrogen atmosphere before measurement. Vacuum distillation was used to reduce the water level below 0.5 Wt.% where applicable.

3.2. Sample preparation

3.2.1. Preparation of Binary Surfactant Gel Phase

The solvent and surfactant were first weighed into glass vials containing a magnetic stirrer. Following this the vessel was sealed and heated to 75°C in an oil bath, unless specified otherwise, with continuous stirring for 30 minutes. The vial was then removed from the oil bath to allow to cool to room temperature for a minimum period of 5 hours undisturbed to allow for quiescent crystallization. The mixtures were stored at room temperature until required for characterisation.

3.2.2. Preparation of Ternary Mixtures Containing SDS and Glycerol.

The solvent and surfactant were first weighed into glass vials containing a magnetic stirrer. Ternary components, including water, 1-dodecanol, or NaCl, were added thereafter. The vessel was sealed and heated to 75 °C in an oil bath, unless specified otherwise, with continuous stirring for 30 minutes. The vial was then removed from the oil bath to allow to cool to room temperature, for a minimum period of 5 hours undisturbed to allow for quiescent crystallization. The mixtures were stored at room temperature until required for characterisation.

3.2.3. Preparation of Ternary and Quaternary Mixtures Containing Carrageenan, Glycerol, Water, and SDS

The polymer and SDS (where applicable) were first weighed into a glass vial. Glycerol was added, and the mixture was immediately dispersed using a spatula to minimise lumping. The vial was then sealed and placed on a roller mill for 15 minutes. The vial was then removed, and water was added. For unheated samples, the sample was then placed on a roller mill for a minimum of 12 hours. For heated samples, a stirrer bar was added, and the sealed vial was heated to 75°C for one hour in an oil bath. After this the stirrer bar was removed and the mixture was allowed to quench quiescently for 5 hours. SDS containing mixtures were not mixed on a roller mill following cooling to maintain crystal aggregate integrity and stored at room temperature. Samples not containing SDS were placed on a roller mill for a minimum of 12 hours.

3.3. Analytical Methods

3.3.1. Polarised Optical Microscopy

Optical microscopy images were recorded at 2.5x, 10x, and 20x magnification using an Axio Scope A1 fluorescence microscope (Zeiss, Jena, Germany) equipped with an Axiocam 105 colour camera. Polariser and analyser crossed at 90° to each other were used for collecting POM images. To minimise flow, which can lead to crystal aggregate break up, the material was delicately and slowly transferred from the vessel to a glass microscope slide using a spatula. A coverslip was then gently placed over the sample and the images acquired. Zen Lite (Zeiss, Oberkochen, Germany) software package was used to operate the instrument and process the collected images.[1]

For isothermal cooling measurements, the temperature was controlled using a THMS600 microscope heating stage (Linkam Scientific, Tadworth, UK). Samples were loaded into a coverslip- gap (in place with an Oring) – coverslip sandwich with a diameter of 22 mm and thickness of 1 mm. This assembly was then heated to 80 °C for 5 minutes to achieve thermal equilibrium, monitored by the loss of birefringence, before quenching at 30 °C min^{-1} until a desired cooling temperature is reached. This temperature is then maintained, and a frame was recorded every 60 seconds, until no change in the shape or size of the crystals were observed and the measurement was ceased.

3.3.2. X-ray Scattering

3.3.2.1. Equipment and Sample Processing

SAXS measurements of anhydrous SDS powders, SDS mixtures in glycerol, analogous *n*-alkyl sulfate mixtures, SDS/glycerol/water mixtures, SDS/glycerol/dodecanol mixtures (elevated temperature) and SDS/NaCl/glycerol mixtures, and isothermal crystallization of SDS mixtures, were performed on a Xenocs Xeuss 2.0 SAXS laboratory beamline with a metal jet X-ray source (GaKα-radiation, wavelength = 1.3414 Å) (Excillum, Kista, Sweden), and Pilatus 1M pixel detector (Dectris, Baden-Daettwil, Switzerland) using transmission mode. SAXS patterns were recorded at the University of Sheffield over a scattering vector range of 0.02 $Å^{-1} < q < 1.2$ $Å^{-1}$ (or 0.02 $Å^{-1} < q < 1.0$ Å), where $q = \frac{4\pi}{\lambda} sin\theta$ and θ is half the scattering angle. Simultaneous small and wide angle scattering (SWAXS) was measured using the same instrument, with the small angle being data recorded over a scattering range of 0.02 $Å^{-1} < q <$ 1.20 $Å^{-1}$. Wide angle scattering captured during SWAXS was recorded using a Pilatus 100K pixel detector over a scattering range of 1.22 $Å^{-1} < q < 3.52$ $Å^{-1}$. Borosilicate capillaries (2 mm-outer diameter, 0.01 mm wall thickness) were used as sample containers (WJM-Glass Muller GMBH, Berlin, Germany) for the X-ray measurements. For elevated temperature measurements, the temperature was controlled using a HFSX350-CAP capillary heating stage (Linkam Scientific, Tadworth, UK). Samples were heated to 60 °C unless specified otherwise and equilibrated for 10 minutes before recording. For isothermal crystallization measurements, samples were initially heated to 60 °C for 5 minutes to achieve thermal equilibrium, in the dissolved state, before quenching at a rate of 30 °C min^{-1} until a desired temperature is reached. SAXS frames were repeatedly acquired using an exposure length of 59 seconds, and a total cycle time of 60 seconds, for either 120 minutes or until the intensity of the Bragg peaks remained constant.

SAXS patterns for sodium hexadecyl sulfate in glycerol, sodium tetradecyl sulfate in ethylene glycol, all other 12-carbon chained surfactant (sodium dodecanoate, sodium dodecyl benzenesulfonate, sodium dodecyl sulfonate) mixtures in a polyol solvent, (glycerol, propylene glycol or ethylene glycol), and SDS/glycerol/dodecanol (room temperature), were recorded over a range of 0.06 $Å^{-1} < q < 0.9$ $Å^{-1}$ using a Bruker Nanostar laboratory SAXS instrument (Bruker AXS, Karlsruhe, Germany) modified with a GeniX 3D X-ray source (Cuα-radiation, wavelength = 1.5418 Å) and motorized collimating scatterless slits (Xenocs, Grenoble, France) at the University of Sheffield. Borosilicate capillaries (2-mm-outer diameter, 0.01 mm wall thickness) were used as sample containers (WJM-Glass Muller GMBH, Berlin, Germany) for the X-ray measurements.

SAXS patterns of carrageenan in glycerol/water mixtures were recorded over a range of 0.01 $Å^{-1} < q <$ 0.11 $Å^{-1}$ with a Bruker Nanostar laboratory SAXS instrument (Bruker AXS, Karlsruhe, Germany) using a metal jet X-ray source (GaKα-radiation, wavelength = 1.3414 Å) (Excillum, Kista, Sweden) at the Materials Innovation Factory (Liverpool) in conjunction with Unilever. Proprietary quartz capillary (1.5 mm OD) in measuring cells (Bruker AXS, Karlsruhe, Germany) were used for the x-ray measurements.

For all apparatus, *q* was calibrated using silver behenate powder.[2] Two-dimensional SAXS patterns were transformed into one-dimension (1D) curves by an azimuthal integration using software supplied by the instrument manufacturer. Where applicable, scaling of scattering data to absolute intensity (cm^{-1}) was achieved by measuring the incoherent scattering of water. Calibration of the SAXS patterns and the background scattering subtraction were performed using Irena SAS macros for Igor Pro.[2]

3.3.2.2. Kinetic Analysis of Crystallization

Peak intensities and positions of the SDS-glycerol crystal phase recorded from isothermal cooling of SDS/glycerol mixtures were obtained using the powder diffraction/WAXS procedure within the Irena macros available for IGOR Pro 8 software.[3] Peak intensity was subsequently plotted against time, with the data normalised to the highest intensity peak fit. For kinetic measurements, a modified Johnson–Mehl–Avrami–Kolmogorov (Avrami) equation was employed (Equation 3.1),[4–6] using the custom nonlinear modelling function in GraphPad Prism version 9, selecting the robust fitting method chosen (GraphPad Software, San Diego, California USA.)[7]

$$X(t) = 1 - e^{-k(t-t_{init})^n} \qquad \text{eq. 3.1}$$

Where $X(t)$ is the volume fraction of crystallized species, t is time, t_{init} is the lag time, n is the Avrami exponent, and k is the overall crystallization rate constant.

3.3.2.3. Electron Density Profile Reconstruction from Small Angle Scattering Data.

The electron density distribution of one-dimensional periodic lamellar structures can be expressed (along the layer normal) at a point z in space, as a Fourier series $F(z)$, such that:

$$F(z) = \frac{1}{L}\sum_{l=-\infty}^{\infty} S(l) \cdot e^{-2\pi i \frac{lz}{L}} \qquad \text{eq. 3.2}$$

Where S(l) is a structure factor (Fourier term in the series) corresponding to the specific Miller index l, and L is the lamellar period along the layer normal. Since S(l) and S$(\bar{l})$ are conjugate quantities, Equation 3.2 can be written as:

$$F(z) = \frac{1}{L}[S(0) + 2 \cdot \mathrm{F}'(\mathrm{z})] \qquad \text{eq. 3.3}$$

Whereby,

$$F'(z) = \sum_{l=1}^{\infty} |S(l)| \cdot cos\left(\frac{2\pi lz}{L} - \delta(l)\right) \qquad \text{eq. 3.4}$$

Where, $|S(l)|$ is the structure factor amplitude. *n*-alkyl sulfate molecules crystallize into bilayer motifs, and therefore the electron density projection against the layer normal is symmetrical with respect to the layer centre. For a centrosymmetric symmetry, or structures containing a plane of symmetry, or rotation (screw) axis parallel to the lamellae layer normal, the phase angle, $\delta(l)$, can exist in two states: 0 or π. Thus, Equation 3.4 can be simplified further:

$$F'(z) = \sum_{l=1}^{\infty} m(l) \cdot |S(l)| \cdot cos\left(\frac{2\pi lz}{L}\right) \qquad \text{eq. 3.5}$$

Where $m(l) = \frac{S(l)}{|S(l)|} = \pm 1$ is the phase sign coefficient associated with a particular Miller index (l). $F'(z)$ represents the electron density profile, which is used for determination of molecular packing along the layer normal. The structure factor amplitudes for Equation 3.5 can be calculated from the corresponding total diffraction peak intensities, I_{00l}, of the lamellar structure:

$$|S(l)|^2 = \frac{I_{00l}}{LG} \qquad \text{eq. 3.6}$$

In which $LG = \frac{1}{sin\theta \cdot sin2\theta}$ is the Lorentz-geometrical factor. The polarisation factor can be approximated to ~1 at small angles of diffraction, and therefor can be excluded from calculations.

Diffraction peak intensities and the positions of *n*-alkyl sulfate-glycerol phases were obtained by fitting Pseudo-Voight functions using the Peak Analyser tool in Origin(Pro) 2020b.[8] Peak splitting caused by the Ga Kα-doublet was negligible at small angles and was not considered in the analysis. Periodic Bragg peaks of lamellar structures were identified for each SAXS pattern and assigned to a known (or likely) crystal phase.

Mercury (4.0) software was used to calculate structure factors for the anhydrous SDS crystal structure from literature data,[9] in order to reconstruct and compare electron density distribution along the SDS layer normal with the experimental data.

3.3.2.4. Modelling of Micelle SAXS Patterns at Elevated Temperatures

SAXS patterns were initially fit using core-shell variants of sphere, cylinder, and ellipsoid models for SDS and SDS/dodecanol in glycerol/water mixtures at 60 °C. Core-shell ellipsoid was the only model that gave good correlation to the scattering patterns up to q= 0.65 Å^{-1} for all samples, while exhibiting physically realistic size or shape. Accordingly, it was used as the sole form-factor, in agreement with previous studies of SDS.[10-12] The core-shell ellipsoid model function (2.1.5 Modelling soft materials) was used,[13,14] with the model code being adapted by Illavksy to work with the Irena macro,[15] from the code created by Steven Kline for the NIST model package.[16] For patterns of SDS in water rich solvents, the scattered intensity at high values of q (q $\rightarrow$1 Å^{-1}) experienced an upturn due to amorphous scattering in the wide angle region.[17] Therefore SAXS patterns were fit between a range of 0.25 Å$^{-1} \leq q \leq$ 0.65 Å^{-1} for all samples.

The fitting algorithm was a least squares optimisation. The SLD of the core and solvent were determined using the Irena scattering contrast calculator, with density data obtained from literature sources. The solvent was treated as a homogeneous volume-average in the case of glycerol and water.[18–21] The volume fraction of the scatterers was calculated by defining SDS as a constant density (1.01 cm^{-3}).[12] The scattered intensity variation observed for SDS in binary glycerol/water mixtures meant that fitting with either a calculated or literature value for its SLD was not possible. Therefore the shell SLD was fitted at a uniform thickness. The aspect ratio for the core was left unrestricted and was set to an initial value of unity.

Because of the an ionic nature of the SDS surfactant, the Hayter-Penfold mean spherical approximation structure factor was employed to account for intermicelle repulsion.[22,23] This was included using the structure factor tool within the Modelling II window in the Irena macro.[2,14] The dielectric constant of the solvent was obtained from literature.[24] It was deemed that a decoupling approximation sometimes used to account for ellipsoidal and spherical particles (charged structure factors)[14] would have minimal impact on the fitted structure factor values, and was not used. This is because of the high noise at low q, as well as the small flexible nature of the relatively small micelles in the semi-dilute concentration regime.[10,25]

3.3.2.5. Characterisation of Carrageenan Scattering.

The inbuilt Irena power law fitting tool was used to determine the gradient of the low *q* slope relating to fractal like scattering originating from undissolved particles or network-type structures.[3] In the mid *q* range, the polyelectrolyte structure factor peak was fitted using a Gaussian function, using the inbuilt modelling II function in the Irena macro.

3.3.3. Infrared Spectroscopy

Fourier transform infrared (FT-IR) spectra were recorded between 400 and 4000cm^{-1} with 1 cm^{-1} resolution on a Perkin Elmer 100 (PerkinElmer, Buckinghamshire, UK) instrument equipped with a universal attenuated total reflection (ATR) accessory. A background spectrum was recorded for each measurement and subtracted manually. Scans were exported using the in house software and processed using GraphPad Prism 9.

3.3.4. Differential Scanning Calorimetry

Thermal analysis was conducted using a Discovery DS 25 (TA Instruments, New Castle, DE, USA). SDS solutions in glycerol that had previously undergone heating and subsequent quiescent cooling, were weighed (~50 mg) and hermetically sealed in aluminium sample pans. Each sample was then transferred into the measurement chamber at 15 °C using the autosampler module, so as to not disrupt the crystal phase. Samples comprising SDS and glycerol and SDS/dodecanol/glycerol mixtures were heated at 0.5 °C min^{-1} to 65 °C. For SDS/NaCl/glycerol mixtures the sample was then heated at 1 °C min^{-1} up to 115 °C. Data were analysed using TRIOS software,[26] where the onset of melting and the peak temperature was measured using the Peak Integration (enthalpy) tool implementing a linear baseline. The end set was measured using the Endset Point analysis tool.

3.3.5. Rheology

Steady-state and oscillatory measurements on SDS dissolved in glycerol and glycerol/water mixtures, and viscosity curve measurements of iota-carrageenan in glycerol/water mixtures were conducted using an MCR 502 rheometer equipped with a variable-temperature Peltier plate and hood (Anton Paar GmbH, Graz, Austria), and a cone plate geometry (15 mm diameter, 4° cone angle). Samples previously subjected to a heating and quiescent cooling cycle were loaded into the rheometer. The mixture was

first heated up to 80 °C at 30 °C min^{-1}, where the temperature was held for 5 minutes to remove thermal history. Following this, the mixture was quenched at 30 °C min^{-1} to 20 °C. The mixture was then held at 20 °C for 5 hours before measurement, with a constant oscillatory frequency and amplitude being recorded during this time (0.1% strain, 10 rad s^{-1}). A form of the Avrami equation (Equation 3.7),[27] was employed to analyse the G' data, allowing the crystallized volume fraction to be obtained ($\mathrm{X(t)}$).

$$\ln\left[1-\ln\left(1-\frac{G'(t)-G'(0)}{G'(\infty)-G'(0)}\right)\right]=\mathrm{n}(\ln(\mathrm{t}-t_{init}))-\ln(k) \qquad \text{eq. 3.7}$$

Where $G'(t)$ is the G' at any given time, $G'(0)$ is the initial value of G', and $G'(\infty)$ is the infinite (plateau) value for G'. Eq (3.7) can be plotted, and a linear regression performed, where the gradient is the Avrami exponent. The lag time, t_{init}, was determined as a deviation of G' from the initial linear trajectory, whereas $G'(\infty)$ was determined as the highest observed value of G'. Due to varying stages of crystallization (e.g. a plateau region where the majority of surfactant in the liquid phase is depleted), deviation from power law behaviour was observed at the extremities of the Avrami plot and such data were not included in the linear regression.

For steady shear measurements of SDS (2 Wt. %) in glycerol/water mixtures, viscosity curves were recorded after in situ cooling: 50 measurements were recorded at shear rates ranging from 0.05 s^{-1} to 500 s^{-1}, with intervals increasing in a logarithmic fashion. For steady shear measurements of carrageenan in glycerol/water mixtures, 30 measurements recorded at shear rates ranging from 0.01 s^{-1} to 500 s^{-1}, with intervals increasing in a logarithmic fashion. The interval time was determined by the rheometer software to mitigate time-dependent structure breakdown, and hence record equilibrium viscosity where possible. In the case of successive viscosity curves, the samples were initially formed in situ, with no disturbance to the rheometer or sample in between measurements.

Amplitude sweep measurements for SDS (2 Wt.%) in glycerol (oscillatory mode) were recorded following in situ cooling, with 30 data points recorded at strains ranging from 0.01 % to 500 % (at 10 rad s^{-1}), with intervals increasing in a logarithmic fashion. A 20 second time interval between points was used, as oscillatory measurements cause less morphology damage than steady shear measurements. Frequency sweeps (SDS in glycerol) were conducted following in situ cooling, with 30 data points being recorded at a frequency range of 0.01 rad s^{-1} to 100 rad s^{-1} (at 0.1 % strain), using a 30 second time interval between points. Frequency sweeps for carrageenan in glycerol/water mixtures was conducted on an Anton Paar DSR301 with ASC using a vane geometry (40 mm length 22 mm diameter, 27 mm sample holder diameter). In each case 30 data points were recorded from 100 rad s^{-1} to 0.1 rad s^{-1} (at 1 % strain) with a time interval of 10 seconds.

Creep-recovery measurements were conducted following in situ cooling of SDS (2 Wt.%) in glycerol. Firstly, a constant stress of 5 Pa was applied for 300 seconds, and measurements recorded with intervals increasing from 0.01 to 25 seconds in a logarithmic fashion. Recovery was subsequently measured by determination of steady-state conditions, which were determined automatically with a steady-state threshold range of 10%.

SIPLI rheology measurement were conducted on an Anton Paar 301 instrument, equipped with a mechano-optical (SIPLI) attachment, variable-temperature Peltier plate and Peltier hood. A plate-plate geometry was geometry consisting of a 25 mm polished steel (top) plate and a glass bottom base plate. The sample gap was set to 1 mm to allow the observation of birefringence. The sample was illuminated using an Edmund Optics 150 W MI-150 fibre optic white light (high intensity) source. Polariser and analyser were positioned at 90°, and images were recorded using a Lumenera Lu165c colour CCD camera. The samples of SDS (2 Wt.%) in glycerol were initially loaded into the rheometer, before being heated for 10 minutes at 60 °C, and subsequently cooled for 150 minutes at 20 °C. Completion of crystallization was confirmed by the plateau of G' values from fixed amplitude and frequency oscillatory measurements during cooling. Birefringence images were recorded before, during and immediately after an application of constant steady shear (100 s^{-1} for 2000 seconds).

3.3. References

1 *ZEN lite 3.2 (Blue edition)*, ZEISS Microscopy, Oberkochen, Germany.
2 M.Nyam-Osor, D. V.Soloviov, Yu. S.Kovalev, A.Zhigunov, A. V.Rogachev, O. I.Ivankov, R. V.Erhan, and A. I.Kuklin, Journal of Physics Conference Series, 2012, **351**, 012024
3 J. Ilavsky and P. R. Jemian, *Journal of Applied Crystallography*, 2009, **42**, 347–353.
4 M. Avrami, *The Journal of Chemical Physics*, 1940, **8**, 212–224.
5 M. Avrami, *The Journal of Chemical Physics*, 1941, **9**, 177–184.
6 M. Avrami, *The Journal of Chemical Physics*, 1939, **7**, 1103–1112.
7 *GraphPad Prism version 9.0.0 for Windows*, GraphPad Software, San Diego, USA.
8 *Origin(Pro) 2020b*, OriginLab Corporation, Northampton, MA, USA.
9 C. F. MacRae, I. Sovago, S. J. Cottrell, P. T. A. Galek, P. McCabe, E. Pidcock, M. Platings, G. P. Shields, J. S. Stevens, M. Towler and P. A. Wood, *Journal of Applied Crystallography*, 2020, **53**, 226–235.
10 S. L. Gawali, M. Zhang, S. Kumar, D. Ray, M. Basu, V. K. Aswal, D. Danino and P. A. Hassan, *Langmuir*, 2019, **35**, 9867–9877.
11 M. Bergström and J. S. Pedersen, *Physical Chemistry Chemical Physics*, 1999, **1**, 4437–4446.
12 B. Hammouda, *Journal of Research of the National Institute of Standards and Technology*, 2013, **118**, 151-166.
13 S. S. Berr, *Journal of Physical Chemistry*, 1987, **91**, 4760–4765.
14 M. Kotlarchyk and S. H. Chen, *The Journal of Chemical Physics*, 1983, **79**, 2461–2469.

15 J. Ilavsky, SAXS_IgorCode/User form factors for Irena at master · jilavsky/SAXS_IgorCode, https://github.com/jilavsky/SAXS_IgorCode/tree/master/User form factors for Irena, (accessed 16 April 2021).
16 NIST, *SANS Model Function Documentation*, 2012.
17 N.S. Murthy and H. Minor, *Polymer*, 1989, **31**, 996–1002.
18 A. Volk and C. J. Kähler, *Experiments in Fluids*, 2018, **59**, 75-78.
19 J. V. Joshi, V. K. Aswal and P. S. Goyal, *Journal of Physics: Condensed Matter*, 2007, **19**, 196219.
20 T. Zemb and P. Charpin, *Journal de Physique Paris*, 1985, **46**, 249–256.
21 M. A. Saleh, S. Akhtar, S. Begum, M. S. Ahmed and S. K. Begum, *Physics and Chemistry of Liquids*, 2004, **42**, 615–623.
22 J. B. Hayter and J. Penfold, *Molecular Physics*, 1981, **42**, 109–118.
23 J. Hansen and J. B. Hayter, *Molecular Physics*, 1982, **46**, 651–656.
24 *Physical properties of glycerol and its solutions*, Glycerine Producers' Association, New York, 1963.
25 D. G. Greene, D. V. Ferraro, A. M. Lenhoff and N. J. Wagner, *Journal of Applied Crystallography*, 2016, **49**, 1734–1739.
26 TRIOS Version 5.0, *TA Instruments–Waters LLC*, New Castle, USA.
27 J. Y. Chen, Z. Komeily-Nia, L. P. Fan, Z. Y. Li, B. Yuan, B. Tang and J. L. Li, *Journal of Colloid and Interface Science*, 2018, **526**, 356–365.

4. Binary Mixtures of Anionic Surfactants in Polyols

4.1. Introduction

Sodium dodecyl sulfate (SDS, Figure 4.1a) is a ubiquitous molecule within the personal care industry.[1,2] It is considered to be an anionic ideal model surfactant due to its physical properties. The monodisperse alkyl tail, combined with an electron rich, polar head group facilitates its structural determination using x-ray scattering.[3–6] Depending on end usage, SDS is most commonly found in consumer goods at semi-dilute concentrations above the CMC, or higher in dilutable formulations such as washing up detergent.[7,8] Glycerol (Figure 4.1b) is also widespread as it provides cost-effective humectancy,[9] and can increase the stability of foam as a viscosifier.[10] Hence both glycerol and SDS are often complementary ingredients in fast moving consumer goods (FMCGs) such as toothpastes and hair.[11,12]

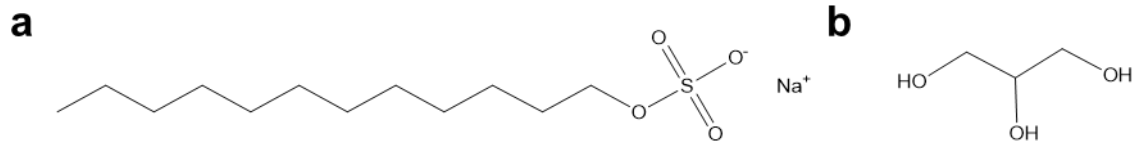

Figure 4.1: Chemical structure of a) sodium dodecyl sulfate b) glycerol.

There is a body of work detailing SDS behaviour in glycerol-water mixtures, including critical micelle concentration (CMC) determination, Krafft temperature, and thermodynamic parameters.[13–17] As glycerol concentration is increased in the aqueous glycerol mixtures, the polarity of the solvent decreases,[18] reducing the degree of solvation for the charged head groups and increasing the CMC and Krafft temperature.[17] While some authors have described hydrated crystals forming in glycerol/water solutions,[17,19] there was little work detailing the crystallization of SDS in glycerol at room temperature when this project was conceived. After most of the work was complete, an article by Matthews et al. detailing similar mixtures of SDS in glycerol was published.[14] Discussion of results in the context of this publication are included at the end of this chapter.

To understand the behaviour of analogous systems of SDS and glycerol, the underlying interactions that determine co-assembly require examination. Controlling molecular shape and H-bonding moieties are common methods for designing and improving supramolecular-based gels. Can this be achieved with other commonly available components? By exploring the solvent type, tail, and headgroup, in structurally similar analogues to the SDS and glycerol pair, it is possible to determine the structure property relationships which governs the self-assembly process.

4.2. Results and Discussion: SDS-Glycerol Binary Mixtures

4.2.1. Visual and Microscopical Observations of the SDS-glycerol Gel Phase

SDS is insoluble in glycerol at room temperature. When SDS in glycerol is heated above the Krafft temperature,[17] and subsequently cooled quiescently for a minimum of 5 hours, a homogeneous translucent suspension is formed, similar to the phase shown by Abdel-Rahem's studies.[19] Above 2 Wt. % a freestanding gel formed (Figure 4.2b), and similar behaviour is observed in samples tested up to 16 Wt. %. Samples at or above 30 Wt. % did not exhibit gelling behaviour when cooled but instead formed a viscous slurry (Appendix 8.1). Concentration ranges typical for industrial formulations were chosen as the primary focus of the study, especially 2 Wt. % SDS due to the high degree of structuring (Figure 4.2b) at low concentrations.

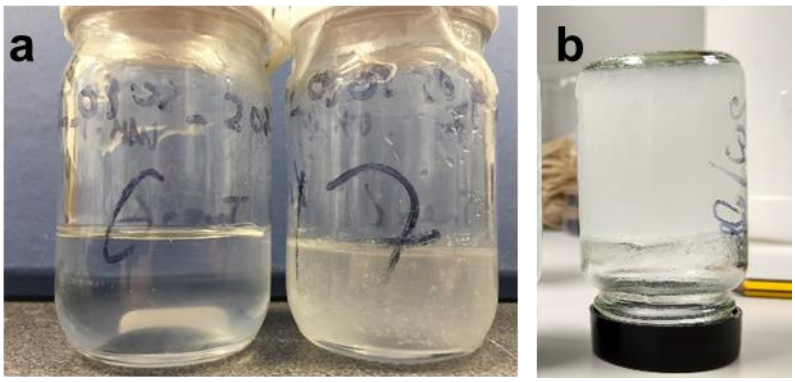

Figure 4.2: a) 0.8 Wt.% (6) and 1 Wt.% (7) SDS in glycerol cooled quiescently. b) Freestanding gel formed of 2 Wt.% SDS in glycerol cooled quiescently .

When gelled mixtures were studied by polarised optical microscopy (POM); large birefringent, twisted ribbons/fibres were observed (Figure 4.3). Birefringence is often indicative of structural order, e.g. crystals or liquid crystals. Furthermore, samples at higher concentrations (Figures 3b and 3c) also contain ribbons, albeit at shorter length scales due to greater nucleation resulting from higher degrees of supersaturation.[20] It is evident the ribbon species form an entangled network which causes gelation.[21] For all samples, length and diameter of the fibres/ribbons were polydisperse, with lengths above 500 µm at low concentrations. The polydisperse nature of these fibres contrasts with nanosized supramolecular assemblies which typically form smaller, more uniform assemblies.[22,23] However, the material does look similar to certain supramolecular assemblies e.g. SaFiNs. Nevertheless, this may be an effect of temperature, causing similar sized crystal aggregate growth. [24]

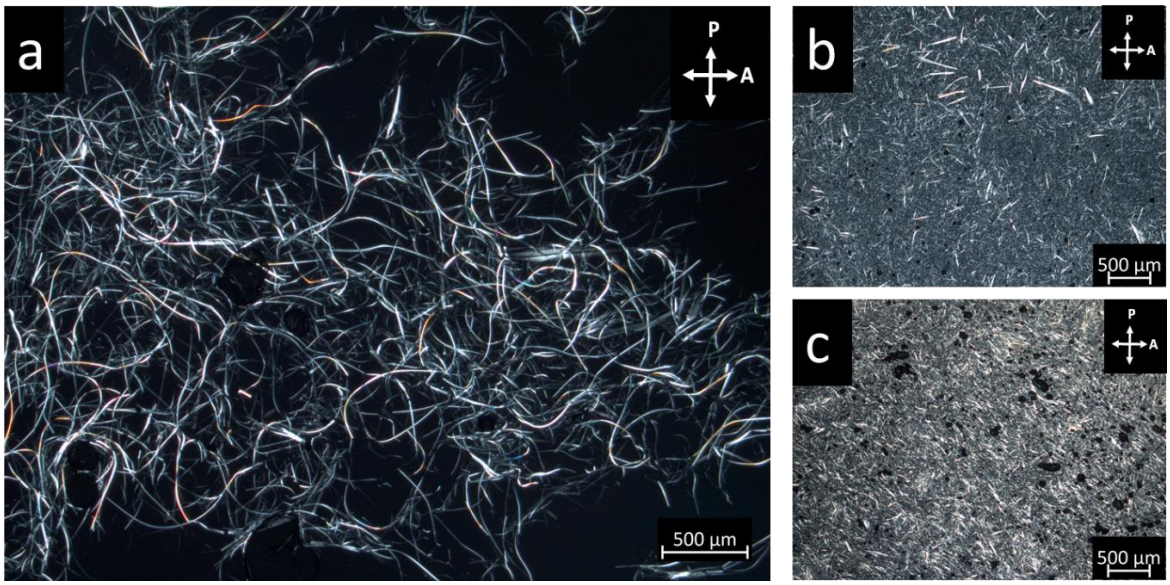

Figure 4.3: Polarised optical microscopy images of SDS in glycerol, subjected to heating at 75°C before being cooled quiescently overnight, at a) 2 Wt. % SDS, b) 8 Wt. % SDS, c) 16 Wt. % SDS. Direction of polariser and analyser indicated by P and A, respectively.

Fibres observed using POM (Figure 4.3), exhibit morphologies similar to coagels,[25–27] which are hydrated surfactant crystals or semi-crystalline aggregates.[28] The characteristic twist of the fibres can be attributed to one or two possibilities. Firstly, chirality can cause asymmetric packing to occur, and the crystal aggregates can propagate to form structures with periodic twists.[29] However, this seems unlikely as SDS is achiral and glycerol is prochiral, and the structure appears to form irregular twists (Figure 4.3a). Alternatively, is that during the fibre formation, SDS molecules organise into bilayer motifs. The stacks of bilayers subsequently experience stress during growth, causing unbalanced growth and subsequent twisting of the crystal aggregate.[30] This behaviour is commonly observed in the crystallization of achiral polymers.[30] To better understand the structure of the SDS molecules, small angle, and wide angle x-ray scattering (SAXS/WAXS) was performed on the SDS/glycerol solutions, following heating and quiescent cooling (thermal cycle). Characterisation of the phase initially focused on 2 Wt. % solutions. Subsequent studies were undertaken at higher concentrations.

4.2.2. Small and Wide Angle X-Ray Scattering Measurements for Structural Determination and Formation Kinetics

SAXS analysis of a representative 2 Wt.% solution of SDS in glycerol following a thermal cycle result in a series of four unique, prominent Bragg peaks with their position corresponding to integer ordering (Figure 4.4b). The peak ordering is indicative of a lamellar symmetry, found in all other SDS crystal types,[31,32] where SDS is arranged in bilayers along the primary axis. The 4th order reflection was not prominent, compared to 1st, 2nd, 3rd, and 5th peak orders. The first order peak showed a spacing of 55.4 Å, which is 15.5 Å larger than the literature value of anhydrous SDS,[33] and 16.8 Å larger than experimental results from SDS powder measured in this study (Figure 4.4a). SAXS was performed on SDS/glycerol mixtures up to 30 Wt.% SDS (Appendix 8.2), with the new lamellar phase present as the predominant species up to 16 Wt.%. Moreover, the bilayer spacing did not vary as the concentration of SDS changed, indicating a more fixed (stoichiometric) structure than species such as fluid bilayers.[34,35] From 30 Wt.% SDS, anhydrous crystals predominate with no evidence of the new lamellar structure. For 10 Wt.% and 16 Wt.% SDS mixtures, anhydrous crystals are present, but with low peak intensity equating to ~1% abundance (Appendix 8.2). This may be due to crystallization conditions, or presence of small quantities of impurities such as water or synthetic precursors of SDS or glycerol.

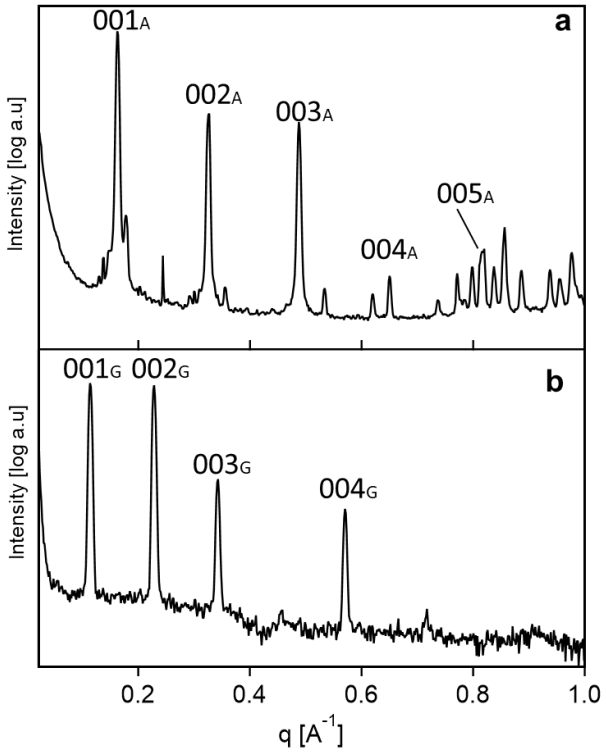

Figure 4.4: Background corrected 1D SAXS pattern of a) anhydrous SDS powder b) gelled 2 Wt.% SDS in glycerol mixture. $00l_G$ and $00l_A$ are Miller indices used to denote lamellar peaks of the respective phases (anhydrous SDS and gelled SDS in glycerol phase).

A larger d_{001} spacing suggests a significant change in the packing or structure of the crystal, as in the case of hydrated and anhydrous crystals of SDS.[31,33] One hypothesis is that a change in spacing is solely due to altered molecular tilt. However, the magnitude of the d_{001} spacing between anhydrous SDS and the SDS glycerol crystal phase is distinctly different. Considering the packing of anhydrous SDS, with 15 °, and a 2 Å intermolecular spacing between chain,[36] the maximum length of an SDS bilayer at zero tilt is ~43 Å, which is much smaller than that observed for SDS-glycerol phase. Therefore, the change in d_{001}-spacing cannot be only due to tilt. When considering the evidence within the literature for solvate crystals and co-crystals,[31–33,37] it is possible that glycerol is incorporated within the crystal structure about the SDS headgroup, causing the (d_{001}) bilayer spacing to increase.

Time-resolved SAXS measurements during isothermal crystallization of a SDS (2 Wt.%) solution in glycerol were undertaken at both 20 °C and 0 °C to determine whether the crystals were a result of an initial unstable phase transformation, or the primary nucleation of a new phase.[38] Polymorph transformation was a distinct possibility and this is exhibited by molecules with crystallizable alkyl chains, e.g. fats and fat mixtures.[39] By exploring two temperatures, an indication for the kinetic favourability of the phase can be observed, much like with SDS hydrate crystal formation in aqueous solution.[12] The development of the crystal structure was observed by measuring Bragg peak data from the background-corrected SAXS patterns over time (Figures 4.5a and 4.5b). As crystallization occurs through a primary pathway and not polymorphic interconversion, the first order peak was fit with a Gaussian function, normalized to the maximum intensity (equating to the volume fraction of the crystal[40]) and plotted against time (Figure 4.5c).

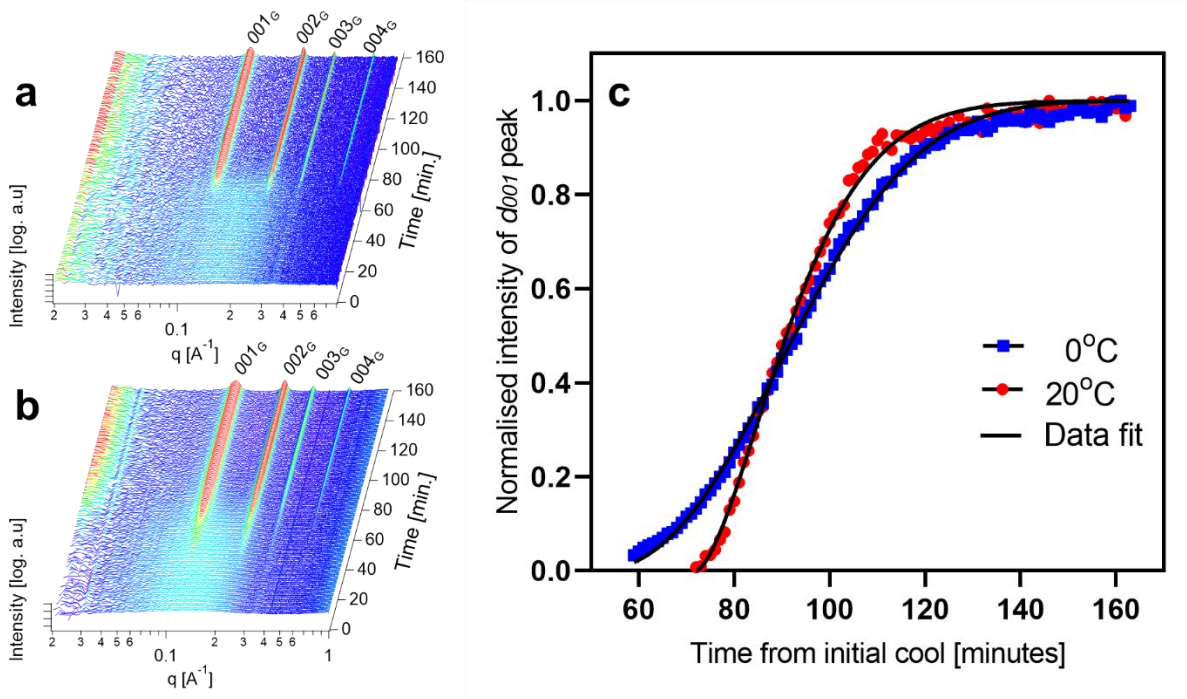

Figure 4.5: Time-resolved background-corrected SAXS patterns recorded for 2 Wt.% SDS in glycerol quenched at 30 °C min^{-1} from 60 °C to a) 20 °C and b) 0 °C and held isothermally for 160 minutes where 00l$_G$ are Miller indices used to denote lamellar peaks of the SDS-glycerol phase. c) Plot measuring relative intensity of the first order 001$_G$ peak during isothermal cooling, with fitted Avrami equation. Output model parameters are shown in Table 4.1.

The four characteristic peaks were the only ones observed at both cooling temperatures (Figures 4.5a and 4.5b). The highest intensity peak, 001$_G$, was evident after 72 minutes at 20 °C, which was reduced to 59 minutes at 0 °C. For both samples, a period of growth was seen over the following 40 minutes as shown by an increase in intensity of the Bragg peaks. In the middle of *q* region, at around 0.1-0.2 Å^{-1} the initial enhanced intensity can be attributed to micelle scattering.[5,41–43] This shortly disappears following the appearance of the peaks. With no evidence of other phases (Figures 4.5a and 4.5b), it can be concluded that direct formation of the new phase from a micellar solution is the dominant pathway. Both samples exhibited faster rates of crystallization than initial visual observation in vials. This is attributed to factors such as surface area, heat transfer and the presence of an x-ray beam, which may have increased nucleation events.[44] Intensity of the Bragg peaks is directly proportional to the volume fraction of species present, therefore kinetic behaviour can be established by comparing integrated peak intensity over time (Figure 4.5c). Phase changes, including crystallization formation have been studied using the Kolmogorov–Johnson–Mehl–Avrami (Avrami) equation,[45–47] enabling the determination of growth type in terms of dimensionality and spontaneity. It is not the only growth equation that has been successfully used for modelling crystallization. For example, the Malkin crystallization equation may be suitable for polymers.[48] In the case of fats, modified Gompertz and

Foubert models have been used.[49,50] However, the Avrami equation has been used to characterise fibre-type low molecular weight gelators,[51] fats,[52,53] and even SDS crystals.[12] Given its theoretical underpinning (as opposed to purely empirical models), it was deemed that the Avrami equation would be the most appropriate for this analysis.

A linearized derivative of the Avrami equation is often attempted for ease of modelling and has been Previously used for SAXS data analys.[54,55] However, it was decided that non-linear modelling should be used to gather as much information as possible about the crystallization process. Considering this, the output parameters can be observed (Table 1).

Table 4.1: Output parameters for Avrami fit of normalised diffraction peak intensity over time for 2 Wt. % SDS isothermally cooled at two temperatures, showing Avrami constant (K), lag time (t_{init}) and Avrami exponent (n).

Equation parameter	0 °C	20 °C
K	7.00×10^{-5}	6.54×10^{-3}
t_{init} *[min.]*	49.2	72.0
n [dimensionless]	2.44	1.59

SDS generally forms 2D platelets and 1D needles, respectively. This means that unless spherulitic growth occurs, the Avrami constant (n) could be 1-3. For the SDS crystals formed in glycerol, the Avrami exponent value at 20 °C was 1.59 (Table 1), which is closest to rod- like growth with sporadic nucleation (n=2).[56] While integer ordering is expected, non-integer values can arise from multiple sources, although 'consecutive growth of different crystalline units' can be discounted due to the isotropic 2D pattern of a single crystal phase.[55] One suggestion is that crystallization occurs through a mixed pathway of both instantaneous and sporadic nucleation. However, this is unlikely as the high lag time and slow growth would indicate that spontaneous growth is unlikely. Instead, either heterogeneous crystallization occurs due to high surface area to volume ratio, or there is secondary nucleation e.g. leading to branching.[57] Branching appeared to be minimal in the quiescently cooled microscopy images (Figure 4.3), although the twisting of the ribbon may also affect growth kinetics. Nevertheless, the Avrami exponent (when rounded) is consistent with the expected behaviour and crystal morphology.

At 0 °C, the Avrami exponent increases to 2.4, which still can be rounded to 2. This would appear to suggest that 2D or 3D growth occurs if there is primary homogenous nucleation.[56] However, the same

crystalline microstructure forms when quenched to 20 °C, although this does not discount a change in crystal habit. An increase in heterogenous nucleation seems likely, although secondary nucleation and tip branching should not be discounted.[58] In summary, the experimental results indicate a high kinetic barrier for the formation of the SDS-crystal phase, due to the long initial lag time (t_{init}), followed by rod-like nucleation (similar to both LMWGs and crystals).[58–60]

WAXS was performed on 2-8 Wt. % SDS solutions in glycerol to determine the nature of the lamellar structure, as well as any inherent crystallinity without the presence of other crystal types (e.g. anhydrous SDS) observed at higher concentrations. However, this resulted in minimal additional structural information due to presence of amorphous scattering from glycerol, even after centrifugation. Therefore, to obtain better quality structural information, a higher concentration of SDS in glycerol (8 Wt.%) was studied using simultaneous SAXS and WAXS (SWAXS), to provide a higher signal to noise ratio in corresponding scattering patterns. The resulting patterns after background subtraction, indicated a high degree of order, with at least ten identifiable diffraction orders present in the 00*l* plane (Figure 4.6). Furthermore, a significant number of additional Bragg peaks most likely corresponding to other (non-lamellar) crystallographic planes indicate the crystalline nature of the SDS-glycerol phase.

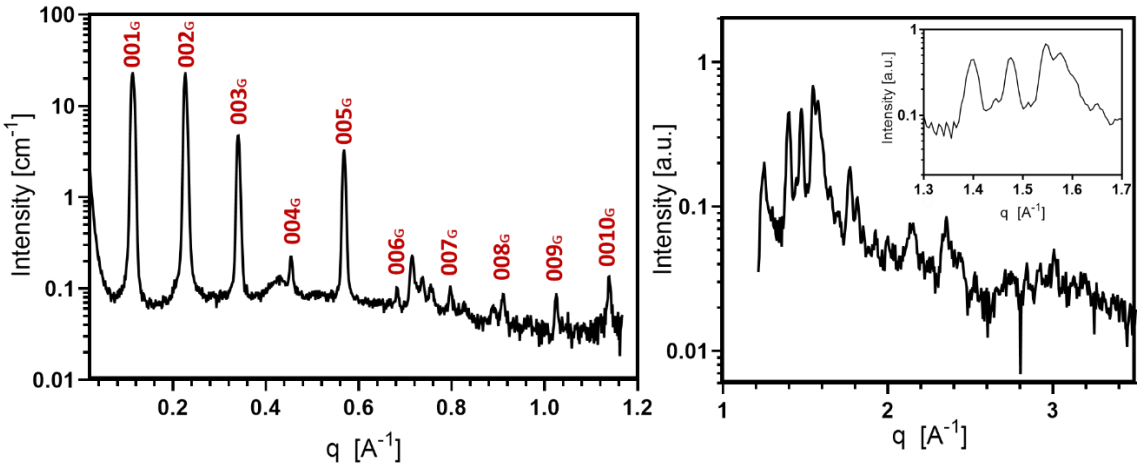

Figure 4.6: Background-corrected 1D SWAXS pattern with Left) SAXS component and Right) WAXS component, with inset showing characteristic short spacings, of 8 Wt.% SDS in glycerol cooled quiescently from 75 °C. 00l_G are Miller indices used to denote lamellar peaks of the SDS-glycerol phase. Both scattering patterns were captured using a Xenocs Xeuss 2.0 instrument, with the SAXS pattern recorded with a Pilatus 1M pixel detector, as well as WAXS recorded using a Pilatus 100K pixel detector located within the sample chamber.

The additional peaks can be identified in the WAXS pattern (Figure 4.6), specifically between q =1.3-1.7 Å $^{-1}$ (Figure 4.6 inset). These characteristic 'short spacings' peaks could be related to the sub-cell formed as a result of *n*-alkyl chain packing.[61] Although not indicative of the unit cell geometry, detection of the

characteristic WAXS peaks enables estimation of packing geometries, and has been used for fat crystals[62] as well as SaFiNs.[63] When alkyl chains are packed parallel to the bilayer normal (Figure 4.7a), a hexagonal structural motif called a 'rotator phase' occurs,[64–66] which produces a single 100 peak at ~4.1 $Å^{-1}$. However, if there is directional ordering about the zigzag plane, an orthorhombic sub cell occurs (Figure 4.7b), which typically forms two peaks at ~ 4.2 $Å^{-1}$ and ~ 3.7 $Å^{-1}$ (indexed as 110 and 200, respectively) for *n*-alkanes such as polyethylene. If there is additional tilt against the layer normal (Figure 4.7c), the terminal methyl groups in the space between chains cause a series of peaks to form, suggesting a monoclinic or triclinic subcell.[61] In Figure 4.6, four peaks are observed, with the latter two are overlapping as a result of scan resolution and proximity. The number of peaks therefore suggests that the sub cell of the SDS glycerol crystal phase is of low symmetry corresponding to triclinic or monoclinic syngony.

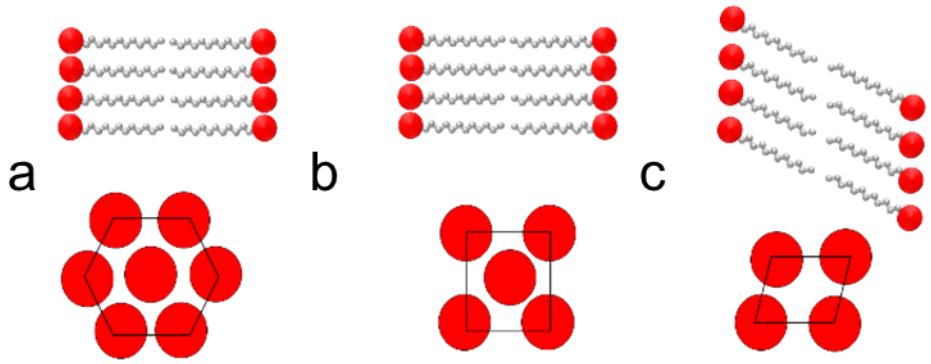

Figure 4.7: Idealised potential subcell geometries for SDS packing, modified from the most common polymorphs of triacyl glycerol (TAG) crystals with view along (top) and perpendicular (bottom) to the packing layer normal. a) hexagonal (rotator phase) structure, b) orthorhombic structure, c) triclinic (and monoclinic) structure.

Considering the characteristic WAXS scattering, it is likely that the *n*-alkyl chains present in the SDS-glycerol crystal phase are tilted with respect to the layer normal (Figure 4.7c). It is also reasonable to expect that some of the peaks could be associated with the glycerol packing. However, in order to confirm the geometry of the SDS molecule packing, including the sub cell geometry, more details must be elucidated from the scattering data.

4.2.3. Electron Density Profiles Constructed from Scattering data for Structural Analysis Along the Layer Normal

As the new SDS-glycerol structure is lamellar in nature, it is possible to estimate packing along the long axis or layer normal using an inverse Fourier transformation.[67,68] This method is versatile and has been applied to both crystalline materials such as triacylglycerols, and non-crystalline materials such as fluid lipid bilayers.[61,69–71] Using a Fourier series allows the characterisation of structure factor amplitudes from experimental diffraction peak intensities which, in turn, enables calculation of electron density along the layer normal. This allows the packing of atoms to be estimated, as well as confirming presence of interlamellar species such as water.[72] For molecules such as SDS, electron density varies along the molecule, with the alkyl chain consisting of lower electron density (lighter atoms) than the sulfate head group (heavier atoms). Subsequently, positions of high and low electron density along a bilayer can be ascribed to the position of certain atoms. Furthermore, as glycerol has an intermediate electron density, its position can be verified, as well as estimation of its stoichiometry with respect to SDS. As the electron density profile is dependent on scattered peak location and intensity in the diffraction pattern, the resolution depends on how many reflections are observed and subsequently included.

To determine an electron density profile, the phase sign coefficient m(l) for a particular Miller index must be defined for the Fourier terms, where m(l) is ± 1 (Section 3.3.2.3, Equation 3.5). When there are n reflections used to construct the electron density profile, there are 2^n variants that require assignment . The 'phase problem' that arises from multiple reflections is often overcome by referring to analogous systems, or by systematically altering the bilayer spacing e.g. the swelling method used for characterising lipid bilayers.[34] Although electron density profiles (EDPs) of SDS in various mixed systems are available,[73–75] there is no record of EDPs for SDS crystal phases. For this system, the phase problem was overcome through a combination of complimentary methods. Firstly, analysis of the resulting electron density profile is compared to EDPs for the known anhydrous crystalline phase of SDS.[33] However, to mitigate discrepancies relating to experimental factors (i.e. crystal defects, data collection and processing), a comparison between EDPs created from experimental SAXS data and simulated scattering data using known atomic positions was performed for anhydrous SDS (Appendices 8.3, 8.4 and 8.5).[33] Given the relative resolution of the electron density profile, five orders of reflection were decided as the optimal number which gave a manageable number of variants (n=5, 2^5 = 32).

Identifying the correct EDP for anhydrous SDS, provided an estimation of electron density throughout the bilayer. Two methods were employed (Figure 4.8); firstly simplistic location of scattering length density[5] as a proxy for electron density, consisting of a head and tail region, located through atomic positions from crystallographic data (Figure 4.8a).[33] Secondly, following work by Aray et al.,[36] bond

electron densities calculated through computational methods utilising 'Quantum Theory of Atoms in Molecules' (QTAIM)', were plotted at midpoints of the corresponding atoms to give an alternative, higher resolution picture of electron density throughout the bilayer. Unfortunately, the geometrical information of the optimised structure was not given, and hence atomic positions were obtained from the aforementioned crystallographic data.[33] This compromise is adequate due to the low probability for significant deviation of atomic positions in the bilayer.

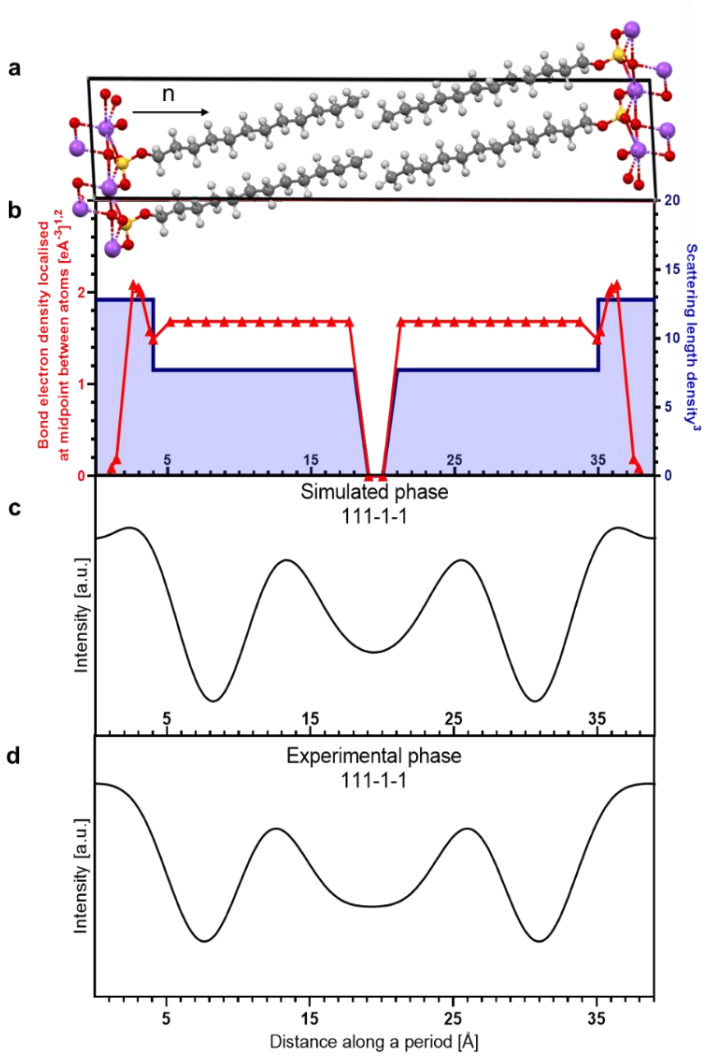

Figure 4.8: a) Packing of anhydrous crystalline SDS along the layer normal (n) created using Mercury crystallographic software.[76] b) Schematic representation of electron density distribution along the bilayer normal (n), using two regions of electron density (using scattering length density as a proxy), and bond electron densities calculated from QTAIM.[36] c) Projection of electron density along the layer normal, reproduced from structure factors calculated from single crystal data of anhydrous sodium dodecyl sulfate. d) Projection of electron density along the layer normal, calculated from experimental SAXS data of anhydrous crystalline SDS (Figure 4.4). Set of signs shown as +/- 1 for each EDP represents the Fourier term phase sign [m(l)] coefficients for the four structure factor amplitudes observed in the SAXS pattern.

Determination of the correct phase for anhydrous SDS is possible (Figures 8C and 8D) despite multiple similar EDPs (Appendices 8.3 and 8.5). In both cases, a region of lower electron density is observed in the centre, with the outermost two peaks indicating the presence of the head group. Both experimental and simulated data show similar profiles in this respect, with similar relative head and tail intensities. The simulated pattern provides a slightly more precise profile, with a dip in electron density at the outer edge of the head group. Such a phenomenon can be interpreted through bond electron density in Figure 4.8B, with the outermost Na-O region experiencing the lowest electron density.[36] The small reduction in intensity is not seen in Figure 4.8D, with a plateau being observed instead. It is expected that growth of an equilibrated single crystal with a small number of defects and imperfections would increase similarity between EDPs. However, it is reassuring to observe similar experimental results to the simulated pattern, allowing comparison with other crystal phases.

Identification of head and tail motifs expressed in anhydrous crystals allows for the development of a structural model, which can be used in turn to describe the SDS-glycerol crystal phase. Phases with analogous structural motifs containing a head and tail were identified (Figure 4.9a) for EDPs of the SDS-glycerol crystal phase, constructed from peak intensities measured from the scattering pattern of 8 Wt.% SDS in glycerol (following heating and cooling) (Appendices 8.6 and 8.7). Like the electron density profile of anhydrous SDS powder, the chosen SDS-glycerol EDPs contained two maxima representing the head groups, separated by an identical region of lower electron density. However, unlike the anhydrous electron density profile, a new region of electron density can be identified outside of the SDS bilayer. It is hypothesised that this region contains glycerol, which is incorporated within the overall crystal structure. An additional difference to the anhydrous electron density profiles is the atoms which are represented in the head group maxima. In the anhydrous crystals, the halfwidth of the peak (with plateau or subsequent decrease) represents a single head group. Comparing this result with the peak width observed for the SDS-glycerol phase is likely to suggest that the most pronounced peaks represent a single SDS head group. This is due to positioning of the head groups across the bilayer, whereby anhydrous crystals exhibit head to head stacking. This is unlikely in the SDS-glycerol crystal phase as the glycerol acts as a spacer between the adjacent bilayers. Nevertheless, the similarity of head group peaks allows for comparison, with the caveat of resolution that occurs when limited Fourier terms (relating to peaks in the experimental SAXS pattern) are used to construct electron density profiles. Another difference between anhydrous SDS and the SDS-glycerol phase, is the observance of a single well-defined electron density profile for anhydrous SDS. In contrast, four possible variants are

identified for the SDS-glycerol phase (constructed from 5 orders of reflections), which differ marginally in their spacing.

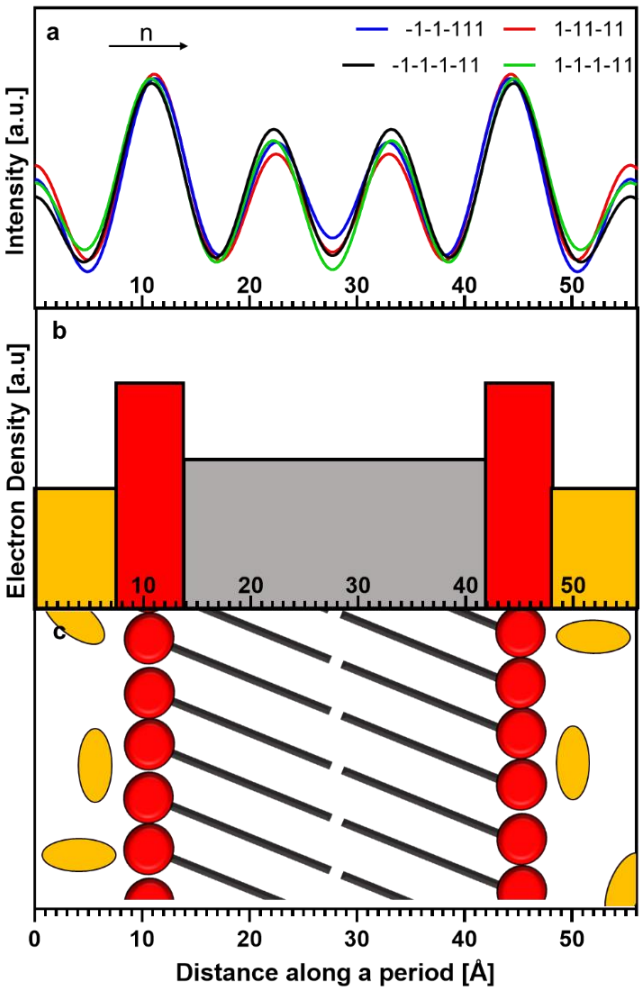

Figure 4.9. A) Most suitable projections of electron density profiles along the bilayer normal (n), constructed from experimental SAXS lamellar peaks of the SDS-glycerol phase. Set of numbers in the EDP corresponds to m(l) coefficients representing the Fourier term phase signs for the four structure factor amplitudes observed in the SAXS pattern. B) Schematic of the electron density distribution relating to the position of the constituents [head group (red) and hydrocarbon tail (grey) and glycerol (orange)] along the SDS-glycerol layer normal. C) Packing of SDS (coloured by red and grey) and glycerol (yellow) molecules along the layer normal. The orientation and conformation of glycerol is not determinable with the set of data, and therefore has been represented as a range of conformations in which glycerol may lie.

Chain tilt relative to the primary axis can be estimated through inspection of the EDP for the SDS-glycerol crystal phase. Like the anhydrous EDP pattern for SDS (Figures 4.8C and 4.8D), the maxima within the SDS-glycerol profiles corresponds to the centre of the head group where sulfur is present. However, as the precise phase cannot be directly determined from the four variants, a range of head to head distances are observed from 33.0-33.8 Å. Considering the distance between sulfur and the

terminal hydrogen (17.5 Å), as well as an in-plane distance between opposing terminal hydrogens in the bilayer; a 'zero degree tilt' head to head distance is estimated as 35.6 Å. Estimation of the head-to-head distance for the (simulated) anhydrous SDS electron density profile (Figure 4.8c) returns a tilt of 17°, an overestimation of 2° compared to literature data.[33] The overestimation of ~10% reveals one of the primary sources of error in this method: the discounting of tilt in the non-primary axis. However, if the magnitude of additional tilt is negligible, as for most SDS molecules,[31–33] then the tilt of the SDS-glycerol phase is estimated to be 18-22°. Furthermore, short spacing information from WAXS (Figure 4.6), suggests a triclinic (or monoclinic) sub cell, implying tilted alkyl chains.[61] The only means of reducing uncertainty for the estimate tilt is single crystal diffraction, which is beyond scope of this work. However, given the potential for large fibres to be formed, it is likely this can be achieved in the future.

Surprisingly, the electron density found in the outer layer containing glycerol is less than that expected for all potential phases when atomic composition and electron density of the molecules are considered. As glycerol contains carbon, hydrogen, and oxygen, its electron density is expected at equimolar ratio to be higher than that of the SDS tail group (containing just carbon and hydrogen) and also lower than the SDS head group (containing sulfur and oxygen). However, for all potential electron density profiles, the apparent electron density of glycerol within the EDP is either lower or equal to the alkyl chain. Therefore, it is likely that glycerol exists within the crystal at less than equimolar stoichiometry, in an approximate 1:2 molar ratio with respect to SDS. The limited resolution of the profile and assumption that molecular tilt in a non-primary axis is negligible account for the observed electron density of the glycerol region. Furthermore, orientation of glycerol is ambiguous from the electron density profile information alone. When considering the sublayer depth, glycerol should span the majority of the distance by existing parallel to the layer normal, otherwise larger minima in electron density would be observed. Single crystal diffraction data would also confirm the stoichiometry and orientation of glycerol.

4.2.4. Infrared Spectroscopy Measurements for the Determination of Order within the Glycerol Sublayer

The high degree of order indicated by multiple Bragg reflections in the SWAXS indicates that SDS is highly crystalline within the SDS-glycerol phase. Furthermore, POM indicates discrete, polydisperse crystalline-like fibres. However, the degree of crystallinity for the interlamellar glycerol cannot be confirmed from the SWAXS or microscopy experiments alone. To achieve further information about glycerol crystallinity, infrared spectroscopy can be used to examine the molecular environment (and hence crystallization). Infrared spectroscopy studies were attempted on a 16 Wt.% solution of SDS in

glycerol in order to determine any structural changes compared to the anhydrous crystal and pure glycerol. The composition of this mixture contained more than 99 Wt.% SDS-glycerol crystal phase (Appendix 8.2), with a small amount of anhydrous crystal phase that minimally impacts the spectra. The increased signal resulting from a high SDS-glycerol phase concentration should enable clear identification of peak shifts.

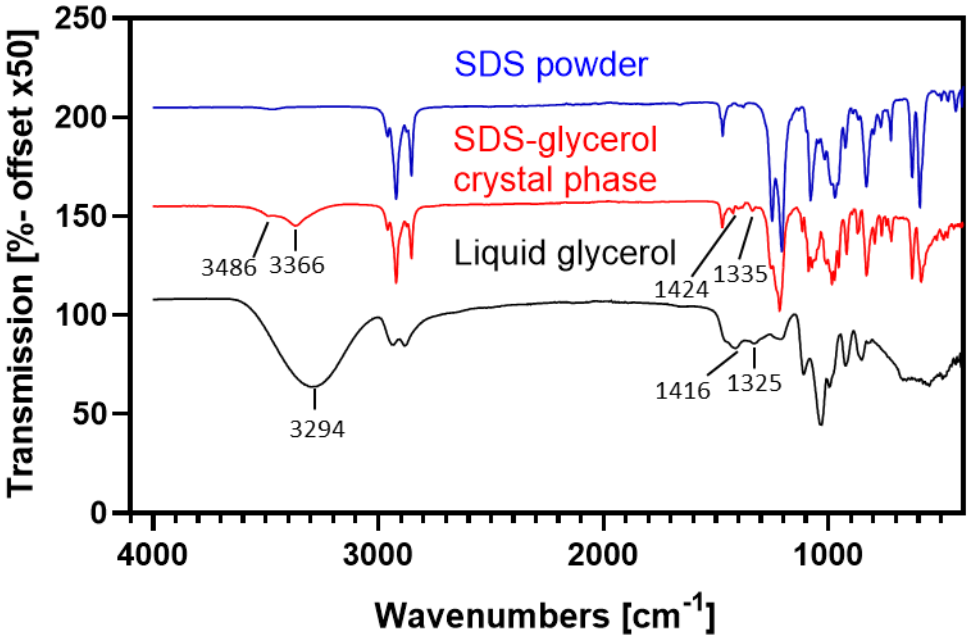

Figure 4.10: Infrared spectra (offset to allow comparison) of (top) SDS Powder, (middle) background subtracted SDS-glycerol crystal phase) and (bottom) liquid glycerol. v-OH vibrations of glycerol observed above 3000 cm^{-1} indicate hydrogen bonding and additional order in the SDS-glycerol crystal phase compared to liquid glycerol. CH bending vibration of glycerol indicated between 1325-1425 cm^{-1} for SDS-glycerol are shifted relative to that for liquid glycerol.

By subtracting the scattering from liquid glycerol from the SDS containing mixture (Appendix 8.8), it was possible to obtain the infrared spectrum for solely the SDS-glycerol phase (Figure 4.10). When identifying peaks in the resulting spectrum, most prominent peaks originating from SDS within the SDS-glycerol phase had similar wavenumbers and relative intensities to those of anhydrous SDS phase, suggesting a similar structural arrangement of the SDS molecules. However, the emergence of new bands at higher wavenumbers, greater than the peak centre of amorphous glycerol, indicates the presence of H-bonding.[77] This indicates the possibility for bound or structured (as opposed to disordered) glycerol within the crystal, much like with bound water in hydrated SDS crystals.[78] (Poly)crystalline glycerol exhibits two predominant bands representing five v-OH vibrational modes at low temperatures (77 K). The temperature difference may account for the polycrystalline glycerol bands

existing at ~100 cm^{-1} lower than the experimental results shown in this work.[79] However, the similarity between literature and experimental data is not a coincidence and is further evidence for the order and crystallinity of the SDS-glycerol system.

4.2.5. Differential Scanning Calorimetry Measurements for Determination of Krafft Temperature

A large induction time for the formation of the SDS-glycerol phase was observed. Hence it was difficult to measure crystallization and Krafft temperatures, even at 0.1 °C min^{-1}. Therefore, a method previously established for the determination of Krafft temperature in coagels was employed. [25,28] The Krafft point of SDS in glycerol has already been measured.[17] However, as micellar solubility varies with temperature, this work predominantly focuses on the Krafft temperature (K_T or critical micelle temperature, CMT) for industrially relevant concentrations. A baseline of pure glycerol was subtracted from samples to negate for any thermal behaviour of bulk glycerol. In general, peaks were broad and relatively easy to identify (Appendix 8.9). All samples were identified as pure SDS-glycerol by SAXS, except for 16 Wt.% SDS in glycerol, which contained small amounts of anhydrous crystal. It is expected that this would have a minor impact on the melting point, but it may cause a slightly lower expected endset temperature (Figure 4.11). Furthermore, the baseline of the resulting DSC curves after the melting point differed between samples (Appendix 8.9), although this is likely to have a minor effect on the endset temperature determination.[80]

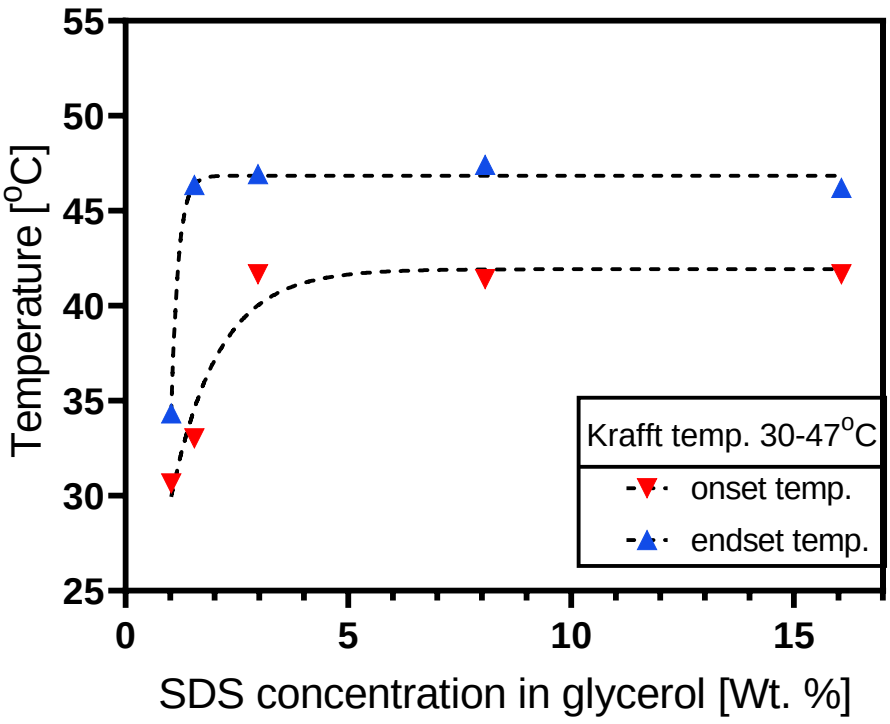

Figure 4.11: Phase diagram of SDS in glycerol either at or below 16 Wt.% SDS, as determined by melting profiles obtained using DSC , where red data points represent onset of melting peaks, blue data points represent endset of peaks, and the range between the points represent the melting range. Dotted lines indicate an exponential plateau fit to visualise the dependence of solubility on temperature. DSC melting profiles are shown in Appendix 8.9.

The Krafft temperature remained relatively constant above 3 Wt. % with a range of 41-46 °C between onset and endset. This is above the reported Krafft point but this is expected due to the higher concentration.[25,81,82] However, the weak signal for the 1 Wt.% sample has a less defined onset and therefore must be considered with caution. Overall, the data show that despite a Krafft point close to room temperature, the SDS-glycerol phase exists at 10-15 °C above the room temperature for industrially relevant concentrations.[17]

4.2.6. Rheological Characterisation of Physical Properties and Formation

Characterisation of physical properties for the SDS-glycerol crystal phase is essential for understanding its potential industrial implications. It is expected that the rheological profile is akin to that for coagels and LMWGs, but also shares similarities with crystalline suspensions, where aggregates can irrecoverably break under shear.[62,83] Initially, high variability was experienced for viscosity curves of SDS in glycerol which was partially attributed to shear-induced breakup prior to the measurements (i.e. sample loading to the rheometer). Two possible methods were available to counteract this artifact: an initial pre-shear stage, or in situ formation of the crystalline gel phase from the micellar solution. The

latter was chosen as it allowed characterisation of low shear behaviour, which is relevant to real world applications, i.e. expulsion of a cream or paste from a tube. Cooling in situ also allowed for control over cooling temperature, giving useful insight into process variability. Before measurements were undertaken, the mixtures were subjected to small amplitude oscillatory strain (10 rad s^{-1}, 0.1% strain) during cooling, to examine the formation of the phase in a rheological context.[84] The storage modulus (G') data was then used to measure Avrami kinetic behaviour at different temperatures (Figures 4.12a-12c), enabling comparison with the SAXS data (Figure 4.5).[24,52,58,85]

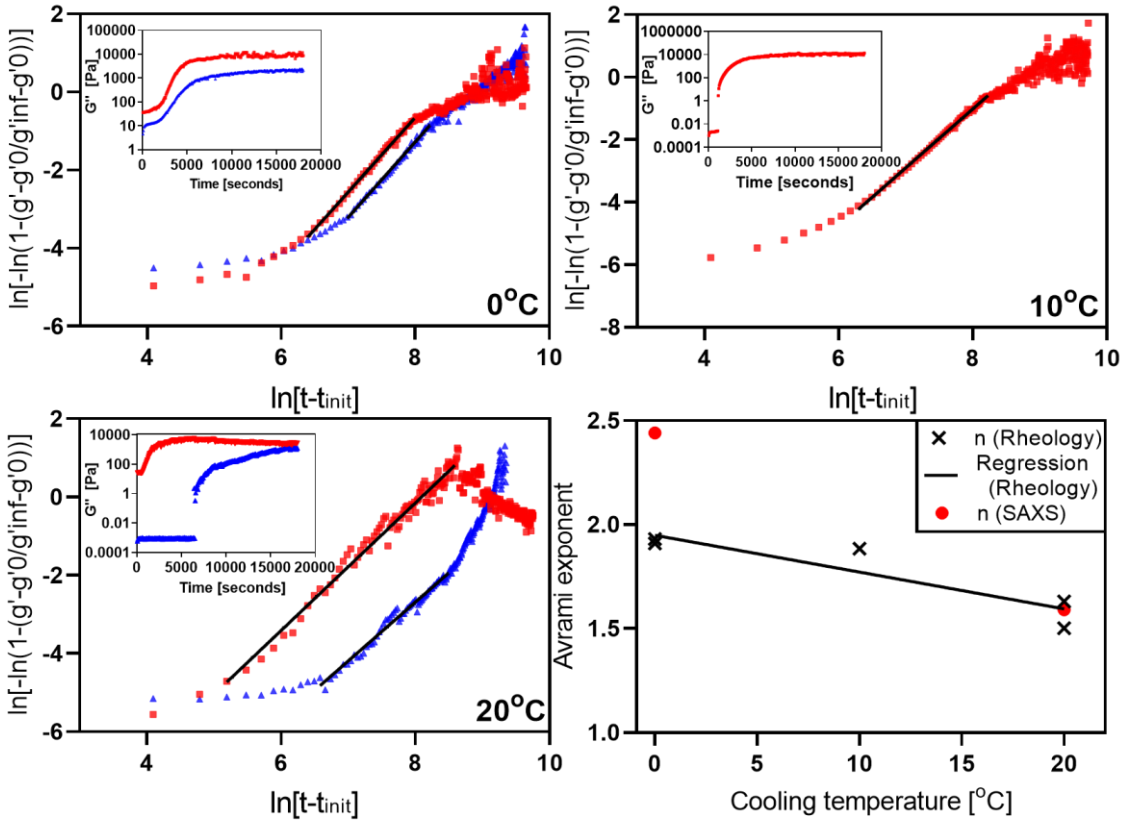

Figure 4.12: Linearised Avrami kinetic graphs measuring isothermal crystallization of 2 Wt.% SDS in glycerol at temperatures of top left) 0 °C, top right) 10 °C, bottom left) 20 °C. Insets shows oscillatory rheology measurements (0.1% strain amplitude at 10 rad s^{-1} angular frequency) measuring G' over time. Bottom right) Avrami exponent vs temperature with linear regression for rheological measurements of isothermal cooling. SAXS Avrami data are included for comparison. Blue and red data points show two separate recorded instances using the same variables (repeats), with both values of Avrami exponent included in bottom right graph.

A lag time was observed, mirroring SAXS data, although this varied widely from 100 to 6500 seconds (Figure 4.12, inserts). Repeats of structure development yielded similar behaviour for 0 °C, although this slightly differed for 20 °C. It is thought that the change in sample temperature may be inhomogeneous, arising from thermal equilibration of the rheometer heating/cooling elements.[86] As

direct observance of the phase abundance was not possible, linearisation of the Avrami kinetic equation was used.[58] The lag time and infinite viscosity were determined, with the former obtained by observing deviation from the initial trajectory, and the latter calculated from the highest G' value. All cooling measurements yielded a linear region for the Avrami plots, with deviation at either extreme. In most cases, this represents a plateau region being reached, whereby the majority of the surfactant is crystallized, and hence a reduction in the Avrami exponent is observed. However, one experiment conducted at 20 °C shows a positive deviation, potentially arising from imprecision in the linearisation method, notably $G'(\infty)$.

For all samples, an Avrami exponent between 1.5 and 2 was observed, with lower values at higher temperatures (Figure 4.12d). This agrees with the SAXS data, where an exponent between 1.6 and 2.4 was observed for 20 °C and 0 °C, respectively (Table 1). It is thought that the higher exponent at 0 °C indicated by SAXS, may be due to the greater surface area to volume ratio using a capillary as a sample holder, which allows for more efficient thermal transfer. However, factors such as geometry, wall material, presence of bubbles may cause the inherent variability in both Avrami exponent (n) and t_{init}. Nevertheless, the growth trends are clear and are coherent between the two different methods, which both indicate either increased branching or increase in dimensionality, with the latter potentially representing a transition from single needles to spherulites

Viscosity measurements of 2 Wt.% suspensions of SDS in glycerol were then performed (Figure 4.13). This was initially conducted using steady-state measurements to discern flow and yielding behaviour compared to toothpaste and common toothpaste structurants, with oscillatory measurements being performed later.[87–89] For the most part, the mixtures measured between 0 °C and 20 °C followed well-defined, shear-thinning behaviour. However, at low shear rates, a highly shear-thinning region is experienced instead of a plateau. Hence the data were treated as two separate regions (with the boundary indicated in Figure 4.13) and the data obtained above 0.35 s^{-1} were modelled using the Cross relationship.[90] Comparing model parameters, there was minimal difference in the degree of shear-thinning, infinite shear viscosity, or critical shear boundary between the different cooling temperatures. Despite similar viscosities throughout the range of shear rates, within the low shear region, sample cooled at 20 °C exhibited higher viscosities below 0.35 s^{-1}, which is most likely the result of larger crystals. This trend is not observed above the initial shear-thinning region, but at the lowest shear rates used as well as fitted η_0 measurements.

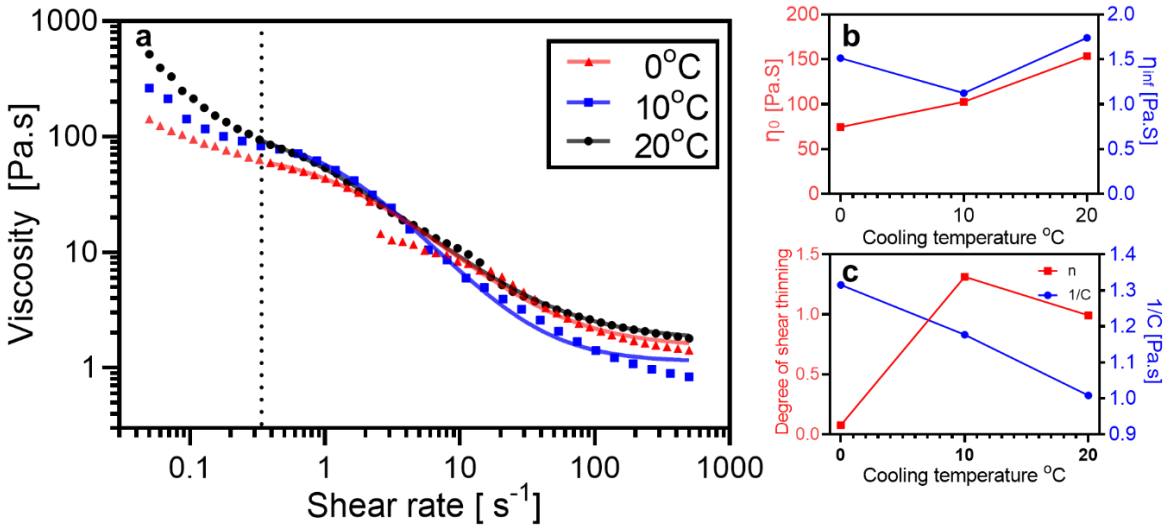

Figure 4.13: a) Steady-state viscosity curve of 2 Wt.% SDS in glycerol, recorded at 20 °C, measured after the quenching from 80 °C to 20 °C at 30 °C min^{-1}, followed by isothermal cooling at 20 °C for 5 hours. Two distinct regions can be observed: a low-shear-thinning region ($\dot{\gamma}$< 0.35 s^{-1}) with power law type scaling, indicated by the dotted line, caused by the network structure formed from the crystal suspension. A higher shear rate region, which exhibits more traditional 'Cross-like' behaviour. b) Cross model output parameters for zero shear (η_0) and infinite shear (η_{inf}) viscosity. C) Cross model output parameters for degree of shear-thinning and shear-thinning boundary (1/C).

The shear-thinning behaviour of SDS-glycerol gels shares similarities to a 'yield stress gel',[95] which typically transforms from solid-like behaviour to liquid-like above a certain yield stress, although oscillatory measurements are needed to confirm this. However, unlike microgel/polymeric equivalents, the SDS-glycerol mixture forms crystalline fibres, which are unlikely to reform. The shear-thinning behaviour arises from the weak network structure that is formed during crystallization, which when disrupted, causes loss in viscosity. It does not explain why shear-thinning behaviour is Cross-like after the initial reduction in the low shear region. Therefore, multiple mechanisms must be occurring to explain this multistage shear-thinning behaviour.[91] Firstly, the temperature dependent low shear viscosity will depend on the crystal network, and hence if the habit remains the same, this can only be logically attributed to relative crystallite size. This is because higher temperatures lead to slower rates of crystal nucleation growth, thus producing larger aggregates. The larger crystal aggregates are stronger and require more force to disrupt and break into smaller aggregates and/or align parallel to the shear direction.[92] Once the network is disrupted, but the majority of fibres are not broken, the first reduction in gradient is reached. As the shear rate is increased, fibres begin to break up and align due to shear.[93] Finally, the remaining aggregates are small enough to align along the shear direction and are likely to suffer minimal further breakage. Hence an infinite viscosity plateau is reached. However, this

cannot be confirmed through viscosity measurements alone. Creep testing was partially successful for 2 Wt.% mixtures of SDS cooled at 20 °C (Appendix 8.10), indicating a transition from elastic to viscous flow at 0.15 %. While some degree of structural recovery was observed, a different testing methodology must be employed to understand the rheological behaviour at higher shear rates.

Shear-induced polarised light imaging (SIPLI) detects birefringence during shear events, which indicate alignment and hence rationalises viscosity behaviour. A 2 Wt.% solution of SDS in glycerol was cooled in situ initially from 80 °C to 20 °C at 30 °C min^{-1}, followed by isothermal cooling for 3 hours at 20 °C. The cooling time was chosen from evidence for complete crystallization using SAXS measurements. A shear rate of 100 s^{-1} was chosen (Figure 4.14) as this considers a high shear scenario where breakdown of fibres is likely to occur, with images recorded throughout the 33 minute measurement time.

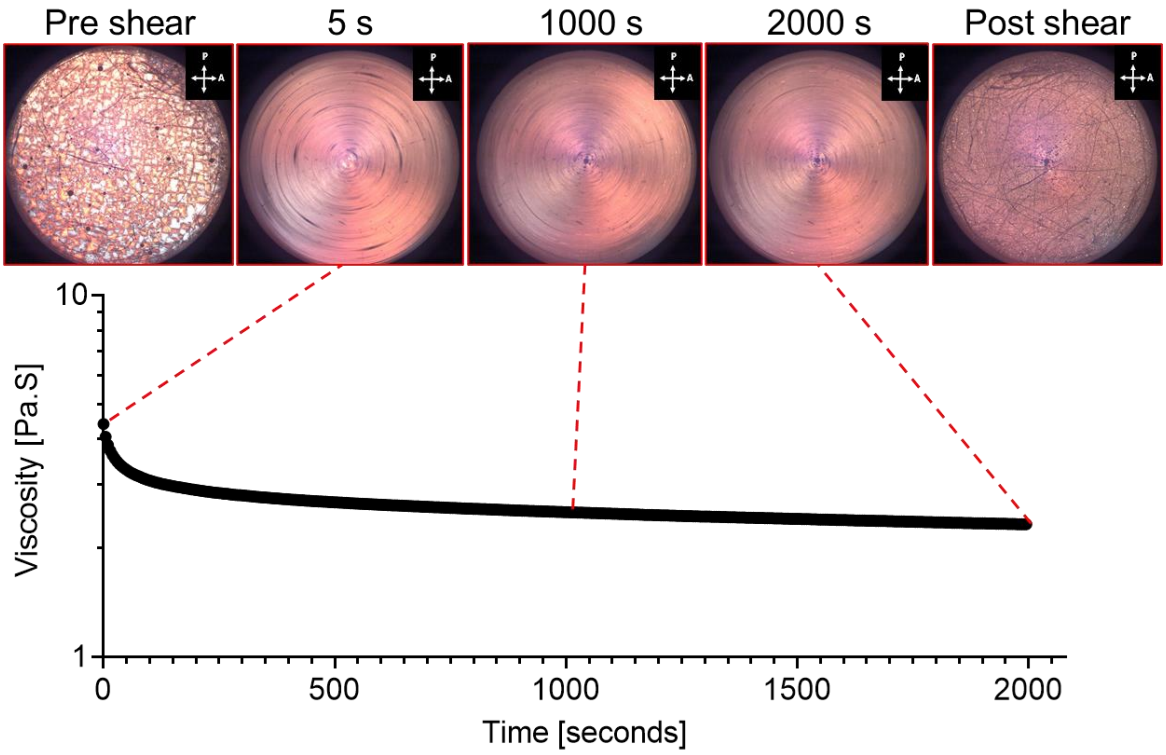

Figure 4.14: Rheo-SIPLI measurements of 2 Wt.% SDS in glycerol, performed at the sample edge shear rate of 100 s^{-1}, recorded at 20 °C, after quenching from 80 °C to 20 °C at 30 °C min^{-1}, followed by isothermal cooling at 20 °C for 3 hours. Representative SIPLI images were recorded throughout the shear profile. Large crystal aggregates (seen initially in the pre shear polarised light image) break down and align under shear, evidenced by the Maltese cross formation and reduction in viscosity.[94] Immediately following the shear event, the majority of material loses orientation. Direction of polariser and analyser indicated by P and A, respectively. Note that artifacts originating from imperfections on the surface of the glass sample plate, as seen 'pre shear' and 'post shear' which is not indicative of sample makeup.

Within the first 5 seconds of shear being applied (Figure 4.14), a Maltese cross begins to form, indicating almost immediate orientation to the direction of shear.[94] Simultaneously, there is a loss in viscosity which is initially steep, but decays exponentially, producing a plateau at half the initial viscosity. The small change in viscosity is accompanied by a modest change in birefringence, with the Maltese cross marginally more evident at 1000 s and virtually no change beyond this timeframe. Finally, immediately after the shear event, the majority of fibres loose orientation, causing a loss in the observed polarisation- albeit only for a small area within the centre. The resulting post-shear mixture is predominantly homogeneous, unlike the pre-shear mixture, for which large crystalline domains are evident. Thus, the SDS-crystal phase is highly sensitive to shear, with immediate break-up of the crystals coinciding with alignment when high shear is applied. Rheo-SIPLI data coincides with successive viscosity curves (Appendix 8.11), whereby the structure behaves similar to a non-recoverable 'yield stress gel'.[95] A general trajectory can be considered during shear (Figure 4.15). Shear causes initial disruption of the network structure, prior to large scale breakup and alignment of the resulting crystalline aggregates.

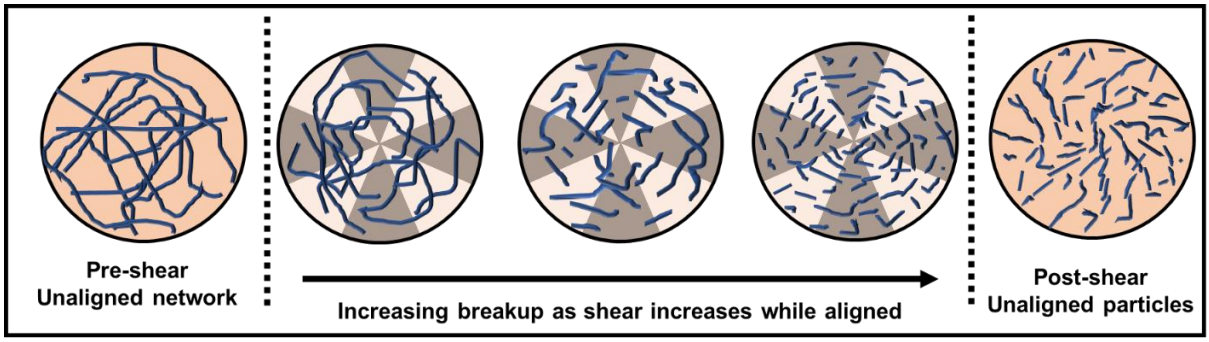

Figure 4.15: Schematic representation of SDS-glycerol crystal fibre breakup over time while experiencing shear, linking both SIPLI and rheological data (Figure 4.14) as well as the viscosity data (Figure 4.13).

Steady-shear rheology indicates the highly shear-thinning nature of the gel phase. However, to establish the full rheological behaviour, oscillatory data are needed. Initially, a strain amplitude sweep was performed to determine the linear viscoelastic range (LVER) (Figure 4.16a) for samples quenched from 80 °C to 20 °C at 30 °C min^{-1} followed by cooling at 20 °C for 5 hours. This temperature profile was chosen due to its proximity to quiescently cooled conditions. The LVER was observed to be narrow, with a maximum strain at ~ 0.15 %, coinciding with the creep recovery test. Therefore, the structure is characterised as brittle, due to its limited elasticity. Notably, G' exceeds G'' up to ~ 4 % strain, where a crossover occurs. This corresponds to 'yield-stress gel' like behaviour, as the material is G'' dominated (hence more liquid like) once the structure is broken.

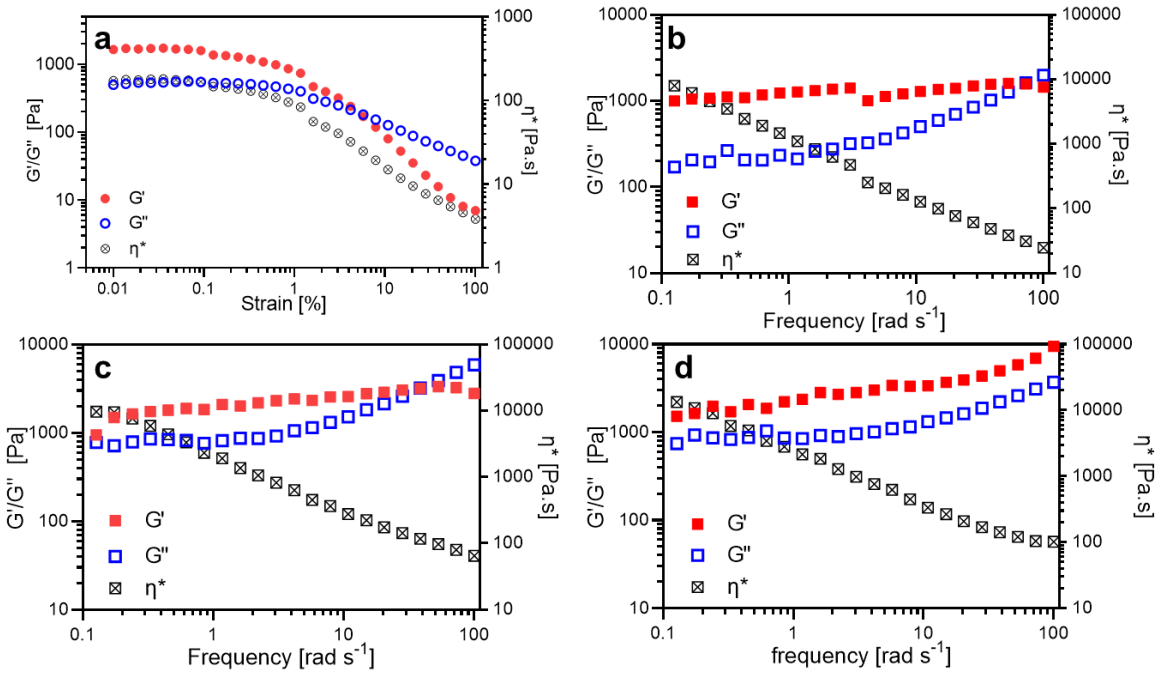

Figure 4.16: Oscillatory rheology of 2 Wt.% SDS in glycerol solutions measured at 20 °C, after quenching from 80 °C to 20 °C at 30 °C min^{-1}, followed by isothermal cooling at different temperatures for 5 hours. Note that following cooling, the mixture was brought to the measurement temperature of 20 °C and equilibrated for a further 2 minutes before being studied. a) Strain sweep at an angular frequency of 10 rad s^{-1}, measured following isothermal cooling at 20 °C. b) Frequency sweep (0.1% strain amplitude) measured following isothermal cooling at 20 °C. c) Frequency sweep (0.1% strain amplitude) measured following isothermal cooling at 10 °C d) Frequency sweep (0.1% strain amplitude) measured following isothermal cooling at 0 °C.

From the LVER range determined for the amplitude sweep (Figure 4.16a, < 0.15 %), 0.1 % strain amplitude was chosen for the subsequent frequency sweeps, providing a strong signal response within the LVER. The frequency sweeps were conducted at three temperatures, as in the steady shear measurements. For all samples, G' was significantly greater than G'' for the majority of the frequency region studied, indicating a gel-like material. However samples cooled at 10 °C and 20 °C exhibit a crossover between G' and G''. This indicates a liquid region, meaning that the material is not a true gel and has liquid character, whereas samples cooled at 0 °C can be considered to be a true gel. Moreover, both G' and G'' and by extension η*, are higher as the mixture is cooled to lower temperatures. This is likely due to the more effective network formed from smaller more uniformly dispersed crystals at lower temperatures.

Initially, oscillatory data appear to be inconsistent with the steady-state viscosity curve data: for which the low shear region shows a positive correlation between cooling temperature and viscosity. This is because both experiments describe different shear events. In the frequency sweep data, the material is subjected to a small oscillatory shear that does not break the structure. Comparatively, continuous

shear initially disrupts the networks in the low shear region, before breaking up the crystal structures into smaller particles. This must be considered when designing a formulation such as a toothpaste, where yielding and shear-thinning on application is just as important as stability and gel-like behaviour on its removal from a container or tube.

Overall, the mixtures behave much like a fragile, brittle gel, which yields at exceptionally low strains. The subsequent breaking and aligning of aggregates under continued shear can be evidenced by SIPLI, as well as the inherent variability in crystallization, as seen in both steady-state and oscillatory measurements. Despite this, the degree of structuring that can occur at low concentrations is remarkable and could aid formulation design by boosting viscosity without polymer additives. However, the rheological behaviour is quite unlike polymers and hence further exploration is warranted.

4.2.7. Comparison to the Literature Data

Shortly after the majority of the experimental work in this project was completed, Mathews et al. reported that a presence of an SDS-glycerol 'microfibrillar gel phase' was formed above the CMC.[14] Microscopy indicated an identical fibre morphology and SAXS confirmed similar increases in lamellar spacing when compared to anhydrous SDS (Table 4.2). Rheological measurements indicated similar structuring behaviour; with identical observance of gelation at ~ 2 Wt.%, and G'' dominated behaviour at high strain rates measured during amplitude sweep. Unfortunately, no-in situ gel formation had been attempted while measuring rheology, which might lead to lower than expected viscoelasticity values. An example of this is in strain analysis where the LVER is observed below 0.1 % strain. This could indicate a less structured mixture, with a reduction in elasticity resulting from disruption to the gel network. However, a similar frequency sweep for the 2 Wt.% SDS in glycerol cooled at 0 °C was observed for a 4 Wt.% sample of SDS in glycerol (quiescently cooled), with no crossover between G' and G'' at high frequencies. This is most likely due to the increased entanglements when more ribbon crystals are present at higher concentrations.

However, characterisation of the microstructure of the gel phase can be achieved through simplistic model parameterisation, in which a glycerol region and a bilayer region is identified. The work presented in this chapter is close in agreement with that of Matthews et al. for the glycerol sublayer thickness, as well as the lamellar period. However, work conducted in this thesis is considered to be a more robust method for obtaining structural information. Analysis of electron density profiles enabled further study of the SDS-glycerol phase, with an estimate of the bilayer tilt to be 18-22°. This information, together with diffraction peaks observed by SAXS/WAXS and microscopy data, suggests

that the 'microfibrillar phase' is highly crystalline. Moreover, IR spectroscopy studies indicate an ordered crystalline glycerol layer. A summary of key findings with regard to the microstructural parameters, is provided in Table 4.2.

Table 4.2: Comparison of structural parameters between work described by Matthews et al., and this work regarding the SDS-glycerol phase.[14] While main structural features remain similar, a distinction can be drawn between stoichiometry and crystallinity.

	Matthews et al.[14]	This work
Lamellar period [Å]	55.6	55.4
Thickness of glycerol region [Å]	8	7
Molecular tilt [degrees]	N.A.	20
Glycerol: SDS stoichiometry	1:1.5-2.0	< 1:1
Phase characterisation	Paracrystalline mesophase	Co-crystal

4.3. Results and Discussion: *n*-Alkyl Sulfates in Polyols

4.3.1. Room Temperature Behaviour of *n*-Alkyl Sulfate Homologues in Glycerol

Initially, anionic amphiphiles that are structurally analogous to SDS (e.g. sodium dodecanoate, sodium dodecyl benzenesulfonate, sodium dodecyl sulfonate) were examined as 2 Wt.% solutions in various polyols (glycerol, 1,3-propanediol and ethylene glycol) via a thermal cycle, to determine if similar fibre co-assemblies could be formed. However, such studies did not result in any gelation or fibre phase. In contrast, when linear (even chained) alkyl sulfates with a range of chain lengths from C10 to C18 in glycerol were tested, more promising results were obtained. To account for different Krafft temperatures, heating at 100 °C was used to fully dissolve the surfactant initially. As well as SDS, C14-C18 alkyl sulfates exhibited gel formation. POM images indicated polymorphic crystal structures comprising a predominantly fibre morphology for C14 and C18, with platelets and needles being present as well (Figure 4.17). Unfortunately, owing to the small amount of material available at the time, the C16 glycerol phase was not captured using microscopy, but characterised by SAXS alone. C10 alkyl sulfate solution remained soluble at room temperature, suggesting that fibre formation might occur at lower temperatures. The fibres seen in Figure 4.17 display a similar size and morphology to those formed by SDS. This suggests a similar structural motif, whereby glycerol is intercalated between SDS bilayers.

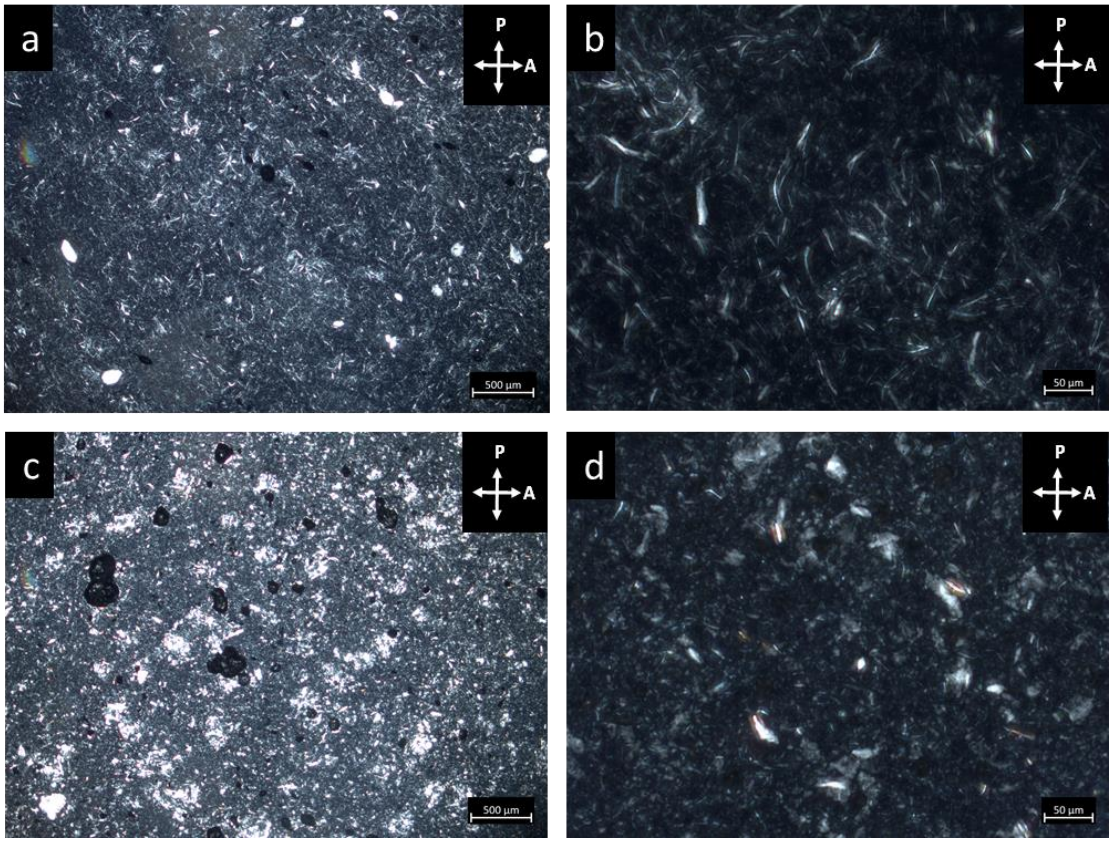

Figure 4.17: Polarised optical microscopy images of a) and b) 2 Wt.% sodium n-tetradecyl sulfate in glycerol (a and b) and 2 Wt. % sodium n-octadecyl sulfate in glycerol (c and d) following heating at 100 °C and quiescent cooling overnight. C. Both samples show a mixed phase with ribbons associated with SDS-glycerol crystal phase, and other morphologies (e.g. platelets) associated with hydrated and anhydrous crystal types. Direction of polariser and analyser indicated by P and A, respectively.

It is hypothesised that the formation of mixed phases of alkyl sulfate crystals is caused by (i) the lower purity of the starting materials, with the likely presence of synthetic precursors and other impurities,[14] and (ii), the increased Krafft temperature causing more rapid crystallization under quiescent conditions. This may be the reason why C18 shows a higher presence of a) non fibre species and b) smaller fibre motifs, despite being cooled quiescently. Nevertheless, both C14 and C18 form fibres similar to that of SDS-glycerol (Figure 4.3). SAXS patterns further confirm crystal polymorphism with the presence of varying solvates and anhydrous crystals (Appendices 8.6, 8.12, 8.13, and 8.14). The origin of such hydrates is thought to be residual water within the starting materials. Nevertheless, all samples from C14-18 contained phases with a larger than expected lamellar period. When first order peak spacing of the glycerol containing crystals (001_G) is plotted against alkyl chain number, a highly linear trend is seen (Figure 4.18).

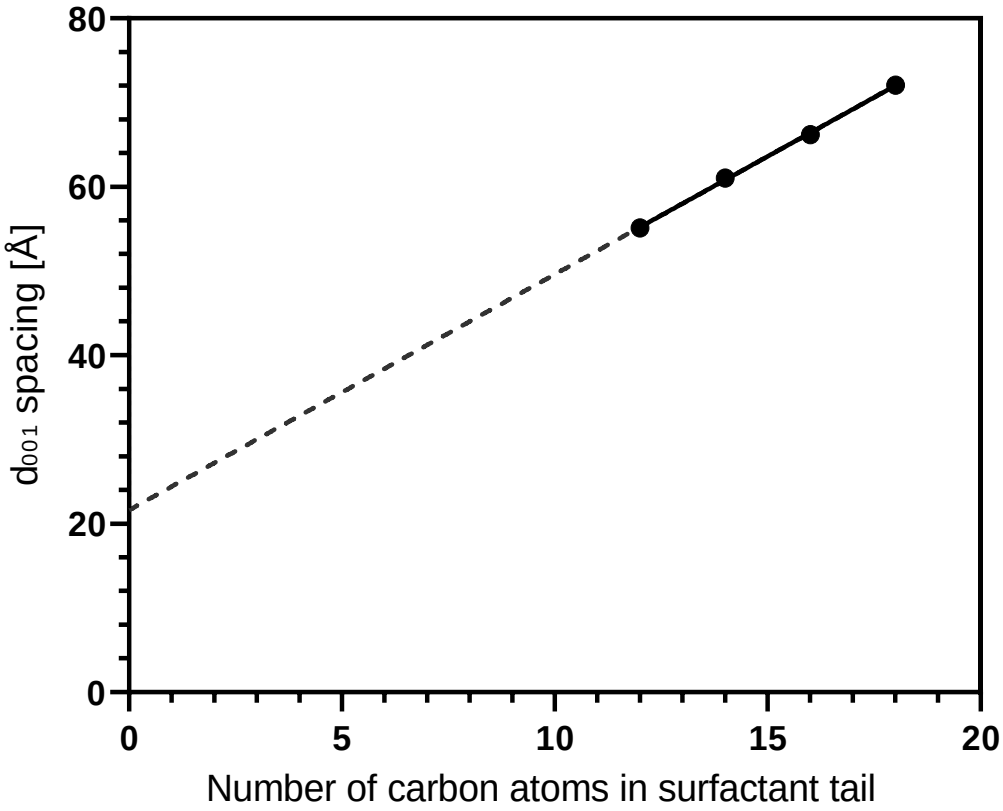

Figure 4.18: Lamella (d_{001}) spacing determined from SAXS patterns for a homologous series of n-alkyl sulfate surfactants in glycerol mixtures. This is plotted against number of n-alkyl carbon atoms. Linear regression is extrapolated to the theoretical '0 carbon chain' for an n-alkyl sulfate molecule exhibiting an n-alkyl sulfate-SDS crystal phase. 1D scattering patterns and associated fits are presented in Appendices 8.6, 8.12, 8.13, and 8.14.

By exploring the relationship between number of carbons and d_{001}-spacing, a linear trend can be extrapolated to zero carbon atoms. It can be assumed that the change in alkyl chain tilt is either systematic (unlikely) or negligible (more likely). Therefore, an estimation of the sublayer for alkyl sulfate-glycerol crystals , which contains the sulfate head region and glycerol, can be established. This value is 21.6 Å, which can be compared with the values observed for the electron density profile of SDS alone. Sublayer information from structural analogues suggests the 'whole' headgroup (as well as glycerol) exists within the 11.3 Å each side of the bilayer. Interestingly, both the -1-1-1-11 and 1-1-1-1-1 phases for the EDP of SDS exhibit peak maxima at the same sublayer measurement distance. However, this represents the distance from the centre of the headgroup outwards, defining a slightly different region. The main atom to fall outside of this region is the oxygen molecule adjoined to the carbon chain, where the atomic centre lies 1.2 Å towards the centre with respect to the layer normal. The difference is likely to be an effect of resolution of the EDP or the assumption of zero tilt in the non-primary axis, slightly altering sublayer values. Nevertheless, the congruence between EDP and d_{001}-spacing of alkyl sulfate-glycerol crystals is a clear indication of the accuracy of the electron density

model, and the ubiquity and uniformity of the alkyl sulfate-glycerol cocrystal structure. Determination of crystal structure (through single crystal diffraction) would allow confirmation of glycerol stoichiometry and is the next step in characterisation of the species.

4.3.2. Room Temperature Behaviour of Sodium Tetradecyl Sulfate in Ethylene Glycol

It has been shown that the self-assembly of sulfate surfactants and polyols is not limited to a single molecule (SDS) but is also possible for homologous analogues. To understand the driving force for co-assembly, C12 and C14 alkyl sulfates were tested in solutions of ethylene glycol and propanediol (4 Wt.%). While no phase change occurred in propanediol, C14 exhibited gel formation at 4 Wt.% when heated and cooled above the Krafft temperature in ethylene glycol. C12 was soluble at room temperature, and even cooling at 0 °C did not yield crystals. POM studies of C14 revealed similar crystalline fibres to that observed for SDS and glycerol (Figure 4.19).

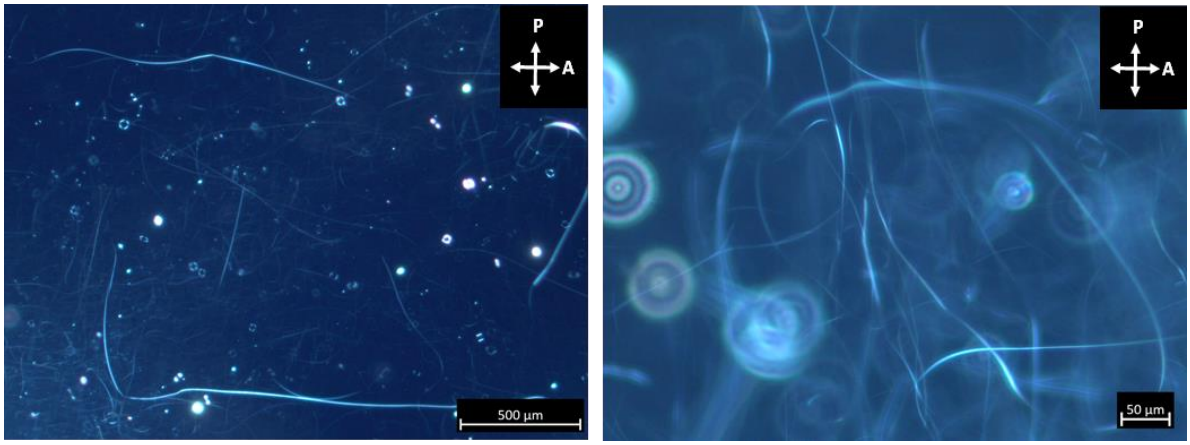

Figure 4.19: Polarised optical microscopy images of 4 Wt. % sodium tetradecyl sulfate in ethylene glycol after isothermal quiescent cooling overnight from 75 °C. Ribbon crystal formation suggests a similar mode of assembly to that for alkyl sulfate-glycerol crystal phases, indicating that ethylene glycol becomes intercalated within a sublayer region between surfactant headgroups. Note that the blueness of the images is not as a result of the sample, but incomplete auto-white balance during image acquisition. Direction of polariser and analyser indicated by P and A, respectively.

Remarkably, a fibre motif is observed when C14 is cooled quiescently in ethylene glycol. Fibres show a degree of anisotropy with irregular twists, and polydisperse lengths. Despite ethylene glycol being a toxic substance and therefore not relevant for personal care products, these results show that both the surfactant and solvent type can be altered and tuned, while still achieving gelation. To confirm the inclusion of ethylene glycol (EG) within the structure, SAXS analysis was performed. Due to the inferior

equipment used, 4 Wt.% solutions were employed to ensure higher signal to noise ratios. The resulting mixture was compared to sodium tetradecyl sulfate powder (Figures 4.20).

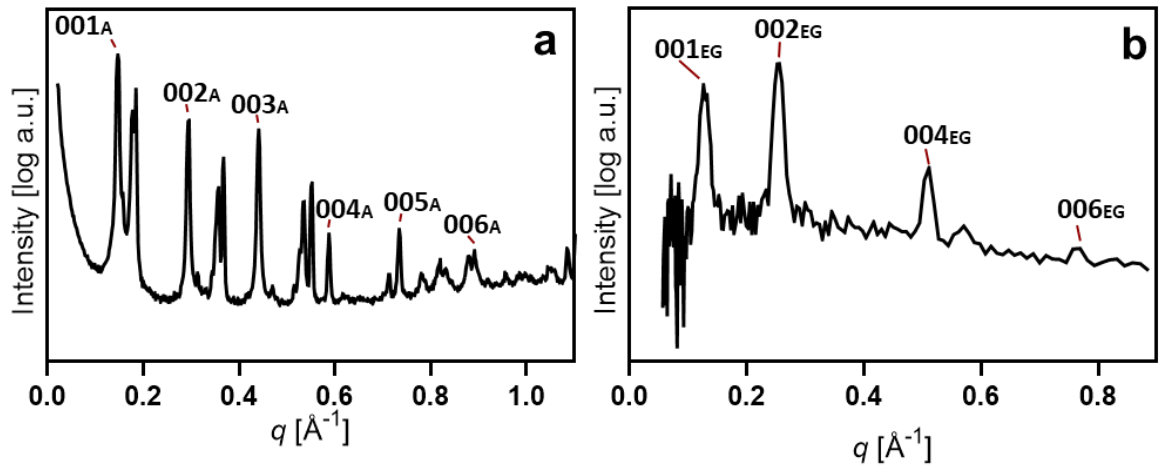

Figure 4.20 a) SAXS pattern recorded for sodium n-tetradecyl sulfate (C14) powder as received (undried). Hydrate crystal phase labelling has been omitted for ease of reading. b) Background corrected 1D SAXS pattern of gelled 4 Wt.% C14 in ethylene glycol mixture. $00l_A$ and $00l_{EG}$ are Miller indices used to denote lamellar peaks of the respective phases. (anhydrous SDS and gelled C14 alkyl sulfate-ethylene glycol phase).

Within the SAXS pattern (Figure 4.20b) the 1st, 2nd, 4th, and 6th order 00*l* peaks were most prominent for the STS (C14)-ethylene glycol phase. With limited literature crystallographic data for C14 (sodium *n*-tetradecyl sulfate)[96] and poor resolution of the STS-ethylene glycol SAXS pattern, it was not possible to reconstruct EDP's with a high degree of certainty owing to the phase problem. However, this could be achieved in future work by obtaining crystallographic information for sodium tetradecyl sulfate, followed by better quality (higher signal to noise) scattering data for C14 in ethylene glycol. Comparing the SAXS pattern of C14 in ethylene glycol to its constituent powder form (prior to drying), an increase in spacing from 42.5 Å to 49.3 Å is observed. The d_{001} spacing is noticeably smaller than the STS (C14)-glycerol phase (61.0 Å). Despite ethylene glycol containing one less carbon/alcohol group, the considerable difference in spacing can only be rationalised by an appreciable change in tilt. The evidence in d_{001}-spacing change, along with the formation of fibres indicate that co-assembly during crystallization of alkyl sulfates and other polyols can occur. Furthermore, both ethylene glycol and glycerol, which are known for their cryoprotectant properties,[97] can form crystalline, ordered assemblies. It is noteworthy that alkyl sulfates in 1,3- propanediol did not gel or form fibres, suggesting that two adjacent hydrogen bond donating groups may be important to interact and co-assemble, or simply a high hydrogen bond density. This may be because the solvent molecule can form multiple hydrogen bonds with the sulfate group, in accordance with Etter's rule,[98] although future work screening a larger solvent range could Identify systematic behaviour.

In both crystallography and LMWGs, attempts have been made to provide a theoretical underpinning into the science of co-assembly.[99] This has been met with varying success[100] and different strategies have been employed, including the predictive use of Hansen solubility parameters.[101] While water readily forms hydrated crystals in aqueous media, its polarity and ability to hydrogen bond is superior to that for other solvents (Table 4.3). Despite being less polar, with a reduced hydrogen bonding, both glycerol and ethylene glycol exhibit co-assembly, despite their solubility with alkyl sulfates.

Table 4.3. Comparison of selected physical properties of polar protic solvents, which undergo co-assembly or solvate (co)crystallization with n-alkyl sulfates. Green cells indicate observed (or literature) co-assembly behaviour, and red indicates no observed co-assembly.

	1,3-Propanediol	Ethylene Glycol	Glycerol	Water
Dielectric constant	35.0†[102]	38.66 †[103]	41.14†[18]	80.37†[18]
Hansen solubility parameter – H-bonding component (δh) [$MPa^{1/2}$]	23.2[101]	26.0[101]	29.3[101]	42.3[101]

†Measurements at 20 °C

1,3-Propanediol is the least polar (as well as a lower δh) solvent shown in the selection (Table 4.3), but it is only marginally less polar than ethylene glycol. This shows the limitation of using solubility parameters to define co-assembly in a quantitative manner, as recognized by Lan et al.[100] It is this therefore suggested, that further investigations of alkyl sulfate crystal gel phases must be carried out with geometry of the constituents undergoing assembly in mind. Although multiple H-bonding sites in close proximity may not be critical for co-assembly,[37] the work presented here suggests a crucial relationship with the sulfate head group, and the diol motif within the solvent, particularly for fibre formation. While evaluation of alternative head groups proved unsuccessful, the cocrystallization and fibre formation was less specific with regard to towards tail composition. Therefore, possible future directions for this research are include identifying the importance of a diol motif, surfactant, or solvent in regard to hydrogen bonding that leads co-assembly. Alternatively, tail composition, including branching, unsaturation, and odd carbon numbered chain lengths which will effect packing of the surfactant, can also be explored. If successful, such changes will also change the physical properties, and potentially improve the desirable qualities of the structuring system, e.g. the crystallization rate, Krafft temperature and degree of branching of the fibres.

4.4. Conclusion and Future Work

A novel gel phase was identified in glycerol-SDS binary mixtures below the Kraft temperature and above the CMC. Rheological characterisation indicated a highly structured material that exhibited elastic properties (and hence G' dominated behaviour) within the LVER. However, amplitude sweep and steady shear data indicated a brittle network with irrecoverable loss of structure even at low shear rates. The mixtures therefore behave like crystal networks, where aggregates are physically broken in shear events, causing yielding, flow, and alignment, similar to a non-recoverable yield-stress gel.[83] The structure arises from growth of fibre-like crystal aggregates, which entangle and gel, as indicated by SAXS, microscopy and rheology studies. These aggregates grow to large sizes (> 500 µm), facilitated by slow growth and limited primary nucleation in quiescent conditions. The layer structure was identified by SWAXS to be novel and have considerably larger period than all known crystal phases of SDS, with a high degree of order and tilted alkyl chains within the layer. Electron density distribution information was elucidated from the scattering data and rationalised in the context of the anhydrous crystal phase. The SDS-glycerol crystal phase was shown to contain glycerol intercalated in between SDS bilayers. Moreover, the tilt of the bilayers were estimated to be 18-22°, which is similar to anhydrous SDS. Measurement of the Krafft temperature at industrially relevant concentrations indicated an increase from the Krafft point.[17] While expected, this s has important implications for storage, production, and use in personal care formulations. While the crystallinity of the structure was evident through the high degree of order exhibited in the scattering data, and aggregate formation in POM, the crystallinity of glycerol within the sublayer could not be verified. This was therefore achieved by recording infrared spectra, to reveal defined ν-OH vibrations, suggesting order and H-bonding motifs similar to that of polycrystalline glycerol.[79] Thus, the structure is as almost wholly crystalline, as opposed to a supramolecular (aggregated) nanosized assembly, which has implications for the mechanism of formation. Nevertheless, similarities between fibrous gels such as SaFiNs are clear with similarities in fibre-like morphologies and structures[104] and rheological behaviour.[105] The characterisation of this phase leads to an improved view of the SDS-glycerol phase and of work conducted by others in parallel to this study,[14] whereby the phase is considered as a microfibrillar gel that is also paracrystalline.

Studies of analogous crystalline gel systems based on alkyl sulfate homologues in glycerol were also undertaken. It was observed that a common structural motif of a layered structure was present, whereby glycerol existed within an intercalated sublayer. Furthermore, a linear increase in the layer period with carbon chain length was observed, consistent with original sublayer measurements made for SDS in glycerol. In principle, further structural information could be obtained by growth of single crystals in order to obtain diffraction data. This is because the method of electron density profile

reconstruction, while successful, was limited by resolution, causing some degree of ambiguity with regard to the sublayer depth. In the short term, preparation of more concentrated gels may allow unit cell determination, if single crystal formation is not possible. Despite no surfactants with alternate head groups able to form gels in a range of protic polyol solvents, sodium *n*-tetradecyl sulfate in ethylene glycol was shown to form crystalline structures similar to the equivalent glycerol mixtures. This suggests the importance of multiple H-bonding sites with appropriate directionality for gel formation, as opposed merely polarity effects. This is an exciting discovery which opens the door for surfactant and solvent design employing diol (or equivalent non-covalent) bonding motifs, much like the work conducted with water and ascorbate surfactant derivatives, which enabled coagel formation.[106] The present study introduces a means of structuring for non-aqueous personal care or drug formulations, without the use of polymers and using common ingredients, which may be modified to tailor of physical properties.

4.5. References

1 C. Edser, *Focus on Surfactants*, 2018, **2018**, 1–2.
2 A. Kunal and S. Singh, *Glycerol Market Trends Analysis 2018-2024 World Industry Report*, 2018.
3 G. V. Jensen, R. Lund, J. Gummel, T. Narayanan and J. S. Pedersen, *Angewandte Chemie*, 2014, **126**, 11708 –11712.
4 O. G. Us 'yarov, *Colloid Journal*, 2016, **78**, 698–704.
5 T. Zemb and P. Charpin, *Journal de Physique Paris*, 1985, **46**, 249–256.
6 S. L. Gawali, M. Zhang, S. Kumar, D. Ray, M. Basu, V. K. Aswal, D. Danino and P. A. Hassan, *Langmuir*, 2019, **35**, 9867–9877.
7 E. Summerton, M. J. Hollamby, C. S. Le Duff, E. S. Thompson, T. Snow, A. J. Smith, C. Jones, J. Bettiol, S. Bakalis and M. M. Britton, *Journal of Colloid and Interface Science*, 2019, **535**, 1–7.
8 E. Summerton, G. Zimbitas, M. Britton and S. Bakalis, *Journal of Crystal Growth*, 2016, **455**, 111–116.
9 R. Ciriminna, C. Della Pina, M. Rossi and M. Pagliaro, *European Journal of Lipid Science and Technology*, 2014, **116**, 1432–1439.
10 T. F. Tadros, *Applied Surfactants: Principles and Applications*, Wiley, Weinheim, 2005.
11 F. Lippert, *Monographs in Oral Science*, 2013, **23**, 1–14.
12 R. M. Miller, A. S. Poulos, E. S. J. J. Robles, N. J. Brooks, O. Ces and J. T. Cabral, *Crystal Growth & Design*, 2016, **16**, 3379–3388.
13 S. E. Friberg, I. Blute and P. Stenius, *Journal of Colloid And Interface Science*, 1989, **127**, 573–582.
14 L. Matthews, Ż. Przybyłowicz, S. E. Rogers, P. Bartlett, A. J. Johnson, R. Sochon and W. H. Briscoe, *Journal of Colloid and Interface Science*, 2020, **572**, 384–395.
15 C. C. Ruiz, L. Díaz-lópez, J. Aguiar, L. Díaz-López and J. Aguiar, *Journal of Dispersion Science and Technology*, 2008, **29**, 266–273.
16 D. J. Lee and W. H. Huang, *Colloid and Polymer Science*, 1996, **274**, 160–165.

17 H. Khan, J. M. Seddon, R. V Law, N. J. Brooks, E. Robles and J. T. Cabral, *Journal of Colloid And Interface Science*, 2018, **538**, 75–82.
18 *Physical properties of glycerol and its solutions*, Glycerine Producers' Association, New York, 1963.
19 R. A. Abdel-Rahem, *Journal of Dispersion Science and Technology*, 2013, **34**, 932–940.
20 S. Datta and D. J. W. Grant, *Crystal Research and Technology*, 2005, **40**, 233–242.
21 J. G. Hardy, A. R. Hirst and D. K. Smith, *Soft Matter*, 2012, **8**, 3399–3406.
22 E. R. Draper, B. Dietrich, K. McAulay, C. Brasnett, H. Abdizadeh, I. Patmanidis, S. J. Marrink, H. Su, H. Cui, R. Schweins, A. Seddon and D. J. Adams, *Matter*, 2020, **2**, 764–778.
23 J. Buendia, E. Matesanz, D. K. Smith and L. Sanchez, *Cryst. Eng. Comm.*, 2015, **17**, 8146–8152.
24 X. Huang, P. Terech, S. R. Raghavan and R. G. Weiss, *Journal of the American Chemical Society*, 2005, **127**, 4336–4344.
25 S. Ogawa, M. Koga, K. Asakura, I. Takahashi and S. Osanai, *Journal of Surfactants and Detergents*, 2017, **20**, 255–261.
26 P. S. Dubey, H. Srinivasan, V. K. Sharma, S. Mitra, V. G. Sakai and R. Mukhopadhyay, *Scientific Reports*, 2018, **8**, 1–16.
27 G. V. Ullio Gamboa, L. A. Benedini, P. C. Schulz and D. A. Allemandi, *Journal of Surfactants and Detergents*, 2016, **19**, 747–757.
28 M. Ambrosi, P. Lo Nostro, L. Fratoni, L. Dei, B. W. Ninham, S. Palma, R. H. Manzo, D. Allemandi and P. Baglioni, *Phys. Chem. Chem. Phys.*, 2004, **6**, 1401–1407.
29 I. A. Nyrkova and A. N. Semenov, *Soft Matter*, 2010, **6**, 501–516.
30 B. Lotz and S. Z. D. Cheng, *Polymer*, 2005, **46**, 577–610.
31 V. M. Coiro, M. Manigrasso, F. Mazza and G. Pochetti, *Acta Crystallogr.*, 1987, **C43**, 850–854.
32 V. M. Coiro, F. Mazza and G. Pochetti, *Acta Crystallogr.*, 1986, **C42**, 991–995.
33 L. A. Smith, R. B. Hammond, K. J. Roberts, D. Machin and G. McLeod, *Journal of Molecular Structure*, 2000, **554**, 173–182.
34 R. J. Alsop, R. Maria Schober and M. C. Rheinstädter, *Soft Matter*, 2016, **12**, 6737–6748.
35 F.-G. Wu, H.-Y. Sun, Y. Zhou, R.-G. Wu and Z.-W. Yu, *RSC Advances*, 2014, **4**, 51171–51179.
36 Y. Aray, J. G. Parra, R. Paredes, L. J. Álvarez and A. Diaz-Barrios, *Heliyon*, 2020, **6**, e04199.
37 H. Hirata and N. Iimura, *Journal of Colloid and Interface Science*, 1998, **199**, 111–122.
38 K. Sato and S. Ueno, *Current Opinion in Colloid and Interface Science*, 2011, **16**, 384–390.
39 D. Kalnin, P. Lesieur, F. Artzner, G. Keller and M. Ollivon, *European Journal of Lipid Science and Technology*, 2005, **107**, 594–606.
40 F. Xue and S. Jiang, *Polymers*, 2014, **6**, 2116–2145.
41 J. Narayanan, A. S. Abdul Rasheed and J. R. Bellare, *Journal of Colloid and Interface Science*, 2008, **328**, 67–72.
42 T. Arnold, A. J. Jackson, A. Sanchez-Fernandez, D. Magnone, A. E. Terry and K. J. Edler, *Langmuir*, 2015, **14**, 9.
43 S. L. Gawali, M. Zhang, S. Kumar, V. K. Aswal, D. Danino and P. A. Hassan, *Communications Chemistry*, 2018, **1**, 1-8
44 V. Martis, S. Nikitenko, S. Sen, G. Sankar, W. Van Beek, Y. Filinchuk, I. Snigireva and W. Bras, *Crystal Growth and Design*, 2011, **11**, 2858–2865.
45 M. Avrami, *The Journal of Chemical Physics*, 1940, **8**, 212–224.
46 M. Avrami, *The Journal of Chemical Physics*, 1941, **9**, 177–184.
47 M. Avrami, *The Journal of Chemical Physics*, 1939, **7**, 1103–1112.
48 A. Y. Malkin, V. P. Beghishev, I. A. Keapin and S. A. Bolgov, *Polymer Engineering & Science*, 1984, **24**, 1396–1401.
49 I. Foubert, K. Dewettinck and P. A. Vanrolleghem, *Trends in Food Science and Technology*, 2003, **14**, 79–92.
50 W. Kloek, P. Walstra and T. Van Vliet, *JAOCS, Journal of the American Oil Chemists' Society*, 2000, **77**, 389–398.

51 Y. Liu, R. Y. Wang, J. L. Li, B. Yuan, M. Han, P. Wang and X. Y. Liu, *CrystEngComm*, 2014, **16**, 5402–5408.

52 J. F. Toro-Vazquez, E. Dibildox-Alvarado, M. Charó-Alonso, V. Herrera-Coronado and C. A. Gómez-Aldapa, *JAOCS, Journal of the American Oil Chemists' Society*, 2002, **79**, 855–866.

53 S. Padar, S. A. K. Jeelani and E. J. Windhab, *Journal of the American Oil Chemists' Society*, 2008, **85**, 1115–1126.

54 K. Mita, H. Okumura, K. Kimura, T. Isaki, M. Takenaka and T. Kanaya, *Polymer Journal*, 2013, **45**, 79–86.

55 E. L. Heeley, D. J. Hughes, Y. El Aziz, P. G. Taylor and A. R. Bassindale, *European Polymer Journal*, 2014, **51**, 45–56.

56 A. G. Marangoni, in *Kinetic Analysis of Food Systems*, Springer International Publishing, Cham, 2017, pp. 113–134.

57 S. A. Chelaghma, O. De Almeida, P. Margueres, J. C. Passieux, J. N. Perie, A. Vinet and B. Reine, *Polymer Crystallization*, 2020, **3**, e10141.

58 J. Y. Chen, Z. Komeily-Nia, L. P. Fan, Z. Y. Li, B. Yuan, B. Tang and J. L. Li, *Journal of Colloid and Interface Science*, 2018, **526**, 356–365.

59 E. Carretti, V. Mazzini, E. Fratini, M. Ambrosi, L. Dei, P. Baglioni, P. Lo Nostro and P. Lo Nostro, *Phys. Chem. Chem. Phys.*, 2016, **18**, 8865–8873.

60 M. A. Rogers, X. Liu, V. A. Mallia and R. G. Weiss, *CrystEngComm*, 2015, **17**, 8085–8092.

61 O. O. Mykhaylyk and C. M. Martin, *European Journal of Lipid Science and Technology*, 2009, **111**, 227–235.

62 A. G. Marangoni and L. H. Wesdorp, *Structure and properties of fat crystal networks*, CRC Press, Boca Raton, Second Edition, 2013.

63 S. Wu, J. Gao, T. J. Emge and M. A. Rogers, *Crystal Growth & Design*, 2013, **13**, 1360–1366.

64 E. B. Sirota, H. E. King, H. H. Shao and D. M. Singer, *Journal of physical chemistry*, 1995, **99**, 798–804.

65 G. Ungar and N. Mašić, *Journal of Physical Chemistry*, 1985, **89**, 1036–1042.

66 H. E. King, E. B. Sirota, H. Shao and D. M. Singer, *Journal of Physics D: Applied Physics*, 1993, **26**, 8–136.

67 O. O. Mykhaylyk and I. W. Hamley, *Journal of Physical Chemistry B*, 2004, **108**, 8069–8083.

68 K. Akabori and J. F. Nagle, *Soft Matter*, 2015, **11**, 918–926.

69 N. Y. D. Li, Š. Perutková, A. Iglič and M. Rappolt, *Elektrotehniski Vestnik*, 2017, **84**, 69–75.

70 T. J. McIntosh and S. A. Simon, *Biochemistry*, 1986, **25**, 4948–4952.

71 S. Tristram-Nagle, Y. Liu, J. Legleiter and J. F. Nagle, *Biophysical Journal*, 2002, **83**, 3324–3335.

72 G. Pabst, M. Rappolt, H. Amenitsch and P. Laggner, *Physical Review E - Statistical Physics, Plasmas, Fluids, and Related Interdisciplinary Topics*, 2000, **62**, 4000–4009.

73 P. Degen, D. C. F. Wieland, S. Leick, M. Paulus, H. Rehage and M. Tolan, *Soft Matter*, 2011, **7**, 7655–7662.

74 F. Bresme and E. Artacho, *Journal of Materials Chemistry*, 2010, **20**, 10351–10358.

75 H. Inouye, H. Tsuruta, J. Sedzik, K. Uyemura and D. A. Kirschner, *Biophysical Journal*, 1999, **76**, 423–437.

76 C. F. MacRae, I. Sovago, S. J. Cottrell, P. T. A. Galek, P. McCabe, E. Pidcock, M. Platings, G. P. Shields, J. S. Stevens, M. Towler and P. A. Wood, *Journal of Applied Crystallography*, 2020, **53**, 226–235.

77 C. H. Chen and E. M. Terentjev, *Langmuir*, 2009, **25**, 6717–6724.

78 R. P. Sperline, *Langmuir*, 1997, **13**, 3715–3726.

79 J. L. Beaudoin, A. Manisse and J. Vadorin, *Optics Communications*, 1973, **7**, 184–186.

80 L. C. Thomas, *Ta instruments*, 2010, **TA039**, 1–5.

81 H. Matsuki, R. Ichikawa, S. Kaneshina, H. Kamaya and I. Ueda, *Journal of Colloid and Interface Science*, 1996, **181**, 362–369.

82 C. H. Chen, I. Van Damme and E. M. Terentjev, *Soft Matter*, 2009, **5**, 432–439.

83 P. Thareja, *Rheologica Acta*, 2013, **52**, 515–527.
84 G. Ben Messaoud, P. Le Griel, D. Hermida-Merino, S. L. K. W. Roelants, W. Soetaert, C. V. Stevens and N. Baccile, *Chemistry of Materials*, 2019, **31**, 4817–4830.
85 A. B. Matheson, V. Koutsos, G. Dalkas, S. Euston and P. Clegg, *Langmuir*, 2017, **33**, 4537–4542.
86 D. A. Barker and D. I. Wilson, *Rheologica Acta*, 2006, **46**, 23–31.
87 A. Ahuja and A. Potanin, *Rheologica Acta*, 2018, **57**, 459–471.
88 A. Benchabane and K. Bekkour, *Colloid and Polymer Science*, 2008, **286**, 1173–1180.
89 J. Y. Kim, S. Bak, B. Chung, W. Ha and Y. Jung, *Bulletin of the Korean Chemical Society*, 2020, **41**, 1211–1216.
90 M. M. Cross, *European Polymer Journal*, 1966, **2**, 299–307.
91 R. Piramuthu Raja Ashok, M. S. Thomas and S. Varughese, *Soft Matter*, 2015, **11**, 8441–8451.
92 O. O. Mykhaylyk, N. J. Warren, A. J. Parnell, G. Pfeifer and J. Laeuger, *Journal of Polymer Science, Part B: Polymer Physics*, 2016, **54**, 2151–2170.
93 E. Tarabukina, F. Jego, J.-M. Haudin, P. Navard and E. Peuvrel-Disdier, *Journal of Food Science*, 2009, **74**, E405–E416.
94 O. O. Mykhaylyk, *Soft Matter*, 2010, **6**, 4430-4440.
95 B. Ayan, N. Celik, Z. Zhang, K. Zhou, M. H. Kim, D. Banerjee, Y. Wu, F. Costanzo and I. T. Ozbolat, *Communications Physics*, 2020, **3**, 1–14.
96 J. A. Prins and W. Prins, *Nature*, 1956, **177**, 535–536.
97 A. M. Schrader, C.-Y. Cheng, J. N. Israelachvili and S. Han, *The Journal of Chemical Physics*, 2016, **145**, 041101.
98 M.C. Etter, *Accounts of Chemical Research*, 1990, **23**, 120-126
99 G. R. Famini, *Using Theoretical Descriptors in Structural Activity Relationships: 1. Molecular Volume*, 1988.
100 Y. Lan, M. G. Corradini, R. G. Weiss, S. R. Raghavan and M. A. Rogers, *Chemical Society Reviews*, 2015, **44**, 6035–6058.
101 C. M. Hansen, Ed., *Hansen solubility parameters: A User's Handbook*, Taylor & Francis Group, Boca Raton, Second Edition, 2011.
102 E. R. S. Circular, N B S, Arthur A. Maryott, *Table of Dielectric Constants of Pure Liquids*, 1951.
103 M. Zahn, Y. Ohki, D. B. Fenneman, R. J. Gripshover and V. H. Gehman, *Proceedings of the IEEE*, 1986, **74**, 1182–1221.
104 M. A. Rogers and A. G. Marangoni, *Crystal Growth and Design*, 2008, **8**, 4596–4601.
105 Y. Lan and M. A. Rogers, *Crystal Engineering Communications,* **17**, 8031–8038.
106 E. Tempestini, M. Bucci, V. Mastromartino, M. Gori, D. Tanini, M. Ambrosi, E. Fratini, A. Capperucci and P. Lo Nostro, *ChemPhysChem*, 2017, **18**, 1400–1406.

5. Ternary Behaviour of SDS and Glycerol Containing Mixtures

5.1. Introduction

SDS is commonly added as a foaming agent or detergent to complex personal care formulations along with a multitude of other ingredients.[1] In order to characterise behaviour for such multicomponent mixtures, model systems characterising the overall trends in phase behaviour must first be considered. In Chapter 4, binary mixtures of SDS in glycerol were probed, focusing on the formation of the SDS-glycerol crystal phase. The current chapter aims to characterise the viability of this phase in more complex (ternary) mixtures, as well as understand the behaviour over a range of temperatures. Most importantly, the presence of water is studied, which can be either included intentionally, or may be unwittingly present owing to the hygroscopicity of both SDS and glycerol in an industrial setting.[2,3] While ternary mixtures of SDS-glycerol-water have been studied in detail,[4–6] both micelle structure and phase behaviour in glycerol rich mixtures are areas that require further understanding. Additionally, 1-dodecanol is used as a model impurity/cosurfactant to determine its effect on crystal phase and micelle structure. Finally, the impact of ionic strength is tested through the inclusion of a simple monovalent salt.

5.2. Results and discussion

5.2.1. SDS/Glycerol/Water- Crystal Phase Behaviour

5.2.1.1. SAXS & Microscopy

The SDS-glycerol phase has only recently been identified (through this work and that of Matthews et al.),[7] which raises questions as to why this structure has not been observed earlier. In concurrence with previous work, SDS concentration are 2 or 4 Wt.%, with varying water and glycerol content. Initially, SDS (2 Wt.%) in glycerol-water mixtures (0 Wt.%, 3 Wt.% and 6 Wt.% water of solution) were heated above the Krafft temperature and subsequently cooled quiescently. The resulting mixtures were then examined using optical microscopy (Figure 5.1). Fibre-like crystal aggregates indicative of the SDS-glycerol phase is evident in pure glycerol. However, for the glycerol-water mixture containing 3 Wt.% water of solution, a mixed phase was observed, containing both fibres and platelet-like aggregates. By increasing the water content to 6 Wt.% water of solution, the SDS-glycerol crystal phase disappeared and was replaced by a mixture of platelet-like and needle-like morphologies. This suggests the formation of crystals with varying degrees of hydration,[8-10] or perhaps multiple habits of a dominant crystal structure, which is difficult to verify through microscopy alone. Both Abdel-Rahem and Khan

report that hydrated crystals are present below the Krafft temperature in glycerol-water mixtures.[4,5] This suggests a dominant hydrate phase, although there is little direct evidence for this structure.

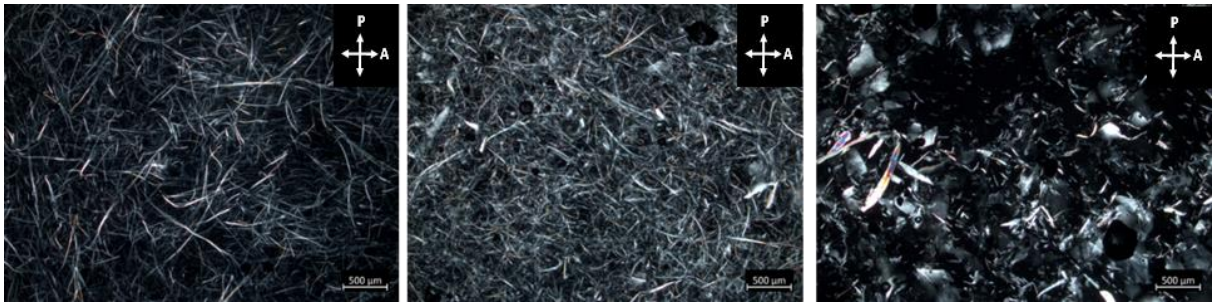

Figure 5.1: Polarised optical microscopy images (POM) of SDS (2 Wt.% of total) in glycerol-water mixtures consisting of (left to right): 0 Wt.% water and 100 Wt.% glycerol, 3 Wt.% water and 97 Wt.% glycerol, and 6 Wt.% water and 94 Wt.% glycerol. Solutions were subjected to heating at 75°C before quiescent cooling for 5 hours. Mixtures show a transition from SDS-glycerol crystal phase to mixed crystal phases and finally platelets and needles of an indeterminate degree of hydration. Direction of polariser and analyser indicated by P and A, respectively.

It is apparent that relatively small amounts of water can disrupt the formation of fibres when cooled quiescently. However, formation of the SDS-glycerol crystal is slow, with long lag times observed (Figure 4.5) during formation, which may indicate kinetic constraints compared to other crystal phases. 2 Wt.% solutions of SDS in glycerol-water mixtures were quenched from 80 °C to 20 °C at 30 °C min^{-1} before being help isothermally at 20 °C while time resolved SAXS measurements were recorded (Figure 5.2), to allow for characterisation of the growing crystal species. The non-fibrelike crystals formed in the presence of small amounts of water was the anhydrous SDS crystal phase (Appendix 8.15), as determined by the near-identical scattering pattern of the high intensity lamellar peaks.[11] When the intensity of the d_{001} peaks are measured against time, abundances of each phase can be quantified, allowing comparison between mixtures with different solvent compositions. For some scattering patterns containing SDS in glycerol/water mixtures, large textured (anhydrous) crystals caused variations in the plateau intensity after crystallization. The calculation of a plateau intensity average appeared to mitigate the effect, allowing for comparison between crystal types. When the relative crystal composition was plotted against water content, a sigmoidal curve (Figure 5.2a) was obtained, whereby SDS-glycerol crystals were replaced in favour of anhydrous crystals as the water content is increased.

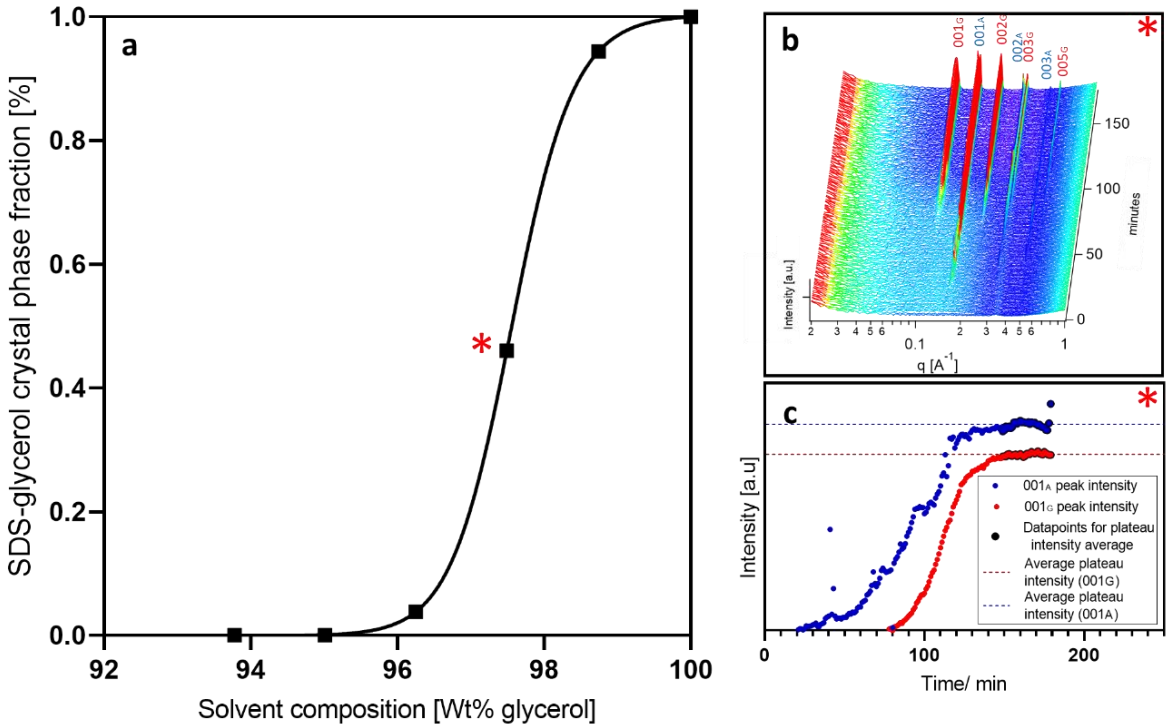

Figure 5.2: a) Volume fraction of SDS-glycerol crystal phase with respect to the anhydrous crystal phase and its dependence on glycerol concentration in glycerol-water mixtures, calculated from averages of intensity plateaus of 001_G and 001_A diffraction peak intensity from 2 Wt.% solutions isothermally cooling at 20 °C of SDS, after an initial quench at 30 °C min^{-1} from 80 °C to 20 °C (Appendix 8.15, 8.16). b) Representative time resolved 1D SAXS pattern showing evolution of anhydrous and SDS-glycerol crystals with a solvent composition containing 97.5 Wt.% glycerol and 2.5 Wt.% water. c) Representative fitted d_{001I} peak intensity over time, determined from b, with indication of a mean peak plateau intensity for a solvent mixture containing 97.5 Wt.% glycerol.

Anhydrous crystals also showed the same or lower t_{init} than the SDS-glycerol phase (Appendix 8.15,8.16), which is hypothesised to be a result of the anhydrous crystal exhibiting a lower kinetic barrier to formation.[11] The reduction in solvent viscosity through addition of water may also be a contributing factor, which in turn allows for faster diffusion.[12] It is initially unclear why anhydrous crystals form in preference to either hydrated crystals or the SDS-glycerol phase, as hydrate crystals typically dominate when cooled in purely aqueous solution.[8-10] One aspect is the kinetic favorabilty; for anhydrous crystals to form, only organisation of the SDS must occur. Whereas the SDS-glycerol and SDS-hydrate crystal phases require organisation of two components, lowering entropy and increasing the kinetic barrier. This aligns with Ostwald's rule of stages[13] whereby cocrystals are the thermodynamic product with their formation driven by enthalpy, although this is not always the case.[14]

To further examine the nature of phase formation during crystallization, a solution of 2 Wt.% SDS in glycerol-water mixture (3 Wt.% water of solution) was isothermally cooled and studied by time resolved POM. This was then compared to SDS in pure glycerol (Figure 5.3). The presence of water increased the crystallization growth rate by approximately a factor of two, in agreement with the SAXS data. In the presence of 3 Wt.% water of solution, both fibre and feather-like morphologies were present, suggesting a dendritic mode of growth.[15] This corresponds to the same anhydrous crystal species observed during quiescent cooling (Figure 5.1, middle) and isothermal cooling by SAXS, despite being a different crystal habit to the expected platelet or needles.[8,9,16-19] Re-examining the initial observations of POM images of SDS (2 Wt.%) solutions at varying water concentrations (Figure 5.1), it is feasble that feather morphologies were initially present but were destroyed by shear during loading of the sample. Nucleation occurred in a sporadic fashion for both mixtures and also propagated from the surface of bubbles.

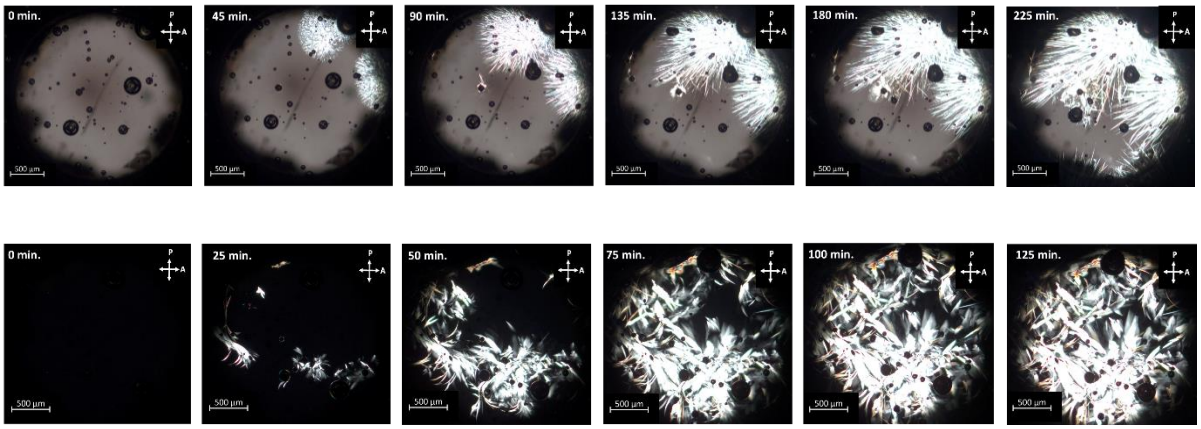

Figure 5.3: Time resolved polarised optical microscopy measurements for solutions initially quenched at 30 °C min^{-1} from 80 °C to 20 °C, followed by isothermal cooling at 20 °C containing (upper row) 2 Wt.% SDS in glycerol, with the SDS-glycerol crystal phase forming phase consisting of fibre crystals through sporadic nucleation, (Lower row) SDS (2 Wt.%) in glycerol-water mixture (3 Wt.% water and 97 Wt.% glycerol), forming a mixed phase consisting of SDS-glycerol crystals and feather-like crystals of either anhydrous or hydrated SDS through sporadic nucleation. Different acquisition times were used for each solvent mixture to prevent overexposure due to the difference in birefringence for each sample, causing a difference in background brightness. Direction of polariser and analyser indicated by P and A, respectively.

One possibility is that feather-like crystal formation is a result of the SDS-glycerol crystal phase acting as a seeding agent.[20] Alternatively, glycerol or water may adsorb onto specific crystal faces, influencing growth.[21] Another factor that can affect habit is the viscosity of the system, where the increased viscosity of glycerol-rich formulations causes slower diffusion and hence higher incidences of secondary nucleation and branching.[22] The formation of feather morphologies is not limited to low water content and is observed for crystals formed in 10 Wt.% water as well (Figure 5.4). Therefore the SDS-glycerol

phase does not influence the habit of the anhydrous crystals. It is only when the water content is increased up to 20 Wt.% water of solution (Figure 5.4) that crystals with the expected needle-like habits are observed. Hence high glycerol content (or low water content) seems to be the cause of the feather-like crystal habit.

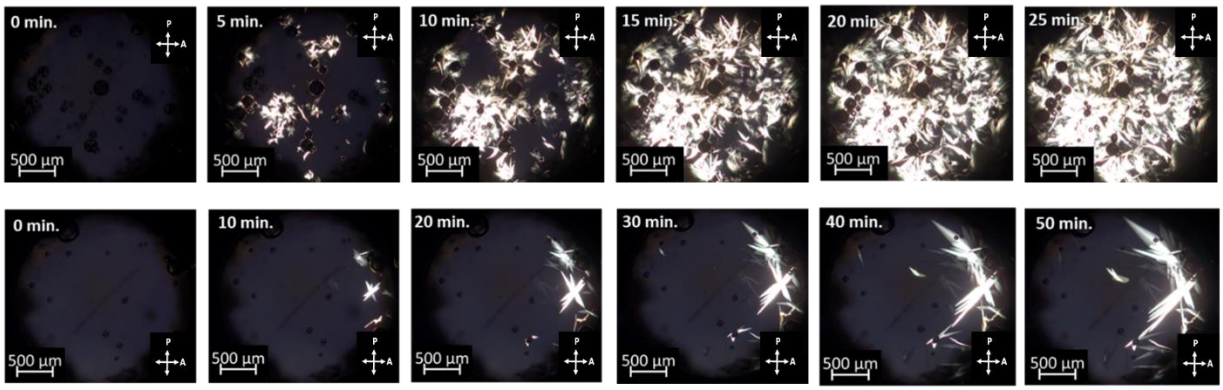

Figure 5.4: Time resolved polarised optical microscopy measurements for solutions initially quenched at 30 °C min^{-1} from 80 °C to 20 °C, followed by isothermal cooling at 20 °C containing (upper row) SDS (2 Wt.%) in glycerol-water mixture containing 10 Wt.% water 90 Wt.% glycerol solvent, forming a phase consisting of feather-like crystals of either anhydrous or hydrated SDS through sporadic nucleation, (Lower row) SDS (2 Wt.%) in glycerol-water mixture containing 20 Wt.% water 80 Wt.% glycerol solvent, forming a phase consisting of needle -like crystals of either anhydrous or hydrated SDS through sporadic nucleation.

Isothermal cooling measurements at different temperatures can enable the identification of kinetic and thermodynamic products of crystallization, where higher degrees of undercooling produce a higher proportion of the kinetic product.[11] Therefore measurement of crystallization during isothermal cooling at two different temperatures, 15 °C and 0 °C were undertaken (following an initial quench from 80 °C at 30 °C min^{-1}) for 2 Wt.% solutions of SDS in a glycerol-water (3 Wt.% water of solution) allowing comparison with previous measurements at 20 °C. Initial observations of time-resolved microscopy (Figure 5.5) indicate faster growth at lower temperatures, with instantaneous (as opposed to sporadic) nucleation occurring at 0 °C. Mixtures with a greater degree of undercooling are expected to crystallize faster due to the lower activation energy for nucleation.[23] Crystalline aggregates were both smaller and primarily needle-like when cooled at 0 °C, suggesting predominant anhydrous or hydrate formation. At 15 °C, similarly to 20 °C, sporadic nucleation and slow growth leads to the formation of distinct fibre and feather-like crystals, with bubbles acting as the main nucleation sites.

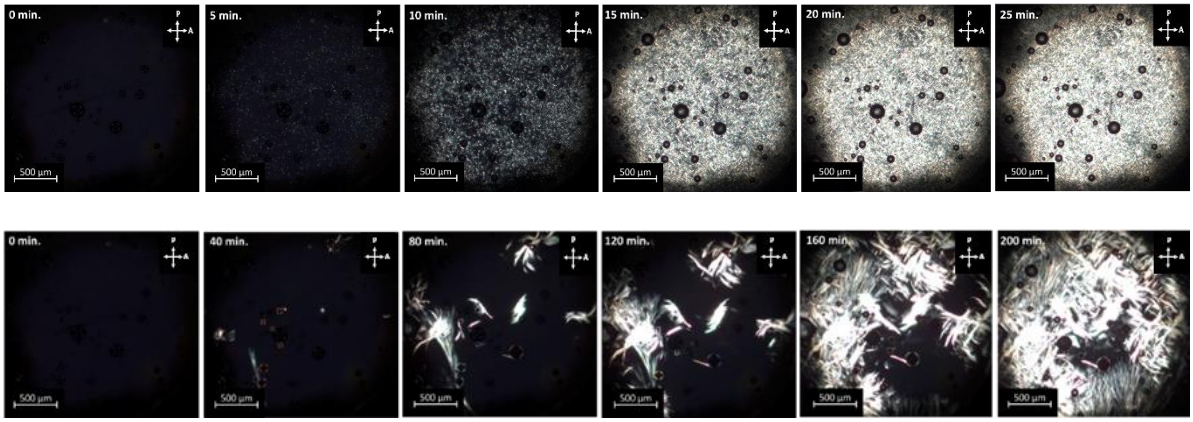

Figure 5.5: Time resolved polarised optical microscopy measurements of SDS (2 Wt.%) in a glycerol-water solution (3 Wt.% water and 97 Wt.% glycerol) isothermally cooled at (Upper row) 0 °C preceded by an initial quench at 30 °C min^{-1} from 80 °C, (Lower row) 15 °C preceded by an initial quench at 30 °C min^{-1} from 80 °C. Cooling at 0 °C yields a phase consisting of small needle -like crystals of either anhydrous or hydrated SDS through instantaneous nucleation. Comparatively. cooling at 15 °C yields a mixed phase consisting of SDS-glycerol crystals and feather-like crystals of either anhydrous or hydrated SDS through sporadic nucleation. Direction of polariser and analyser indicated by P and A, respectively.

Crystallization of mixtures under the same conditions was then assessed using time-resolved SAXS. Cooling at 0 °C (Figure 5.6b, 5.6d) yielded predominantly anhydrous crystals with only ~5% abundance of the SDS-glycerol phase, in contrast to the near-equal abundance for both phases when cooled at 20 °C. The anhydrous phase also had a t_{init} of 10 minutes i.e. 15 minutes lower than the SDS-glycerol phase, coinciding with microscopy observations of spontaneous nucleation (Figure 5.5). The data confirm the kinetic favourability of the anhydrous crystal in glycerol-rich binary aqueous solvents, in agreement with Ostwald's rule of stages.[13] For the sample cooled at 15 °C, (Figure 5.6b, 5.6d) a plateau intensity had not been reached by the end of the experiment and further repeats over a longer timescale are needed to verify relative abundance. However, despite similar ratios of anhydrous crystal and SDS-glycerol phase compared to those at 20 °C, a small amount of another crystal phase (001u) is observed, with a first order d001 -spacing (31.9 Å) that does not coincide with known crystal phases.[8-10,16-19] This may be due to the lower temperature affecting the d_{001}-spacing of a known hydrate, or perhaps a new crystal phase with indeterminate composition. An alternative explanation is the formation of hexagonal intermediate phases reported by Mathews et al.,[24] although this does not correlate with the microscopy observations or with the assigned crystal phases. Further work to determine structure and favourability of the unknown phase could be examined using different cooling methods (including non-isothermal regimes), as well as varying concentrations of SDS. However, isothermal cooling at higher temperatures proved difficult, because the large crystal aggregate size leads to non-representative relative intensity measurements.

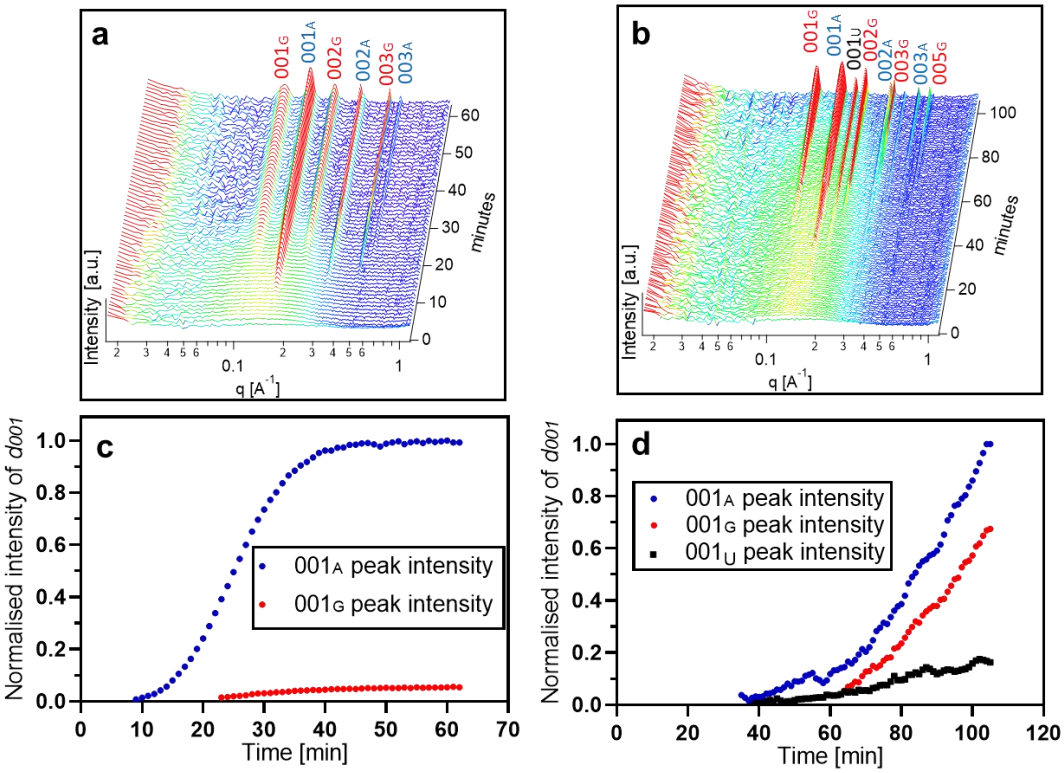

Figure 5.6: Top: time-resolved 1D SAXS pattern of 2 Wt.% SDS in glycerol-water solvent (3 Wt.% water and 97 Wt.% glycerol solution) isothermally cooled at a) 0 °C preceded by an initial quench at 30 °C min^{-1} from 80 °C, b) 15 °C preceded by an initial quench at 30 °C min^{-1} from 80 °C. C) d_{00l} peak fitted intensity over time for mixtures cooled at 0 °C. b) d_{00l} peak fitted intensity over time for mixtures cooled at 0 °C. Where $00l_G$, is SDS-glycerol crystal phase, $00l_A$ is the anhydrous crystal phase, $00l_u$ is the new/unknown SDS crystal phase.

With evidence for preferential formation of anhydrous crystals being exaggerated at lower temperatures, it can be concluded that anhydrous SDS is the kinetic product in glycerol-water mixtures. The behaviour extends to other compositions, with quiescently cooled SDS (4 Wt.%) in glycerol-water mixtures containing up to 40 Wt.% water of solution also forming anhydrous crystals (Appendix 8.17). However, two important questions remain. Firstly why do hydrates not form more readily? And secondly, why does the anhydrous phase become the kinetic product only when water is present?

The answers to both these questions are linked to the locality and behaviour of water. Both SDS and glycerol are highly soluble in water, and readily form solutions. For SDS, it has been shown through scattering experiments that the shell of micelles is highly hydrated in aqueous solutions, with up to 50% of the shell volume composed of water.[25] This may be the case for glycerol-water solutions of SDS, where there could be a significant presence of water in the micelle shell, that could disrupt co-ordination of glycerol to SDS during crystallization. However, if this is the sole mechanism affecting crystallization, it would be expected that hydrate SDS crystals would form more readily. Alternatively,

water is also known to readily disperse in glycerol, which is highly hygroscopic, and binary solutions display low water activity.[26,27] The presence of water may affect crystallization by tying up glycerol in a H-bonded solvent network. This would explain the formation of anhydrous crystals over both hydrated and glycerol crystal phases. However, this cannot be determined from crystallization information alone, and either process (or both) could occur. The behaviour of water molecules in solution can be assessed using either Raman or NMR spectroscopy.

4.3.1.2. Rheology

The high aspect ratio crystal fibres in the glycerol phase is what enables freestanding gels to form, which then break up under shear to enable flow. Other crystal morphologies with lower aspect ratios, are less likely to entangle and subsequently gel or structure at the same concentrations, although aggregates will still break up under shear. Therefore, the rheology of SDS mixtures in glycerol-water solvent with different compositions (0 Wt.%, 3 Wt.%, 6 Wt.% water of solution), were measured to determine the effect of changing the crystal type on shear-thinning behaviour. Viscosity curves were conducted following in situ isothermal cooling within the rheometer for mixtures of SDS (2Wt.%) in glycerol-water mixtures (0 Wt.%, 3 Wt.%, 6 Wt.% water of solution). Initial G' measurements recorded during crystallization (Figure 5.7) show similar behaviour to the SAXS isothermal cooling data, where mixtures containing water tend to crystallize quicker due to growth of the anhydrous crystal. However, as multiple crystal types are present, it is not applicable to measure Avrami kinetic behaviour through rheology alone, which cannot distinguish between multiple coexisting crystal types. Thus this technique is less informative than other methods such as SAXS.[28]

For SDS solutions containing 0 Wt.% and 3 Wt.% water of solution, higher peak and plateau values of G' (Figure 5.7) are obtained, compared to the solution containing 6 Wt.% water of solution. This is due to the presence of the SDS-glycerol phase, which can form entangled networks. For all samples, a reduction in viscosity was observed following the peak maxima, which represents the end of crystal growth. This was not expected as a plateau should occur instead of a decrease.[29] In the mixture containing 6 Wt.% water of solution, G' is reduced from 1300 Pa (peak value) to 200 Pa by the end of the measurement. It is hypothesised that this is a result of equilibration of the crystal material and perhaps relaxation from stresses endured during crystallization. After the peak value of G' (Figure 5.7a), the subsequent loss and plateau value coincides with a greater dampening factor, equating to a less elastic structure. While not representative of the whole frequency range, it is an indication that the

network-like behaviour is affected after the initial growth. The formation of crystal structures with lower aspect ratios, such as platelets and feathers may enhance this effect due to the lower degree of entanglement.[30] It is less likely this behaviour is seen at higher concentration regimes, because of the reduction in degrees of freedom and increased between of crystal aggregates.

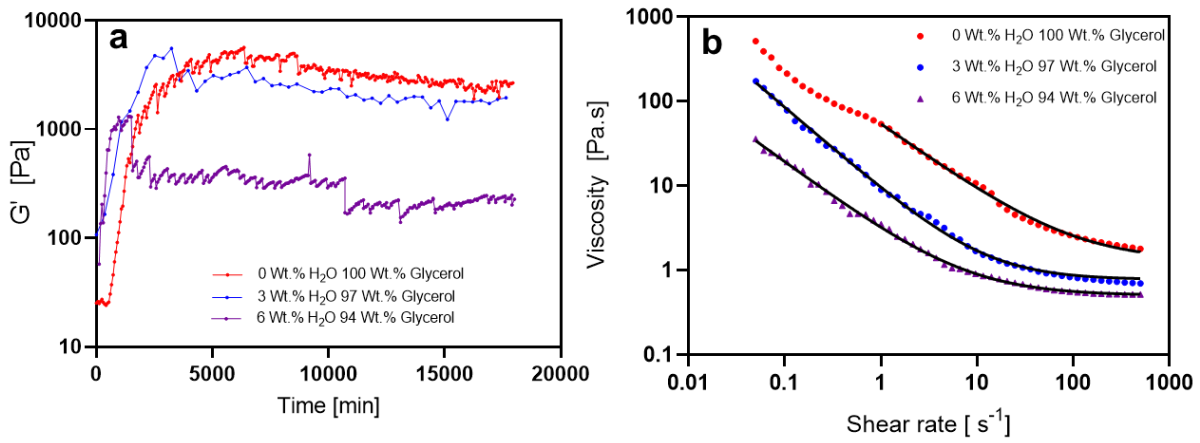

Figure 5.7: 2 Wt.% SDS in glycerol water mixtures isothermally cooled in situ for 5 hours at 20 °C, following an initial quench at 30 °C min^{-1} from 80 ° to 20 °C, containing 0% water and 100% glycerol (red), 3 Wt.% water and 97 Wt.% glycerol (blue), 6 Wt.% water and 94 Wt.% glycerol (purple) solvent mixtures. a) G' evolution over time owing to the crystallization and network formation of SDS. b) Corresponding viscosity curves for the resulting crystalline suspension with a Sisko model fit.[31] N.B. The sample in glycerol (red) is the same dataset as that shown in Figures 4.12 and 4.13.

Shear-thinning behaviour also differs for different solvent compositions (Figure 5.7b). While no true zero shear viscosity plateau is observed, the SDS solution in pure glycerol exhibits a depression in gradient at approximately 0.35 s^{-1} Further shear-thinning occurs below this value and such behaviour was repeatable at different temperatures (Figure 4.13). This is not the case for samples containing water, where a power law-type behaviour is observed. The Sisko model[31] was employed to fit the degree of shear-thinning (n) and infinite viscosity plateau (η_{inf}). All samples exhibited similar values of n, with this exponent ranging from 0.8 to 1.0. This suggests that the effect of shear is similar for all samples, with a proportional loss in viscosity. All samples show different values of η_{inf}, which approaches the value expected for the solvent viscosity.[12] Despite different crystal types and habits, the breakdown under shear is identical. Furthermore, the solvent viscosity has a large effect on structure after a continuous shear event, which must be considered when designing a toothpaste formulation. It is not possible to distinguish between the inherent structuring properties through viscosity curve measurements. However, further creep analysis as well as oscillatory (frequency and amplitude sweep) data would provide insight into the structure and gelation of the mixture. Oscillatory data would also

show whether the samples containing water are best described as gels, semisolids, or liquids within the LVER.

5.2.2. SDS/Glycerol/Water Mixtures – Elevated Temperature Behaviour

While the micelle behaviour of SDS in glycerol has only recently been observed,[7] the behaviour of SDS in aqueous and mixed aqueous systems have been studied much more intensively.[4–6] However, the rationalisation of micelle structure throughout the whole solvent composition range for glycerol and water has not been well established and was therefore attempted in this work. This was achieved for 2 Wt.% and 4 Wt.% SDS solutions as an extension of previous formulations. During preliminary analysis of scattering patterns of SDS (2 Wt.%) in glycerol, it was found that a core-shell ellipsoid model produced a satisfactory fit to the data, while remaining consistent with other small angle measurements of SDS in various solvent.[32–36] Due to the concentrations studied, a Hayter-Penfold (HP) structure factor for charged spherical particles[37,38] was used as a first approximation to account for intermicellar repulsions. Measurements were conducted at 60 °C, which is a relevant temperature for processing all formulations above the Krafft temperature.[4] The formulations were created using weight fractions, with volume fraction contribution accounted for within the fitting parameters (Appendix 8.18).

Samples containing 30 and 40 Wt.% water produced a relatively low intensity scattering signal exemplified by a lower maximum of the observed form factor 'peak' (Figure 5.8d and 5.8e) relative to otherr patterns (Figure 5.8). This was not an experimental error, as future studies showed similar behaviour. It is expected that contrast matching between the solvent SLD and the SDS SLD was the likely cause for this observation. Considering that most studies indicate high degree of mixing at this solvent composition,[39] large scale partition of solvent is deemed unlikely. There is also limited potential for solvent transfer into the micelle core due to the large difference in polarity. The cause of the intensity variation was initially thought to be a change in micelle shell composition through hydration of micelle head groups. This is because some cases within the literature report that the volume fraction of water associated with the head group in an anionic micelle can account for more than 50% of the shell volume fraction.[32] However, it was hypothesised, that in this system, the dynamic equilibrium of water between the shell and the bulk in glycerol-aqueous mixtures, causes the micelle head groups to be partially solvated by water. Thus, as the water content is increased, more water is located in/round the surfactant head groups, causing the effective shell thickness to increase and the shell SLD (or average electron density) to decrease. To assess this phenomenon, the micelle shell parameters were chosen to be variables fo the fitting model. Furthermore, it was assumed for the analysis that the SDS mass

density is 1.01 g cm^{-3}, based on the known SDS density in aqueous micellar solutions (1.00-1.01 g cm^{-3}).[40–42] Although it is recognised that the micellar density of SDS is likely to change in different solvent mixtures and temperatures, its effect on the overall volume fraction is expected to be minimal at this concentration when compared to the volume change associated with the different solvent compositions (which are accounted for). Thus this allows for the determination of the dramatic change in scattering intensity. Fixing the SDS mass density minimised structural model over-parameterization, whereby over-fitted outputs of concentrations were initially obtained.

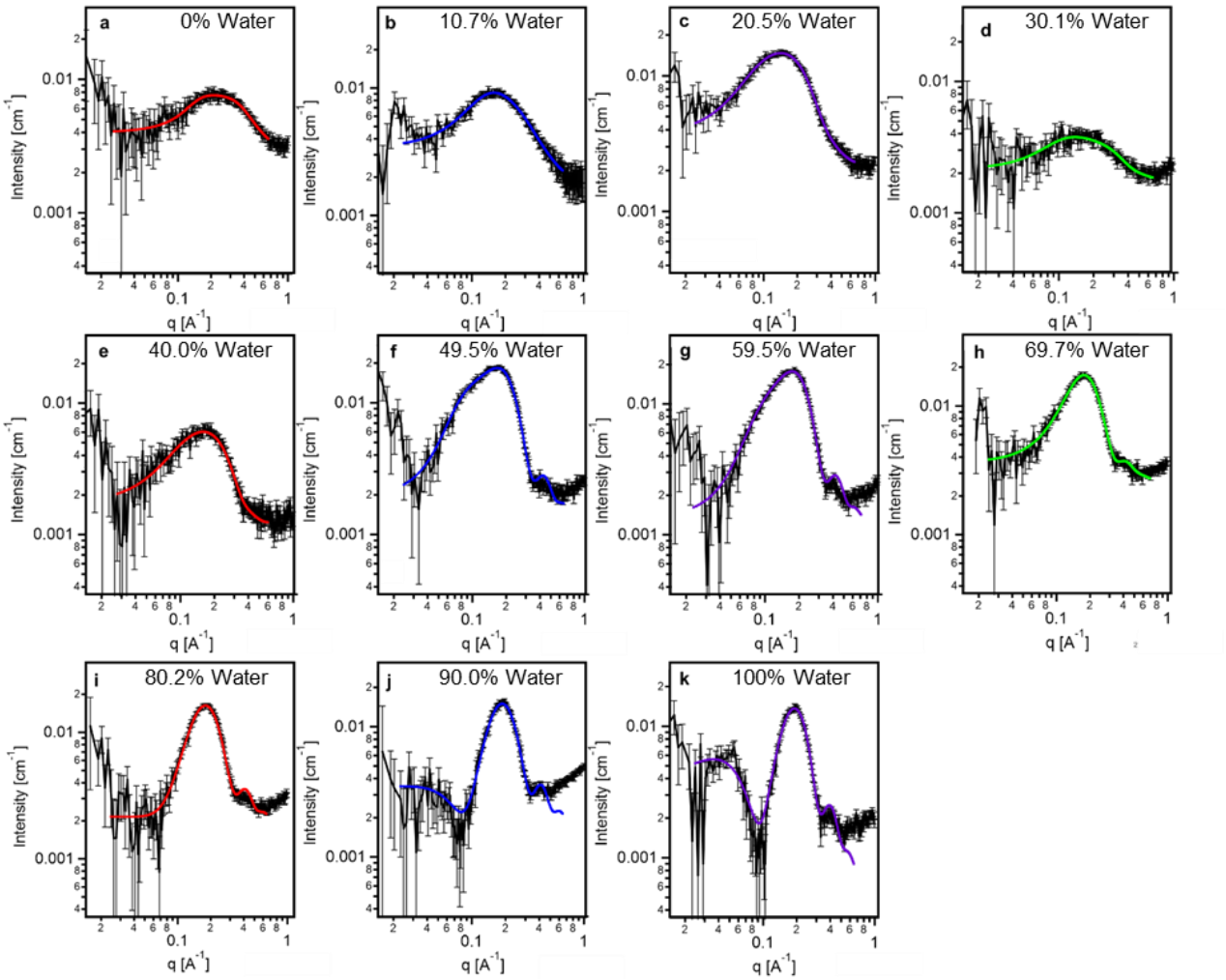

Figure 5.8: 1D SAXS patterns of SDS (2 Wt.%) in glycerol-water solutions at 60 °C, fitted with models comprised of a core-shell ellipsoid form factor with Hayter-Penfold mean spherical approximation structure factor for charged spherical particles , with solvent compositions of a) 100 Wt.% glycerol, b) 10.7 Wt.% and water 89.3 Wt.% glycerol, c) 20.5 Wt.% water and 79.5 Wt.% glycerol, d) 30.1 Wt.% water and 69.9 Wt.% glycerol, e) 40 Wt.% water and 60 Wt.% glycerol, f) 50.5 Wt.% water and 49.5 Wt.% glycerol, g) 59.5 Wt.% water and 40.5 Wt.% glycerol, h) 69.7 Wt.% water and 30.3 Wt.% glycerol, i) 80.2 Wt.% water and 19.8 Wt.% glycerol, j) 90 Wt.% water and 10 Wt.% glycerol, k) 100 Wt.% water. A full list of fitting parameters is given in Appendix 8.18.

The core-shell ellipsoid form factor used,[43] in combination with the HP structure factor built in the Irena macro for Igor Pro produced good fits to the experimental data (Figure 5.8 and Table 5.1).[38,44] Due to the upturn at low and high *q*, even after background correction, all fittings were performed within the *q* range 0.25 $Å^{-1} \leq q \leq 0.65$ $Å^{-1}$. This mitigated the problem but there was a broader distribution of the sum of the squares of independent standard normal variables (χ^2) at higher water concentrations. The upturn was less of a problem in glycerol rich solvent due to more intense scattering at high *q*. A series of trends are apparent for the fitted models: the best fit for SDS micelles in glycerol-rich solvents is an oblate ellipsoid, wheras water rich-systems can be fitted assuming a prolate ellipsoid.[40] This may indicate that there is an intrinsic property of a solvent, or an interaction between the SDS surfactant and the solvent, that causes the observed variation in ellipticity, unfortunately this could not be further explored within this work owing to time constraints.

The core radius of the SDS micelles initially increased minimally in glycerol-rich binary solvents (Figure 5.8 and Table 5.1), with a more dramatic increase being observed when shifting to water-rich solvents. This was followed by a gradual increase in size as more water was present. The inverse trend in size versus glycerol concentration is consistent with literature data, which typically show a higher aggregation number.[5,6] This is typically as a result of reduced interfacial tension between the bulk and micelle phase, which equates to lower Gibbs energy of micellization that causes lower aggregation numbers.[453] The Gordon parameter can be used to describing solvent properties (and the ability to form non-covalent interactions): and is concurrent with the trend in Gibbs free energy of micellization.[5,45] On the other hand, the effect of water in glycerol-rich mixtures, if localised near the head group, may have the potential to increase the interfacial tension in a nonlinear fashion. This would explain the apparent plateau in core size in the fitted data for the glycerol-rich solvent region. Generally, glycerol-rich mixtures afforded more polydisperse SDS micelles, although this may be as a result of a lower signal-to-noise ratio for the scattering patterns.

Table 5.1: Fitted parameters of the core-shell ellipsoid form factor with Hayter-Penfold structure factor obtained for 2 Wt.% SDS solutions in glycerol-water mixtures at 60 °C (Figure 5.8). Full fitting parameters are given in Appendix 8.19.

Wt.% water of solvent	Equatorial core radius [Å]	Polydispersity index* [σ/r_{core}]	Aspect ratio	Shell thickness [Å]	Shell SLD [$x10^{10}$ cm^{-2}]	Charge	HP radius [Å]	Reduced χ2
0	11.3	0.293	0.416	4.83	13.1	6.80	8.99	0.91
10.7	11.9	0.176	0.408	3.87	12.2	3.93	9.61	0.91
20.5	13.4	0.294	0.648	7.21	12.0	4.22	14.1	1.40
30.1	10.2	0.073	0.367	7.06	10.9	4.32	11.7	0.98
40	13.4	0.002	0.503	9.46	10.8	3.85	11.7	0.89
50.5	13.3	0.087	1.58	4.91	12.0	7.75	16.8	1.82
59.5	14.6	0.122	1.24	2.92	13.2	3.52	11.5	2.48
69.7	14.9	0.135	1.29	2.96	13.3	2.41	10.0	1.63
80.2	14.9	0.092	1.57	3.34	12.8	4.18	8.83	1.94
90	15.0	0.075	1.63	3.31	12.9	3.96	9.54	10.02
100	15.7	0.101	1.42	2.91	13.1	2.81	12.6	3.84

**Polydispersity index is defined as the core radius standard deviation (σ) divided by core radius (r_{core}).*

Due to the high noise, the low *q* region was more problematic than the mid *q* range. This manifested in the wide variation in structure factor fitted parameters, including charge, volume fraction and the equatorial micelle core radius. Measurements over a lower *q* range would be greatly beneficial to obtain more accurate fits. Alternatively, employing the use of component SLD contrast matching such as contrast variation SANS could be beneficial.[33]

While the shell radius was expected to remain constant, the fittings reveal an increase in shell thickness for mixtures of SDS in glycerol-rich binary mixtures. This is reduced to a lower plateau when in water-rich mixtures (Table 1). Mirroring the trend, is a reduction in the fitted shell SLD. The shell thickness maximum occurs at 40 Wt.% water, which is at the same point of the SLD minima. This may be explained by the larger volume that the shell occupies at 40 Wt.% water, when the greater core size is considered. Finally, it must be noted that the SLD values (at 30 or 40 Wt.% water of solution) for the SDS micelle shell are below that of glycerol, indicating that the change in size and SLD is more likely the result of water localisation.

A conceptual model can be established to rationalise the findings (Figure 5.9a). Glycerol is a comparatively poor solvent for SDS. In this respect, SDS form small oblate micelles in glycerol only at elevated temperatures (Table 1). On addition of water, the polarity, and polarisability of the solvent increases, leading to greater solvation of the SDS head groups and a gradual increase in SDS micelle size. Although glycerol is highly compatible with water, it competes with SDS (sulfate group), thus creating a dynamic equilibrium for the water between the surface of the micelle and the bulk solvent. At low concentrations of water (< 10 Wt.%), the effect on the micelle shell is minimal, but at higher concentrations more water molecules become localised near the head groups, causing a large, hydrated thick shell. When water becomes the primary solvent, the hydration layer is less observable, as the glycerol is dissolved in the water. A similar phenomenon has been verified for scattering experiments involving proteins in glycerol/water mixtures. In this case partial replacement of glycerol in the hydrated surface of the protein occurs above 50% glycerol (v/v).[46] This aligns with the experimental fitted SLD results, which indicate a maximum at 60 Wt.% glycerol. Conversely, glycerol localisation in dipalmitoyl phosphatidylcholine monolayers and liposomes has also been reported in mixed aqueous solutions,[47] which further complicates data interpretation.

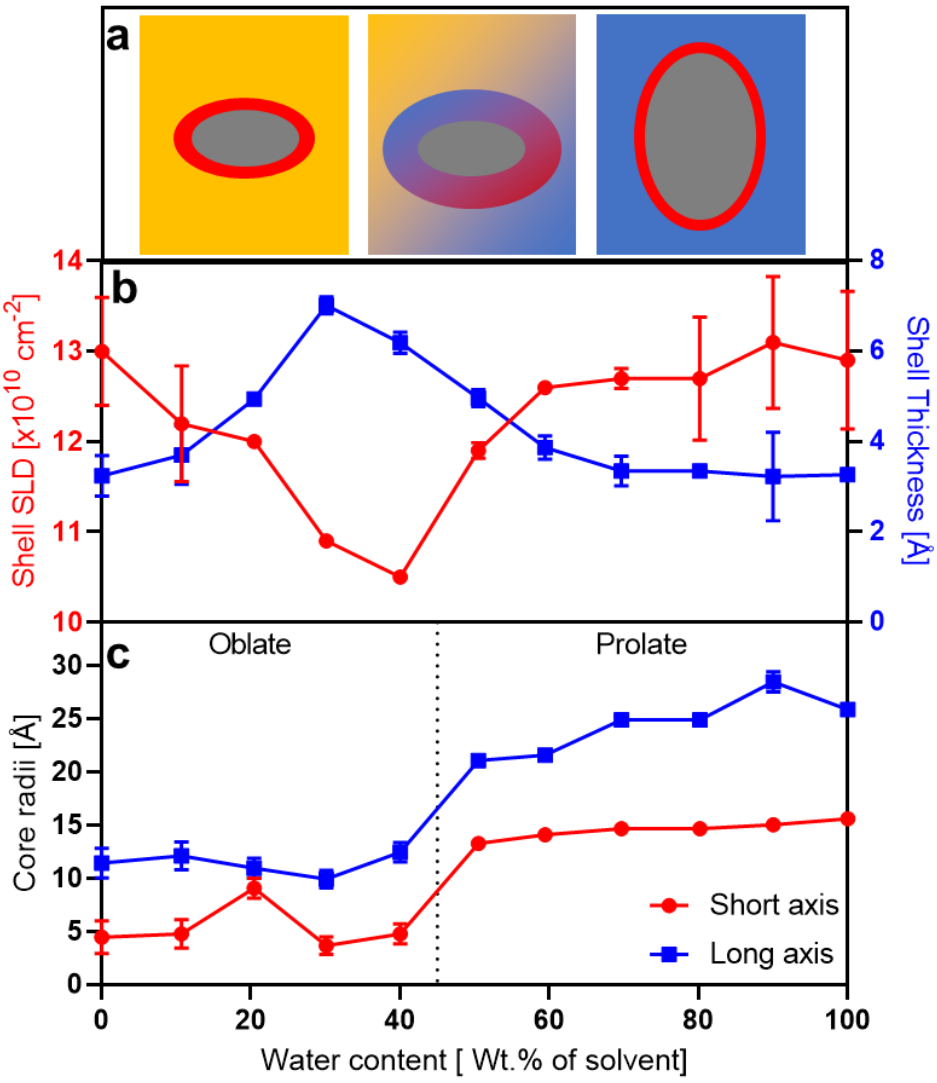

Figure 5.9: a) Representation of fitted micelle shape and structure formed by SDS (2Wt.%) in aqueous glycerol mixtures at 60 °C. Here the small oblate micelle gradually increases in size with the addition of water, with the additional hydration of the shell with water, until a water-rich solvent is present whereby larger, more traditional prolate SDS micelles are observed. B) Variation of fitted shell SLD and shell thickness with water content, indicating preferential hydration of water about the shell in the 20-40 Wt.% water region. C) Variation of fitted micelle core radii with water content, displaying a marked increase in size in water-rich mixtures, whereby the micelles also become prolate. Error bars correspond to the uncertainties in data fitting procedure. A full list of fitting parameters is given in Appendix 8.19.

While the SAXS data can be used to characterise micelle size and shapes, these findings suggest large changes in the nature of the micelle structure in aqueous-glycerol mixtures. While much of the fitting parameters related to the solvent properties have been obtained from literature sources,[12,26,48–51] the large changes in scattering can only be rationalised through changes in micelle morphology. However, to determine whether the formation of the hydrated shell was a function of concentration, or even occurred at different concentrations, SAXS was also performed on SDS 4 Wt.% mixtures, at various

water-glycerol compositions (Figure 5.10). It was considered that the higher concentration of scattering objects should also increase the scattered X-ray intensity and hence improve the signal-to-noise ratio. The same fitting procedure was attempted for all samples, yielding a similar trend (Table 2) with slightly more variance. One sample (40 Wt.% water of total solvent) could not be modelled owing to the poor contrast. While this did not occur at 2 Wt.%, it is unsurprising due to the previously observed SLD variation of the shell. Like lower SDS concentrations, samples at 4 Wt.% exhibited a reduction in scattering intensity from 20 Wt.% water of solution, with intensity increasing in water-rich media (60-100 Wt.% water of solution).

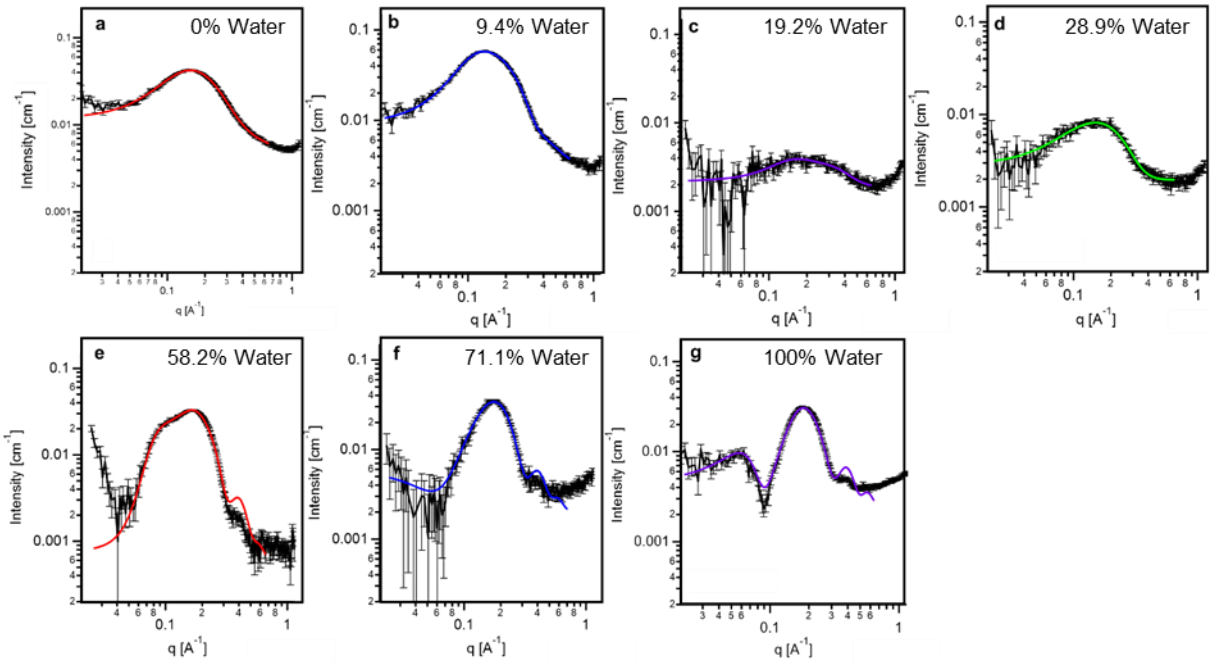

Figure 5.10: 1D SAXS patterns of SDS (4 Wt.%) in glycerol-water solutions at 60 °C, fitted with a core-shell ellipsoid form factor coupled with a mean spherical approximation (Hayter Penfold) structure factor, with solvent compositions of a) 100 Wt.% glycerol, b) 9.4 Wt.% water and 90.6 Wt.% glycerol, c) 19.2 Wt.% water and 80.8 Wt.% glycerol, d) 28.9 Wt.% water and 71.1Wt.% glycerol, e) 58.2Wt.% water and 41.8Wt.% glycerol, f) 78.7 Wt.% water and 21.3 Wt.% glycerol, g) 100 Wt.% water. A full list of fitting parameters is given in Appendix 8.19.

The trends in fitting agree reasonably well with the results obtained for mixtures of 2 Wt.% SDS, albeit with a larger micelle size, which is expected due to the effect of concentration on the extent of micelle aggregation.[52] There were some variations in equatorial core radius in glycerol-rich mixtures, although this may be due to a relatively weak scattering signal from the sample causing a poor fit. Nevertheless, the increase in shell thickness coincides with a reduction in shell SLD. The best data fit indicated that the ellipticity differed in glycerol and aqueous mixtures, with oblate micelles dominating in glycerol-rich media. Mirroring the increase in the equatorial core radius, the micelle charge, which is related to the SDS aggregation number (N_{agg}), increases.

Table 5.2: Fitted parameters of the core-shell ellipsoid form factor with Hayter-Penfold structure factor obtained for 4 Wt.% SDS solutions in glycerol-water mixtures at 60°C (Figure 5.9). Full fitting parameters and given in Appendix 8.19.

Wt.% water of solvent	Equatorial core radius [Å]	Polydispersity index* [σ/r_{core}]	Aspect ratio	Shell thickness [Å]	Shell SLD [$x10^{10}$ cm^{-2}]	Charge	HP radius [Å]	Reduced χ2
0	13.7	0.260	0.608	4.66	13.1	3.27	12.57	1.35
9.4	15.4	0.178	0.668	4.84	12.8	5.13	14.58	1.09
19.2	7.4	0.149	0.492	7.81	101.0	4.79	11.48	1.11
28.9	10.0	0.321	0.662	12.33	10.9	3.26	14.21	1.01
58.2	31.2	0.083	2.280	7.08	11.5	16.47	19.51	9.08
78.7	25.6	0.087	1.635	3.09	13.4	0.10	13.06	2.82
100	26.0	0.066	1.599	3.19	13.1	15.34	20.33	12.82

**Polydispersity index is defined as the core radius standard deviation (σ) divided by core radius (r_{core}).*

Figure 5.11 shows similar behaviour for the fitted micelle structure compared to 2 Wt.%, where the absolute values of the SLD are in close agreement (Figure 5.9b). Absolute shell thicknesses are larger, notably at 20-30 Wt.% water of solution. This may be because of the higher SDS concentration, with more sulfate headgroups present per micelle. Nevertheless, the trend appears to hold true at various SDS concentrations, which is an supports the hypothesis of water localisation within the structure.

While the mean spherical radius presents a more varied spread of data, this can be rationalised by the fact that the HP structure factor for charged spherical particles is less suitable for the structural analysis of elliptical particles at higher concentration, and thus can be considered as an 'apparent' structure factor.[53,54] Kotlarchyk introduced a decoupling method by using a correction factor to account for both non-spherical and polydisperse micelles,[53] while Greene et al. showed that this method is valid for more spherical or oblate objects at lower concentrations.[55] It has also been shown that the spherical HP approximation copes reasonably well for describing SDS micelles with lower ellipticities.[33] In the present work, the higher noise at low *q* also affects fitting of the structure factor peak. Therefore, in order to obtain more representative structure factor fitting, SAXS patterns should be recorded at lower *q* and decoupling approximations should be employed.

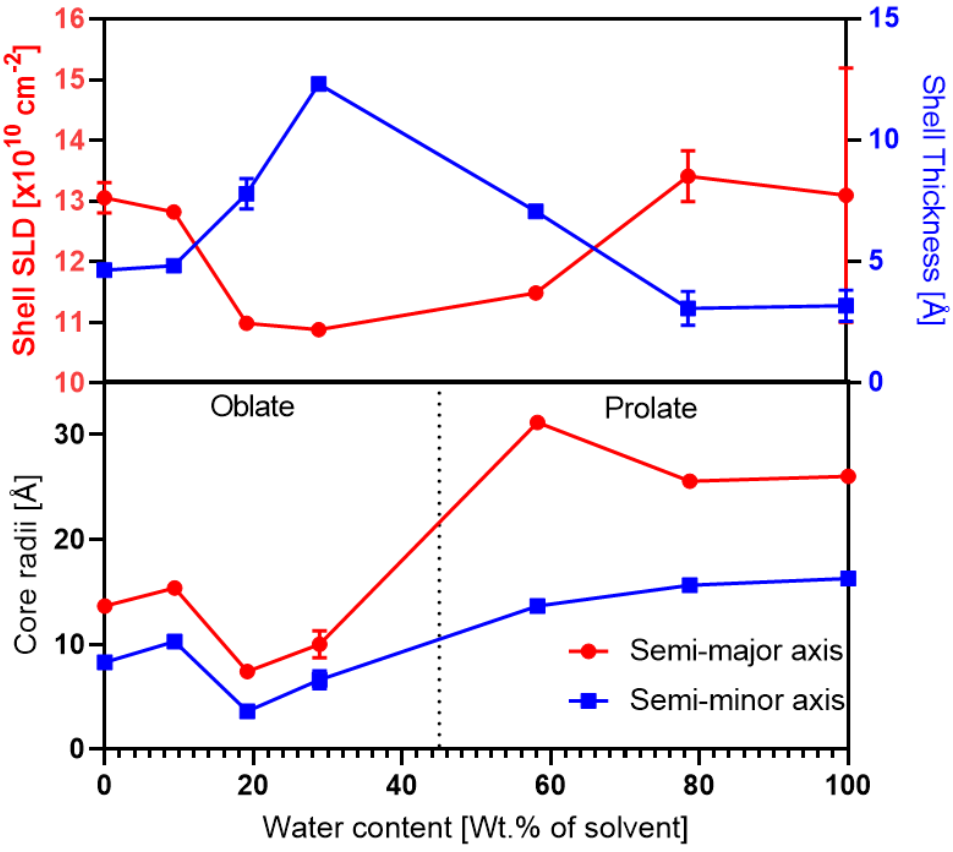

Figure 5.11: Representation of micelle shape and structure formed by SDS (4 Wt.%) in glycerol aqueous mixtures at 60 °C with top) variation of fitted shell SLD and shell thickness with water content, indicating preferential shell hydration at water concentration of 20-30 Wt.%. Bottom) variation of fitted micelle core radii with water content, displaying a marked increase in size in water-rich mixtures, whereby the micelles also become prolate. Error bars correspond to the uncertainties in data fitting procedure.

Overall the fittings suggest that water localises around the surface of an ionic micelle, even in polar water-miscible solvents such as glycerol. However, SLD variation at different SDS concentrations is reassuring, suggesting that it is a genuine phenomenon and not a result of a particular concentration. Following work by Zhao et al.,[46] specific ions and ionic conditions may alter hydration in glycerol-water mixtures, and hence it would be worthwhile exploring surfactant analogues with alternative counterions. More parameters could be measured to improve the accuracy of the models, e.g. measuring the density of SDS at all glycerol/water ratios through regression of solution density measurements. Even with the current set of parameters, it is unlikely that the refined SDS density would change the results significantly. More in depth experiments to probe the nature of water localisation would be useful, either Raman or infrared (IR) spectroscopy and contrast variation small-angle neutron scattering. The former should allow detection of different states for the water molecules, which could

be in turn be used to quantify the amount and locality of water if it is in dynamic equilibrium with the micelle surface. SANS would enable measurement of the SDS micelle shell composition and/or the presence and location of water molecules.

Considering the micelle behaviour in the context of crystallization, the localisation of water complicates matters. For example, above 20 Wt.% water, crystal morphologies of platelets and needles form, whereas feather crystals form at lower concentrations (>6 Wt.% of solution).[8,9,16-19] This suggests viscosity is not the only factor when considering the crystallization habit for glycerol-water mixtures. Furthermore, does the hypothesised hydration of headgroups disrupt SDS-glycerol cocrystal formation? SAXS data would need to be collected at lower water concentrations (c.a. 3-6 Wt.% of solution) to address this question. Moreover, if water does preferentially localise at the SDS head groups, why are hydrates not more common than anhydrous crystals? It is more likely that the dynamic equilibrium of water inhibits the SDS-glycerol phase, such that large quantities of water become associated with the head group only when the volume of water is substantial (but still less than that of glycerol).

While this work was conducted independently to that of Matthew et al., it is important to rationalise differences between these findings.[7] It was reported that SDS forms short cylindrical micelles in glycerol, which would be a departure of the known behaviour for SDS in water.[7] While SDS is known to form ellipsoidal micelles in water, it is possible that the packing parameter cab be altered to further form cylinders.[4] Despite overall similarities in shape, an oblate micelle will 'shield the micelle core more effectively. In a non-capped cylinder, the core of the micelle may be exposed. When considering the micelle fit for 4.4 W.t% SDS in glycerol at 70 °C,[7] the face of the cylinder accounts for ~60% of the total surface area (Figure 5.12). This seems unlikely as the exposed core would induce restructuring of the solvent and entropic penalties associated with the hydrophobic effect would be incurred.

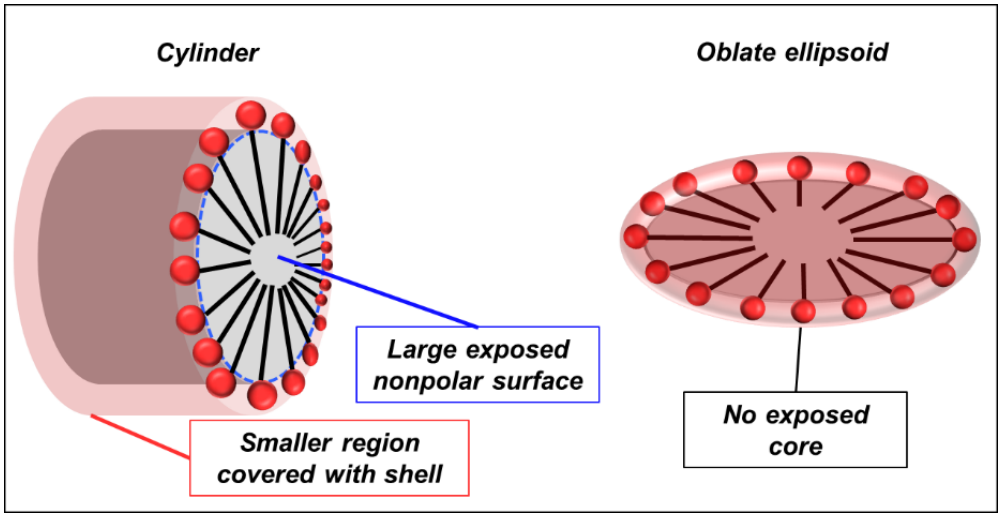

Figure 5.12: Comparison of form factor models for SDS micelles in glycerol at elevated temperatures.[7]

The behaviour of this ternary mixture of SDS, water, and glycerol is complex, and this initial work represents a foundation for others to build on. Both micelle and crystal behaviour exhibit novel phase behaviour and transitions, with the focus being on depth as opposed to breadth of the formulation space. Nevertheless, the behaviour shown here is unique, and has implications for formulation in more complex scenarios. Moreover, addition of more polar substances may alter the equilibria observed for this simple system. However, the formulation sensitivity of some phases, such as the SDS-glycerol phase in the presence of water has been shown to dramatically alter physical properties, particularly the rheology (Figure 5.7).

5.2.3. SDS/1-dodecanol/Glycerol – Crystal Phase Behaviour

1-Dodecanol is a key synthetic precursor for many surfactants including SDS.[56] It consists of a C12 alkyl tail with a single terminal hydroxyl group, and it is much less amphiphilic and polar than SDS. Summerton et al. reported the crystallization of SDS in the presence of 1-dodecanol in aqueous mixtures: 1-dodecanol acts as a seed causing morphological changes including cocrystallization.[57] It is possible that addition of 1-dodecanol to SDS in glycerol may cause similar behaviour. Furthermore, 1-dodecanol is known to act as a cosurfactant,[58] influencing the packing parameter and hence the micelle shape.[59] Therefore both crystalline and solution structures were studied. This also provided complimentary data to previous work, while focusing on lower SDS/dodecanol concentrations.[60] ~4 Wt.% SDS solutions were studied to emphasise any trends that occurred as a function of SDS/1-dodecanol molar ratio, while still being industrially relevant. Initially, solutions containing SDS, 1-

dodecanol and glycerol (Table 3) were heated to 75°C and cooled quiescently. The resulting mixtures were then studied at room temperature using optical microscopy and DSC.

Table 5.3: Composition of 3 tertiary mixtures containing SDS, glycerol and 1-dodecanol.

	SDS [Wt.%]	Dodecanol [Wt.%]	Glycerol [Wt.%]
SDD1	3.05	0.00	97.0
SDD2	3.80	0.33	95.9
SDD3	3.74	0.97	95.3
SDD4	3.73	1.73	94.5

Microscopy images indicate a significant difference in morphology for each sample. Compared to only SDS in glycerol, birefringent fibres characteristic of the SDS-glycerol phase become shorter, and less defined when 0.33 Wt.% 1-dodecanol is included (Figure 5.13a, 5.13b). At considerably higher 1-dodecanol concentrations (Figure 5.13c, 5. 13d), there is a lower proportion of fibres, which are replaced by ill-defined clumps.

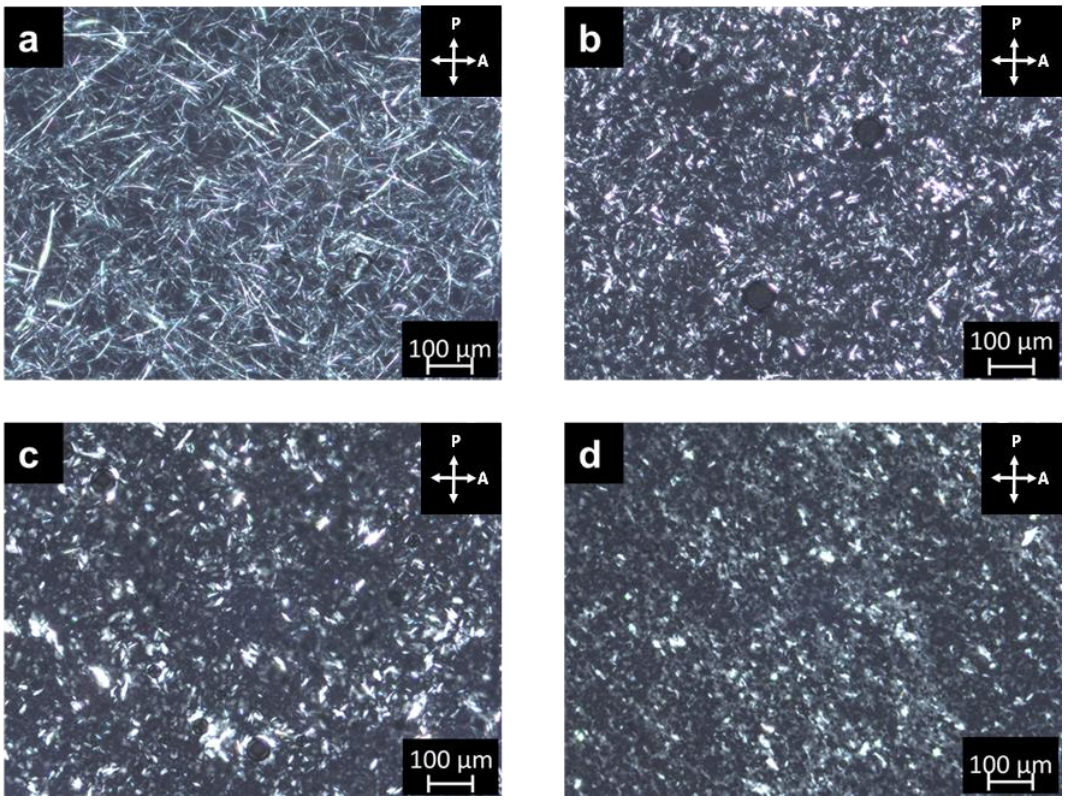

Figure 5.13: Polarised optical microscopy images of ternary mixtures of SDS, 1-dodecanol and glycerol heated to 75 °C and quiescently cooled overnight. Sample composition shown in Table 5.3 where a) SDD1 b) SDD2 c) SDD3 d) SDD4. In general, a transition from fibre morphology to ill-defined aggregates occurs as 1-dodecanol concentration is increased, indicating loss of the SDS-glycerol crystal phase.

The stark change in crystal morphology suggests similar behaviour to the literature data,[57] where 1-dodecanol acts as a seeding agent and crystallizes with SDS. Despite inhibition of the fibre phase occurring over a narrower concentration range than that observed for water, the SDS:1-dodecanol molar ratio must be considered. Thus inhibition of this phase is unlikely if 1-dodecanol is merely present as a minor impurity. However, if the crystal morphology is affected as shown by POM, there may be implications for gelation owing to the lower aspect ratio morphologies which do not entangle in the same manner.[29] The microstructure and physical properties of the clumped phase cannot be confirmed through microscopy alone, and incorporation of 1-dodecanol into this crystal structure is not yet proven.

The next step for characterising the phases observed in Figure 5.13, was the use of DSC to measure melting ranges. In water, 1-dodecanol inclusion resulted in an increase in melting temperature for both 1-dodecanol and SDS.[57] For SDS, 1-dodecanol and glycerol, there are generalised peak ranges (A, B, and C) which vary with the 1-dodecanol concentration (Figure 5.14). SDS in glycerol exhibits a single broad melting peak (Figure 5.15a Peak C), which is indicative of the SDS-glycerol phase at 44 °C. Addition of 0.33 Wt.% 1-dodecanol results in a marginally lower melting range, with a single peak observed at 42 °C for SDD2, although it is more well-defined. This is because of the large crystal aggregate size in SDD1 which melts slower due to the smaller surface area to volume ratio. A shoulder is also observed, although its origin is unknown. Increasing the 1-dodecanol concentration causes three peaks to be observed, suggesting a change in crystal phase. While the peak attributed to the SDS-glycerol crystal phase is present in both samples, this feature is downshifted by 2°C. It is unknown whether this corresponds to the anhydrous crystal, SDS-glycerol crystal or an SDS-1-dodecanol crystal .

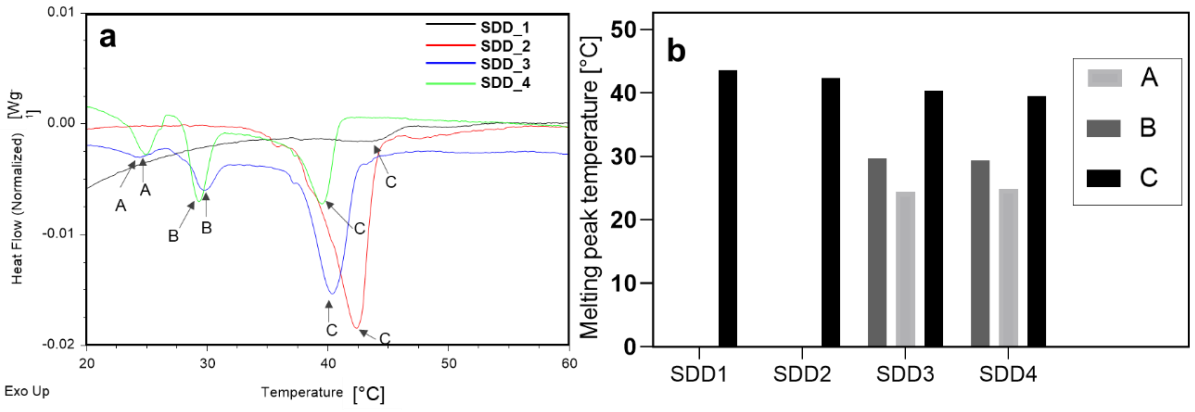

Figure 5.14: a) DSC melting profile of tertiary mixtures of SDS, 1-dodecanol and glycerol, with compositions shown in Table 5.3. Three separate and prominent peaks are identified and labelled as A,B,C, corresponding to the likely transition of 1-dodecanol, SDS-dodecanol cocrystal, and SDS-glycerol or anhydrous SDS crystals. b) Representation of fitted peak transitions in Figure 13a with different compositions compared against one another. Samples were initially prepared by being heated to 75 °C followed by quiescent cooling overnight before measurement.

The presence of two additional peaks (A and B Figure 5.14) most likely corresponds to SDS/1-dodecanol (B) cocrystal and crystallized 1-dodecanol (A). However, only a single melting point was observed for SDS/1-dodecanol mixtures in Summerton's work.[57] This is due to the higher solubility of 1-dodecanol in aqueous SDS mixtures and the heating profile used in this work, where any 1-dodecanol not incorporated into the SDS structure precipitate and crystallises at 15 °C sample. Additionally, the relative reduction in peak magnitude (enthalpy) of peak C, and increase in peak A and B, indicates that the crystal containing SDS (and no 1-dodecanol) is replaced for a cocrystal as 1-dodecanol is increased. Peak A closely aligns with the literature melting behaviour of 1-dodecanol and peak B aligns with the melting transition reported by Summerton et al. for the SDS-dodecanol co-crystal.[57,61]

Therefore a transition from the SDS-glycerol crystal to the SDS-dodecanol crystal is likely as the relative 1-dodecanol concentration is increased, according to microscopy observations and DSC measurements. To confirm this, SAXS was performed on quiescently cooled 4 Wt.% SDS solutions in glycerol containing varying amounts of 1-dodecanol (Figure 5.15). Two predominant phases were initially identified throughout the concentration range, which corresponded to the SDS crystal phase (001_G= 54.9 Å) and an unknown crystal phase with a d_{001}-spacing of 35.4 Å (001_D). Another minor phase was observed at 31.6 Å, which is close to the peak found in SDS/glycerol/water (3 Wt. % water of solution), but this featured was not observed anywhere else.

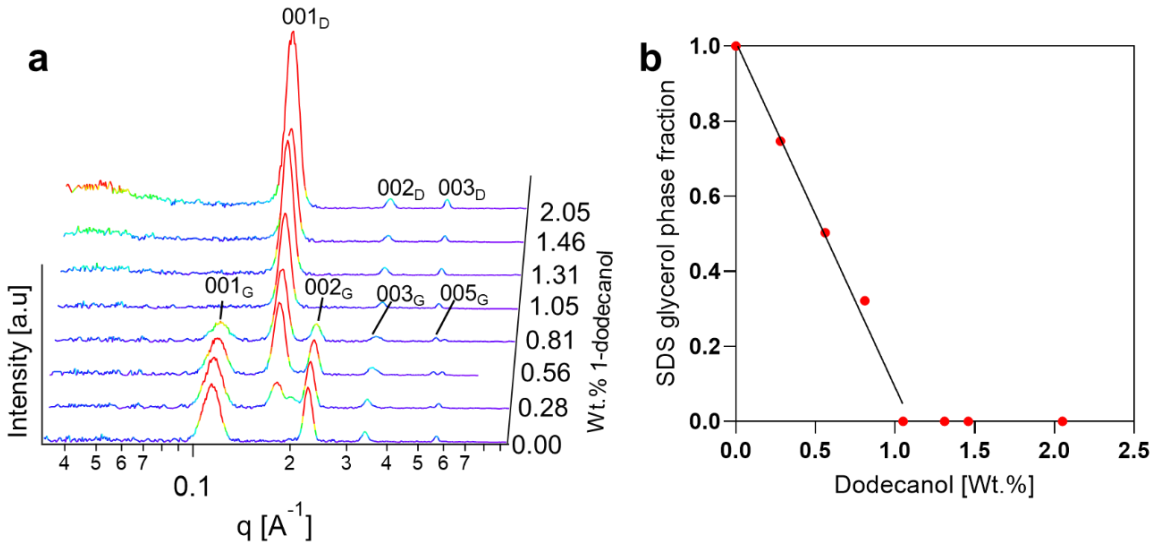

Figure 5.15: Tertiary mixtures of SDS (4 Wt.%), 1-dodecanol and glycerol heated to 75 °C and quiescently cooled overnight. A) 1D SAXS pattens plotted against 1-dodecanol concentration where $00l_G$ is the SDS-glycerol crystal phase and $00l_D$ is the SDS-dodecanol cocrystal phase. B) Linear trend of reduction in SDS-glycerol phase in preference to SDS-dodecanol phase as 1-dodecanol concentration is increased. A 1:4 1-dodecanol: SDS mass ratio, corresponding to a 0.42:1 molar ratio is required for complete inhibition.

The trend in crystal abundance is linear (Figure 5.15b) with respect to the 1-dodecanol concentration, with SDS-dodecanol crystals formed in preference to the SDS-glycerol crystal phase. Full inhibition of the SDS crystal phase occurred with dodecanol concentratios above 1 Wt.% (which equates to SDS with a 79% purity by mass). However, significant morphological change in crystal habit occurs before this. The SDS-dodecanol cocrystal phase appears to be non-stoichiometric and differs depending on the SDS and 1-dodecanol concentrations. This is evidenced by the small yet measurable change in d_{001}-spacing (Figure 5.16), where the higher 1-dodecanol concentration produces a marginally larger bilayer spacing. It can be concluded that 1-dodecanol plays a very similar role in SDS-glycerol mixtures as it does in SDS-water mixtures in that it acts as a nucleating agent, causing cocrystals with ill-defined stoichiometry to form. Although small amounts of 1-dodecanol impurity may be inconsequential for phase behaviour within a formulation, the effect on the SDS-glycerol crystal aspect ratio may cause loss of entanglement and network formation. Therefore oscillatory rheology should be employed to determine this effect.

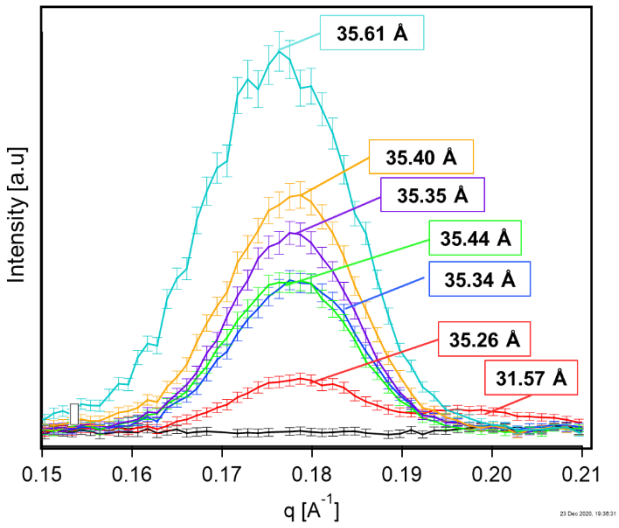

Figure 5.16: Magnified regions of the d_{001} peak of the SDS-dodecanol crystal obtained from SAXS data (Figure 5.15), for tertiary mixtures of SDS (4 Wt.%), 1-dodecanol and glycerol heated to 75 °C and quiescently cooled overnight. Fitted peak centres show a small but noticeable decrease in peak position, corresponding to an increase in d_{001}-spacing as the 1-dodecanol concentration is increased. Peaks contain the following amount of 1-dodecanol, listed from highest intensity to lowest intensity: 2.05 Wt.%, 1.46 Wt.%, 1.31 Wt.%, 1.05 Wt.%, 0.81 Wt.%, 0.56 Wt.%, 0.28 Wt.%, With the lowest intensity (0.28 Wt.%) sample showing two peak centres.

5.2.4. SDS/1-dodecanol/Glycerol – Elevated Temperature Behaviour

It is equally as important to understand the solution behaviour as well as crystallization because changes in micelle shape can alter the solution's physical properties. For example a spherical micelle to wormlike micelle transition can result in an increase in viscoelasticity.[62] SDS (4 Wt.%) and 1-dodecanol

(up to 2 Wt.%) in glycerol were heated to 60 °C, to allow comparison with previous micelle data. The fitting was conducted at 0.03 $A^{-1} < q < 1\ A^{-1}$, to mitigate the effect of backstop scattering (low q) and amorphous (high q) scattering. The data were fitted using the core-shell ellipsoid model with a HP structure factor. This approached indicated an oblate ellipsoid similar to previous measurements. As absolute intensity calibration was not possible for this dataset; the scale parameter was not fixed but fitted. Moreover, the SLD change for the micelle shell on addition of 1-dodecanol was treated as negligible, as the hydroxyl group was considered to make a minimal contribution the shell density due to its relative small size. All models fitted the scattering patterns to a high degree, although the χ^2 values increased at high 1-dodecanol concentrations (Table 4). This is due to the increase in scattered intensity, causing larger absolute values.

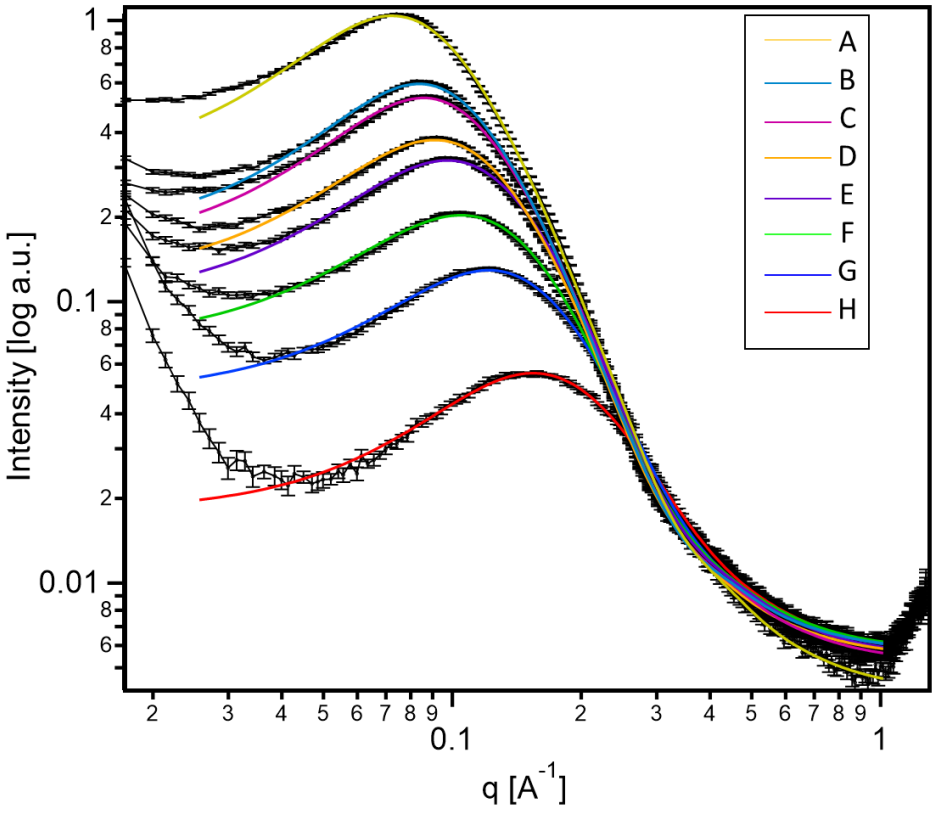

Figure 5.17: 1D SAXS patterns of SDS (4 Wt.%) and 1-dodecanol in glycerol solutions at 60 °C, fitted with a core shell ellipsoid form factor coupled with a charged mean spherical approximation (Hayter Penfold) structure factor. Samples contain A) 0 B) 0.28 Wt.% C) 0.56 Wt.% D) 0.81 Wt.% E) 1.05 Wt.% F) 1.31 Wt.% G) 1.46 Wt.% H) 2.05 Wt.% 1-dodecanol. The shift to low q is indicative to core swelling. Full fitting parameters are providedin Appendix 8.20.

All patterns converge at a similar low q value (Figure 5.17) and the peak maxima correlates with the 1-dodecanol concentration. The shift in these maxima, and hence increase in micelle size (Table 5.4) is explained by swelling of the core, as well as a reduction in the aspect ratio as the 1-dodecanol

concentration is increased.[63] However, the aspect ratio decreases because the alcohol group aligns at the glycerol interface. Thid causes a causing slightly lower packing parameter, as the shell is composed of both primary alcohol and sulfate groups.

Due to the oblate ellipsoid form factor, the spherical HP structure factor is not optimised to account for non-sphericality,[55] which may slightly alter the fitted parameters. For example, while inter-micelle repulsion exists due to the presence of charged SDS molecules, the addition of 1-dodecanol should have a negligible effect on overall micelle charge. However the fitted charge value is observed to increase (Table 4). It is expected that the inclusion of a decoupling method, may increase the validity of the fitted structure factor, as higher aspect ratios lead to poorer fits of the data.[53] Furthermore, the scattering from the beam stop causes an upturn at low *q* which influences the fit, despite the low *q* fitting limit used, as evidenced by the lack of upturn in the measurement of SDS (4 Wt.%) in glycerol (Figure 5.10a).

Table 5.4: Fitted parameters of models composed of a core-shell ellipsoid form factor with a Hayter-Penfold structure factor for ternary solutions containing SDS (4 Wt.%) with 1-dodecanol and glycerol at 60°C (Figure 5.17). Full list of fitting parameters is given in Appendix 8.20.

Wt.% 1-dodecanol	Equatorial core radius [Å]	Polydispersity index* [σ/r_{core}]	Aspect ratio	Shell thickness [Å]	Charge	HP radius [Å]	Reduced χ2
0	12.64	0.64	0.64	4.12	9.30	9.30	2.14
0.28	13.31	0.75	0.75	3.26	8.93	8.93	2.09
0.56	17.06	0.63	0.63	3.75	11.69	11.69	2.22
0.81	18.60	0.61	0.61	3.56	12.46	12.46	2.36
1.05	16.98	0.72	0.72	3.02	13.03	13.03	8.58
1.31	20.90	0.57	0.57	3.36	13.53	13.53	4.75
1.46	21.50	0.55	0.55	3.05	13.12	13.12	22.6
2.05	24.25	0.50	0.50	3.10	13.52	13.52	2.14

**Polydispersity index is the core radius standard deviation (σ) divided by core radius (r_{core}).*

The fitting parameters show an increase in core radii on addition of 1-dodecanol (Table 4, Figure 5.18). However, the formation of structures associated with a lower packing parameter (i.e. worms) was not observed. Instead, a slight reduction in aspect ratio was observed, although this was highly variable.

This suggests that while affecting the shape of the micelle, the presence of 1-dodecanol influences micelle shape less than other additives on micelle shape such as salt.[64]

The shell thickness slowly and consistently reduced in size up to 25%. This is explained by the presence of the hydroxyl groups of the 1-dodecanol at the interface, which lowers the average thickness. This raises questions regarding the decision to fix the shell SLD, as it was expected the effect of 1-dodecanol on the shell would be minimal. However, this may cause over-parameterization as normalized absolute intensity measurements were not possible for this dataset. A general trajectory can be envisioned (Figure 5.18) where the micelles become larger and slightly more oblate and may have the potential to form wormlike micelles at higher alcohol concentrations.[65]

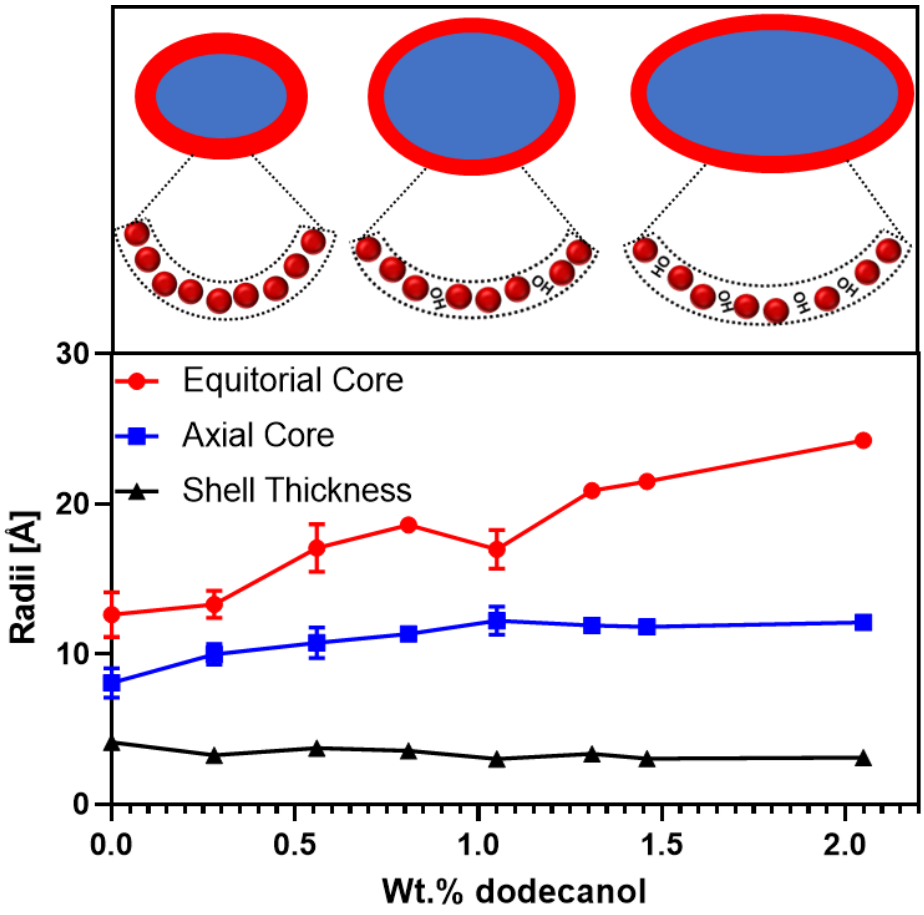

Figure 5.18: Top) Visualisation of micelle fitted size and shape form factor parameters (Table 5.4) for SDS (4 Wt.%), 1-dodecanol and glycerol ternary mixtures at 60 °C. Rationalisation of shell thickness and curvature are visualized in the packing of SDS headgroups and the 1-dodecanol OH group. Bottom) Fitted parameters from SAXS model fitting (Table 4) versus 1-dodecanol content. Error bars correspond to the uncertainties in data fitting procedure.

The data provide some for understanding of the structures formed in the presence of a potential impurity in commercial SDS, which can cause changes in physical properties and affect product performance. While the behaviour was well defined at the concentration studied, the measurement of physical properties, such as rheology, would be invaluable in future experiments to quantify the difference in crystal morphology. Moreover, the effect of crystallization at different temperatures is likely to play a large role in crystal formation, which may favour different crystal types.

5.2.5. SDS/Glycerol/NaCl Crystal Phase Behaviour

Inorganic salts are often present in a wide range of personal care formulations, for example to provide therapeutic benefit in the case of fluoride salts for enamel protection, or the addition of NaCl in shampoo formulations to form viscosifying wormlike micelles.[65,66] SDS (2 Wt.%) glycerol solutions with added NaCl were prepared in order to determine phase composition and to examine whether the SDS crystal phase would be inhibited. Solutions containing 1, 2, and 3 Wt.% NaCl were subjected to heating and quiescent cooling, whereby a higher heating and mixing interval of 100 °C for 1.5 hours was used to ensure dissolution of NaCl.

The resulting mixtures contain different structures, as indicated by POM studies (Figure 5.19). While the reference solution showed formation of large crystal fibres, solutions containing salt (Figure 5.19b to 5.19c) contain much smaller crystalline aggregates. For samples containing 1 Wt.% and 2 Wt.% NaCl, fibre morphologies were interspersed with other minor amounts of large platelets. The smaller size of the fibres suggests more rapid growth, possibly through instantaneous nucleation. Closer inspection of the sample containing 3 Wt.% NaCl (Figure 5.19c, 5.21) indicates the presence of platelets and needles, thus differing in morphology to that observed for glycerol-water mixtures.

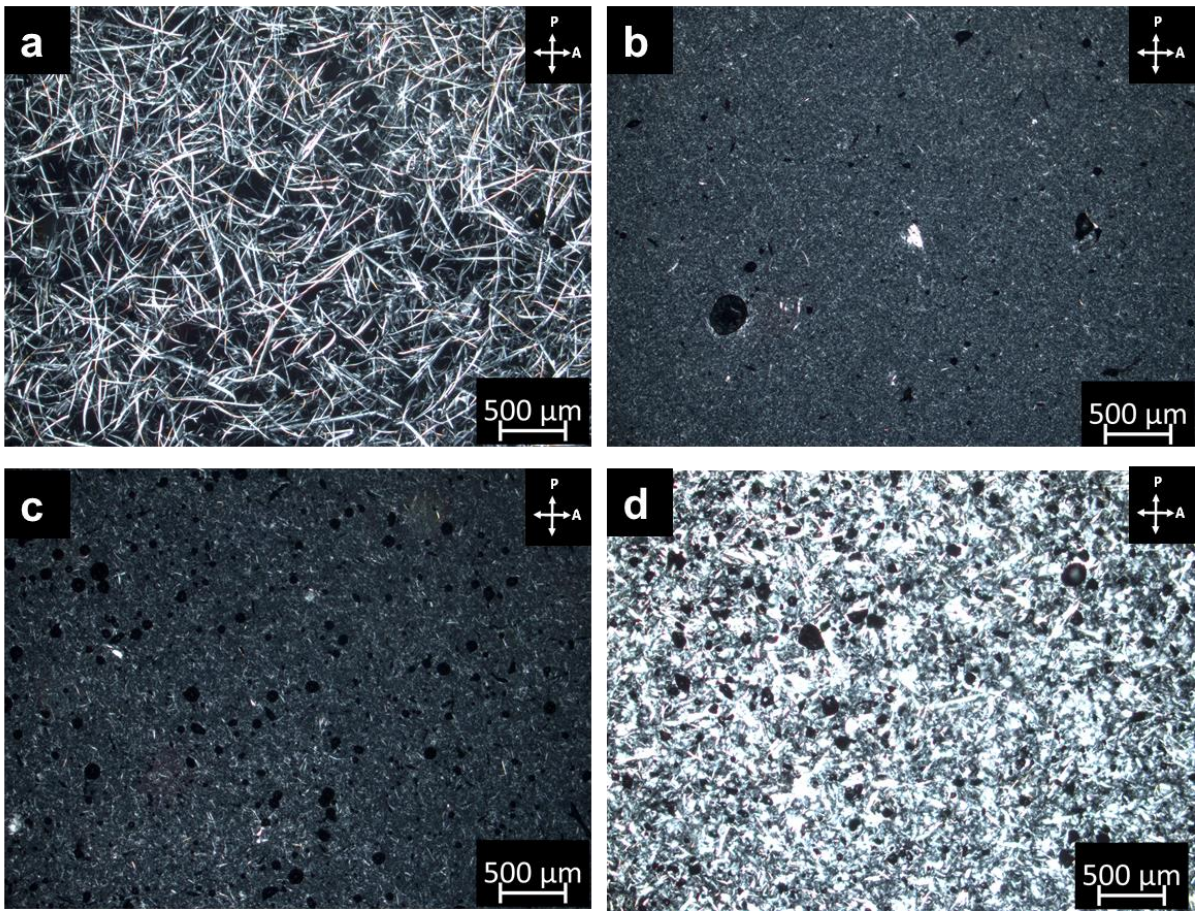

Figure 5.19: Polarised optical microscopy images of tertiary mixtures of SDS (4 Wt.%), NaCl and glycerol following heating at 100 °C and quiescent cooling overnight. a) 0 Wt.% NaCl b) 1 Wt.% NaCl c) 2 Wt.% NaCl and d) 3 W.t% (NaCl). In b and c, a fibre morphology is dominant along with a small number of unknown aggregates, where the crystal aggregate size is much smaller than in zero salt samples. At high salt concentration (d) an entirely new phase is obtained that does not contain any fibres.

Literature data shows a minimal impact on Krafft temperature when adding small quantities of NaCl to SDS in water/glycerol mixtures.[4] DSC studies performed on 4 Wt.% solutions of SDS in glycerol containing 0.5 Wt.% and 4 Wt.% NaCl showed an increased melting range (+30 °C) at high NaCl concentrations (Appendix 8.21), although this was still well below the processing temperature used. This may mean that different crystal morphologies or phases are formed as a result of differing degrees of undercooling, despite being quiescently cooled. To determine the phase composition, SAXS studies were performed (Figure 5.21).

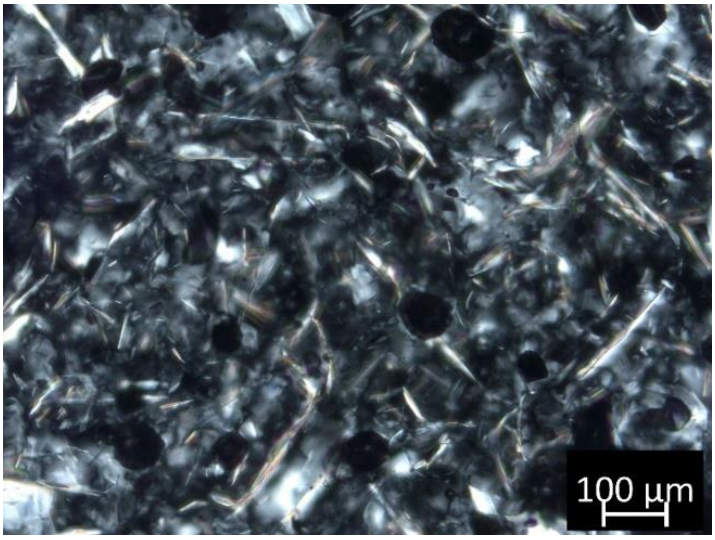

Figure 5.20: Polarised optical microscopy image of SDS (4Wt.%) in NaCl (2 Wt.%) and glycerol solution following heating at 100 °C and quiescent cooling overnight (same sample as Figure 5.19c). Mixture shows needles and platelets of indeterminate composition.

A new crystal structure is observed at 3 Wt.% NaCl (Figure 5.21) and is present as a minor constituent along with the SDS-glycerol crystal at both 1 and 2 Wt.% NaCl. The new crystal structure had a d_{001}-spacing of 31.5 Å (001_N) , which is similar to the phase found in mixtures of SDS (2 Wt.%) in 3 Wt.% water and 97 Wt.% glycerol cooled at 15 °C, as well as the minor constituent found in quiescently cooled SDS (4 Wt.%) and 1-dodecanol (0.28 Wt.%) in glycerol (d001- 31.9 Å). However, it cannot be verified if the species are the same. It is not obvious what this phase is, as its d_{001}-spacing does not correspond to the most common (hydrate or anhydrous) phases of SDS. [8-10,16-19] The microscopy images suggest that this phase is likely crystalline, as opposed to the 'hexagonal phase' reported by Matthews et al.[24]

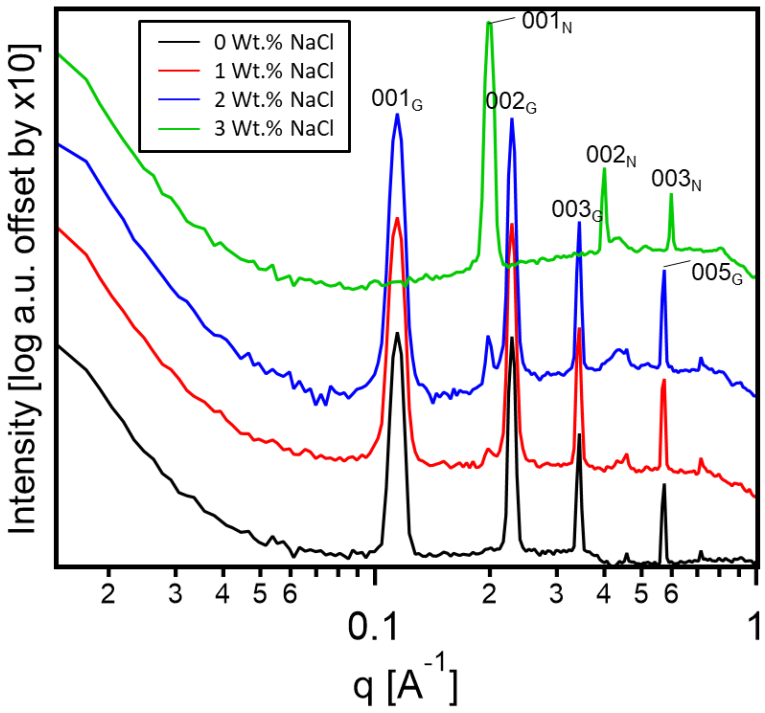

Figure 5.21: Offset 1D SAXS patterns of the tertiary mixtures of SDS (2 Wt.%), NaCl and glycerol following heating at 100 °C and quiescent cooling overnight. While the sample without salt is comprised of only the SDS-glycerol crystal phase ($00l_G$) , samples containing 1 and 2 Wt.% NaCl show low intensity of an alternate crystal type of SDS ($00l_N$), concurrent with microscopy (Figure 5.19). Samples containing 3 Wt.% NaCl contain only an alternative crystal of SDS, with unknown composition.

The unknown phase exists in all ternary mixtures studied, and therefore cannot be related to anything other than glycerol and SDS. There are two possible explanations: a hithertoo undiscovered polymorph of anhydrous SDS or a polymorph of the SDS-glycerol phase. The second is less likely (but possible), owing to the limited number of geometrical conformations that glycerol and SDS could adopt to satisfy the d_{001}-spacing, although this could be compensated by significant tilt in both the primary (lamellar) and non-primary axis. It was not possible to construct electron density profiles that informed the structure as the profile from three orders of magnitude did not yield sufficiently high resolution. Stoichiometry was estimated to be sub-equimolar for the SDS-glycerol phase, which may indicate different accessible stoichiometries – much like hydrate equivalents. However, it is entirely likely that the phase could be both anhydrous and polymorphic. Moreover, SDS and NaCl are both sodium salts, so any change in crystallization from different counterions is not possible.[67] However, the crystal may form as salts are often found at the Stern layer of a micelle,[1] potentially affecting glycerol-sulfate interactions. If so, more work would be needed to confirm this hypothesis. Single crystal diffraction (or powder diffraction) in the wide angle range would provide more structural information because the higher number of lamellar peaks should enable the construction of detailed electron density profiles to aid characterisation.

5.3. Comparison of Crystal and Micelle Behaviour

For molecules containing crystallizable alkyl chains, packing is a key factor in the formation of crystals. Ionic surfactants also have headgroup interactions that can affect crystallization.[66] The work shown in this chapter indicates the wide range of crystallization behaviour dictated by solvent properties and interactions with the sulfate head group of SDS. It was expected that hydrate crystals would form in the presence of water. However, this was generally not the case, with preference for the formation of anhydrous crystals instead. Both NaCl and 1-dodecanol additives induced different crystal structures. While this was expected in the presence of 1-dodecanol due to the compatibility of its alkyl tail enabling cocrystallization, the new crystal formed in the presence of NaCl was surprising. The SDS-glycerol phase was generally kinetically inaccessible in tertiary mixtures with respect to other phases and small amounts of tertiary additive led to large changes in structure. This has implications for formulation and design and more precise formulation and processing may be required to target a certain phase. The nature of the crystal phase was shown to have an impact on industrially relevant physical properties, e.g. unwanted melting and crystallization of SDS crystals caused by a negative shift in melting point in the presence of 1-dodecanol. A summary of the primary crystal types is shown in Figure 5.22.

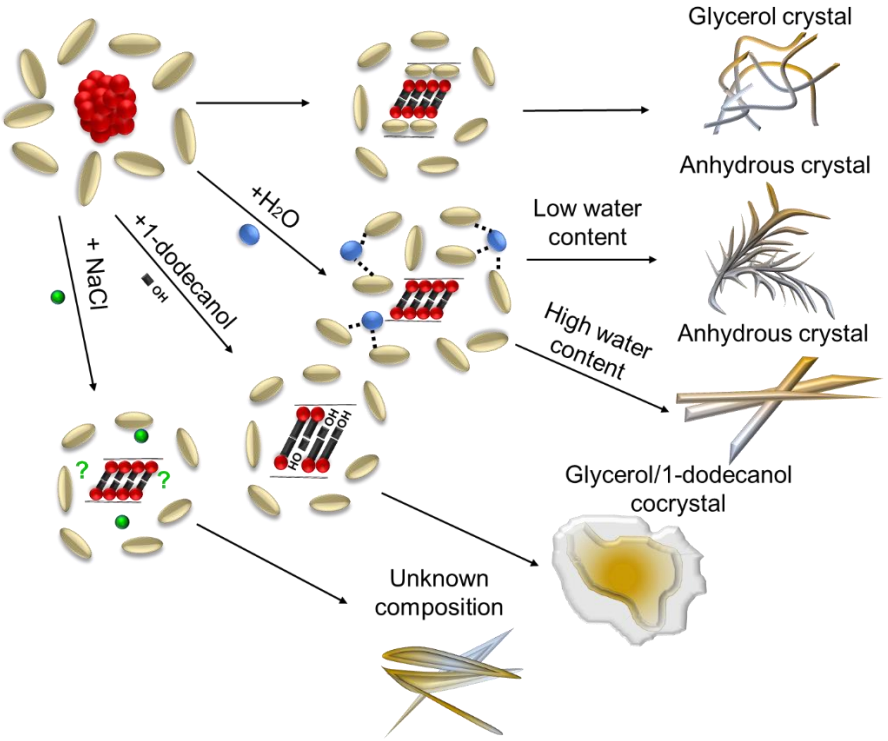

Figure 5.22: Summary of observed crystallization at lower degrees of under-cooling (20 °C and above) for SDS in glycerol. The effect of different additives on crystal structure and subsequent morphology (habit) are shown. While all other phases are characterised, the samples containing NaCl require further characterisation in future work.

Micelle structures at elevated temperature were generally well described by ellipsoidal structures. Water-rich SDS micelles tend to give prolate ellipsoids, whereas glycerol rich micelles tended to give oblate micelles. However, often the quality of the data fit between prolate and oblate ellipsoid is similar and the shape can be almost identical aside from the aspect ratio.[68] This is not the only piece of work to report a tuneable difference in ellipticity based on mixture composition, although micelle ellipticity in micelles is still debated.[69,70] While the proposed shape of the SDS/glycerol micelles is different from that reported by Matthews et al.,[7] some commonality is observed in that a shorter cylinder is modelled, with an aspect ratio of less than unity. One shape that was not considered was a triaxial ellipsoid, which has been reported to give better data fits than standard biaxial models.[71] Oliver et al. showed that adjustment of the chain length for surfactants, while affecting micelle size, does not alter ellipticity to a large degree.[72] Packing of the surfactant, with particular focus on head group arrangements, has been used to rationalise the preferred formation of ellipsoids.[27,73] This suggests that the effective size of the surfactant headgroup, which is affected by solvation, could be the key as to why SDS in glycerol forms oblate micelle (vs prolate in aqueous solutions).

5.4. Conclusions

The work contained in this chapter begins to quantify the complex crystallization behaviour that arises when other compounds are introduced, each with different mechanisms. Water was shown to inhibit SDS-glycerol crystals, with the predominance of the anhydrous SDS phase above 6 Wt.% water of solution. This has implications in terms of structuring, as glycerol is hygroscopic and atmospheric water ingress could cause a change in crystallization for water contents achievable through the humectancy of glycerol alone.[74] Isothermal crystallization measurements at different temperatures suggested that the anhydrous crystal was the kinetic product, with a previously unknown kinetic barrier to SDS-glycerol crystal formation. It was hypothesised that this was a result of either hydration (of water) at the micelle surface prior to crystallization, or the interaction between glycerol and water 'tying up the glycerol' through a H-bonded liquid network. More likely, water is present in a dynamic equilibrium between the bulk solvent and micelle surface. SAXS data appeared to agree with this, with glycerol-rich binary aqueous mixtures experiencing greater shell hydration, resulting in a thicker micelle shell with a lower SLD than expected. Furthermore, a feather crystal morphology, indicative of a high degree of secondary nucleation, was also observed for anhydrous SDS crystals in solutions with low water contents. This gave way to needles at 20 Wt.% water of solution. The cause could not be determined but may also be affected by interactions between water and SDS.

Shell swelling occurred in SDS micelles at elevated temperatures in mixed solvents for both 2 and 4 Wt.% SDS. While the SAXS data fits at different concentrations were self-consistent, amorphous scattering at high *q*, noise at low *q*, spherical approximation of the structure factor suggest that numerous experimental parameters could still be improved upon, when revaluating the system. This could be achieved through scattering experiments with a wider *q* range. Complimentary techniques such as SANS and Raman spectroscopy are the next logical step for micelle characterisation, as these techniques can probe local water structure in greater detail.

The behaviour of 1-dodecanol within the SDS-glycerol system provided a means of understanding the effect of likely impurities or cosurfactant on cocrystallization and micelle structure. Micelle scattering was much as expected, with swelling of the core and a modest increase in ellipticity. The formation of an SDS-dodecanol cocrystal, with layer spacing that was dependant on 1-dodecanol concentration, was consistent with the findings reported by Summerton et al. for aqueous SDS mixtures.[57] The melting behaviour of SDS-dodecanol cocrystals was the opposite to that reported by Summerton et al., with a reduction in melting temperature due to the different solvent and Krafft temperature. Future work should focus on rheological effects, given the drastic change in crystal morphology.

The effect of adding NaCl unexpectedly produced a new crystal type with a different morphology and d_{001}-spacing. Many questions still remain regarding the precise composition, but this work certainly introduces another factor to consider when designing formulations that contain SDS and glycerol. In the future, better resolved scattering patterns at higher scattering angles should enable electron density profile reconstruction without the need to form single crystals.

5.5. References

1 T. F. Tadros, *Applied Surfactants: Principles and Applications*, Wiley, Weinheim, 2005.
2 M. L. Sheely*, Industrial and Engineering Chemistry*, 1932, **24**, 1060–1064.
3 R. Boerefijn, P.-R. Dontula and R. Kohlus, *Handbook of Powder Technology*, 2007, **11**, 673–703.
4 H. Khan, J. M. Seddon, R. V Law, N. J. Brooks, E. Robles and J. T. Cabral, *Journal of Colloid And Interface Science*, 2018, **538**, 75–82.
5 R. A. Abdel-Rahem, *Journal of Dispersion Science and Technology*, 2013, **34**, 932–940.
6 C. C. Ruiz, L. Díaz-lópez, J. Aguiar, L. Díaz-López and J. Aguiar*, Journal of Dispersion Science and Technology*, 2008, **29**, 266–273.
7 L. Matthews, Ż. Przybyłowicz, S. E. Rogers, P. Bartlett, A. J. Johnson, R. Sochon and W. H. Briscoe, *Journal of Colloid and Interface Science*, 2020, **572**, 384–395.
8 R. M. Miller, A. S. Poulos, E. S. J. J. Robles, N. J. Brooks, O. Ces and J. T. Cabral, *Crystal Growth & Design,* 2016, **16**, 3379–3388.
9 R. M. Miller, O. Ces, N. J. Brooks, E. S. J. Robles and J. T. Cabral, *Crystal Growth & Design*, 2017, **17**, 2428–2437.

10 L. A. Smith, R. B. Hammond, K. J. Roberts, D. Machin and G. McLeod*, Journal of Molecular Structure*, 2000, **554**, 173–182.
11 F. Tian, H. Qu, A. Zimmermann, T. Munk, A. C. Jørgensen and J. Rantanen, *Journal of Pharmacy and Pharmacology*, 2010, **62**, 1534–1546.
12 N. S. Cheng, *Industrial and Engineering Chemistry Research*, 2008, **47**, 3285–3288.
13 J. W. P. Schmelzer and A. S. Abyzov, in *Thermal Physics and Thermal Analysis*, Springer, Cham, 2017, pp. 195–211.
14 M. Svärd, D. Ahuja and Å. C. Rasmuson*, Crystal Growth & Design*, 2020, **20**, 4243–4251.
15 H. J. Wood, J. D. Hunt and P. V. Evans, *Acta Materialia*, 1997, **45**, 569–574.
16 V. M. Coiro, F. Mazza and G. Pochetti, *Acta Crystallographia*., 1986, **C42**, 991–995.
17 V. M. Coiro, M. Manigrasso, F. Mazza and G. Pochetti, *Acta Crystallographia*., 1987, **C43**, 850–854.
18 S. Sundell, *Acta Chemica Scandinavica*, 1977, **A31**, 799–807.
19 L. A. Smith, A. Duncan, G. B. Thomson, K. J. Roberts, D. Machin and G. Mcleod, *Journal of Crystal Growth*, 2004, **263**, 480–490.
20 R. M. Miller, J. T. Cabral, E. S. J. Robles, N. J. Brooks and O. Ces, CrystEngComm, 2018, **20**, 6834–6843.
21 X. Li and Q. Zhang, *Crystals*, 2020, **10**, 24.
22 H. Wang, Q. Lin, X. Dou, T. Yang, Y. Han, *Crystals*, 2017, **7**, 357-367.
23 A. G. Marangoni, in *Kinetic Analysis of Food Systems*, Springer International Publishing, Cham, 2017, pp. 113–134.
24 L. Matthews, M. C. Stevens, R. Schweins, P. Bartlett, A. J. Johnson, R. Sochon and L W. H. Briscoe, *Colloids and Interface Science Communications*, 2021, **40**, 100342.
25 P. C. Griffiths, A. Paul, R. K. Heenan, J. Penfold, R. Ranganathan and B. L. Bales, *Journal of Physical Chemistry B*, 2004, **108**, 3810–3816.
26 *Physical properties of glycerol and its solutions*, Glycerine Producers' Association, New York, 1963.
27 H. Nakagawa, T. Oyama, *Frontiers in Chemistry*, 2019, **7**, 1–9.
28 A. Kelarakis, S.M. Mai, C. Booth, A.J. Ryan, *Polymer*, 2005, **46**, 2739–2747.
29 G. Ben Messaoud, P. Le Griel, D. Hermida-Merino, S. L. K. W. Roelants, W. Soetaert, C. V. Stevens and N. Baccile, *Chemistry of Materials*, 2019, **31**, 4817–4830.
30 P. Thareja, *Rheologica* Acta*,* 2013, **52**, 515–527.
31 A.W. Sisko, Industrial & Engineering Chemistry Research, 1958, **50**, 1789-1792
32 P. C. Griffiths, A. Paul, R. K. Heenan, J. Penfold, R. Ranganathan and B. L. Bales, *Journal of Physical Chemistry B*, 2004, **108**, 3810–3816.
33 S. L. Gawali, M. Zhang, S. Kumar, D. Ray, M. Basu, V. K. Aswal, D. Danino and P. A. Hassan, *Langmuir*, 2019, **35**, 9867–9877.
34 M. Bergström and J. Skov Pedersen, *Physical Chemistry Chemical Physics*, 1999, **1**, 4437–4446.
35 C. Seguin, J. Eastoe, R. K. Heenan and I. Grillo, *Journal of Colloid and Interface Science*, 2007, **315**, 714–720.
36 H. Chen, E. Zhang, X. Dai, W. Yang, X. Liu, X. Qiu, W. Liu and X. Ji, *Journal of Polymer Research*, 2019, **26**, 39.
37 J. Hansen and J. B. Hayter, *Molecular Physics*, 1982, **46**, 651–656.
38 J. B. Hayter and J. Penfold, *Molecular Physics*, 1981, **42**, 109–118.
39 H. Nakagawa and T. Oyama, *Frontiers in Chemistry*, 2019, **7**, 1–9.
40 B. Hammouda, *Journal of Research of the National Institute of Standards and Technology*, 2013, **118**, 151.
41 C.-H. Tung, G.-R. Huang, S.-Y. Chang, Y. Han, W.-R. Chen and C. Do, *Journal of Physical Chemistry Letters*, 2020, **11**, 7334–7341.
42 K. Limbu, S. K. Shah and A. Bhattarai, *Bibechana*, 2018, **16**, 131–136.

43 https://github.com/jilavsky/SAXS_IgorCode/tree/master/User form factors for Irena, (accessed 30 December 2020).
44 J. Ilavsky and P. R. Jemian, *Journal of Applied Crystallography*, 2009, **42**, 347–353.
45 A. Rodríguez, M. Del Mar Graciani, M. Angulo and M. L. Moyá, *Langmuir*, 2007, **23**, 11496–11505.
46 L. Zhao, L. Pan, Z. Cao and Q. Wang, *Journal of Physical Chemistry B,* 2016, **120**, 13112–13117.
47 W. Terakosolphan, J. L. Trick, P. G. Royall, S. E. Rogers, O. Lamberti, C. D. Lorenz, B. Forbes and R. D. Harvey, *Langmuir*, 2018, **34**, 6941–6954.
48 A. Volk and C. J. Kähler, *Experiments in Fluids*, 2018, **59**, 75.
49 R. Behrends, K. Fuchs, U. Kaatze, Y. Hayashi and Y. Feldman, *The Journal of Chemical Physics*, 2006, **124**, 144512.
50 G. E. McDuffie, R. G. Quinn and T. Litovitz, in *Journal of Chemical Physics*, 1962, **37**, 239–242.
51 K. Takamura, H. Fischer and N. R. Morrow, *Journal of Petroleum Science and Engineering*, 2012, **98**–**99**, 50–60.
52 D. Myers, *Surfactant Science and Technology*, John Wiley & Sons, Hoboken, 2020.
53 M. Kotlarchyk and S. H. Chen, *The Journal of Chemical Physics*, 1983, **79**, 2461–2469.
54 N. J. Wagner, R. Krause, A. R. Rennie, B. D'Aguanno and J. Goodwin, *The Journal of Chemical Physics*, 1991, **95**, 494–508.
55 D. G. Greene, D. V. Ferraro, A. M. Lenhoff and N. J. Wagner, *Journal of Applied Crystallography*, 2016, **49**, 1734–1739.
56 S. Rebello, A. K. Asok, S. Mundayoor and M. S. Jisha, in *Pollutant Diseases, Remediation and Recycling*, Springer, Cham, 2013, pp. 277–320.
57 E. Summerton, G. Zimbitas, M. Britton and S. Bakalis, *Journal of Crystal Growth*, 2016, **455**, 111–116.
58 S. Shirzad and R. Sadeghi, *Journal of the Iranian Chemical Society,* 2018, **15**, 1365–1375.
59 S. E. Anachkov, G. S. Georgieva, L. Abezgauz, D. Danino and P. A. Kralchevsky, *Langmuir*, 2018, **34**, 4897–4907.
60 S. E. Friberg and P. Liang, *Colloid & Polymer Science*, 1986, **264**, 449–453.
61 J. Zuo, W. Li and L. Weng, *Energy and Buildings*, 2011, **43**, 207–210.
62 T. H. Ito, R. K. Rodrigues, W. Loh and E. Sabadini, *Langmuir*, 2015, **31**, 6020–6026.
63 C. Totland and A. M. Blokhus, *Physical Chemistry Chemical Physics*, 2017, **19**, 7708–7713.
64 G. V. Jensen, R. Lund, J. Gummel, T. Narayanan and J. S. Pedersen, *Angewandte Chemie*, 2014, **126**, 11708 –11712.
65 J. G. Méndez-Bermúdez and H. Dominguez, *Journal of Molecular Modeling*, 2016, **22**, 1–9
66 A. Joiner, F. Schafer, M. M. Naeeni, A. K. Gupta and D. T. Zero, *Journal of Dentistry*, 2014, **42**, S53–S59.
67 S. Hayashi and S. Ikeda, *Journal of Physical Chemistry*, 1980, **84**, 744–751.
68 S. Vass, J. S. Pedersen, J. Pleštil, P. Laggner, E. Rétfalvi, I. Varga and T. Gilányi, *Langmuir*, 2008, **24**, 408–417.
69 R. C. Oliver, J. Lipfert, D. A. Fox, R. H. Lo, J. J. Kim, S. Doniach and L. Columbus, *Langmuir*, 2014, **30**, 13353–13361.
70 J. N. Israelachvili, D. J. Mitchell and B. W. Ninham*, Journal of the Chemical Society, Faraday Transactions 2: Molecular and Chemical Physics,* 1976, **72**, 1525–1568.
71 M. T. Ivanović, M. R. Hermann, M. Wójcik, J. Pérez and J. S. Hub, *Journal of Physical Chemistry Letter*s, 2020, **11**, 945–951.
72 R. C. Oliver, J. Lipfert, D. A. Fox, R. H. Lo, S. Doniach and L. Columbus, *PLoS ONE*, 2013, **8**, e62488.
73 J. Iyer and D. Blankschtein, *Journal of Physical Chemistry* B, 2012, **116**, 6443–6454.
74 C. Miner and Dalton NN, Glycerine: An Overview, The Soap and Detergent Association, New York, 1990.

6. Ternary Behaviour of Iota-Carrageenan Glycerol-Water mixtures, and Implications for SDS Crystal Formation

6.1. Introduction

The majority of structuring polymers in personal care have been designed to work in aqueous systems.[1] However, for the characterisation of industrially-relevant polymer mixtures containing glycerol and water it is essential to understand "low water" formulations. Iota carrageenan (ι-carrageenan) was studied in various glycerol-water mixtures, to determine its structure and properties across the formulation range. Carrageenan shows unique structuring in binary aqueous mixtures containing alcohols and polyols such as ethanol and sugars, respectively. [2–5] This behaviour is partly associated with the binding and exclusion of cosolvents to the polymer and is also observed for other biopolymers.[6–8] There is, however, some debate to the nature of the structure of carrageenan with x-ray scattering evidence for the formation of double helices.[9,10] More recent work using atomic force microscopy (AFM) indicates the formation of single helices (for ι-carrageenan) that can assemble to form twisted higher order self-aggregated (tertiary) double helices or multiple-chain aggregated (quaternary) structures (Figure 6.1).[11] However, some authors still envision double helices.[12] In the light of this situation, schematic representations of carrageenan are shown as single (rather than double) helices as it is difficult to probe the precise conformation.

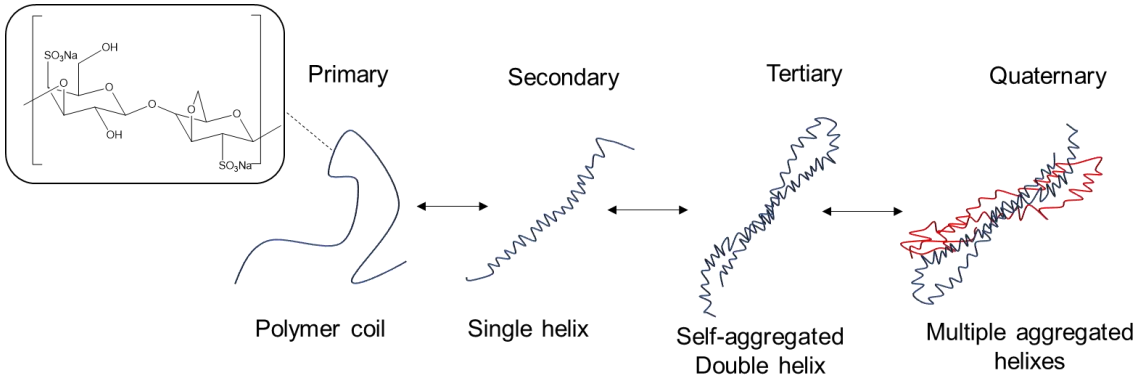

Figure 6.1: Structure of ι-carrageenan (inset), and its possible hierarchical conformational arrangements. Depending on the chemical environment and temperature, this polymer can form a single helical structure, which can in turn either self-aggregate, or form aggregates comprising multiple chains. Figure adapted from Diener et al.[11]

Microstructural characterisation by SAXS and microscopy was performed alongside rheology studies, to understand structure-property relationships for this polymer. Owing to the confidentiality agreement between the supplier and Unilever, detailed chemical characterisation could not be

undertaken. However, the polymer can be considered to be a high molecular weight carrageenan with predominant iota composition (Figure 6.1 inset). Much like SDS, processing can have a large effect on its structure and properties. Therefore, 1 Wt.% ι-carrageenan mixtures were first prepared by processing at room temperature. This enabled initial characterisation, as well as informing behaviour prior to any thermal treatment, which could have implications for processing e.g. viscosity effects on mixing. Following this, 1 Wt.% ι-carrageenan mixtures were prepared via an initial heating and mixing step, followed by quiescent cooling and mixing. The rheological behaviour was then compared to determine the influence of structure and properties. Finally, the effect of carrageenan on SDS-glycerol crystal formation (with and without the prescence of water) is studied to inform the direction of future investigations into structuring.

6.2. Results and Discussion

6.2.1. ι-carrageenan/Glycerol/Water- Unheated Processing

Initially, viscosity measurements were undertaken on 1 Wt.% ι-carrageenan in a series of binary glycerol-water mixtures, ranging from 100% glycerol to 100% water. The polymer was studied at an industrially relevant concentration, most likely corresponding to the semi-dilute unentangled concentration regime.[13,14] During the addition of water or water-containing solvent, clumping of the powder was observed,[15] resulting in large agglomerates with a gelled surface due to rapid solubilisation.[16] To reduce the need for high shear dispersants to homogenise such clumped particles, the polymer was initially dispersed in glycerol before the desired volume of water was added.[16] For the resulting viscosity data, all samples displayed two regions: a zero-shear viscosity plateau and a shear-thinning region (Figure 6.2). The infinite shear viscosity plateau was not observed for most samples but this regime may require higher shear rates or higher polymer concentrations.[17] Due to the lack of an infinite shear plateau for the majority of the viscosity curve data, tangent analysis was performed in lieu of the Cross model. [18,19]

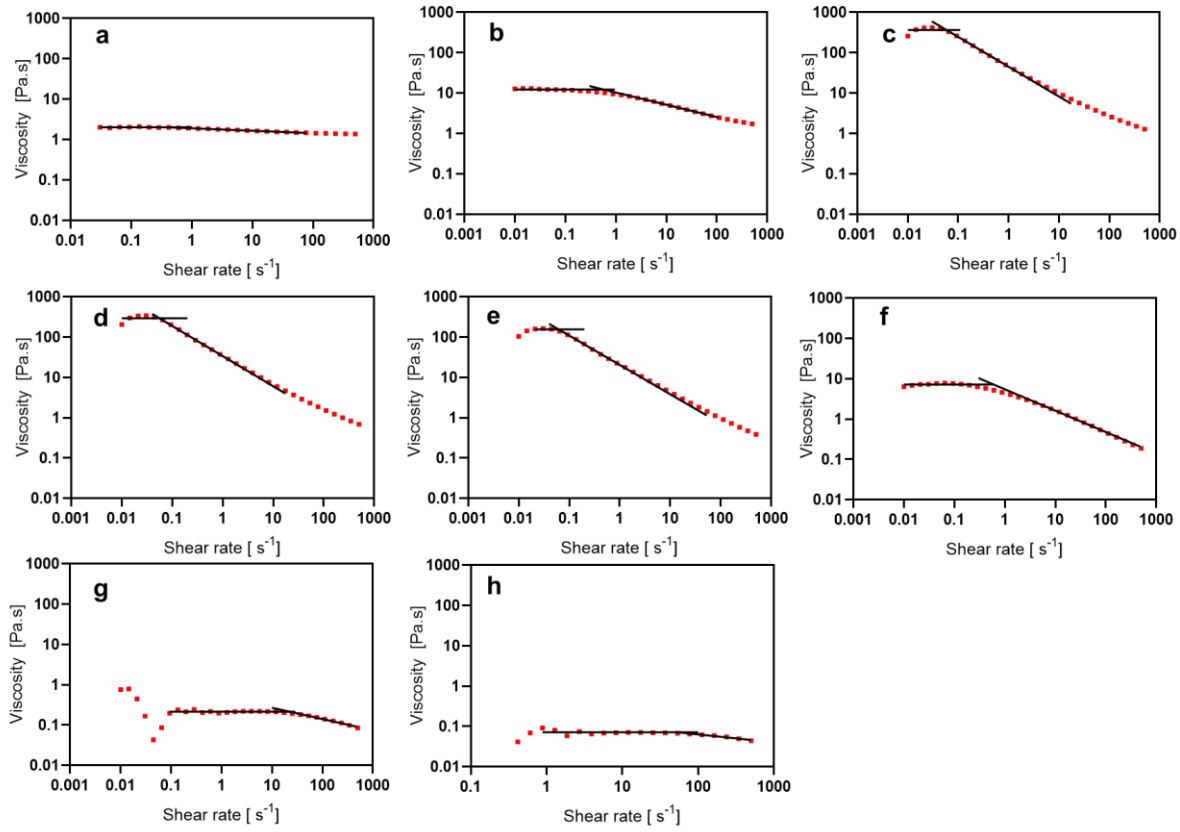

Figure 6.2: Viscosity vs. shear rate curves for 1 Wt.% iota-carrageenan in glycerol water mixtures prepared using unheated processing with solvent compositions of a) 0 Wt.% water and 100 Wt.% glycerol b) 1.0 Wt.% water and 99.0 Wt.% glycerol c) 10.3 Wt.% water and 89.7 Wt.% glycerol d) 20.0 Wt.% water and 80.0 Wt.% glycerol e) 31.3 Wt.% water and 68.7 Wt.% glycerol f) 50.1 Wt.% water and 49.9 Wt.% glycerol g) 75.5 Wt.% water and 24.5 Wt.% glycerol h) 0 Wt.% water and 100 Wt.% glycerol. Tangent analysis has been attempted (black) to determine shear-thinning parameters.

The zero shear viscosity degree of shear-thinning, and the onset of shear-thinning were plotted against the weight fraction of water present in the solvent (Figure 6.3). To complement this, polarised optical microscopy (POM) studies were performed (Figure 6.3a-6.3,c) to examine the phase behaviour.

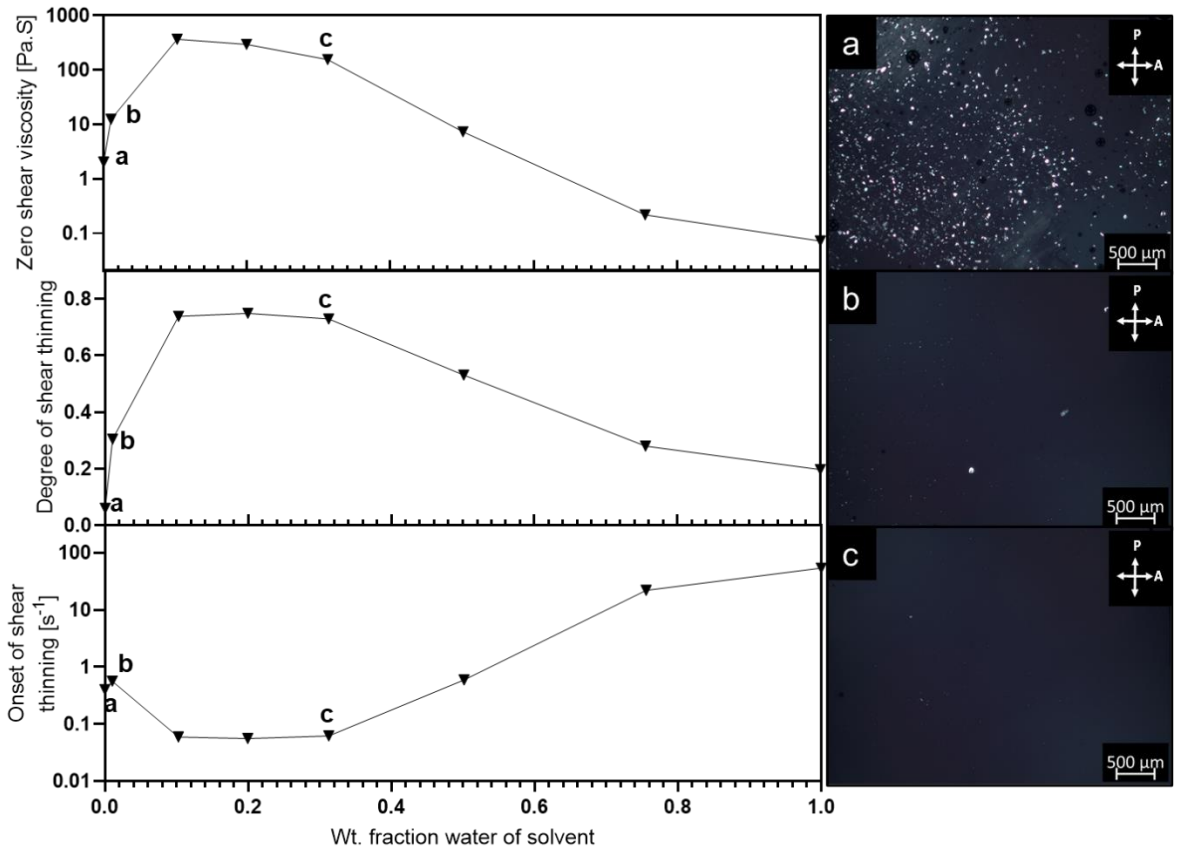

Figure 6.3: Fitted parameters from tangent analysis of the viscosity curves obtained for unheated 1 Wt.% iota-carrageenan in glycerol/water mixtures (Figure 6.2): (top) zero-shear viscosity, (middle) degree of shear-thinning, (bottom) onset of shear-thinning. Associated polarised optical microscopy of chosen solutions with a) 0 Wt.% water and 100 Wt.% glycerol b) 1.0 Wt.% water and 99 Wt.% glycerol c) 31.2 Wt.% water and 68.8 Wt.% glycerol.

The trends in zero shear viscosity (η_0), degree of shear-thinning (*m*), and onset of shear-thinning (*c*) for 1 Wt.% solutions are non-linear in each case, with an asymmetric parabola (or inverse parabola for *c*) shape (Figure 6.3). The trend in η_0 cannot be attributed to the solvent viscosity, which decreases in an exponential-like fashion as the (weight percent) of water increases.[20] Therefore the increase and subsequent decrease in η_0, as well as the mixtures' response to shear, is a result of the changing microstructure of the polymer. Polarized optical microscopy provides further information: birefringent objects (Figure 6.3a) are indicative of semicrystalline agglomerates and do not contribute to a meaningful increase in viscosity for these mixtures. The viscosity curve, with η independent of flow rate, is indicative of a Newtonian fluid and is the expected behaviour for a particulate dispersion. This state may be kinetically limited e.g. due to poor solvency of glycerol for the polymer compared to water, or reduced diffusion due to higher solvent viscosity.[21] Thus, there is potential for aging effects, where the partially solvated particles slowly interact further with the solvent and hence increase the solution viscosity over time.[22] Addition of water up to 10 Wt.% of solution resulted in an increase of both *m* and

η_0. This is accompanied by a lower critical shear rate for the onset of shear-thinning. Microscopy analysis of samples containing 1 Wt.% water indicates that the majority of carrageenan interacts with the solvent and is not in powder form. At higher water contents, both η_0 and *m* begin to fall, with *c* increasing proportionally. The apparent increase in structuring for binary solvent mixtures is also consistent with solutions/gels of iota and kappa carrageenan in aqueous alcohol and polyol mixtures.[2,8,23,24] Parallels can also be drawn between experimental η_0 measurements, and literature viscometry measurements of sodium carboxymethylcellulose (SCMC), where a parabolic trend is also seen.[25] For SCMC such behaviour can be rationalised in two ways: through synergistic interactions of glycerol and SCMC,[26] or the increasing dispersion of SCMC and gradual dissolution of its ionic functional groups as the water level is increased, leading to swelling followed by dissolution.[25] While either reason may be the cause of similar behaviour for ι-carrageenan, for SCMC there is still some debate regarding its helical nature,[27] whereas it is well known that carrageenan forms a helical secondary structure. The degree to which helices form is influenced by physical conditions and the presence of other dissolved molecules such as salt, which has been studied by various authors.[11,13,28–30]

The physical properties that highlight the changing nature of the carrageenan are exhibited through viscoelasticity measurements. An increase in G' suggests an increase in a network-type structure that yields gels and viscous solutions. This property was probed using frequency sweeps for the 1 Wt.% solutions, with the rheometer operating in oscillatory mode (Figure 6.4). Due to the highly viscoelastic nature of these solutions, a rheometer with a vane and cup instead of the standard cone and plate geometry (which is used for viscosity curves) was used in order to minimise wall slippage at high frequency oscillations.[36] This did not manifest within the steady shear measurements where no slip type behaviour was seen.[31–33] The frequency sweep showed a liquid-like solution in glycerol, with G'' dominating at all frequencies. The introduction of water led to higher G' and G'' values, indicating interactions between the polymer and the solvent. At 24.2 Wt.% water of solution, G' dominated at most frequencies, although G' fell below G'' at low frequencies. Although the material displays gel-like behaviour, it is not a true gel, because G' does not dominate at all frequencies.

Nevertheless, the structuring that can be obtained by simply tuning solvent parameters is considerable. In water-rich solvents, the solutions become dominated by G'' once more, while still retaining higher G' values than those in glycerol. As with the trend in viscosity for the flow sweep measurements, the solvent viscosity contributes to lower G'' values as the water content is increased, although it is not the sole factor.

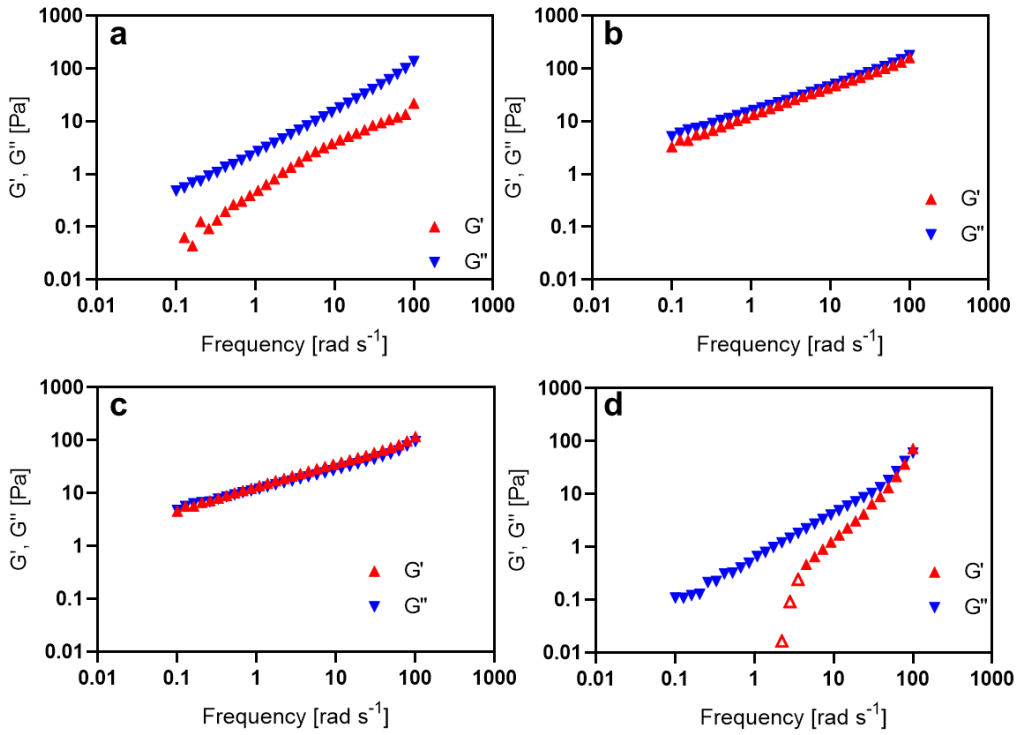

Figure 6.4: Frequency sweeps for unheated solutions of 1 Wt.% iota carrageenan in glycerol-water mixtures containing a) 0 Wt.% water and 100 Wt.% glycerol b) 5.5 Wt.% water and 94.5 Wt.% glycerol c) 24.2 Wt.% water and 75.8 Wt.% glycerol d) 100 0 Wt.% water and 0% glycerol. Open symbols indicate anomalous results from by flow instabilities and should be disregarded .

Considering the rheological and microscopy findings, and in the context of previous studies on carrageenan, it is clear that distinct changes in the structure of unheated polymer solutions occurs within relatively small changes of solvent composition.[3,23] Furthermore, as both the viscosity and viscoelasticity changes considerably, these results have implications for structuring within more complex formulations. The high G' values observed for glycerol-rich, aqueous-mixtures suggest network formation: G' and G" are essentially parallel over three orders of magnitude in frequency suggests an incipient chemical gel – i.e. is a percolated gel.[34,35] although the conformation of the polymer in this network cannot be fully understood by rheology alone. However, SAXS analysis was performed on these carrageenan solutions (Figure 6.5), in order to understand the change in polymer conformation with varying solvent.

The resulting 1D scattering patterns (Figure 6.5) show three distinct regimes as a result of different microstructures. Firstly, in glycerol alone, a decay in intensity following a power law is observed with an exponent value of n = 3.3. This corresponds to scattering from surface fractals (or the scattering

from a diffuse interface of particles) observed from the powder agglomerates observed by microscopy (Figure 6.3). The scattering analysis confirms that the amount of dissolved polymer is minimal, given the lack of any scattering from dissolved chains or ionic repulsion associated with polyelectrolytes. Furthermore, for the processing method used here, behaviour mirrors the dry powder state envisioned by Ramakrishnan and Prudhomme for κ-carrageenan in glycerol.[33] The second scattering motif appears to be a transition region, in which particle agglomerates are present alongside swollen (or partially disaggregated) polymer, in samples with a water content of 1-4 Wt.% water of solution. This can be identified from two features: the presence of fractal scattering causing a power law intensity decay of ~1.5-3 at low *q* (corresponding to powder agglomerates in microscopy as well), and the emergence of a typical 'polyelectrolyte peak' at higher *q*. This peak is a structure factor which occurs due to ionic repulsion from the sulfate functional groups within the carrageenan.[37] For unheated samples, water increases solubility and, at low levels, the amount of solubilised carrageenan is proportional to the water concentration. However, this trend does not follow the concentration/correlation length relationship associated with semi-dilute polyelectrolytes (correlation length $\propto c^{1/2}$).[38,39] The result is consistent with the lower concentration of birefringent particles observed by microscopy analysis of the solution containing 1 Wt.% water (Figure 6.3b). It can be inferred that the reduction of birefringence corresponds to solubilisation/disaggregation of the polymer.

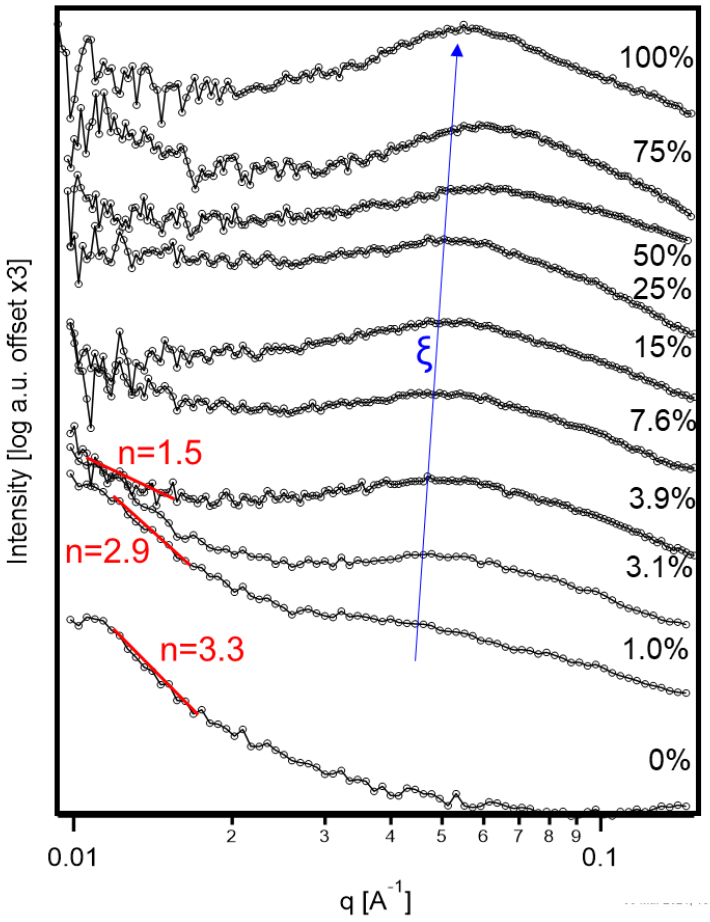

Figure 6.5: SAXS patterns of 1 Wt.% ι-carrageenan solutions in glycerol-water mixtures, ranging from 100 Wt.% water of solution (top) to 100% glycerol (bottom). Initially surface fractal scattering is seen in glycerol solvent with a power law exponential decay (n=3.3). As small amounts of water are added, the scattering patterns display mixed fractal and polyelectrolyte scattering in solvent mixtures containing up to 3.9 Wt.% water and 96.1 Wt.% glycerol with a varying low q power law exponent (n=1.5 to n=2.9). Finally semidilute polyelectrolyte scattering, containing a structure factor peak equating to the correlation length of the polymer solution, ξ , is observed for all other scattering patterns at higher water contents. A general positive trend between water content and the scattering vector of ξ is shown in blue, resulting in a real space decrease. Data are offset by a factor of three for the sake of clarity.

At higher water contents, a third scattering motif is observed, which displays typical semi-dilute polyelectrolyte scattering,[40] i.e a dominant peak at higher q.[41] Intensity scaling at low q is difficult to distinguish from the noise so analysis of this region was not performed. However, the slope in this region could indicate some form of aggregation.[12,42,43] Polyelectrolyte solutions are often envisioned as 'meshes', where extended 'rod-like' polymer conformations arrange themselves to minimise electrostatic repulsion.[43] The polyelectrolyte (structure factor) peak represents the correlation length (ξ) that describes the mesh 'pore size' (Figure 6.6) and can be determined from the position of the peak maxima (where $\xi = \frac{2\pi}{q}$). For these data, a generalised trend can be observed in the reduction of

correlation length as a function of water content of solution (Figure 6.6). However, this is nonlinear and follows a generalised exponential curve. At 1 Wt.% water in the solution, the longest correlation length is observed. The amount of solubilised polymer is relatively low at this stage and the subsequently small amount of dissolved sulfate groups can arrange themselves over large distances to satisfy Columbic repulsons. However, when the water content is increased from 1 to 3 Wt.%, the correlation length decreases dramatically by ca. 20%, corresponding to the increased concentration of solvated polymer.[43] Thereafter, this the reduction in correlation length is more gradual. Considering the initial microscopy data (Figure 6.3), it can be assumed that the majority of the polymer is no longer in 'powder form' and instead interacts with the solvent to some degree above 4 Wt.% water of solution.

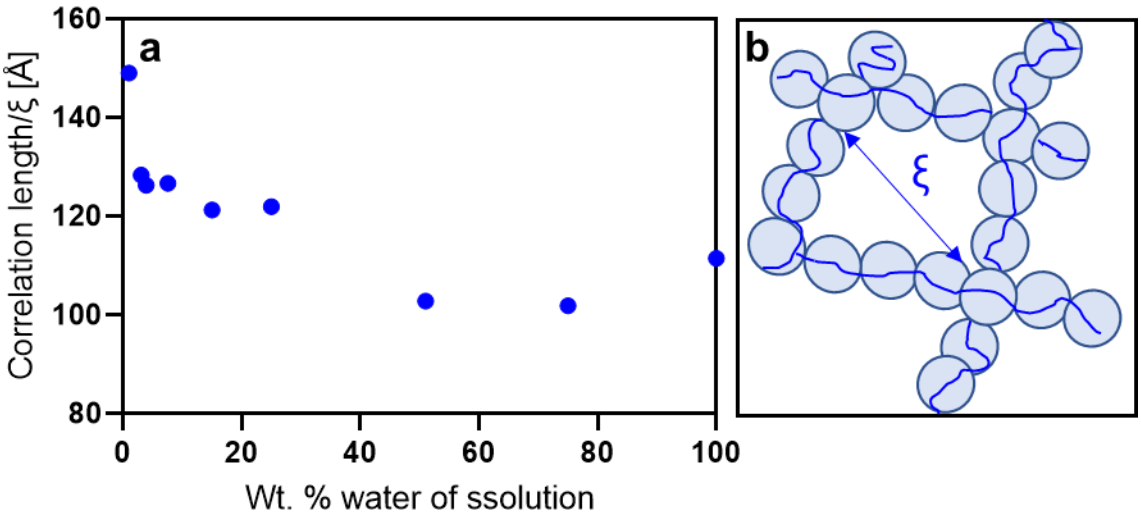

Figure 6.6: a) Real space correlation length (ξ) calculated from polyelectrolyte structure factor peak maxima in SAXS scattering profiles (Figure 6.5) of ι-carrageenan (1 Wt.%) in glycerol/water mixtures (unheated processing), plotted against the weight fraction of water in the solution. Visualisation of correlation length in semi-dilute polyelectrolyte solutions using the mesh model, where polymer chains orientate to minimise electrostatic repulsions with neighbouring chains containing ionic functional groups.[14,41]

The unusual structuring of biopolymers in mixed solvents requires an explanation not only in terms of increasing dispersion and solubilisation of polymer, but also in terms of the contribution of the solvent quality and the highly nonlinear rheological behaviour. While many binary solvents act as a homogeneous mixture, some authors have sought to explain the changes in microstructure of the polymer in the context of the changing solvent quality and solvent localisation.[7,8,24] For example, Stenner et al.[8] utilized Kirkwood-Buff theory to rationalise gelation[7] through a coil to helix conformation change, which allows for preferential exclusion of cosolvents.[8] In water-rich regions, the coil phase dominates, and polyols are excluded from the surface of the carrageenan. Conversely, helical motifs

become the prevailing structure in glycerol rich media, where polyols preferentially bind to the helix due to the exposed less polar helical backbone, compared to the charged functional groups that are better solvated by water. This concept was previously used to rationalise the increase in gel strength that occurred on addition of ethanol to iota carrageenan mixtures.[23] However, for semi-dilute polymers at concentrations below the critical entanglement ($c^* < c < c_e$), large changes in viscosity and viscoelasticity are unlikely to occur in the same manner for carrageenan. Moreover, larger changes in correlation length would be expected if the polymer chains were simply expanding as a result of increasing solvent quality.[44]

Kirkwood-Buff theory accounts for earlier results within this chapter and provides an explanation for property changes that occur with solvent composition. In glycerol alone, a powder suspension exists, which is kinetically limited and cannot confer structure. The addition of water enables solubilisation (and hence conformational change) of the polymer; with a stiff helical network that begins to viscosify and ultimately gels the mixture. As the water content increases, a higher proportion of carrageenan exists as chains, with the network becoming more flexible. These changes are facilitated by the preferential exclusion of water at low concentrations and the exclusion of glycerol at high water concentrations (Figure 6.7). One incongruous element is the increase in correlation length observe for samples containing 75% water of solution and 100% water, where a plateau (or decrease) might be expected. While the majority of analyses were conducted in glycerol-rich media, more comprehensive analysis in water-rich media might explain this potential anomaly. It is also unclear whether ternary and quaternary carrageenan superstructures exist within the system.[11] In principle, this could be probed bythrough atomic force microscopy (AFM) analysis.

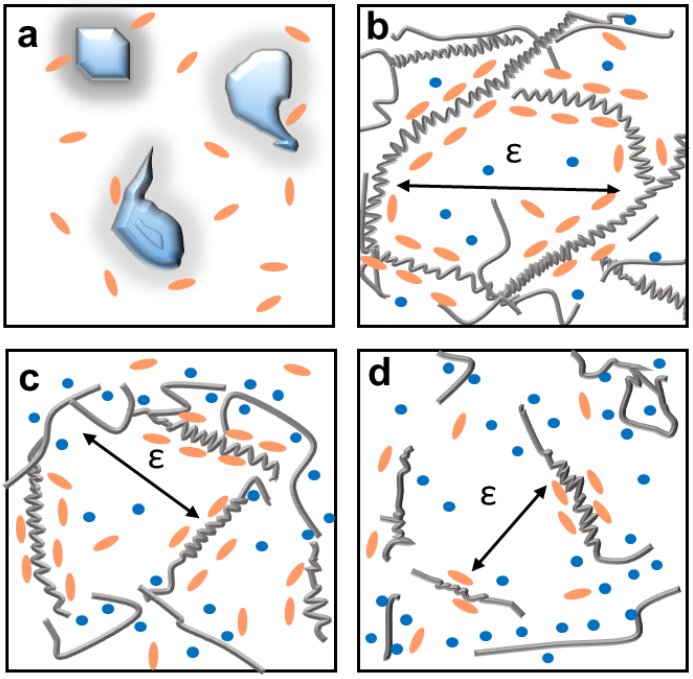

Figure 6.7: General schematic of ι-carrageenan microstructural behaviour in (1 Wt.%) glycerol/water mixtures (visualised as orange for glycerol and blue for water). a) In glycerol alone, the material exists as powder agglomerates and there is limited interaction with the solvent. b) In glycerol-rich (≤25% Wt.% water) solutions, the majority of polymer exists as stiff helices, facilitated by preferential binding of glycerol along the secondary structure, which results a network like arrangement responsible for viscosifying solutions. C) As the water content is increased from 25 to 50 Wt.% water, more polymer exists in coil form, resulting in a less stiff network with lower aggregation. D) in water-rich (> 50 Wt.% water) mixtures, this network structure is lost, and a high proportion of the polymer exists in its coil form, with little aggregation and more typical 'sol like' behaviour.

6.2.2. ι-carrageenan/Glycerol/Water- Heated Processing

Carrageenan is known to undergo large changes in structure with temperature, so it was investigated whether heated samples displayed similar rheology and structure as that of unheated samples. While processing of materials often involves heating, ambient temperature processing is still relevant because a rapid viscosity increase could affect mixing rates.[45] Carrageenan is known to form molecularly dissolved chains (coils) on heating, both in glycerol and water.[3] Therefore, it is only on cooling that the polymer changes conformation (e.g. from helices), potentially gelling mixtures. To test the impact of heating on physical properties and structure, 1 Wt.% ι-carrageenan solutions were prepared via a heating step. After cooling to room temperature and subsequent mixing, the viscosity curves of the resulting solutions were measured (Figure 6.8) and the data were correlated with POM images.

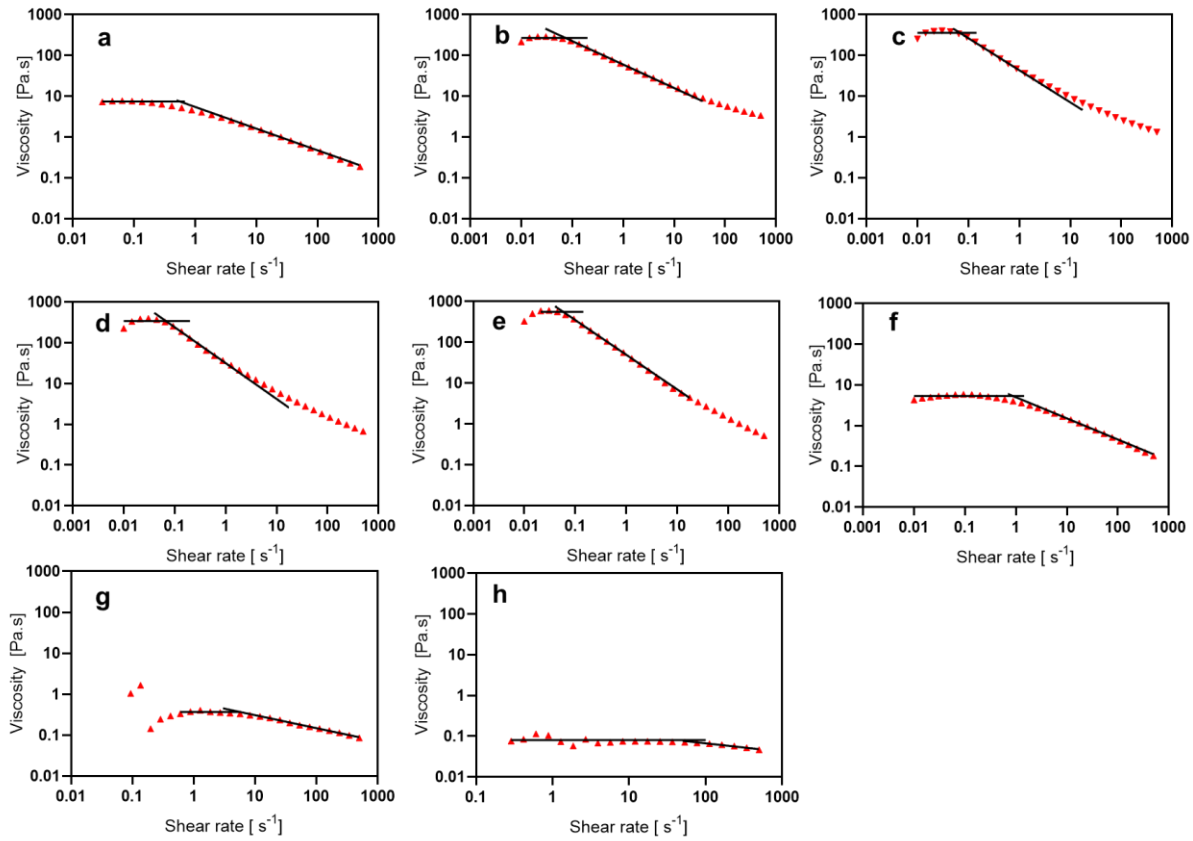

Figure 6.8: Viscosity curves of 1 Wt.% ι-carrageenan in glycerol water mixtures prepared using a heated processing stage with compositions of a) 0 Wt.% water and 100 Wt.% glycerol b) 1.0 Wt.% water and 99.0 Wt.% glycerol c) 10.3 Wt.% water and 89.7 Wt.% glycerol d) 20.0 Wt.% water and 80.0 Wt.% glycerol e) 31.3 Wt.% water and 68.7 Wt.% glycerol f) 50.1 Wt.% water and 49.9 Wt.% glycerol g) 75.5 Wt.% water and 24.5 Wt.% glycerol h) 0 Wt.% water and 100 Wt.% glycerol. Tangent analysis has been attempted (black) to determine shear-thinning parameters.

A parabolic trend for both η_0 and *m* was observed (Figure 6.9), with *c* displaying a similar trend as the data obtained for unheated samples. However, relative to unheated samples large differences were observed pure glycerol and also for solutions containing just 1 Wt.% water of solution. In both cases η_0 increased: by a factor of around four for glycerol (from 2 $Pa.s^{-1}$ to 7.5 $Pa.s^{-1}$) and a factor of twenty for solutions containing 1 Wt.% water of solution (from 12 $Pa.s^{-1}$ to 270 $Pa.s^{-1}$). All other solvent mixtures showed generally similar viscosities. This suggests that heating causes significant changes in the microstructure of carrageenan at low water concentrations.[3] For comparison, the heated solution containing 1 Wt.% water had a degree of shear-thinning, *m*, that was almost double that of its unheated counterpart. Moreover, the behaviour of the glycerol solution was transformed from a Newtonian dispersion of solid particles to a shear-thinning polymer solution. The corresponding POM images shown in (a) clearly indicates that there are still some particles present, but the onset of shear-thinning also demonstrates that there is significant polymer in solution at concentrations above c*. For other

samples in glycerol-rich solutions (< 50 Wt.% water of solution), heated samples exhibited marginally higher *m*, although values were similar in water-rich solvents (> 50 Wt.%). This may be due to the homogeneous nature of the heated samples, in contrast to the particulate domains observed for unheated samples. Finally, while the polymer in pure glycerol displayed similar values for onset of shear-thinning, the heated solution containing 1 Wt.% water gad a *c* value of 0.07 s^{-1} as opposed to 0.56 s^{-1}, while other solvent compositions showed similar behaviour.

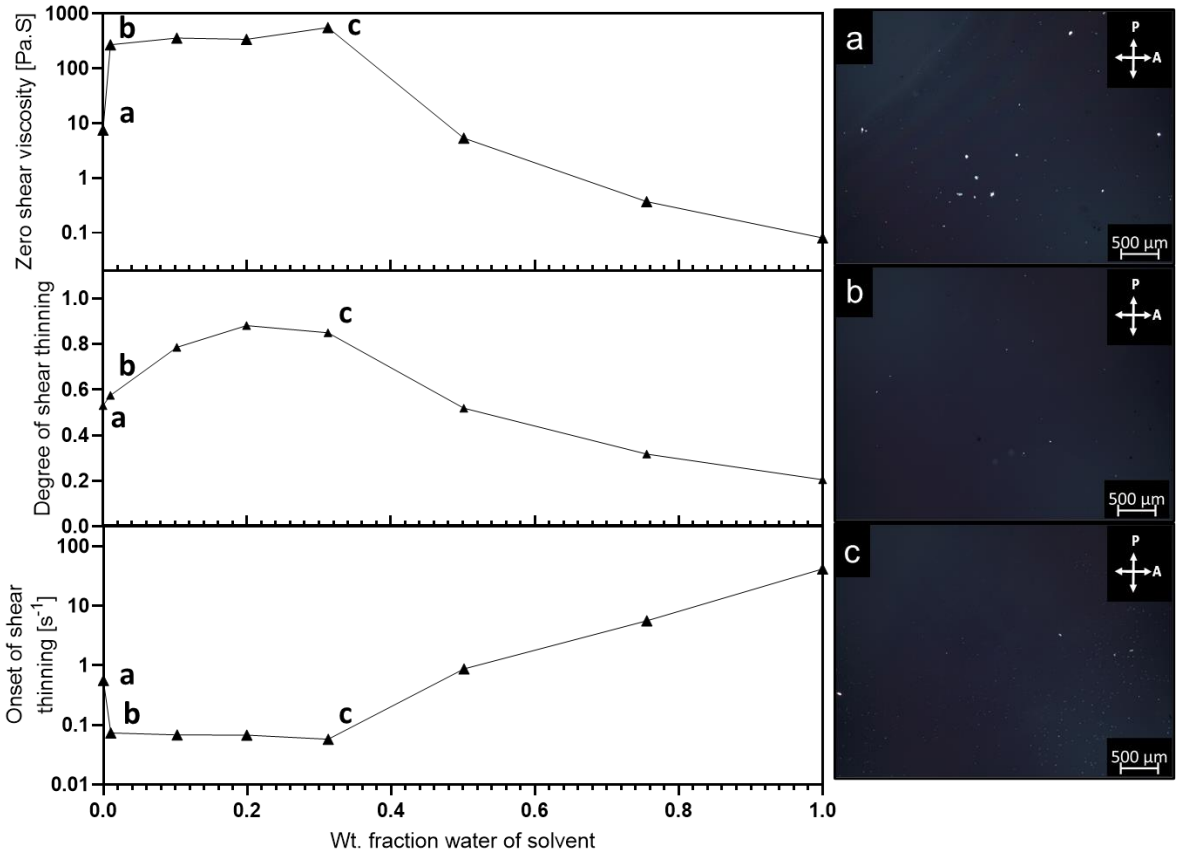

Figure 6.9: Fitted parameters of tangent analysis performed on viscosity curves of unheated 1 Wt.% ι-carrageenan in glycerol/water mixtures (Figure 6.8): top) Zero shear viscosity middle) Degree of shear-thinning bottom) Onset of shear-thinning. Associated polarised optical microscopy images for chosen solutions with a) 0 Wt.% water of solution b) 1.0 Wt.% water of solution c) 31.2 Wt.% water of solution.

The large difference in rheological behaviour at low water contents can be attributed to a change in the degree of dissolution of the polymer, which is limited when unheated. POM analyses confirm this, where samples heated in glycerol resulted in a significant reduction in birefringent agglomerates (Figure 6.9a), equating to dissolution of the majority of the polymer chains. It is likely that a more stringent heating/shear regime would lead to greater polymer dissolution, and the zero shear viscosity would increase proportionally to the sample containing 1 Wt.% water. Since a small number of particles were observed in unheated solutions containing water (Figure 6.9b,c) it can be concluded that most

carrageenan particles melted to form coils upon heating and on cooling formed network-like aggregates that causes the structuring behaviour. The fact that a parabolic or plateau in viscosity is still observed despite heating and cooling indicates that the viscosifying interaction with the solvent is independent of processing parameters (although it may be kinetically limited at very low water contents). As rheological behaviour in water-rich solutions is identical, and SAXS analysis of unheated solutions suggest similar structures, it can be concluded that this formulation region is minimally impacted by processing. SAXS was therefore performed to compare heated and unheated solutions of ι-carrageenan (1Wt.%) in glycerol to understand the differing rheological (and microscopy) behaviour .

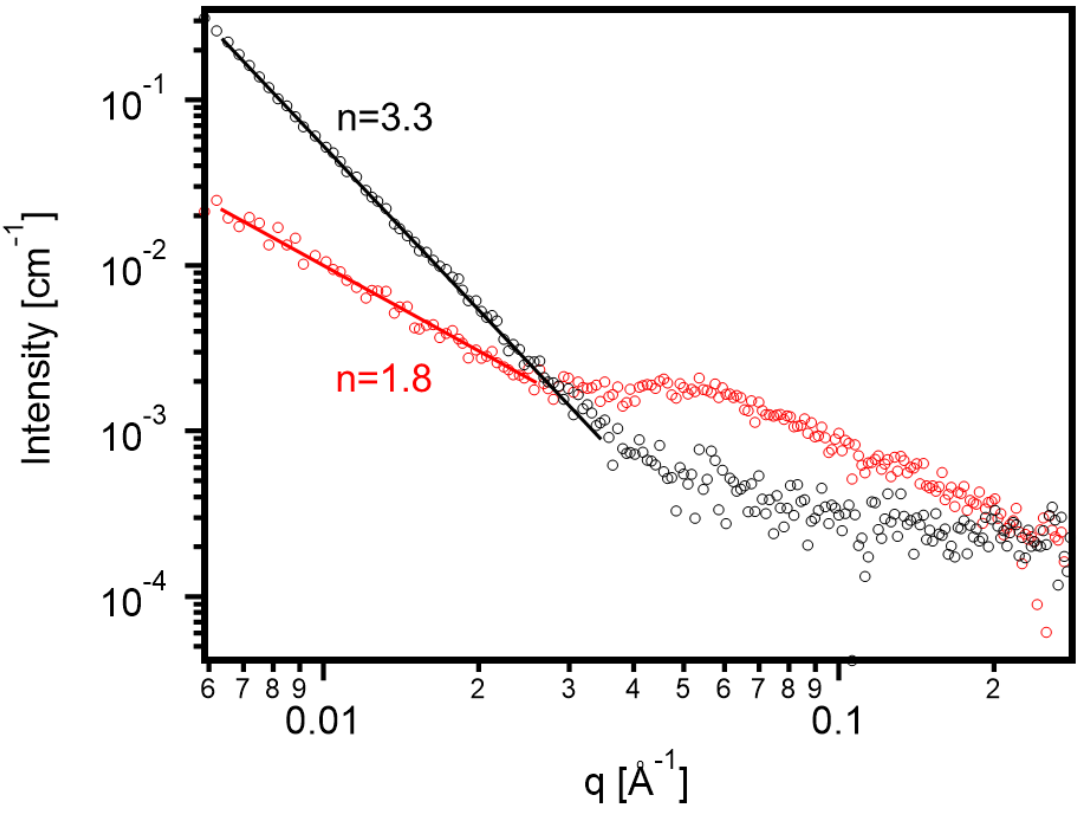

Figure 6.10: 1D SAXS patterns of ι-carrageenan (1 Wt.%) in glycerol, prepared with (red) a heating step during processing and without (black). The SAXS pattern from the unheated sample is indicative of fractal scattering, whereas the heated sample displays a polyelectrolyte structure factor peak resulting from ionic repulsions of dissolved polymer. Low q power law scaling with an exponent (n) of 1.8 is observed in heated solution and may result from inhomogeneities arising from un-melted powder agglomerates.

A power law dependence (n = 3.3) corresponding to fractal scattering is observed for the unheated solution (Figure 6.10), while a polyelectrolyte type scattering motif is observed for the heated solutions, in addition to a low *q* power law intensity decay (n = 1.8). The low *q* slope in the heated sample is most likely the result of inhomogeneities relating to scattering from powder agglomerates, as well a partial

contribution from clustering of chains or helices.[42] The structure factor peak corresponding to the correlation length is similar to that for the unheated solution containing 3 Wt.% water. However, the correlation length is far shorter for the heated solution than the unheated solution for 1 Wt.% water. By extension, a reduction in correlation length for the heated solution containing 1 Wt.% water may occur, although this needs to be confirmed by future work. Nevertheless, it appears that a network structure exists for all heated glycerol-rich solutions, whereas increasing amounts of soluble polymer coils are obtained at higher water contents. When no water is present, it appears that meaningful structuring only occurs on heating and cooling, which may be desirable to improve processability. However the ι-carrageenan tests showed the highest viscosifying properties in glycerol-rich aqueous glycerol mixtures.

6.2.3. Effect of ι-Carrageenan on Phase Composition of SDS /Glycerol/Water Mixtures

The crystal formation of SDS in glycerol/water mixtures showed high sensitivity to water, with the dominance of the anhydrous SDS crystal phase in place of the structuring SDS-glycerol phase above 6 Wt.% water of solution (see Chapter 5.2.1). A complex interplay between ι-carrageenan, SDS and water can therefore be envisioned in terms of structuring. In particular, loss of structure could occur via preferential formation of an anhydrous SDS crystal (rather than the SDS-glycerol phase) in the presence of water, which could be offset by the greater structuring conferred by the carrageenan. Alternatively, with the potential for water molecules to localise around the polymer chains, it is also possible that the phase behaviour of SDS may be altered owing to the activity of the water, leading to differing crystal states. To examine his hypothesis, quaternary mixtures containing SDS (2 Wt.%), ι-carrageenan (1 Wt.%), glycerol and water were prepared and subjected to heating and subsequent quiescent cooling. Moreover, microscopy was conducted to further explore the nature of the resulting crystal phases.

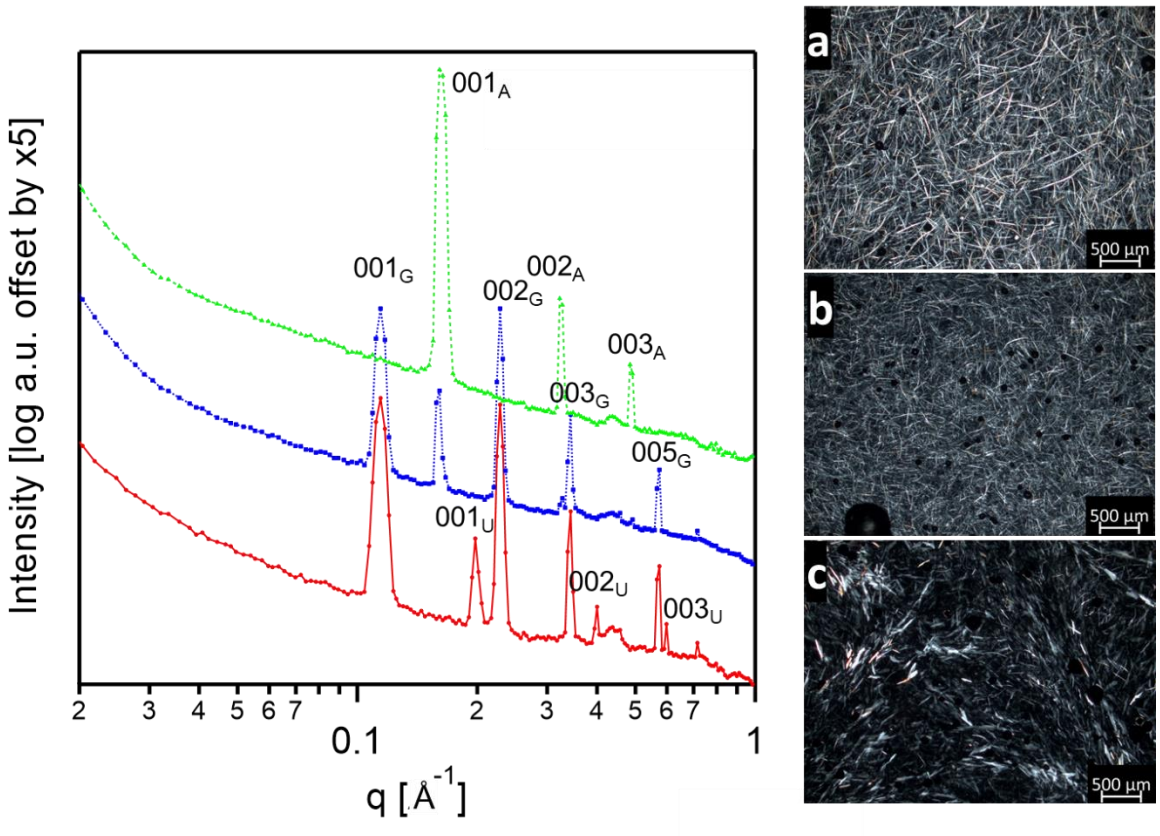

Figure 6.11: 1D SAXS patterns of SDS (2 Wt.%) and ι-carrageenan (1 Wt.%), in glycerol-water mixtures heated to 75 °C and cooled quiescently overnight. Solvent composition varied from 100% glycerol (red), 3 Wt.% water and 97 Wt.% glycerol (blue), and 6 Wt.% water and 93 Wt.% glycerol (green). Solutions in glycerol alone exhibit SDS-glycerol phase (001_G) formation predominantly, corresponding to ribbons observed by microscopy, as well as a minor fraction of unknown crystal (001_U). In 3Wt.% water and 97 Wt.% glycerol, the mixture contains both SDS-glycerol phase and anhydrous SDS (001_A), similar to results in the absence of carrageenan. In and 6 Wt.% water and 93 Wt.% glycerol, the anhydrous crystal phase dominates, similar to mixtures prepared without any carrageenan. The anhydrous crystal phase is found to form unusual, jagged needles, which has not been seen before. SAXS patterns are offset for comparison.

Initially, the introduction of carrageenan in SDS and glycerol (only) mixtures led to the formation of the usual SDS-glycerol crystal phase, with associated ribbon formation. However, minor crystal phase was alsoobserved (*00l*$_u$, Figure 9a), which had the same d_{001}-spacing as that observed for ternary mixtures of SDS/glycerol/NaCl (Figure 19 Chapter 4). This illustrates the subtle effect of additional ionic species even in non-aqueous systems . A lamellar ordering of the other "u" crystal phase was also observed with first, second, and third order peaks (Figure 9). Matthews et al.[46] reported a hexagonal phase for a similar scattering pattern in SDS and glycerol, although identification of this phase microscopically is challenging, and images captured at higher magnification indicated semi-translucent particles (Figure 6.12). It is not known whether these particles are platelets correspond to the crystal phase, or swollen polymer aggregates. Small birefringent platelets could be distinguished in some instances; so this

mixture may contain both. Moreover, the change in crystal type caused by carrageenan was surprising, given the similarity of its ionic sulfate groups to the SDS headgroup.

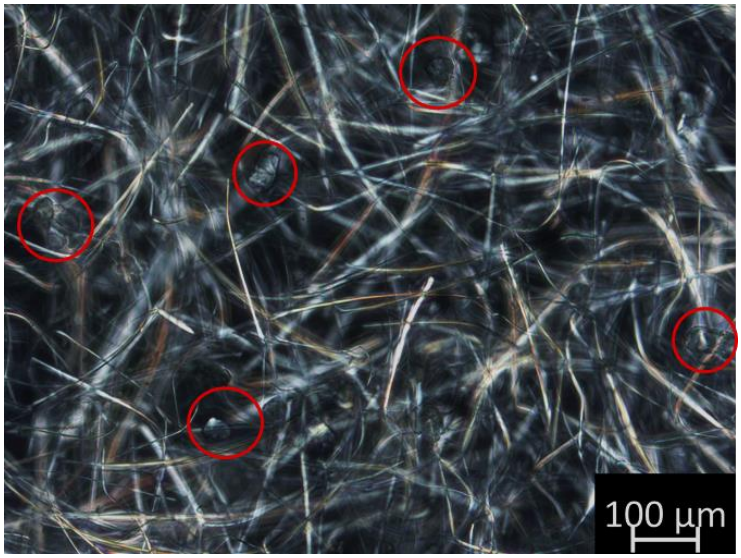

Figure 6.12: Microscopic evidence for alternate crystal motifs observed in mixtures of SDS (2 Wt.%), ι-carrageenan (1 Wt.%) in glycerol following heating and quiescent cooling. Red circles indicate non-ribbon species which are either carrageenan particles or an alternative crystal phase.

Much like results collected in the absence of polymer, the addition of water appears to disrupt SDS-glycerol crystal formation, with mixtures containing 3 or 6 Wt.% water of solution yielding similar amounts of each crystal type (Chapter 5.2.1). In both cases, anhydrous SDS crystals form as before. Thus it can be concluded that, despite the preferential exclusion of cosolvents, the addition of ι-carrageenan has little effect on phase abundance with respect to the anhydrous phase and the SDS-glycerol phase. Interestingly, it appears that the additional unknown crystal phase (001_U = 31.7 Å) also disappears in the presence of water. The same mode of inhibition may be relevant for this crystal type as well as for the SDS-glycerol phase. This also raises a question regarding the composition of this phase and whether it contains glycerol. However, higher resolution diffraction data at a wider *q* range would be necessary to resolve this issue. Finally, the generalised habit of the crystal formed in the presence of 6 Wt.% water is different from solutions containing no polymer. Without ι-carrageenan; a feather-like or platelet/needle could be observed, but jagged planar rods are are the only species (Figure 9c). This suggests that while carrageenan does not inhibit anhydrous crystal formation, as there may be a secondary effect on the macroscopic structure. Crystal growth in gels and polymers is an established field.[47] Many paramters can influence growth, including viscosity, convection currents and adsorption.[4,48,49] This chapter acts as a starting point for further exploration of this field with respect to the effect of biopolymers on SDS crystallization.

6.3. Conclusion

ι-Carrageenan, a commercially available naturally-derived biopolymer, enhances the viscosity of glycerol-rich aqueous media. In this chapter, enhanced structuring occurred more or less regardless of processing history. This is similar to behaviour reported for other carrageenan species and polysaccharides such as SCMC[3,25,26,33] dissolved in binary aqueous mixtures containing alcohols or polyols. Such behaviour could be rationalised through preferential binding or exclusion of cosolvents. This the conformation of the polymer, transitioning from helices to chains in the presence of increasing water content, affecting both the network formation and aggregation in the mixture.[8,23,24] SAXS analysis indicated the largest changes were observed for unheated samples with low water contents (<10 Wt.% water of solution). In this case a change from powder aggregates to dissolved polyelectrolytes was observed, and a transition region in which both co-existed for unheated solutions containing 1-4Wt.% water. At higher water contents, scattering was typical for that of dissolved polyelectrolytes. However, shorter correlation lengths corresponding to a reduction in mesh size were observed, which indicates conformational changes. Despite many rheological similarities, samples subjected to heating exhibited markedly higher viscosity and shear-thinning behaviour at low water contents (1 Wt.% water or lower), which is explained by partial dissolution of the polymer (as confirmed by SAXS). More stringent processing, including longer heating times or higher temperature, would most likely ensure full dissolution of the polymer.

The presence of carrageenan in SDS/glycerol/water mixtures had little effect on the structure of the aqueous SDS crystals (as opposed to the SDS-glycerol phase) when quiescently cooled. However, habit modification from feather-like crystals to jagged needles was observed. Furthermore, when the SDS-glycerol phase was present, it appears that SDS crystals, previously reported for SDS/NaCl/glycerol solutions, are a minor component. Further characterisation of such lamellar crystals with and without polymer is the next logical step for determining the phase composition. Controlled cooling would allow for more detailed analysis of crystal composition, kinetics, and formation. Much is still to be explored with regard to the behaviour of carrageenan in solution. Fitting am appropriate model to SAXS data, such as the 'string of beads' model,[50,51] or others,[35] should enable better characterisation of both the form factor and the structure factor of the sample without additional experimentation.

6.4. References

1 A. Patil and M. S. Ferritto, *Polymers for Personal Care Products and Cosmetics*, Royal Society of Chemistry, Cambridge, 2016.
2 Z. Yang, H. H. Yang and H. H. Yang, *Food Research International*, 2018, **107**, 738–746.
3 S. Ramakrishnan and R. Prud'homme, *Carbohydrate Polymers*, 2000, **43**, 327–332.
4 Z. Yang, H. Yang and H. Yang, *Food Hydrocolloids*, 2018, **75**, 164–173.
5 Y. Liu, K. Zhao and Q. Ma, *Journal of Molecular Liquids*, 2020, **318**, 114268.
6 S. Shimizu and N. Matubayasi, *Journal of Physical Chemistry B*, 2014, **118**, 3922–3930.
7 S. Shimizu and N. Matubayasi, *Journal of Physical Chemistry B*, 2014, **118**, 13210–13216.
8 R. Stenner, N. Matubayasi and S. Shimizu, *Food Hydrocolloids*, 2016, **54**, 284–292.
9 N. S. Anderson, J. W. Campbell, M. M. Harding, D. A. Rees and J. W. B. Samuel, *Journal of Molecular Biology*, 1969, **45**, 86–99.
10 S. Janaswamy and R. Chandrasekaran, *Carbohydrate Research*, 2001, **335**, 181–194.
11 M. Diener, J. Adamcik, A. Sánchez-Ferrer, F. Jaedig, L. Schefer and R. Mezzenga, *Biomacromolecules*, 2019, **20**, 1731–1739.
12 C. Fontes-Candia, A. Ström, L. G. Gómez-Mascaraque, A. López-Rubio and M. Martínez-Sanz, *Algal Research*, 2020, **47**, 101882.
13 N. Mischenko, B. Denef, M. H. J. Koch and H. Reynaers, *International Journal of Biological Macromolecules*, 1996, **19**, 185–194.
14 C. G. Lopez, R. H. Colby, P. Graham and J. T. Cabral, *Macromolecules*, 2017, **50**, 332–338.
15 F. Spyropoulos, A. Lazidis and I. Norton, Eds., *Handbook of Food Structure Development*, Royal Society of Chemistry, Cambridge, 2019.
16 G. Bonacucina, M. Cespi and G. F. Palmieri, *International Journal of Pharmaceutics*, 2009, **377**, 153–158.
17 A. R. del Rio, M. Ramírez-Gilly and A. Tecante, in *Biological Activities and Application of Marine Polysaccharides*, InTech, 2017, vol. 32, pp. 137–144.
18 M. M. Cross, *Journal of Colloid Science*, 1965, **20**, 417–437.
19 M. Larsson and J. Duffy, *Annual Transaction of the Nordic Rheololy Society*, 2013, **21**, 125–138.
20 N. S. Cheng, *Industrial and Engineering Chemistry Research*, 2008, **47**, 3285–3288.
21 A. Marabi, G. Mayor, A. Burbidge, R. Wallach and I. S. Saguy, *Chemical Engineering Journal*, 2008, **139**, 118–127.
22 C. Michon, C. Chapuis, V. Langendorff, P. Boulenguer and G. Cuvelier, *Food Hydrocolloids*, 2005, **19**, 541–547.
23 D. Yang and H. Yang, *LWT - Food Science and Technology*, 2020, **126**, 109281.
24 D. Yang, S. Gao and H. Yang, *Food Hydrocolloids*, 2020, **99**, 105317.
25 Hercules Incorperated, *AQUALON Sodium Carboxymethylcellulose Physical and Properties Chemical properties*, 1999.
26 X. H. Yang and W. L. Zhu, *Cellulose*, 2007, **14**, 409–417.
27 C. G. Lopez, S. E. Rogers, R. H. Colby, P. Graham and J. T. Cabral, *Journal of Polymer Science, Part B: Polymer Physics*, 2015, **53**, 492–501.
28 T. V. Burova, N. V. Grinberg, V. Y. Grinberg, A. I. Usov, V. B. Tolstoguzov and C. G. de Kruif, *Biomacromolecules*, 2007, **8**, 368–375.
29 C. Fontes-Candia, A. Ström, L. G. Gómez-Mascaraque, A. López-Rubio and M. Martínez-Sanz, *Algal Research*, 2020, **47**, 101882.
30 L. C. Geonzon, F. B. A. Descallar, L. Du, R. G. Bacabac and S. Matsukawa, *Food Hydrocolloids*, 2020, **108**, 106039.
31 C. Servais, H. Ranc, C. Sansonnens, S. Ravji, A. Romoscanu and A. Burbidge, 3rd International Symposium on Food Rheology and Structure, 2003, 137–141.
32 R. Buscall, J. I. McGowan and A. J. Morton-Jones, *Journal of Rheology*, 1993, **37**, 621–641.

33 S. Ramakrishnan and R. K. Prud'homme, *Journal of Rheology*, 2000, **44**, 885–896.
34 S.B. Ross-Murphy, Rheologica Acta. 1991, **30**, 401–411.
35 S. Mortimer, A.J. Ryan and J.L. Stanford, Macromolecules, 2001, **34** 2973–2980.
36 F. H. Marchesini, M. F. Naccache, A. Abdu, A. A. Alicke and P. R. de Souza Mendes, *Applied Rheology*, 2015, **25**, 53883- 53,893
37 J. Combet, *EPJ Web of Conferences*, 2018, **188**, 03001.
38 R. M. Fuoss, *Discussions of the Faraday Society*, 1951, **11**, 125-134.
39 A. V. Dobrynin, R. H. Colby and M. Rubinstein, *Macromolecules*, 1995, **28**, 1859–1871.
40 E. Josef, H. Bianco-Peled and D. A. Links, *Soft Matter*, 2012, **8**, 9156–9165.
41 B. Hammouda, F. Horkay and M. L. Becker, *Macromolecules*, 2005, **38**, 2019–2021.
42 W. N. Sharratt, R. O'Connell, S. E. Rogers, C. G. Lopez and J. T. Cabral, *Macromolecules*, 2020, **53**, 1451–1463.
43 K. Salamon, D. Aumiler, G. Pabst and T. Vuletić, *Macromolecules*, 2013, **46**, 1107–1118.
44 W. Essafi, A. Abdelli, G. Bouajila and F. Boué, *Journal of Physical Chemistry B*, 2013, **117**, 731–731.
45 I. Bouwmans and H. E. A. van den Akker, *Institution of Chemical Engineers Symposium Series*, 1990, 1–12.
46 L. Matthews, M. C. Stevens, R. Schweins, P. Bartlett, A. J. Johnson, R. Sochon and W. H. Briscoe, *Colloids and Interface Science Communications*, 2021, **40**, 100342.
47 J. Jennings, M. F. Butler, M. McLeod, E. Csányi, A. J. Ryan and O. O. Mykhaylyk, *Crystal Growth and Design*, 2018, **18**, 7094–7105.
48 W. Fang, H. Zhang, J. Yin, B. Yang, Y. Zhang, J. Li and F. Yao, *Crystal Growth and Design*, 2016, **16**, 1247–1255.
49 A. Moreno and M. J. Rosales-Hoz, *Progress in Crystal Growth and Characterization of Materials*, 2017, **63**, 63–71.
50 I. Dogsa, J. Štrancar, P. Laggner and D. Stopar, *Polymer*, 2008, **49**, 1398–1406.
51 I. Dogsa, J. Cerar, A. Jamnik and M. Tomšič, *Carbohydrate Polymers*, 2017, **172**, 184–196.

7. Conclusions and Future Work

The aim of this work was to characterise the effect of non-aqueous and mixed-aqueous solvents, predominantly containing glycerol and water, on commonly used surfactants, polymers, and their corresponding analogues. This was undertaken to develop the understanding of the constituent materials in personal care formulations such as toothpaste. Detailed characterisation has been achieved for sodium dodecyl sulfate, in glycerol/water mixtures at different temperatures. The effect of addition of electrolytes and alcoholic cosurfactant on the microstructure and phase behaviour has also been studied to simulate complex industrial formulations. Finally a common structuring biopolymer, ι-carrageenan, has been investigated in water-glycerol mixtures with and without SDS. SAXS and optical microscopy were used to probe the microstructure of such systems, with such studies being supplemented by infrared spectroscopy and WAXS data. Rheology was used to quantify the physical properties of the resulting mixtures.

SDS in glycerol was shown to be crystalline at room temperature due to its lower solubility in glycerol compared to aqueous solutions. Formation of an SDS-glycerol crystal phase was confirmed by the presence of ribbon-like crystals following quiescent cooling in solution, which cause gelation at 2 Wt.% SDS and above. By utilising diffraction data from SWAXS experiments, it was possible to characterise the microstructure of the SDS-glycerol phase through reconstruction of the electron density distribution along the crystal bilayer. It was found that the SDS-glycerol phase forms SDS bilayers, as well as distinct sublayers 7 Å wide that contain glycerol. The nature of the sublayer was explored through the formation of homologous n-alkyl sulfate-glycerol crystal phases for even chain surfactants ranging from C12 to C18. Systematic d_{001}-spacing was observed, confirming the presence of a fixed glycerol sublayer. However, it was not possible to obtain pure samples for the homologous series, which resulted in mixed crystal phases. In the future, higher resolution SAXS patterns could be achieved by using higher purity surfactants, thus enabling the reconstruction of electron density profiles. Detailed structural analysis of the SDS-glycerol phase could also be conducted through single-crystal diffraction experiments.

A similar co-assembled structure analogous to the SDS-glycerol phase was formed in mixtures of sodium tetradecyl sulfate (C14) and ethylene glycol. This suggests that high densities of hydrogen bonding and efficient packing at the surfactant headgroup are key factors for co-assembly. Further evidence for this is the lack of co-assembly exhibited by sulfonate-polyol crystals and alkyl sulfate-propylene glycol crystals, which are structurally similar. The work undertaken in this thesis provides initial design rules for the systematic screening of surfactant-solvent mixtures, with a view to understanding their co-assembly.

.

Mixtures containing the SDS-glycerol crystal phase were shown to be highly sensitive to shear, as gelation is facilitated by the high aspect ratio of the crystalline ribbons, which are brittle and can break easily. Cooling temperatures had less impact than expected on the rheological behaviour, with similar viscosity curves and frequency response. Frequency sweep measurements indicated a crossover for G' and G'' at high frequencies for samples of SDS (2 Wt.%) solutions cooled at 20 °C and 10 °C. Samples cooled at 0 °C did not exhibit this behaviour. Future work should examine concentration effects on the SDS-glycerol rheology. SIPLI measurements indicated that at constant high shear, the material broke down and aligned parallel to the shear field. This behaviour may have important implications given the high shear nature of toothbrushing.

At concentrations relevant for industrial formulations, the Krafft temperature (or critical micelle temperature) was significantly higher than that at the Krafft point, when measured from melting points using DSC. The melting range shows there is potential for instability within a product formulation if large temperature fluctuations occur during storage.

The dramatic loss of the SDS-glycerol phase in the presence of small quantities of water showed the sensitivity of the system to modest the changes in the formulation. In most cases, the SDS-glycerol phase was replaced with the kinetically favourable anhydrous crystal. The loss of the SDS-glycerol phase resulted in a reduction in viscosity and shear-thinning behaviour due to loss of the network formation. Formation of anhydrous (rather than hydrated crystals), and the change in crystal habit and type is complex. It is likely that specific interactions between glycerol and water (as well as SDS and water) leads to an equilibrium, with water actively disrupting the formation of SDS-glycerol complexes in the crystal. Solvent viscosity may also play a role both the in crystal habit and the rate of formation. Future work should examine crystallization at significantly higher SDS concentrations to determine whether the crystal behaviour is a function of SDS-water or glycerol-water mass ratios, or both. The implication for an industrial formulation is that reliable creation of the SDS-glycerol phase may be hampered by water ingress which can occur accidentally, for example, because of the highly hygroscopic nature of the formulation.

SDS forms small oblate ellipsoidal micelles in glycerol (aspect ratio = 0.4 for 2 Wt.% SDS), compared to larger prolate ellipsoid micelles in water (aspect ratio = 1.7 for 2 Wt.% SDS) at the same temperature. The smaller size in the former case is expected due to the increased ionic repulsion of the headgroups in less polar solvents. In water-rich binary mixtures, the micelles were generally similar in shape and aspect ratio irrespective of the solvent composition. However, glycerol-rich binary mixtures exhibited a

reduction in shell SLD and an increase in core size from 20-40 Wt.% of solution, which is attributed to hydration of the shell by water. The same behaviour was observed in both 2 and 4 Wt.% solutions of SDS and can be explained by the same dynamic equilibrium of the water between micelle surface and the solvent, which influences crystallization behaviour. This can be confirmed by either studying the water environment, for example by Raman spectroscopy, or by further studying the micelle parameters, for example by SANS, where contrast variation can be exploite. Collection of SAXS patterns at lower *q*, as well as implementation of a decoupling method for the structure factor to account for non-sphericality may also improve fit quality.

Similar research into SDS/glycerol mixtures was independently conducted by Matthews et al. and while there are many similarities in morphology and rheology, these workers proposed a different microstructure and degree of crystallinity. More specifically, Matthews et al. suggested that this phase was paracrystalline, or microfibrillar. The small and wide angle scattering data, as well as the IR spectra presented in this work, suggest the opposite, with a high degree of crystallinity being observed for both SDS and glycerol. Moreover, electron density distribution reconstruction provided a robust method that afforded more information on structure, while still in agreement with the literature value for the sublayer thickness within the SDS/glycerol phase. At elevated temperatures, fitting small angle scattering data to micelle models yielded structures with similar size parameters but different shapes. In particular, this work found that an oblate core-shell ellipsoid was most appropriate, compared to the short core-shell cylinder reported in the literature. This is because the high surface area exposed to the solvent, would cause an entropic penalty due to the hydrophobic effect in the latter case.

Addition of 1-dodecanol for SDS/glycerol mixtures led to similar observations to those reported by Summerton et al. for concentrated aqueous SDS solutions. More specifically, SDS co-crystallized with 1-dodecanol to form ill-defined aggregates. Gradual disruption of the SDS-glycerol phase in favour of the SDS/1-dodecanol phase occurred on addition of 1-dodecanol, and the formation of large ribbon crystals was inhibited in place of ill-formed aggregates. Cocrystallization had the effect of lowering the melting temperature of the surfactant, although multiple DSC peaks could be observed. 1-Dodecanol acted as a cosurfactant at higher temperatures, causing the micelles to swell and become more oblate. Future work should focus on the effect of addition of 1-dodecanol on the rheology of SDS in glycerol. Another compound that influences the crystal structure of SDS is NaCl, which also inhibited formation of the SDS-glycerol phase. However, a new crystal formed instead with a d_{001}-spacing shorter than that of anhydrous SDS. With no observable higher order diffraction peaks, it was not possible to discern structure from electron density profiles. Further exploration of this phase is essential for discerning whether added electrolytes in the stern layer affects co-assembly.

The behaviour of ι-carrageenan in glycerol/water solutions was in good agreement with the literature, where enhanced structuring occurs in aqueous alcoholic solvents. A wide range of solvent compositions was examined, revealing a parabolic trend for zero-shear viscosity and the degree of shear-thinning from viscosity measurements, with maximum structuring occurring at 20 Wt.% water of solution. This is most likely achieved by network formation caused by a coil to helix transition facilitated by preferential exclusion of cosolvents, as rationalised by Kirkwood-Buff theory. SAXS and microscopy studies indicated that for unheated samples, low water contents led to partial dissolution of the polymer, with particles remaining in the solution. Heating the sample reduced this inhomogeneity, with the polymer dissolving on heating and forming the network of helical aggregates on cooling. Hence, heated samples showed stronger rheological structuring at low water contents. At higher water contents (>30 Wt.% water of solution), the rheological behaviour was very similar for unheated and heated samples. The rapid solubilisation and viscosity enhancement in the presence of water must be considered for industrial production. Future work should examine the effect of crosslinking salts such as calcium, which would allow determination of whether the effect of solvent remains constant or can be negated by ionic crosslinking. However, modelling SAXS patterns already collected should provide valuable structural information. Combined with rheological measurements at different concentrations, this could be used to evaluate various industrial formulation protocols. The presence of carrageenan in SDS solutions did not affect the kinetic preference for the anhydrous phase in the presence of water for glycerol rich solvents. The inclusion of carrageenan did, however, lead to the (minor) presence of another crystal, which may be the same type as that formed in the presence of NaCl solutions. Exploration of the relevant processing mechanisms should have implications for rheology and thermal stability of SDS.

The behaviour of SDS in glycerol is often similar to that in water, forming ellipsoidal micelles at higher temperatures and forming co-assembled crystals at low temperatures. The formation of a new, gelling crystal phase comprising SDS-glycerol ribbons is a promising development that may enable structuring of materials without additional polymer. Although not sensitive to the process conditions, the addition of different components causes drastically different behaviour, affecting both the rheology and morphology of the resulting crystals. While this is not ideal for a complex industrial formulation, the addition of a polymer such as iota-carrageenan may mitigate this problem by providing viscosity in the presence of small amounts of water. This work provides fundamental understanding of novel model mixtures, which can be built upon by others to develop robust industrially-relavent formulations.

8. Appendix

8.1: Images of SDS-glycerol solutions following heating at 75 °C for 30 minutes and subsequent quiescent cooling. Left to right: 5 Wt.%, 30 Wt.%, 40 Wt.%, 50 Wt.%, 60 Wt.%, 70 Wt.%, 75 Wt.% SDS. Images show gelation relating to SDS-glycerol phase formation only at 5 Wt.%

8.2: SAXS of SDS-glycerol mixtures following heating at 75 °C for 30 minutes and subsequent quiescent cooling for 2 Wt.%, 8 Wt.%, 10 Wt.%, 20 Wt.%, 30 Wt.% SDS. Results show SDS-glycerol crystal phase presence in all samples aside from 30 Wt.% where anhydrous SDS dominates.

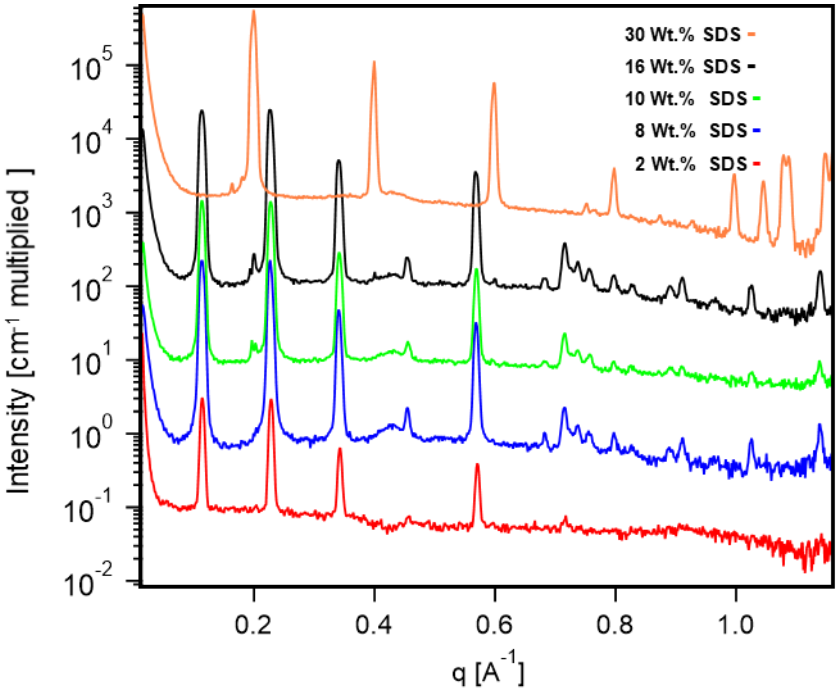

8.3. Electron density profiles constructed from crystal data for anhydrous sodium dodecyl sulfate available from literature,[33] using 5 orders of 00l reflections corresponding to layered structure (1st, 2nd, 3rd, 4th, and 5th order reflections). Structure factor amplitudes were calculated using Mercury 4.0 software. $m(l)$ phase signs of the amplitudes are shown at the top of each profile.

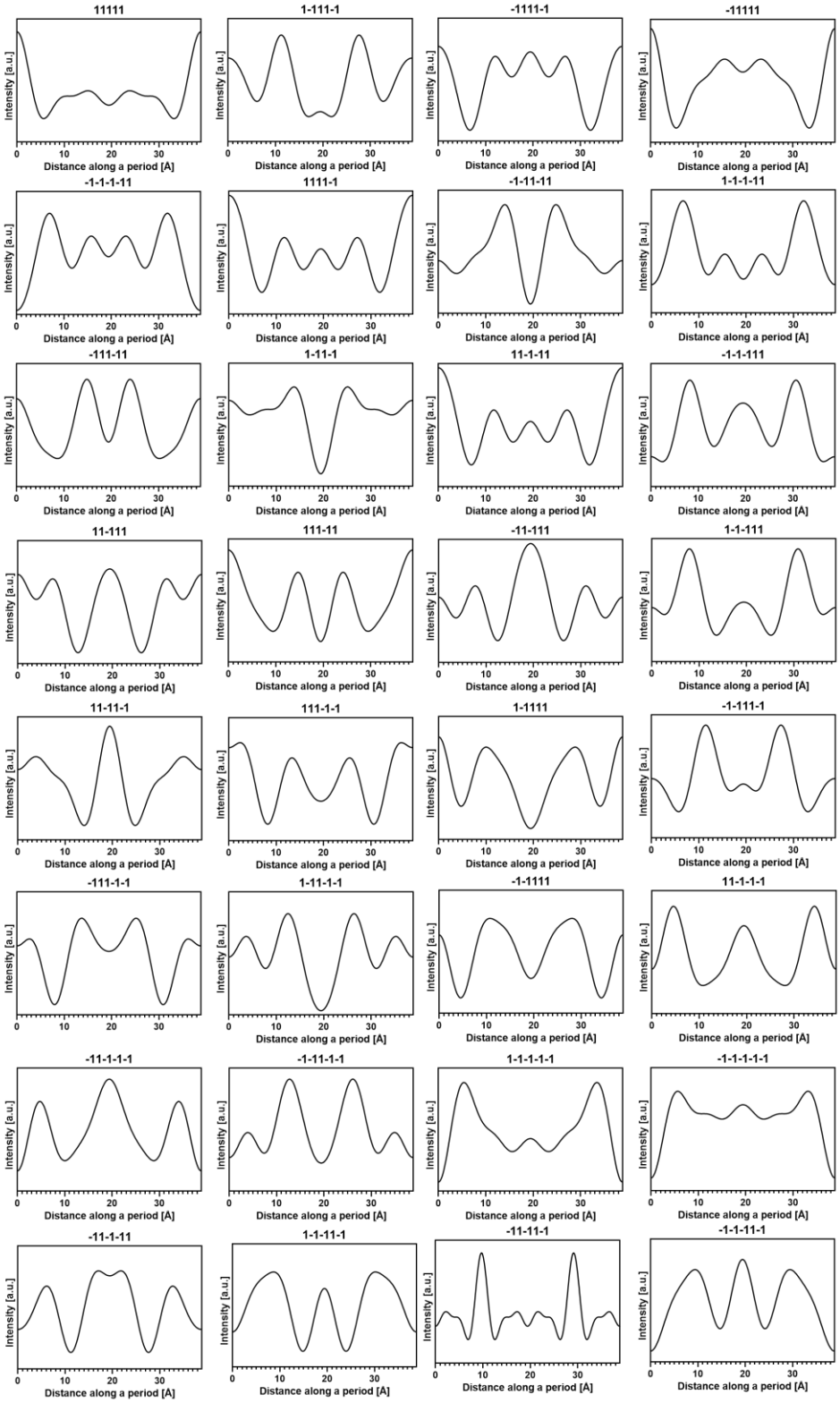

8.4. Top: Peak fitting for sodium dodecyl (C12) sulphate (SDS) powder: experimental SASD pattern (black) with diffraction peaks and scattering background fitted by pseudo-Voight functions using asymmetric least square smoothing, respectively (red line). Inset shows enhanced area containing 4th and 5th order lamellar peak fits. The blue curve below shows residuals from the profile fitting. Bottom: Output of the diffraction peak fitting (peak position, d-spacing and intensity) with crystal phase assignment and Miller indexing.

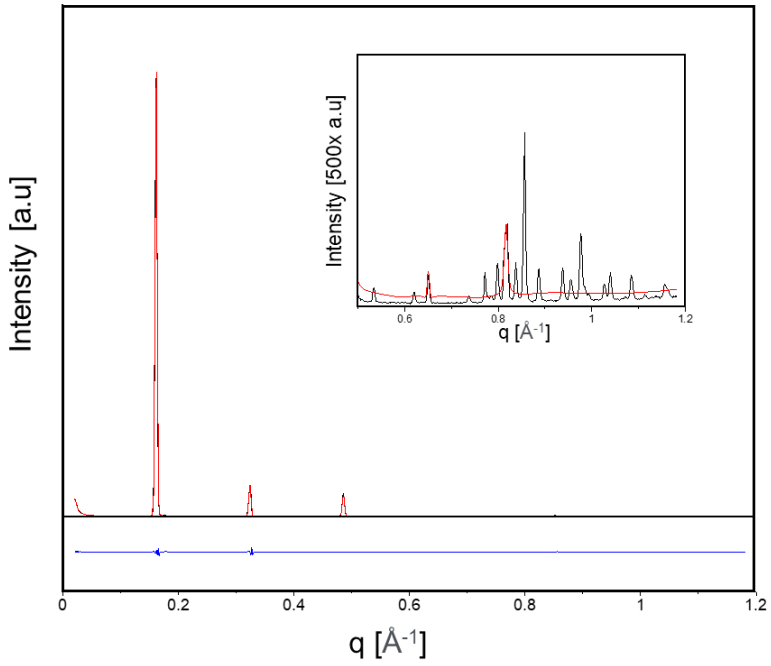

q [Å-1]	d-spacing [Å]	Crystal phase	Miller index	Normalised intensity
0.1627	38.62	anhydrous SDS	001	100.00
0.3256	19.30	anhydrous SDS	002	6.93
0.4879	12.88	anhydrous SDS	003	5.04
0.6502	9.66	anhydrous SDS	004	0.02
0.8164	7.70	anhydrous SDS	005	0.07

8.5. Electron density profiles generated from five 00l reflections of experimental Bragg peak intensities from SAXS scattering patterns of anhydrous crystal data for (dried) sodium dodecyl sulfate powder (Appendix 8.4). $m(l)$ *signs are shown at the top of each profile.*

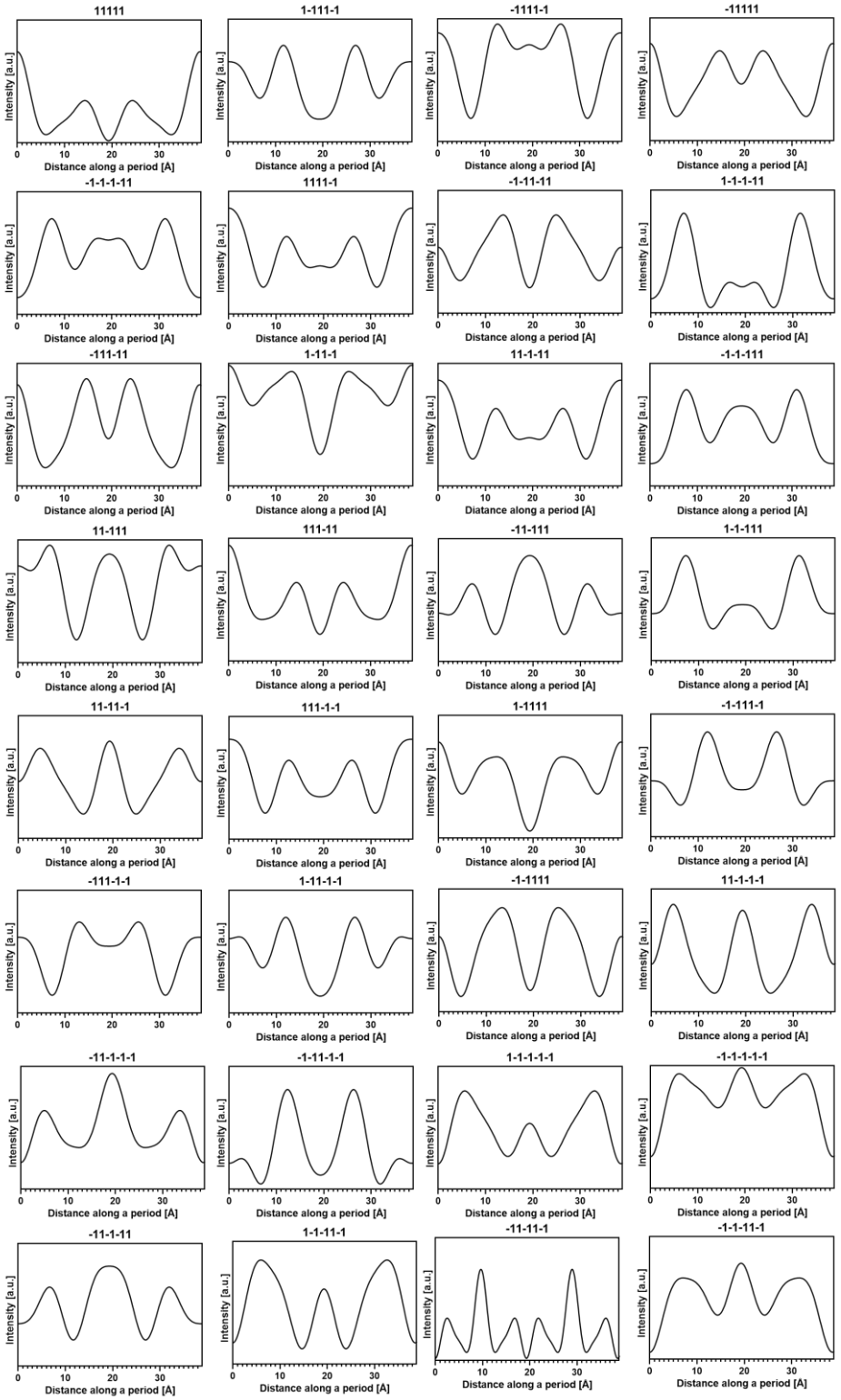

8.6. Top: Peak fitting for SDS (8 Wt.%) in glycerol: experimental SAXS pattern (black) with diffraction peaks and scattering background fitted by pseudo-Voight functions using asymmetric least square smoothing, respectively (red line). Inset shows enhanced area containing higher order peak fits. The blue curve below shows residuals from the profile fitting. Bottom: Output of the diffraction peak fitting (peak position, d-spacing and intensity) with crystal phase assignment and Miller indexing.

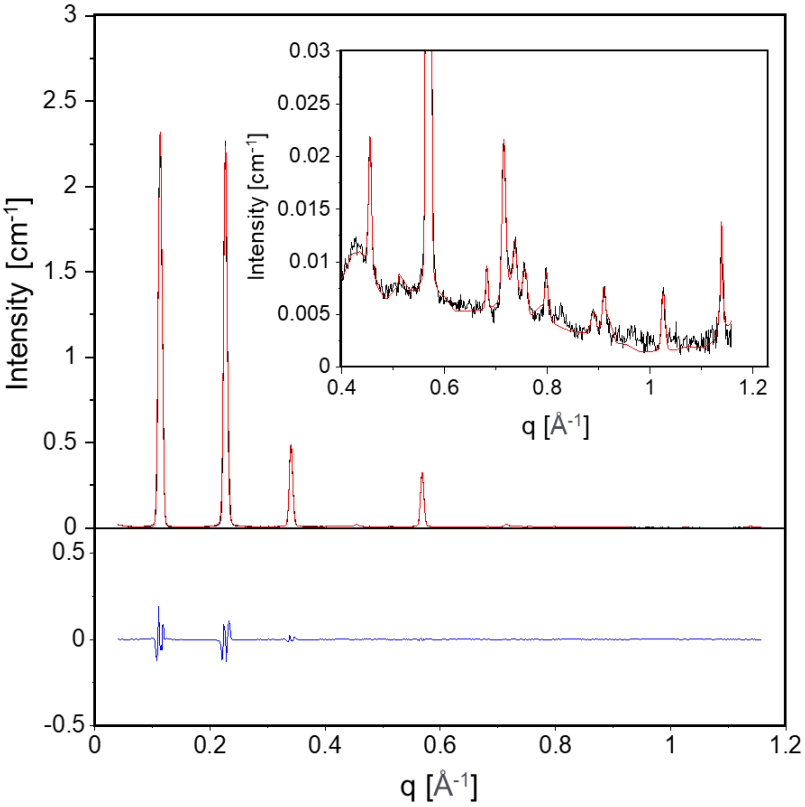

q [Å^{-1}]	d-spacing [Å]	Crystal phase	Miller index	Normalised intensity
0.1133	55.44	glycerol cocrystal	001	100.00
0.2266	27.73	glycerol cocrystal	002	96.25
0.3405	18.45	glycerol cocrystal	003	20.84
0.4546	13.82	glycerol cocrystal	004	0.60
0.5684	11.05	glycerol cocrystal	005	13.76
0.6822	9.21	glycerol cocrystal	006	0.18
0.7151	8.79	glycerol cocrystal	-	0.66
0.7363	8.53	glycerol cocrystal	-	0.34
0.7566	8.30	glycerol cocrystal	-	0.14
0.7981	7.87	glycerol cocrystal	007	0.18
0.8902	7.06	glycerol cocrystal	-	0.10
0.9101	6.90	glycerol cocrystal	008	0.05
1.025	6.13	glycerol cocrystal	009	0.23
1.138	5.52	glycerol cocrystal	0010	0.52

8.7. Electron density profiles generated from five 00l reflections of experimental Bragg peak data collected from SAXS scattering patterns of the SDS-glycerol crystal phase created from 8 Wt.% SDS in glycerol, following heating at 75 °C for 30 minutes and subsequent quiescent cooling (Appendix F). Profiles are grouped into generalised motifs in order to allow for comparison, due to the similar nature of the profiles. $m(l)$ *signs are shown at the top of each profile.*

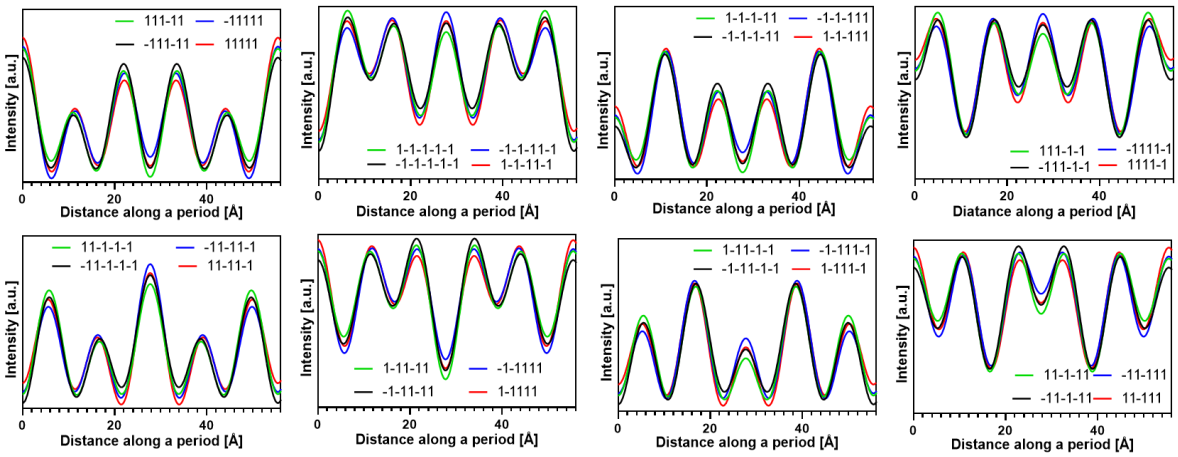

8.8. Infrared spectra of glycerol and 16 Wt.% SDS in glycerol recorded following heating at 75 °C for 30 minutes and subsequent quiescent cooling. Mixture is comprised of the SDS-glycerol crystal phase, and bulk glycerol. Intensity is offset to allow comparison.

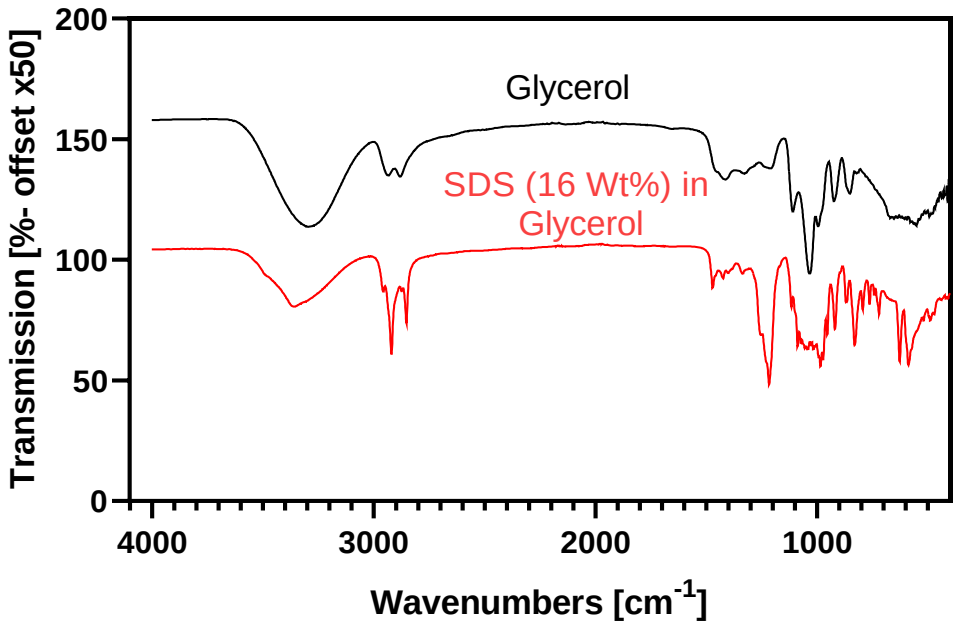

8.9. DSC heating profiles of SDS-glycerol mixtures following a previous heating and cooling cycle (heated to 75 °C for 30 minutes before quiescent cooling): a) overlay of background subtracted heating profiles of SDS in glycerol, b) 1 Wt.% SDS in glycerol, c) 1.5 Wt.% SDS in glycerol, d) 3 Wt.% SDS in glycerol, e) 8 Wt.% SDS in glycerol and f) 16 Wt.% SDS in glycerol. Samples contain SDS-glycerol crystal phase as the sole (or majority) crystalline constituent within the mixtures. Analysis of peak onset and peak temperature is performed using the Peak Integration (enthalpy) tool using a linear baseline. The end set was measured using the Endset Point analysis tool.

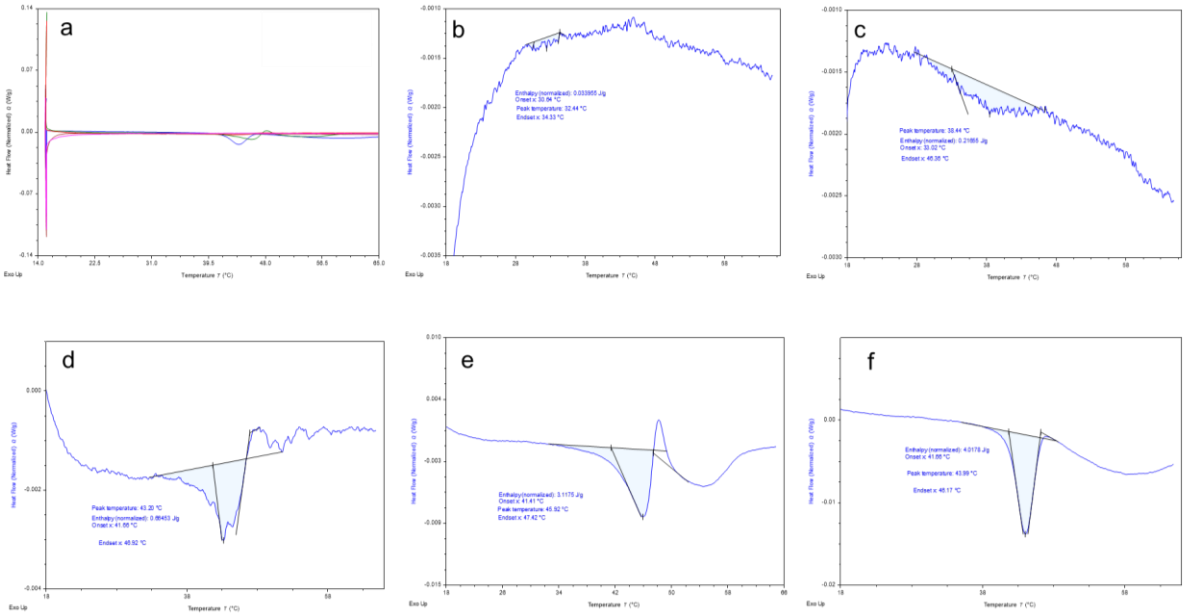

8.10. Creep-relaxation test of SDS (2 Wt.%) in glycerol, heated to 80 °C for 10 minutes before being isothermally cooled at 20 °C for 18000 seconds. Regions are marked where stress is applied (creep) and removed (relaxation).

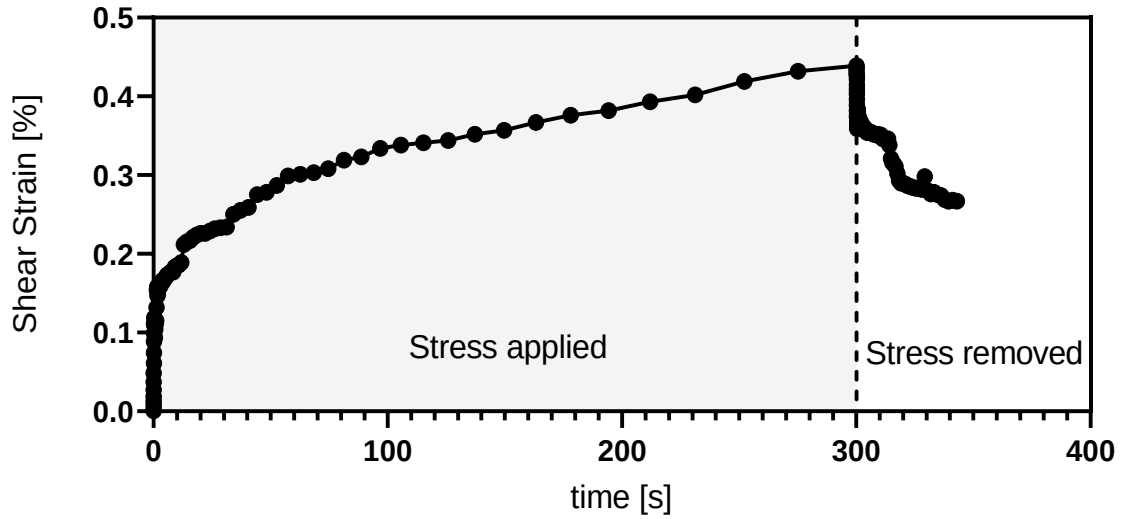

8.11. Successive flow sweeps of SDS (2 Wt.%) in glycerol, heated to 80 °C for 10 minutes before being isothermally cooled at 20 °C for 18000 seconds. Red indicates the first measurement, with 2nd 3rd and 4th runs initiated immediately after. Black was conducted 15 hours later. Minimal change occurs after the first run due to break up of the network formed by crystal aggregates.

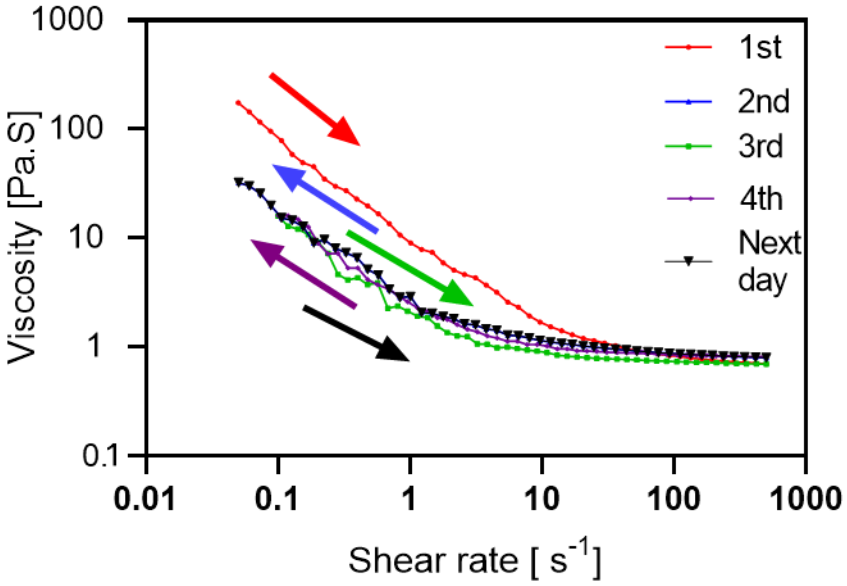

8.12. Top: Peak fitting for C14/sodium tetradecyl sulfate (2 Wt.%) in glycerol, following heating at 100 °C for 30 minutes and subsequent quiescent cooling: Experimental SAXS pattern (black) with diffraction peaks and scattering background fitted by pseudo-Voight functions using asymmetric least squares smoothing, respectively (red line). Bottom: Output of the diffraction peak fitting (peak position, d-spacing and intensity) with crystal phase assignment and Miller indexing. Blue line shows residuals of the fitted peaks and background.

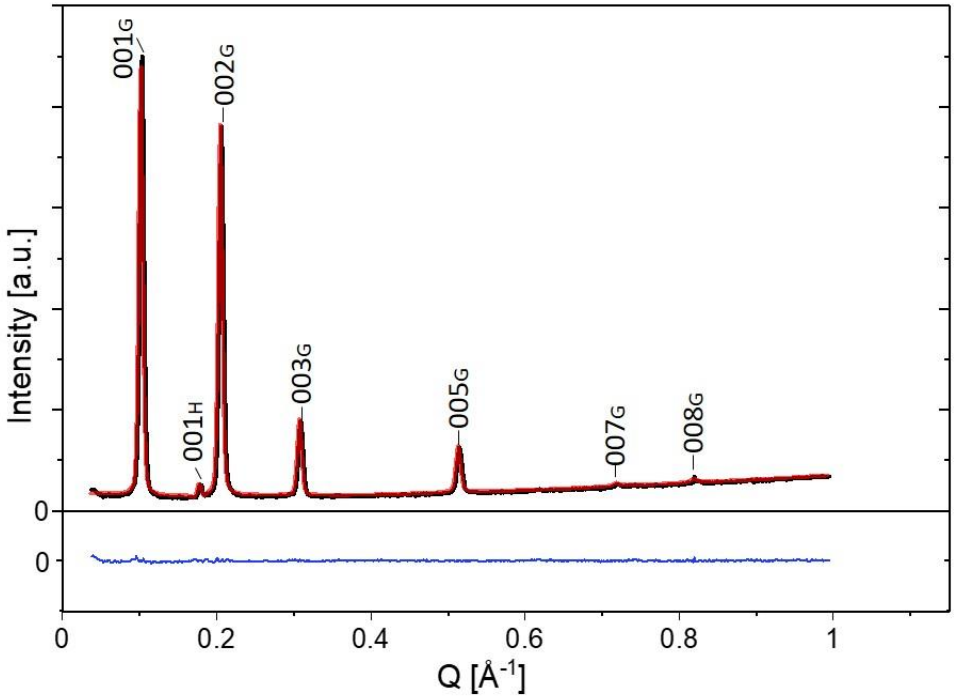

q [Å^{-1}]	d-spacing [Å]	Crystal phase	Miller index	Normalised intensity
0.10296	61.03	C14 (STDS)-glycerol crystal	001_G	100
0.1788	35.15	C14 +H_2O	001_H	84.06
0.2062	30.47	C14 -glycerol crystal	002_G	2.26
0.3090	20.34	C14 -glycerol crystal	003_G	17.19
0.5151	12.20	C14 -glycerol crystal	005_G	10.51
0.7202	8.72	C14 -glycerol crystal	007_G	0.71
0.8214	7.65	C14 -glycerol crystal	008_G	0.75

8.13. Top: Peak fitting for C16/sodium hexadecyl sulfate (2 Wt.%) in glycerol, following heating at 100 °C for 30 minutes and subsequent quiescent cooling: Experimental SAXS pattern (black) with diffraction peaks and scattering background fitted by pseudo-Voight functions using asymmetric least squares smoothing, respectively (red line). Blue line shows residuals of the fitted peaks and background.

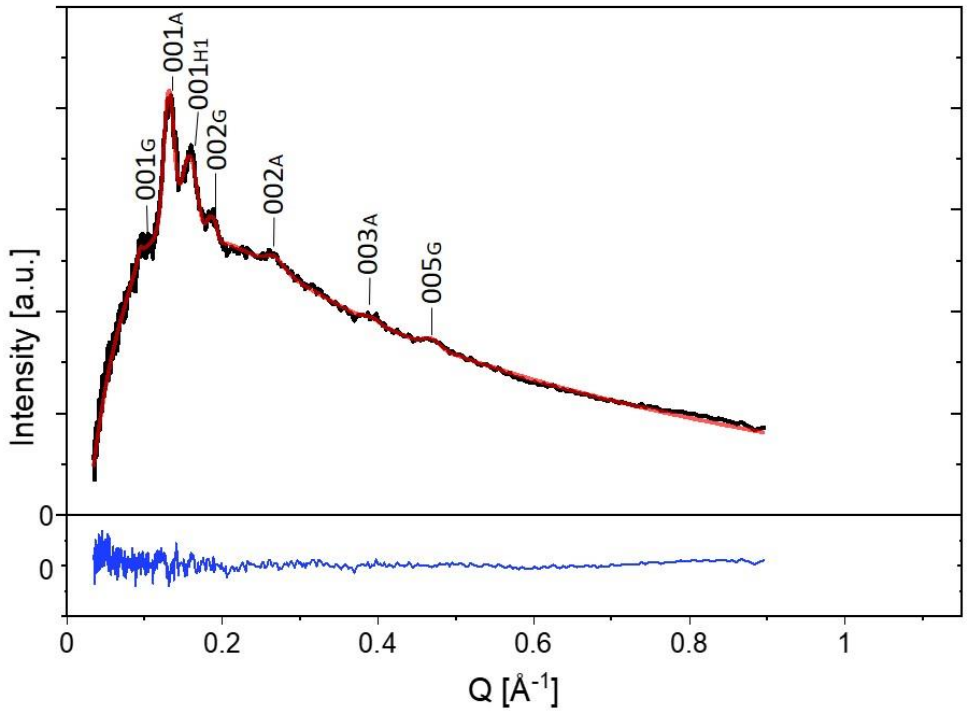

q [Å^{-1}]	d-spacing [Å]	Crystal phase	Miller index	Normalised intensity
0.0949	66.21	C16-glycerol crystal	$d001_G$	11.6
0.1318	47.66	anhydrous SHDS	$d001_A$	100
0.1581	39.72	SHDS+1H_2O	$d001_{H1}$	49.1
0.1869	33.61	C16-glycerol crystal	$d002_G$	12.3
0.2678	23.45	anhydrous SHDS	$d002_A$	10.3
0.3921	16.01	C16-glycerol crystal	$d003_A$	2.29
0.4699	13.37	C16-glycerol crystal	$d005_G$	5.28

8.14. Top: Peak fitting for C18/sodium octadecyl sulfate (2 Wt.%) in glycerol, following heating at 100 °C for 30 minutes and subsequent quiescent cooling: Experimental SAXS pattern (black) with diffraction peaks and scattering background fitted by pseudo-Voight functions using asymmetric least squares smoothing, respectively (red line). Bottom: Output of the diffraction peak fitting (peak position, d-spacing and intensity) with crystal phase assignment and Miller indexing. Blue line shows residuals of the fitted peaks and background.

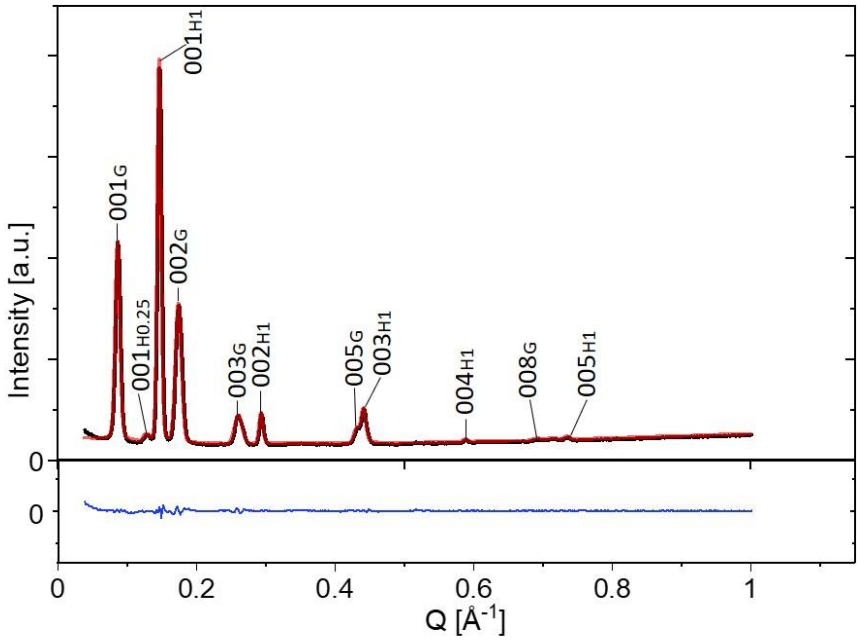

q [Å^{-1}]	*d*-spacing [Å]	Crystal phase	Miller index	Normalised intensity
0.0871	72.08	C18 (SODS)-glycerol crystal	001_G	51.7
0.1284	48.93	C118+0.25H_2O	$001_{H0.25}$	1.33
0.1472	42.67	C18+1H_2O	001_{H1}	100
0.1750	35.89	C18-glycerol crystal	002_G	35.9
0.2616	24.02	C18-glycerol crystal	003_G	7.37
0.2944	21.34	C18+1H_2O	002_{H1}	8.06
0.4321	14.54	C18-glycerol crystal	005_G	3.38
0.4421	14.21	C18+1H_2O	003_{H1}	9.16
0.5894	10.66	C18+1H_2O	004_{H1}	0.54
0.6932	9.06	C18-glycerol crystal	008_G	0.47
0.7361	8.54	C18+1H_2O	005_{H1}	0.85

8.15 Time-resolved 1D SAXS pattern of 2 Wt.% SDS in glycerol/water mixtures during isothermal cooling at 20 °C with compositions containing a)100% Glycerol, (same experimental data used in Chapter 3), b) 98.7 Wt.% glycerol and 1.3 Wt.% water, c) 97.5 Wt.% glycerol and 2.5 Wt.% water, d) 96.2 Wt.% glycerol and 3.8 Wt.% water, e) 95.0 Wt.% glycerol and 5.0 Wt.% water, f) 93.7 Wt.% glycerol and 6.3 Wt.% water. Miller indices are assigned to lamellar diffraction peaks of the SDS-glycerol crystal phase, $00l_G$, and the anhydrous SDS crystals, $00l_A$.

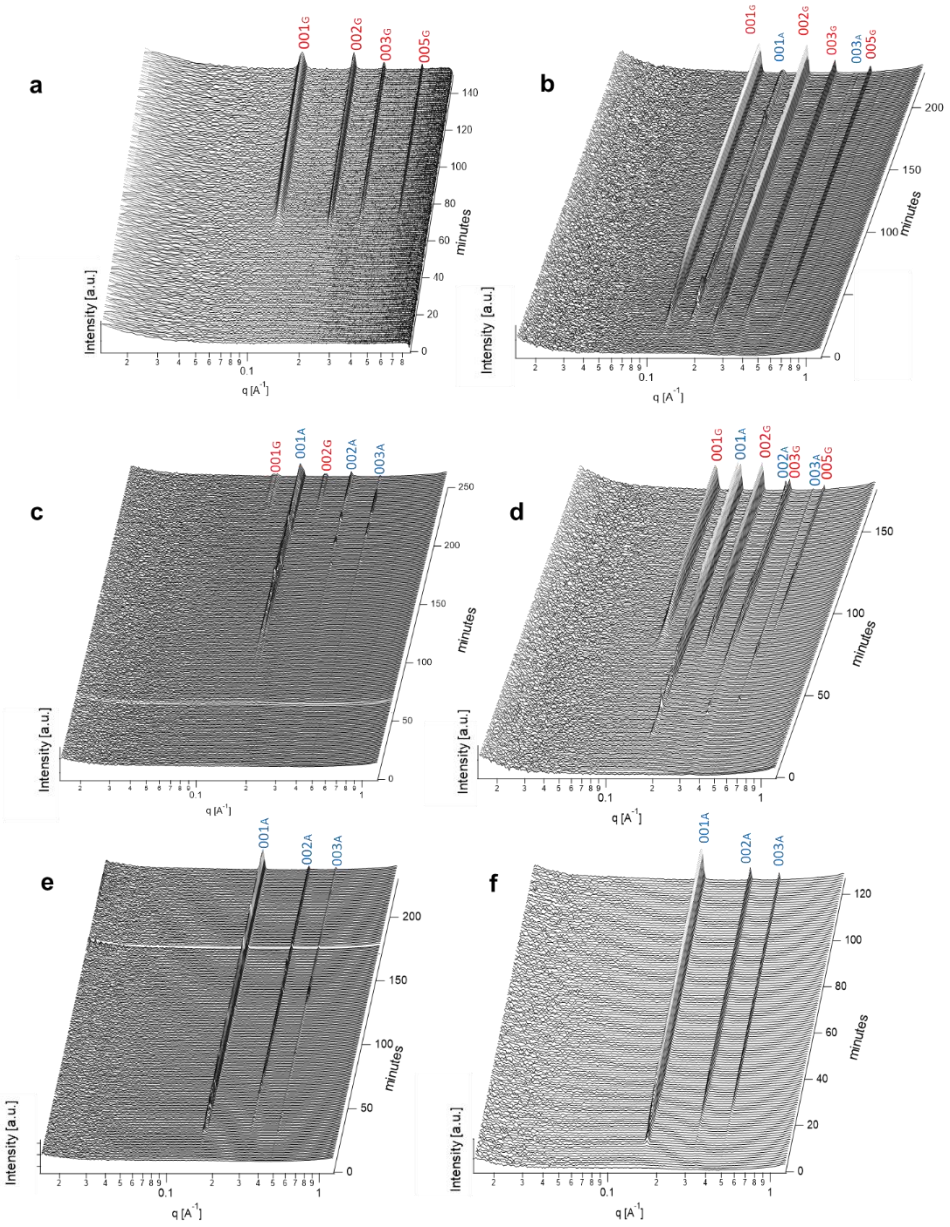

8.16: 001_G and 001_A fitted peak intensity versus the cooling time (right) for 2 Wt.% SDS in glycerol-water mixtures, normalised to the highest plateau intensity average, using scattering data in Appendix A where a)100% Glycerol, (same experimental data used in Chapter 3), b) 98.7 Wt.% glycerol and 1.3 Wt.% water, c) 97.5 Wt.% glycerol and 2.5 Wt.% water, d) 96.2 Wt.% glycerol and 3.8 Wt.% water, e) 95.0 Wt.% glycerol and 5.0 Wt.% water, f) 93.7 Wt.% glycerol and 6.3 Wt.% water.

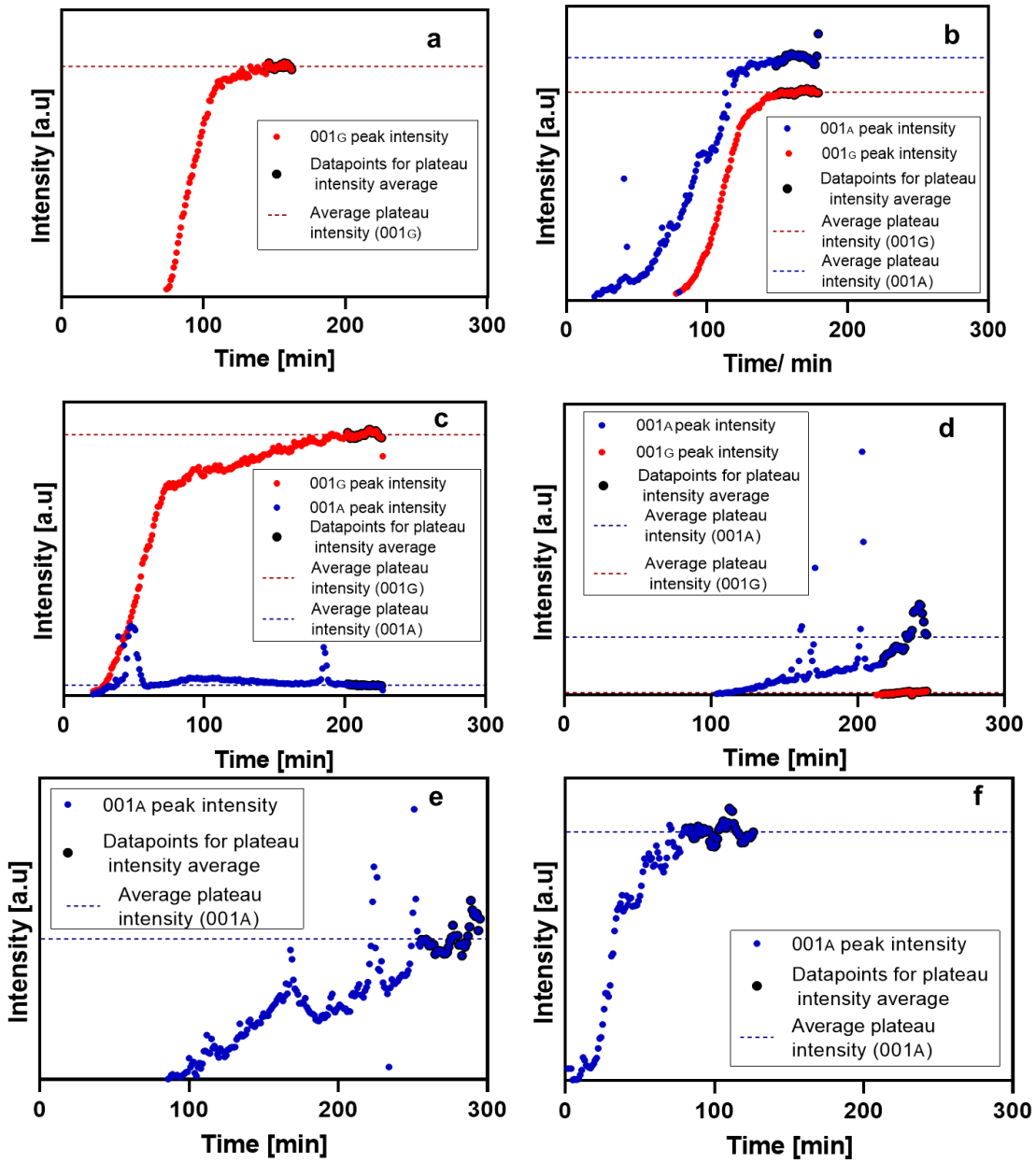

8.17: Background corrected SAXS profiles of SDS (4 Wt.%) containing a) 40 Wt.% water and 60 Wt.% glycerol b) 20 Wt.% water and 80 Wt.% glycerol c) 10 Wt.% water and 90 Wt.% glycerol d) 0 Wt.% water and 100 Wt.% glycerol heated and subsequently quiescently cooled. While the SDS-glycerol phase forms in glycerol, the anhydrous SDS phase forms in all other solvent compositions. $00l_G$ and $00l_A$ are Miller indices used to denote lamellar peaks of the respective phases (SDS-glycerol and anhydrous SDS phase).

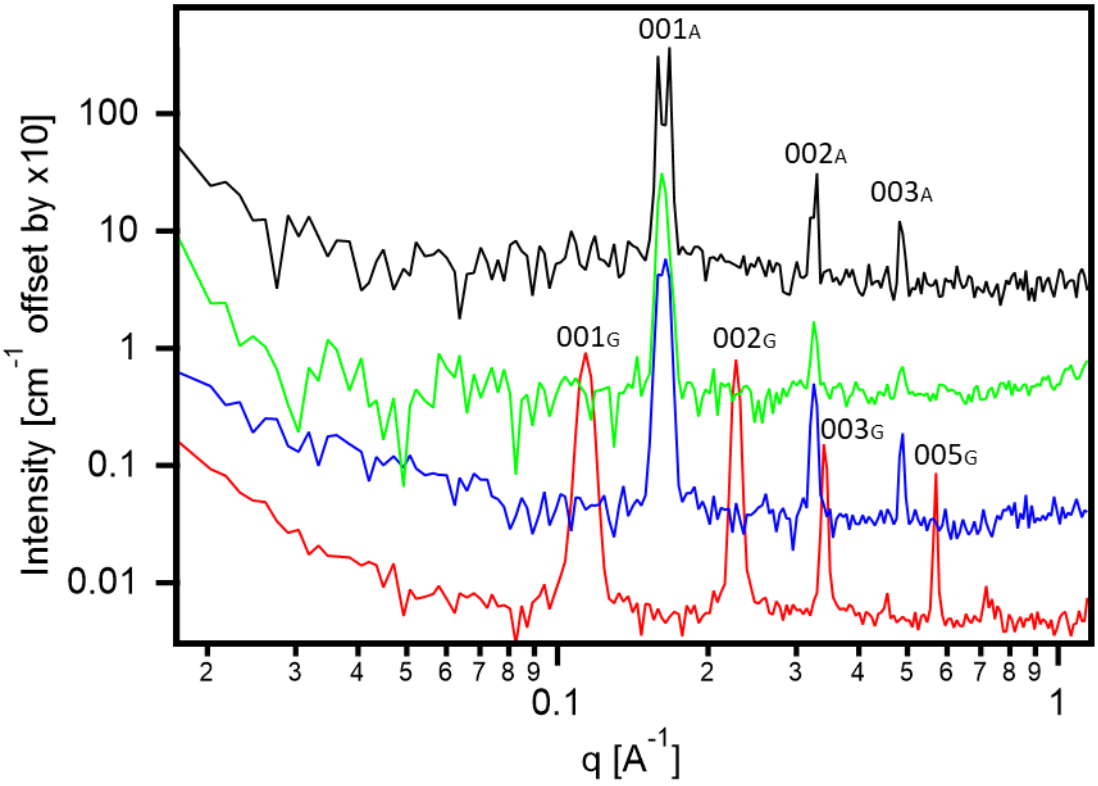

8.18: Fitting parameters of the core-shell ellipsoid form factor with Hayter-Penfold structure factor for SDS (2 Wt.%) micelles in glycerol-water mixtures at 60 °C, where the non-bold column headers indicate fixed parameter and the bold column headers indicate fitted parameters. Note that for all samples, core SLD was fixed at 7.7 x10^{10} cm^{-2}, temperature was fixed at 333.15 K and salt concentration was set to zero.

Wt.% water of solvent	Volume fraction of SDS	**Equatorial core radius [Å]**	**Polydispersity index* [σ/r_{core}]**	**Aspect ratio**	**Shell thickness [Å]**	**Shell SLD [x10^{10} cm^{-2}]**	Solvent SLD [x10^{10} cm^{-2}]	**Charge**	**Structure factor radius [Å]**	Dielectric constant[1]	**Reduced χ2**
0	0.0251	11.3	0.293	0.416	4.83	13.12	11.4	6.80	8.99	33.8	0.91
10.7	0.0244	11.9	0.176	0.408	3.87	12.18	11.2	3.93	9.61	38.2	0.91
20.5	0.0238	13.4	0.294	0.648	7.21	11.97	11	4.22	14.1	42.3	1.40
30.1	0.0233	10.2	0.073	0.367	7.06	10.85	10.7	4.32	11.7	46.3	0.98
40	0.0227	13.4	0.002	0.503	9.46	10.76	10.5	3.85	11.7	50.2	0.89
50.5	0.0222	13.3	0.087	1.58	4.91	11.97	10.3	7.75	16.8	53.4	1.82
59.5	0.0217	14.6	0.122	1.24	2.92	13.25	10.1	3.52	11.5	56.2	2.48
69.7	0.0213	14.9	0.135	1.29	2.96	13.26	9.9	2.41	10.0	59.0	1.63
80.2	0.0208	14.9	0.092	1.57	3.34	12.80	9.7	4.18	8.83	61.6	1.94
90	0.0206	15.0	0.075	1.63	3.31	12.91	9.5	3.96	9.54	64.0	10.02
100	0.0204	15.7	0.101	1.42	2.91	13.09	9.3	2.81	12.6	66.6	3.84

**Polydispersity index is the core radius standard deviation (σ) divided by core radius (r_{core}).*

[1] *Physical properties of glycerol and its solutions, Glycerine Producers' Association, New York, 1963.*

8.19: Full fitting parameters of the core-shell ellipsoid model with Hayter Penfold structure factor, for SDS (4 Wt.%) micelles in glycerol-water mixtures at 60 °C. Where non-bold columns indicate fixed parameter and bold indicates fitted parameters Note that for all samples, core SLD was fixed at 7.7 x10^{10} cm^{-2}, temperature was fixed at 333.15 K and salt concentration was set to zero.

Wt.% water of solvent	Volume fraction of SDS	**Equatorial core radius [Å]**	**Polydispersity index* [σ/r_{core}]**	**Aspect ratio**	**Shell thickness [Å]**	**Shell SLD [x10^{10} cm^{-2}]**	Solvent SLD [x10^{10} cm^{-2}]	**Charge**	**Structure factor radius [Å]**	Dielectric constant[1]	**Reduced χ2**
0	0.0491	13.7	0.260	0.608	4.66	13.0	11.4	3.27	12.6	33.8	1.35
9.4	0.0479	15.4	0.178	0.668	4.84	12.8	11.2	5.13	14.6	38.3	1.09
19.2	0.0469	7.4	0.149	0.492	7.81	11.0	10.9	4.79	11.5	42.3	1.11
28.9	0.0457	10.0	0.321	0.662	12.33	10.9	10.7	3.26	14.2	46.3	1.01
58.2	0.0428	31.2	0.083	2.280	7.08	11.5	10.1	16.47	19.5	50.2	9.08
78.7	0.0410	25.6	0.087	1.635	3.09	13.4	9.7	0.10	13.1	61.5	2.82
100	0.0410	26.0	0.066	1.599	3.19	13.1	9.3	15.34	20.3	66.6	12.82

**Polydispersity index is the core radius standard deviation (σ) divided by core radius (r_{core}).*

[1] *Physical properties of glycerol and its solutions, Glycerine Producers' Association, New York, 1963.*

8.20: Fitting parameters of the core-shell ellipsoid model with Hayter Penfold structure factor, for SDS (4 Wt.%) and 1-dodecanol micelles in glycerol at 60 °C. Where bold columns indicate fixed parameter and non-bold indicates fitted parameters . Note that for all samples, core SLD was fixed at 7.7 x10^{10} cm^{-2}, solvent SLD was fixed to 11.4 x10^{10} cm^{-2}, shell SLD was fixed to 13.1 x10^{10} cm^{-2}, dielectric constant was fixed to 33.8,[1] temperature was fixed at 333.15 K, salt concentration was set to zero.

Wt.% 1-dodecanol	Equatorial core radius [Å]	Polydispersity index* [σ/rc$_{ore}$]	Aspect ratio	Shell radii [Å]	Charge	Volume fraction (SF)	Reduced χ2
0	12.64	0.29	0.64	4.12	9.3	0.027	2.14
0.28	13.31	0.28	0.75	3.26	8.93	0.017	2.09
0.56	17.06	0.23	0.63	3.75	11.69	0.026	2.22
0.81	18.6	0.18	0.61	3.56	12.46	0.024	2.36
1.05	16.98	0.24	0.72	3.02	13.03	0.023	8.58
1.31	20.9	0.17	0.57	3.36	13.53	0.02	4.75
1.46	21.5	0.16	0.55	3.05	13.12	0.018	22.6
2.05	24.25	0.17	0.5	3.1	13.52	0.013	2.14

**Polydispersity index is the core radius standard deviation (σ) divided by core radius (r_{core}).*

[1] *Physical properties of glycerol and its solutions, Glycerine Producers' Association, New York, 1963.*

8.21: DSC melting profiles of SDS (4 Wt.%) in glycerol containing a) 0.5 Wt.% b) 3.8 Wt.% NaCl. The melting temperature is increased by 30 °C between samples indicating a reduction of micellar solubility at high electrolyte concentration.

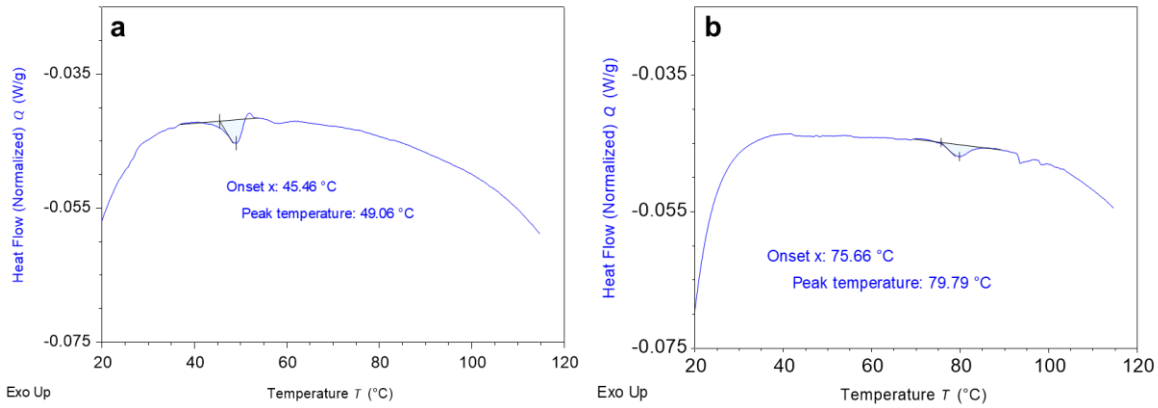

.